MATERIALS CHARACTERIZATION AND ANALYSIS COLLECTION

C. Richard Brundle, *Editor*

Secondary Ion Mass Spectrometry

Applications for Depth Profiling and Surface Characterization

Fred A. Stevie

MOMENTUM PRESS
ENGINEERING

SECONDARY ION MASS SPECTROMETRY

SECONDARY ION MASS SPECTROMETRY

Applications for Depth Profiling and Surface Characterization

FRED A. STEVIE

Analytical Instrumentation Facility, North Carolina State University

MOMENTUM PRESS ENGINEERING

MOMENTUM PRESS, LLC, NEW YORK

Secondary Ion Mass Spectrometry: Applications for Depth Profiling and Surface Characterization

Copyright © Momentum Press®, LLC, 2016.

All rights reserved. No part of this publication may be reproduced, stored in a retrieval system, or transmitted in any form or by any means—electronic, mechanical, photocopy, recording, or any other—except for brief quotations, not to exceed 400 words, without the prior permission of the publisher.

First published by Momentum Press®, LLC
222 East 46th Street, New York, NY 10017
www.momentumpress.net

ISBN-13: 978-1-60650-588-5 (print)
ISBN-13: 978-1-60650-589-2 (e-book)

Momentum Press Materials Characterization and Analysis Collection

Collection ISSN: 2377-4347 (print)
Collection ISSN: 2377-4355 (electronic)

Cover and interior design by Exeter Premedia Services Private Ltd., Chennai, India

10 9 8 7 6 5 4 3 2 1

Printed in the United States of America

This book is dedicated to my wife, Eileen, whose encouragement and support throughout my career helped make possible my contribution to science.

Abstract

Secondary ion mass spectrometry (SIMS) is a mass spectrometric technique for solid materials that can provide elemental analysis at parts per million sensitivity and lateral resolution of 50 nm. When those capabilities are combined with the ability to provide that analysis as a function of depth, SIMS has proved to be a valued technique for a wide range of applications. This book was written to explain a technique that requires an understanding of many details in order to properly obtain and interpret the data. It also will serve as a reference for those who need to provide SIMS data. The book has over 200 figures and the references allow one to trace the development of SIMS and help understand the technique.

KEYWORDS

depth profiling, magnetic sector mass analyzer, mass spectrometry, secondary ion mass spectrometry, time-of-flight mass analyzer, quadrupole mass analyzer

Contents

List of Figures **xiii**

List of Tables **xxi**

Preface **xxiii**

1 Comparison of Surface Analytical Techniques **1**

1.1 Common Elemental Surface Analysis Techniques 1

1.2 Introduction to Mass Spectrometry 3

1.3 Brief History of Mass Spectrometry and SIMS 5

1.4 Types of Mass Spectrometry 7

1.5 Rationale for SIMS 8

1.6 Types of SIMS Data 11

References 12

2 SIMS Technique **19**

2.1 Interaction of Ions with Matter 19

2.2 Sputtering Process 19

2.3 Sputtering Yield 23

2.4 Preferential Sputtering 28

2.5 Secondary Ion Yield 28

2.6 Oxygen Flood (Oxygen Leak, Oxygen Backfill) 30

2.7 Matrix Effects 32

References 34

3 Analysis Parameters **39**

3.1 Parameters of Interest for Depth Profiling 39

3.2 Primary Beam Polarity and Species 39

3.3 Secondary Ion Polarity and Species 43
3.4 Primary Beam Energy 47
3.5 Primary Beam Angle of Incidence 48
3.6 Primary Beam Current, Raster Size 49
3.7 Secondary Beam Energy Distribution—Voltage Offset 49
3.8 Mass Interferences, Mass Resolution 52
References 58

4 Instrumentation 61
4.1 Vacuum System 61
4.2 Overall Instrument 62
4.3 Ion Sources 63
4.4 Primary Ion Column 66
4.5 Sample Chamber and Sample 66
4.6 Secondary Ion Column and Mass Analyzers 67
4.7 Detectors 75
4.8 Focused Ion Beam SIMS (FIB-SIMS) 76
4.9 Computers and Data Manipulation 77
4.10 Related Instruments 77
References 78

5 Depth Profiling (Dynamic SIMS) 81
5.1 Raster and Gate 81
5.2 Depth Resolution 83
5.3 Sputtering Rate 96
5.4 Nonuniform Sputtering, Sample Rotation 96
5.5 Detection Limit, Dynamic Range, Memory Effect 100
5.6 Count Rate Saturation—Detector Dead Time 104
5.7 Small Area Analysis 105
5.8 Nonuniform Distribution 109
5.9 Image Depth Profile—Lateral Resolution 111
5.10 Movement of Species Due to Chemical Effect 111
References 112

6 Quantification **121**
6.1 Need for Secondary Standards 121
6.2 Depth Profile Quantification—Relative Sensitivity Factors 121
6.3 Ion Implanted Standards 124
6.4 Bulk Standards 131
6.5 Matrix and Trace Quantification 132
6.6 Useful Yield 134
6.7 Precision and Accuracy 135
6.8 Quantification in Multiple Matrixes—Cesium Cluster Ions 137
6.9 Static SIMS Quantification 138
6.10 RSF Relationship with Ionization Potential and Electron Affinity 140
References 143

7 Surfaces, Interfaces, Multilayers, Bulk **149**
7.1 Sample Considerations 149
7.2 Surface—Static SIMS 149
7.3 Interfaces 151
7.4 Multilayers 156
7.5 Back Side Analysis 157
7.6 Bulk Analysis 160
References 162

8 Insulators **165**
8.1 Sample Charging 165
8.2 Charge Compensation Methods 168
8.3 Electron Beam Neutralization 169
8.4 Species Mobile Under Ion Bombardment 182
8.5 Buried Insulators 185
8.6 Electron Stimulated Desorption 185
8.7 Summary 186
References 187

9 Residual and Rare Gas Elements **191**

9.1 Residual Gas Elements, Raster Reduction 191

9.2 Rare Gas Elements 200

References 201

10 Applications **205**

10.1 Semiconductors 205

10.2 Organic Materials 223

10.3 Minerals, Ceramics, Catalysts 227

10.4 Metals 229

References 230

11 Analysis Approach **235**

11.1 Initial Considerations 235

11.2 Analysis Sequence 236

Appendix **239**

Index **253**

List of Figures

Figure 1.1. Isotopic abundances. 3
Figure 1.2. High mass resolution mass spectrum of 700 Da. 4
Figure 1.3. Mass spectrometer block diagram. 4
Figure 1.4. AES depth profile. 9
Figure 1.5. SIMS depth profile. 9
Figure 1.6. SIMS mass spectrum y-axis display. 10
Figure 1.7. Zinc oxide mass spectrum. 11
Figure 1.8. SIMS depth profile of BPSG layers. 12
Figure 1.9. Carbon segregation in niobium bicrystals. 12
Figure 2.1. Interaction of ions with matter. 20
Figure 2.2. SIMS process. 20
Figure 2.3. Energy distribution of sputtered particles. 20
Figure 2.4. TRIM simulation at two impact energies. 21
Figure 2.5. Simulation of particle surface interaction. 22
Figure 2.6. Sputtering simulations for SF_5^+. 22
Figure 2.7. Sputtering simulation of C_{60}^+ versus Ga^+ on Ag(111). 23
Figure 2.8. Sputtering yield versus primary energy. 23
Figure 2.9. Sputtering yield versus primary energy. 24
Figure 2.10. Penetration versus incidence angle. 24
Figure 2.11. Distribution of implanted species. 25
Figure 2.12. Sputtering yield versus incidence angle. 25
Figure 2.13. Penetration depth versus energy and incidence angle. 26
Figure 2.14. Angular distribution of sputtered material. 26
Figure 2.15. Sputtering yield versus primary ion atomic number. 27

Figure 2.16. Sputtering yield versus target atomic number. 27

Figure 2.17. Secondary ion yield versus primary energy. 29

Figure 2.18. Secondary ion yield versus incidence angle. 30

Figure 2.19. O_2^+ and oxygen flood remove matrix effect. (a) Yield enhancement in SiO_2 and discontinuity at interface and (b) added oxygen flood removed yield difference between SiO_2 and Si. 31

Figure 2.20. Matrix effect: P in Si versus SiO_2. 32

Figure 2.21. Matrix effect: P in Si versus SiO_2. (a) Raw data: apparent P peaks, (b) referenced to P in Si, and (c) referenced to P in SiO_2. 33

Figure 2.22. Matrix effect and yield enhancement for Pt analysis. (a) Pt^+ in profile of PtSi/Si is enhanced by oxygen because Si is present through the PtSi layer and (b) Pt^+ in profile of Pt/Si is enhanced when Si is encountered below the Pt layer. 33

Figure 3.1. Positive secondary ion yields for O_2^+ impact on Si. 41

Figure 3.2. Negative secondary ion yields for Cs^+ impact on Si. 42

Figure 3.3. Positive secondary Cs-molecular ion yields for Cs^+ bombardment of Si. 43

Figure 3.4. Periodic table summary of optimum primary beam choices. 44

Figure 3.5. AlGaN mass spectrum, 2.8% Al, O_2^+ bombardment. 46

Figure 3.6. Choice of primary beam for detection limit. 47

Figure 3.7. Choice of secondary species: Molecular ions. (a) Impurity + primary beam species, (b) impurity + matrix. 47

Figure 3.8. Angle of incidence dependence on sample voltage. 48

Figure 3.9. Angle of incidence dependence on sample voltage. 49

Figure 3.10. Secondary ion energy distribution. 50

Figure 3.11. Voltage offset. 50

Figure 3.12. Voltage offset. 51

Figure 3.13. Voltage offset on mass spectrum. 52

Figure 3.14. Mass resolution. (a) Completely separated, (b) partial separation, (c) mass regions measured, (d) trapezoidal peak shape. 54

Figure 3.15. Mass interferences. 55
Figure 3.16. High mass resolution separates mass interferences in Si. 56
Figure 3.17. High mass resolution. 56
Figure 3.18. Mass interference for Cu in 0.3 μm SiO_2 film on Si. 57
Figure 4.1. SIMS instrument block diagram. 62
Figure 4.2. Duoplasmatron. 63
Figure 4.3. Cesium microbeam source. 65
Figure 4.4. Liquid metal ion source (LMIS). 65
Figure 4.5. Primary ion column components. 67
Figure 4.6. Quadrupole analyzer. 68
Figure 4.7. Double focusing magnetic sector analyzer. 69
Figure 4.8. Ion trajectories for magnetic sector. 69
Figure 4.9. CAMECA IMS 7f magnetic sector analyzer. 71
Figure 4.10. CAMECA NanoSIMS 50L magnetic sector analyzer. 71
Figure 4.11. Time of flight analyzer. 73
Figure 4.12. TOF-SIMS timing diagram. 74
Figure 4.13. TOF-SIMS reflectron analyzer. 74
Figure 4.14. TOF-SIMS electrostatic analyzer. 75
Figure 4.15. Faraday cup and electron multiplier responses. 76
Figure 5.1. Raster and gate relationship with depth profile shape. 82
Figure 5.2. Beam diameter effect on raster and gate. 83
Figure 5.3. Depth profile characteristics. 84
Figure 5.4. Knock-on and nonuniform sputtering. 85
Figure 5.5. Detected area versus raster size. 85
Figure 5.6. Detected area versus raster size. 85
Figure 5.7. Crater perspective. 86
Figure 5.8. Depth profile parameters for interface. 86
Figure 5.9. Interface location. 87
Figure 5.10. TOF-SIMS depth resolution. 88
Figure 5.11. Depth resolution for delta layer. 88
Figure 5.12. Surface equilibration region. 89
Figure 5.13. Knock-on variation with primary energy. 90

Figure 5.14. Effect of primary beam energy and incidence angle on Sb depth profile in Si. 90

Figure 5.15. Penetration in GaN for CAMECA IMS-6F analyses. 91

Figure 5.16. Absence of equilibration region in SiO_2. 91

Figure 5.17. Cap layer to improve surface analysis. (a) Sample withdrawn from deposition system into clean room between depositions. (b) Wafer left in system between depositions. 93

Figure 5.18. Ultra-shallow analysis approaches. 95

Figure 5.19. Ultra-shallow implant technology. 95

Figure 5.20. Arsenic ultra-shallow analyses. 96

Figure 5.21. Sputter induced roughness on crystalline Si. 97

Figure 5.22. RMS roughness vs. incidence angle. 98

Figure 5.23. Sample rotation during ion bombardment of Al. SEM micrographs of (a) aluminum surface, (b) bottom of crater sputtered through 1 μm aluminum layer into underlying silicon without rotation and (c) with rotation. 98

Figure 5.24. Sample rotation during ion bombardment of Al. 99

Figure 5.25. Sample rotation for multilayer analysis. (a) Without rotation, (b) with rotation. 100

Figure 5.26. K detection limit in Si. 101

Figure 5.27. P detection limit in Si. 101

Figure 5.28. Mesa analysis to reduce sidewall contributions. 102

Figure 5.29. Magnetic sector geometry. 103

Figure 5.30. Quadrupole geometry. 104

Figure 5.31. Dead time issues (count rate saturation). 105

Figure 5.32. Count rate saturation. 105

Figure 5.33. Count rate saturation. 106

Figure 5.34. Analysis region. 106

Figure 5.35. SIMS patterns on silicon patterned wafers. 108

Figure 5.36. 0.35 μm technology CMOS analysis sites. 108

Figure 5.37. Dopant profiles from SIMS test areas. 109

Figure 5.38. Nonuniform distribution. 110

Figure 5.39. Nonuniform distribution—diffusion of implanted Cr in Si. 110

Figure 5.40. Particulates or nonuniform distributions. (a) Depth profile of B implant in Si. Profile shape of Al particle shown. (b) Distortion of first profile due to localized B source, second profile adjacent to first. 111
Figure 5.41. Quantitative 3-D image depth profiling. 112
Figure 6.1. Conversion of raw to reduced data. (a) Raw data. (b) Reduced data. 123
Figure 6.2. Normalization. 124
Figure 6.3. Versatility of ion implanted standards. 125
Figure 6.4. Multiple implants in the same sample. 126
Figure 6.5. NIST standard reference material for As in Si. 127
Figure 6.6. Implant energy considerations. (a) Implant energy too low for Sn → InP. Dose error near surface. (b) Implant energy too high for Be → SiO_2 layer on Si, much of the Be is beyond the SiO_2. 128
Figure 6.7. Fe depth profiles in TiW, TiN, and $TiSi_2$. 129
Figure 6.8. Isotope check. 130
Figure 6.9. Comparison of implant and bulk standards for B in Si. 132
Figure 6.10. Nonlinear region. 133
Figure 6.11. Analysis of SiGe matrix elements. 133
Figure 6.12. Analysis of SiGe impurity elements. 134
Figure 6.13. Precision (reproducibility). 135
Figure 6.14. Dose precision (reproducibility). 136
Figure 6.15. Precision (reproducibility) and accuracy. 136
Figure 6.16. Matrix and impurity element quantification. 138
Figure 6.17. Implant through removable layer. 139
Figure 6.18. Positive secondary ion yields for 80 elements in Si. 141
Figure 6.19. RSF patterns for secondary positive ions. 142
Figure 6.20. RSF patterns for secondary negative ions. 142
Figure 7.1. Polydimethylsiloxane (PDMS). 152
Figure 7.2. Capping layer to analyze and quantify surface species. 153
Figure 7.3. Contaminant at the interface between layers. 153
Figure 7.4. Interface region. (a) Possible Al at the interface, (b) Al is at the bottom of the Si_3N_4 layer, not at the interface. 154

Figure 7.5. Quantification at the interface. 155

Figure 7.6. Quantification of contaminant at the interface. 155

Figure 7.7. Multilayer analysis. 156

Figure 7.8. Back side analysis method. 157

Figure 7.9. Back side analysis: Metal contacts on GaAs. 158

Figure 7.10. Front side analysis of 25 nm hafnium silicate. 159

Figure 7.11. Back side SIMS analysis of 25 nm $Hf_xSi_yO_2$. 160

Figure 7.12. Bulk analysis of HgCdTe. 161

Figure 8.1. Positive primary beam and ejection of secondary electrons cause sample surface to charge positive. 166

Figure 8.2. Depth profiles of F implanted into 500 nm SiO_2/Si with and without neutralizing electron beam. 166

Figure 8.3. Discharge on sample due to Cs^+ bombardment of SiO_2 layer on Si. 167

Figure 8.4. Analysis without electron beam appears to show additional layer at surface. 167

Figure 8.5. Sample charging on Au coated 2% Al in AlGaN. 168

Figure 8.6. SIMS depth profiles of two samples of sphalerite bulk insulator using O^-. 170

Figure 8.7. SIMS craters from $^{16}O^-$ analysis of lithium aluminum silicate. 170

Figure 8.8. Electron yield versus primary electron energy. 171

Figure 8.9. Electron beam induced conductivity (EBIC). 171

Figure 8.10. Example of EBIC analysis. 172

Figure 8.11. Quadrupole geometry. 173

Figure 8.12. GdO^+ intensity versus electron beam current. 174

Figure 8.13. Quadrupole 2 kV electron beam neutralization. 174

Figure 8.14. Quadrupole bulk insulator mass spectral analysis. (a) Watch glass and (b) Pyrex. 175

Figure 8.15. Quadrupole actinic Pyrex analysis. (a) Low actinic Pyrex and (b) expanded view of the surface region. 176

Figure 8.16. $LiNbO_3$ bulk insulator analyzed with PHI-6300 quadrupole. 176

Figure 8.17. CAMECA NEG. 177

Figure 8.18. Magnetic sector negative secondary ion neutralization. 178

Figure 8.19. Cathodoluminescence indication of electron beam irradiation. 179

Figure 8.20. Magnetic sector neutralization for positive secondary ions. 179

Figure 8.21. Magnetic sector analysis of Be in crystalline Al_2O_3. 180

Figure 8.22. High sputtering rate analysis of B implanted bulk SiO_2 using adjacent electron beam method with Au coating. 180

Figure 8.23. TOF analysis for insulator. 181

Figure 8.24. Schematic of Na profiles in SiO_2/Si for Na implanted and analyzed using $^{16}O^-$ and $^{16}O^+$ primary beams. 182

Figure 8.25. Quadrupole insulator analysis of mobile ion species. 183

Figure 8.26. Quadrupole analysis of Li, Na, K implanted SiO_2/Si. 184

Figure 8.27. Magnetic sector analysis of Li, Na, K implanted 1 µm SiO_2/Si coated with 50 nm Au. 184

Figure 8.28. 1 µm SiO_2/Si implanted with Li, Na, K. 185

Figure 8.29. SIMOX analysis. 186

Figure 8.30. Electron stimulated desorption. 187

Figure 9.1. Raster reduction to improve detection limit. 192

Figure 9.2. H detection limit versus instrument vacuum. 193

Figure 9.3. Effect of heat treatments on H in SiO_2. 194

Figure 9.4. H mobility in Nb versus Nb_2O_5. 194

Figure 9.5. C in GaAs. 195

Figure 9.6. Raster reduction to improve detection limit for N in SiC. 196

Figure 9.7. Use of rare isotope. 197

Figure 9.8. Multiple residual gas element implants into GaN. 198

Figure 9.9. Depth resolution. Cs^+ bombardment of Nb. 199

Figure 9.10. Effect of contamination at the surface. 200

Figure 9.11. He in Si using O_2^+ primary beam. 201

Figure 10.1. 0.35 µm technology CMOS. 207

Figure 10.2. SIMS depth profile analysis of epitaxial Si layer. 208

Figure 10.3. Dopant profiles. 209

Figure 10.4. Nitrided gate oxide. 210

Figure 10.5. K in gate oxide. 211

Figure 10.6. Diffusion in barrier layers. 211

Figure 10.7. Borophosphosilicate glass. 213

Figure 10.8. Focused ion beam SIMS of Na Li K using Xe plasma source. 213

Figure 10.9. SIMS analysis of three-level metal structure. 215

Figure 10.10. Fluorine contamination in polymer layers. 216

Figure 10.11. Au plating: Ni diffusion. 216

Figure 10.12. Au plating: Thallium concentration. 217

Figure 10.13. Diffusion of Th in Si. 218

Figure 10.14. InP laser structure. 219

Figure 10.15. GaAs MQW structure. 219

Figure 10.16. GaAs based LED structure. 220

Figure 10.17. AlGaN/InGaN LED structure. 221

Figure 10.18. AlN impurity depth profile. 221

Figure 10.19. AlN structure. 222

Figure 10.20. $LiNbO_3$ doped with Ti. 222

Figure 10.21. ^{13}C labeling in polystyrene analyzed with O_2^+ and Cs^+ beams. 223

Figure 10.22. Improved high mass abundance with C_{60} cluster source. 224

Figure 10.23. Depth resolution improved with sample rotation. 225

Figure 10.24. Depth resolution improved with sample cooling. 225

Figure 10.25. Ar cluster depth profiling. 226

Figure 10.26. Organic light emitting diode. 227

Figure 10.27. Minerals quantification. 228

Figure 10.28. Silicon regions in zeolite. 229

Figure 11.1. Quantification regions. 237

Figure 11.2. Matrix measurement. 237

Figure 11.3. Matrix measurement (profile 1). 238

Figure 11.4. Matrix measurement (profile 2). 238

List of Tables

Table 1.1. Common elemental analysis techniques 2

Table 1.2. Types of mass spectrometry 7

Table 1.3. SIMS advantages and disadvantages 10

Table 3.1. Absolute positive secondary ion yields 40

Table 3.2. Secondary ion species for Ar^+ bombardment of Al 45

Table 3.3. Secondary ion species for O_2^+ bombardment of Si 45

Table 3.4. Common mass interferences 53

Table 4.1. Properties of SIMS sources 66

Table 4.2. Comparison of mass analyzers 76

Table 6.1. TOF-SIMS of implants through SiO_2 139

Table 7.1. Static vs. dynamic conditions 150

Table 7.2. Calculation of atom densities in HgCdTe 161

Table 10.1. Si semiconductor processing steps and related SIMS analyses 206

Table 10.2. Mass interferences in Fe region of labradorite 228

Table A.1. Mass, Abundance, Ionization Potential, Electron Affinity 239

Table A.2. Relative Sputtering Rates 248

Table A.3. Si RSFs 249

Preface

Why this technique? What is the value? This analytical method is not marked by sheer numbers of instruments but by the value of the data obtained. The impact of a depth profile that shows an unexpected contaminant is hard to quantify. In a semiconductor processing facility, the identification of a source of iron contamination can resolve a stoppage of the process line which can be worth millions of dollars per day. The ability to obtain parts per million sensitivity for an element and to locate that element with good depth resolution provides many applications.

What does it take to understand secondary ion mass spectrometry (SIMS)? There are many details and it is necessary to be aware of them. This work is intended to provide a current summary of SIMS depth profiling for those who need to understand SIMS data and those who perform SIMS analyses. Earlier efforts are outdated, and the Wilson, Stevie, Magee book published as a guide is already more than 25 years old. The current offering will be available in print and on the web, and it can be updated.

Depth profiling SIMS has been available for about 40 years, and the understanding and improvements in instrumentation continue to progress. Application examples in this volume include a wide range of materials such as semiconductors, insulators, minerals, metals, and catalysts. But the applications continue to multiply. Plasma ion sources that provide higher ion current density will improve our ability to study interfaces more than 100 μm deep and will increase our understanding of coatings. With the advent of large molecule ion sources such as C_{60} and argon clusters, the method now has progressed into depth profiling of organic materials.

The author has relied on the earlier book for a number of figures. The author is indebted to the contributions from other analysts with whom he has had the privilege of interacting during his career. Of special mention are Bob Wilson and Charles Magee who are the coauthors of our earlier book, and Dave Simons who has provided valued comments to both publications. Dick Brundle and Joe Bennett also reviewed this work and made many contributions.

CHAPTER 1

Comparison of Surface Analytical Techniques

1.1 COMMON ELEMENTAL SURFACE ANALYSIS TECHNIQUES

There are a limited number of commonly available elemental surface analysis techniques. Scanning electron microscopy (SEM) is very widely used and is often accompanied by an x-ray analyzer that provides energy dispersive spectroscopy (EDS) elemental identification with percent level detectability. To categorize the analytical techniques, it is useful to identify the probe and detected species. In this case electrons are the probe and x-rays are detected. Because the electron probe and the analytical volume are small, elemental information can be obtained from a small area. There are two techniques that use electron detection, Auger electron spectroscopy (AES) and x-ray photoelectron spectroscopy (XPS) (also referred to as electron spectroscopy for chemical analysis), and have a better detection limit than SEM-EDS (0.1 percent atomic compared with percent levels). AES uses electron bombardment and detection whereas XPS uses x-ray bombardment and electron detection. Secondary ion mass spectrometry (SIMS) uses ions for bombardment and detection and has a much higher sensitivity (ppma to ppba) than the other techniques and that is a major reason for its usage.

In terms of lateral resolution or minimum analysis area, SEM-EDS can provide elemental analysis results from less than 50 nm and transmission electron microscopy EDS (TEM-EDS) using current instrumentation can identify a single column of atoms [1]. AES can resolve at 3 nm, but XPS has the issue of focusing x-rays so the detected area is often determined

by the focusing properties of the electron analyzer. As a result it is difficult for XPS to have less than 1 μm lateral resolution and the detected area can be on the order of 1 mm for many instruments. SIMS can typically provide lateral resolution less than 1 μm and the NanoSIMS50 can achieve 50 nm lateral resolution. With a liquid metal ion source (LMIS), the beam size can be 5 to 7 nm, but the sensitivity of SIMS is limited for probe beams such as Ga^+. High spatial resolution and ppb sensitivity cannot be achieved at the same time. More detail on small area analysis is provided in Chapter 5.

Table 1.1 provides a comparison of these four techniques most commonly used in elemental analysis. SIMS holds a valued place in the analytical methods, not just because of sensitivity. All elements can be detected including the important element hydrogen, which cannot be detected with the electron beam or x-ray methods. Isotope-specific analysis can also be performed. SIMS analysis can be achieved from less than one monolayer at the surface; however, for depth profiling applications, depth resolution may vary from 2 to 30 nm depending on instrumental conditions. The dynamic range for SIMS is noteworthy. Since this is a mass spectrometric technique, it is possible to have a range from 100 percent to ppm or ppb. Note that the dynamic range or a single species in a depth profile is typically limited to less than 1×10^6 because of memory effects.

Table 1.1. Common elemental analysis techniques

	AES	XPS	SIMS	SEM-EDS
Probe species	Electron	X-ray	Ion	Electron
Detected species	Electron	Electron	Ion	X-ray
Information depth	2 nm	2 nm	0.3–1 nm	0.1–1 μm
Lateral resolution	20 nm	1 μm–1 mm	7 nm–10 μm	50 nm
Elements detected	>He	>He	All	>B
Detection limit	0.1%–1%	0.1%–1%	ppm–ppb	1%
Chemical information	Limited	Yes	Yes	No

1.2 INTRODUCTION TO MASS SPECTROMETRY

Mass spectrometry is an analytical technique that uses a mass spectrometer to separate ions by their mass to charge ratio. All naturally occurring isotopes will be present in natural abundance (except for extraterrestrial, ion implanted samples, or those that may have been intentionally separated, such as lithium, boron, and uranium). As shown in Figure 1.1, chlorine has two naturally occurring isotopes at mass 35 and 37, with the abundances shown. If the Cl dimer ion, Cl_2, is detected, then the isotopic pattern will be a binary expansion of the Cl monomer isotopic pattern. A mass spectrum can be complex because many element combinations are possible and ions can be formed with a charge state higher than one. This complexity can result in multiple species present at the same mass. The species can be resolved if the mass resolution is sufficient as shown in Figure 1.2, which highlights just one mass from a complex mass spectrum for crude oil. All the positive ions shown in the top part of the figure have the same nominal mass 700 [2].

A mass spectrometer block diagram is shown in Figure 1.3. The sample can be inlet as a gas, as vapor from a liquid, or volatilized by laser from a solid and then ionized. Ions can also be generated directly from a solid by interaction with an energetic beam, such as an ion beam. When ions are used they are typically focused in an ion optical column with multiple electrostatic lenses and then scanned over the sample surface to be analyzed. An airlock or exchange chamber makes it possible to insert samples without bringing the analysis chamber up to air. The ions are extracted from the sample interaction region and injected into a mass analyzer. Three types of mass analysis are generally available. Ions can be separated by their mass to charge ratio using quadrupole, magnetic

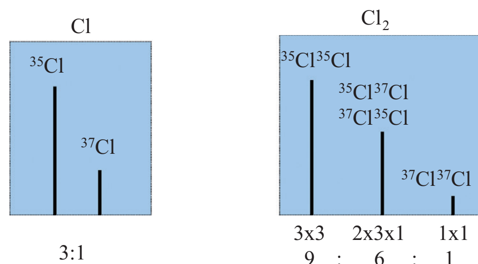

Figure 1.1. Isotopic abundances.

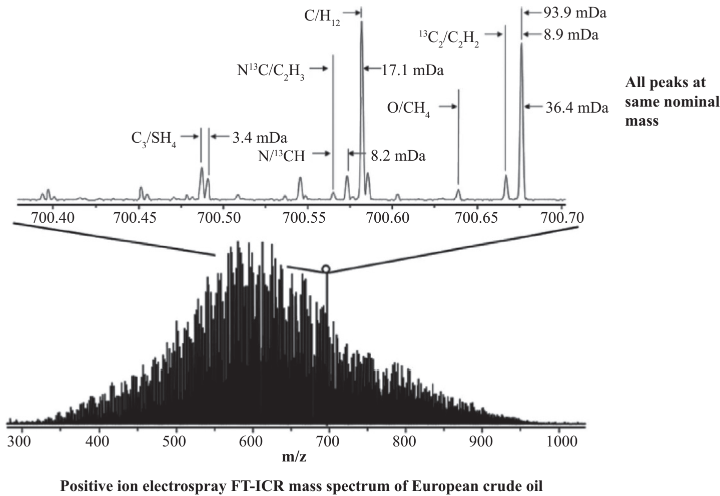

Figure 1.2. High mass resolution mass spectrum of 700 Da.

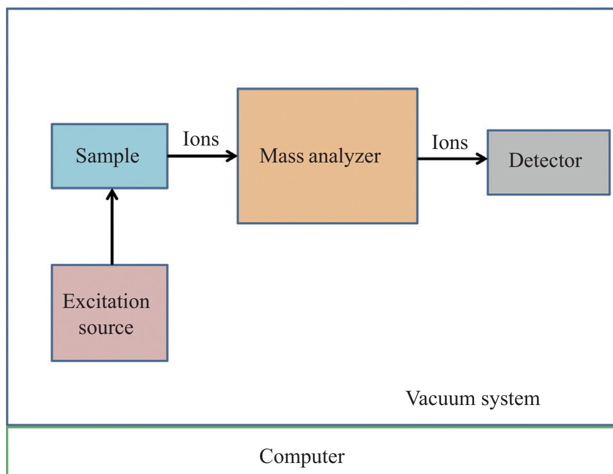

Figure 1.3. Mass spectrometer block diagram.

sector, or time-of-flight (TOF) mass analyzers. The analyzed ions are then detected and processed using counting electronics. The overall instrument operation and the data acquisition and reduction are directed with a computer. The ion beam regions must be under vacuum so a vacuum pumping system is required with the exception of atmospheric pressure ionization systems.

The material to be analyzed can have many elements and the mass of the ion analyzed must be a variable. This means that a mass spectrum, or plot of intensity of each ion as a function of mass to charge ratio, will be obtained. The mass spectrometer measures the mass to charge ratio of the ion of interest. The unit of mass is one Dalton (Da), which is defined as 1/12 the mass of ^{12}C (12.00000). A series of mass spectra taken over a specific time period can provide information on the presence of elements as a function of any parameter that has been varied in the time period. For example, if the sample is being heated, the mass spectra obtained as a function of temperature provide a record of volatile products from the material of interest. If the sample is being sputtered to provide a crater, then the result will be an intensity profile of the species monitored as a function of depth.

Mass spectrometry has been a very successful analytical technique for decades and has been applied to the study of solids, liquids, and gases. It has been used to identify unknown compounds, quantify detected elements, and determine chemical composition. A significant reason for this popularity is the dynamic range from 100 percent to ppm or better. Few techniques can match this capability that can exceed eight orders of magnitude detection and measure bulk and trace constituents. Detection is possible for quantities in the femtogram (10^{-15} g) range. The ability to not only identify elements but also distinguish the isotopes of the elements is a key feature.

1.3 BRIEF HISTORY OF MASS SPECTROMETRY AND SIMS

The mass spectrometer dates back to experiments by J. J. Thomson starting in 1889. Thomson noted that positive secondary ions were generated in a gas discharge tube in 1910 and developed the first mass spectrometer in 1913 by passing ions through a magnetic field [3]. The first modern mass spectrometers are credited to A. J. Dempster in 1918 and F. W. Aston in 1919, who obtained precise atomic weights for ^{20}Ne and ^{22}Ne in 1920 [4]. The double focusing analyzer was developed in 1934 [5]. By 1953 the TOF analyzer had been introduced [6] and the quadrupole analyzer had also been added to the suite of analyzers [7]. Applications in the 1940s were extended from isotope measurements to complex mixtures of hydrocarbons from petroleum fractions. By the 1950s, high molecular weight steroids were analyzed. In the 1960s, gas chromatograph mass spectrometry (GC-MS) was introduced. Many other methods that employ mass spectrometry have subsequently been developed.

The earliest history of SIMS can be traced to Woodcock at the University of Chicago in 1931, who studied negative ions produced by bombardment with Li^+ ions [8]. In 1949, Herzog and Viebock described a SIMS instrument [9]. More SIMS instrumentation began to appear with a magnetic sector analyzer by R. E. Honig in 1958 [10, 11], secondary ion microscope by R. Castaing and G. Slodzian in 1962 [12], and GCA Corporation IMS101 magnetic sector by H. Liebl and R. F. K. Herzog in 1963 [13]. The magnetic sector by G. Slodzian [14] became the prototype for CAMECA magnetic sector instruments starting with SMI-300 (also referred to as IMS-300) in 1968 [15]. In 1969 Benninghoven developed SIMS analysis of the surface, referred to as static SIMS [16]. In the 1970s, a number of commercial magnetic sector SIMS instruments became available such as the CAMECA IMS-3f in 1978 [15] and the Applied Research Laboratories (ARL) IMMA in 1970 [17, 18]. Other instruments such as the Sensitive High Resolution Ion Microprobe magnetic sector [19] and Cherepin instrumentation [20] were also developed in the 1970s. In the same time frame, instruments with quadrupole analyzers were introduced by Wittmaack, Liebl, and Magee [21–25]. Subsequent commercial quadrupole analyzer versions appeared as the Atomika 3000 in 1983, Physical Electronics PHI-6300 in 1984, and Riber MIQ 256. TOF analyzers developed from early work by scientists such as Poschenrieder. [26] The ability to obtain high mass resolution in excess of 10,000 and the injection between analysis pulses of electrons for charge neutralization [27] and ions for sputtering (dual beam depth profiling) have made the TOF-SIMS a highly capable instrument for both the ION TOF [28] and Physical Electronics [29] designs.

Ion sources have seen continual improvement with designs such as the duoplasmatron plasma source [30]. The utility of SIMS was increased significantly in 1977 when a cesium primary beam was developed to enhance negative secondary ion yields [31]. The introduction of the liquid metal ion source (LMIS) provided very high brightness with virtually a point source and the ability to obtain high lateral resolution ion images [32–35]. Ion sources for analysis of organic materials using TOF-SIMS have shown a progression to beams with ever larger ion cluster size starting with SF_5 [36] and continuing with the latest ion sources, C_{60} [37] and Ar clusters [38].

The development of SIMS has been chronicled through a series of biennial international conferences fostered by A. Benninghoven that began in 1977 [39] and continue to be held. Starting with the second meeting, a proceedings book with peer reviewed articles has been published [40–50]. Since SIMS XIII in 2002, the papers have also been published as journal

articles in either *Applied Surface Science* or *Surface and Interface Analysis* that can be easily accessed [51–57]. These books and journal articles represent a significant segment of the early SIMS literature. Unfortunately, many of the proceedings books are difficult to obtain. Other sources of information for SIMS are found in a number of books [58–64] and book chapters [65–71] and at the websites of the American Society for Mass Spectrometry, U.S. SIMS Workshop Series, SIMS in Europe, and International SIMS Society [72–75].

1.4 TYPES OF MASS SPECTROMETRY

There is often confusion over the terms mass spectrometry and mass spectroscopy. Spectrometry refers to the method used to acquire a measurement of a spectrum. Spectroscopy is identified with the study of incident, emitted, and absorbed spectra of materials. Spectroscopy is used to refer to techniques such as AES, and spectrometry is used to identify all the mass spectrometric methods.

The mass spectrometer can be coupled with another technique to produce an instrument with powerful analytical capability. For example, a gas chromatograph separates gases as a function of their ability to pass through a packed column, usually glass. A gas chromatograph mass spectrometer provides a mass spectrometric analysis of each separated portion of the gas mixture inlet into the column. The thermogravimetric mass spectrometer analyzes the volatile portion of a specimen that is being weighed at the same time. Table 1.2 lists several common instrument–mass spectrometer combinations for analysis of different types of materials.

Table 1.2. Types of mass spectrometry

Name	Sample type
Electron impact (EI-MS)	Gas
Inductively coupled plasma (ICP-MS)	Gas/liquid
Gas chromatography (GC-MS)	Gas
Liquid chromatography (LC-MS)	Liquid
Thermal ionization (TIMS)	Solid
Thermogravimetric (TG-MS)	Solid
Glow discharge (GDMS)	Solid
Secondary ion (SIMS)	Solid

Mass spectrometric methods are sorted by the means of ionization. There are many fields in mass spectrometry based on the instrumentation used. Electron impact ionization mass spectrometry is a common method of ionization used for analysis of gases and volatile organic species. The mass spectrum obtained from one ionizing method may be quite different from that obtained using another method. The electron impact method of ionization is very well known and electron impact mass spectra exist for a large number of materials. A significant data item for the analysis of organic materials is the determination of the parent ion, which occurs at the molecular weight of the material. Most ions detected are fragments of the species analyzed. Ion bombardment can break bonds and cause rearrangements, so that some of the ions detected are modifications of the original structure.

Ions ejected from a sample can be analyzed as a function of their location on the sample. By preserving the location, an ion image can be obtained that provides lateral information. If a series of ion images can be obtained during analysis of a specimen, then a three-dimensional representation can be generated.

SIMS utilizes the analysis of detected secondary ions resulting from the bombardment of a surface by primary ions. SIMS has matured to become an essential characterization technique. The semiconductor industry has driven the development of several analytical methods, including SIMS, which has been employed to examine almost every facet of semiconductor fabrication. Developments in instrumentation and quantification have extended the application of this method to many areas other than the semiconductor field.

1.5 RATIONALE FOR SIMS

The major advantages of SIMS are sensitivity, depth resolution, and imaging resolution. These capabilities are achievable for all elements, including hydrogen, and for all isotopes. SIMS is particularly advantageous for sensitivity and depth resolution. The sensitivity of EDS elemental analysis is limited to the percent level and that of AES and XPS to tenths of a percent. Rutherford backscattering spectrometry can surpass AES in sensitivity, especially for higher atomic number elements, but SIMS detection limits are typically orders of magnitude lower. SIMS can detect from 100 percent to ppm or ppb, which is an impressive dynamic range. Parts per trillion detection limits have been obtained under advantageous conditions. The sensitivity of SIMS and the difference between

AES and SIMS can be demonstrated by comparing an AES depth profile for SiO_2/TiN/Al shown in Figure 1.4 with a SIMS depth profile for arsenic implanted in silicon shown in Figure 1.5. The AES profile is quantitative for the matrix species, and shows two orders of magnitude dynamic range plotted with a linear scale. The arsenic in the SIMS profile is plotted with a logarithmic y-axis and shows more than four orders of magnitude dynamic range. The arsenic in this sample would not be detected at all with AES whereas the SIMS detection limit is in the parts per billion atomic range. Note that the detected area for the SIMS profile is 30 μm in diameter and

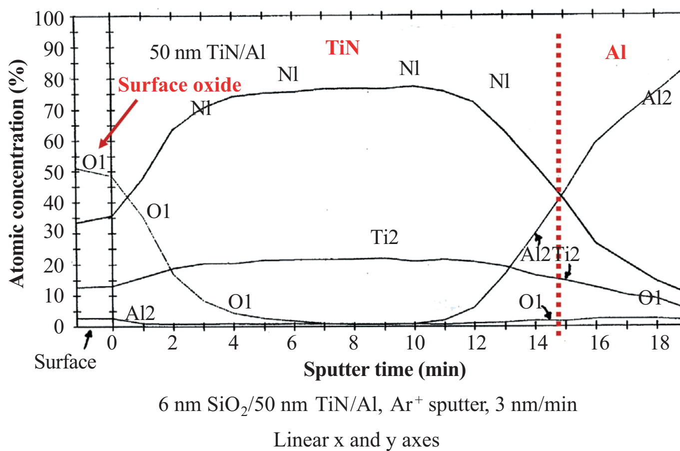

Figure 1.4. AES depth profile.

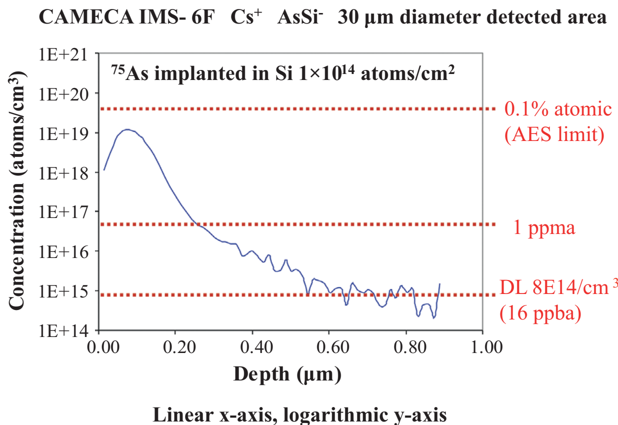

Figure 1.5. SIMS depth profile.

the detected area for AES with a field emission source may be less than 50 nm. Figure 1.6 shows the low mass range of a SIMS mass spectrum for Si plotted with linear and logarithmic y-axis and demonstrates why SIMS data are typically shown with a logarithmic display [76].

SIMS quantification is achieved with standards. Inorganic and organic depth profiles are possible. Much of the organic profiling has been done recently with the availability of cluster ion sources. Table 1.3

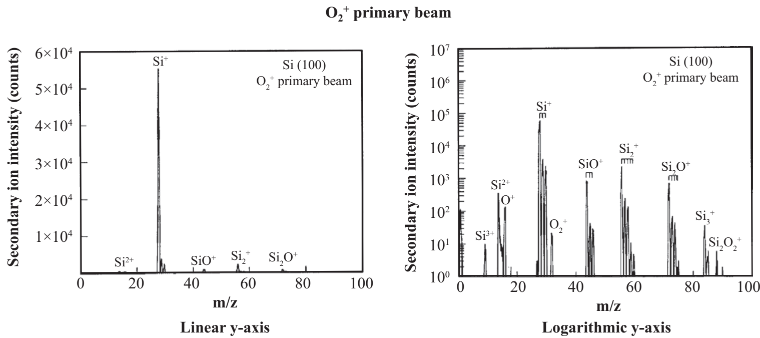

Figure 1.6. SIMS mass spectrum y-axis display.

Table 1.3. SIMS advantages and disadvantages

Advantages
All elements and isotopes detected
Good depth resolution, a few nm typical and can be <1 nm
ppm to ppb sensitivity over periodic table
Dynamic range $>10^8$ possible
Quantitative with standards
Rapid multielement analysis
Two- and three-dimensional analysis possible
Little or no sample preparation
Disadvantages
Destructive technique
Complex mass spectra—many mass interferences
Large variation of secondary ion yields over periodic table
Quantification requires secondary standards
Quantification difficult for matrix species
Secondary ion yield varies with matrix
Charging effects for insulator analysis
Topography formation can affect depth resolution

summarizes the advantages and disadvantages of the SIMS technique. The chapters that follow provide detailed information on these aspects of the technique.

1.6 TYPES OF SIMS DATA

SIMS data are typically presented in three formats: mass spectra, depth profiles, and images. Mass spectra display secondary ion intensity as a function of mass to charge ratio. Figure 1.7 shows a mass spectrum of zinc oxide obtained with O_2^+ primary beam. The spectrum is complex because zinc has five naturally occurring isotopes and molecular ions that contain zinc and oxygen are easily formed. Depth profiles show secondary ion intensity as a function of depth into the sample. For some instrument types, such as quadrupole and magnetic sector, the species profiled must be chosen in advance. For TOF instruments, the complete mass spectrum is obtained at each depth measured and any species in the mass spectrum can be displayed in a depth profile. Figure 1.8 shows a depth profile of an insulator structure, which is coated with gold to aid in charge neutralization. Three layers of borophosphosilicate glass (BPSG) can be distinguished. The layers have a constant phosphorus concentration but a varying boron concentration. Ion images display secondary ion lateral distribution. Figure 1.9 shows carbon ion images from a niobium bicrystal before and after heat treatment. The carbon segregates to the interface after heating.

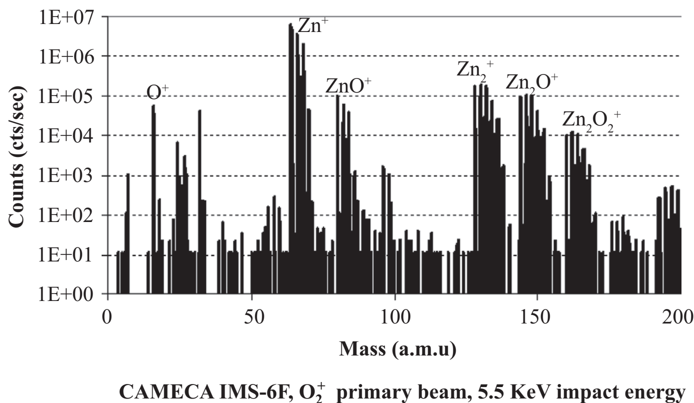

Figure 1.7. Zinc oxide mass spectrum.

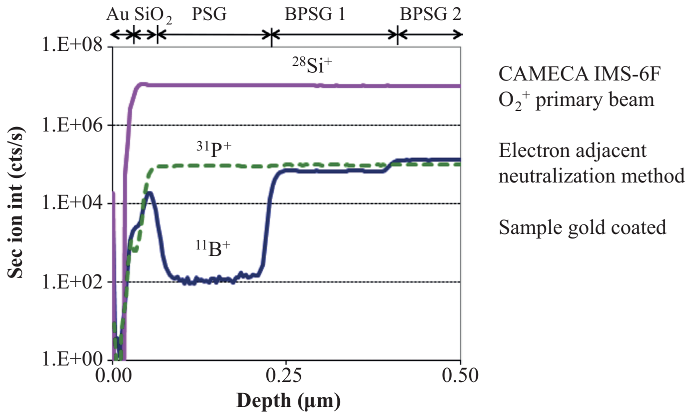

Figure 1.8. SIMS depth profile of BPSG layers.

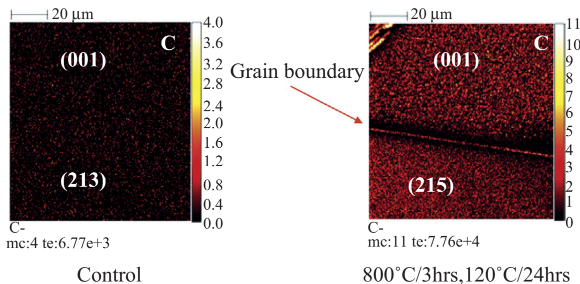

- ION-TOF TOF SIMS V, sputter surface with Cs^+ 10 keV 20 nA
- Analyze with Bi_3^+ 25 keV 0.7 pA over 100 µm × 100 µm area
- Carbon segregates at the grain boundary region after 800˚C/3 hrs, 120˚C/24 hrs heat treatment
- Orientations determined using electron backscatter diffraction (EBSD)

Figure 1.9. Carbon segregation in niobium bicrystals.

REFERENCES

[1] Dycus, J.H., A. Oni, X. Sang, T. Chan, C. Koch, and J.M. LeBeau. 2014. "Observing the Interplay Between Composition and Phonon Transport in $Bi_2Te_{3-x}Se_x$ Alloys Using ADF STEM." *Microscopy and Microanalysis* 20, no. S3, pp. 440–41. doi: http://dx.doi.org/10.1017/s1431927614003924

[2] Marshall, A.G., and R.P. Rodgers. 2008. "Petroleomics: Chemistry of the Underworld." *Proceedings of National Academy of Science* 105, no. 47, pp. 18090–95. doi: http://dx.doi.org/10.1073/pnas.0805069105

[3] Thomson, J.J. 1913. "Rays of Positive Electricity." Proceedings of the Royal S*ociety of London* 89, no. 607, pp. 1–20. doi: http://dx.doi.org/10.1098/rspa.1913.0057

[4] Aston, F.W. 1920. "Constitution of Atmospheric Neon." Philosophical Magazine 39, no. 232, pp. 449–55.

[5] Mattauch J., and R. Herzog. 1934. "About a New Mass Spectrograph." [In German.] *Zeitschrift fur Physik* 89, p. 786. doi: http://dx.doi.org/10.1007/BF01341392

[6] Stephens, W.E. 1953. "A Pulsed Mass Spectrometer with Time Dispersion." *Review of Scientific Instruments* 24, no. 8, p. 616–617. doi: http://dx.doi.org/10.1063/1.1770801

[7] Paul, W., and H. Steinwedel. 1953. "A New Mass Spectrometer Without Magnetic Field." [In German.] *Z. Naturforschg*. 8a, p.448.

[8] Woodcock, K.S. 1931. "The Emission of Negative Ions under the Bombardment of Positive Ions." *Physical Review* 38, no. 9, pp. 1696. doi: http://dx.doi.org/10.1103/physrev.38.1696.

[9] Herzog, R.F.K., and F.P. Viehbock. 1949. "Ion Source for Mass Spectrography." *Physical Review* 76, no. 6, p. 855–56. doi: http://dx.doi.org/10.1103/physrev.76.855

[10] Honig, R.E. 1958. "Sputtering of Surfaces by Positive Beams of Low Energy." *Journal of Applied Physics* 29, no. 3, pp. 549–55. doi: http://dx.doi.org/10.1063/1.1723219

[11] Honig, R.E. 1995. "Stone-age Mass Spectrometry: The Beginnings of 'SIMS' at RCA Laboratories, Princeton." *International Journal of Mass Spectrometry and Ion Processes* 143, pp. 1–10. doi: http://dx.doi.org/10.1016/0168-1176(94)04130-y

[12] Castaing, R., and G. Slodzian. 1962. "Microanalysis by Secondary Ion Emission." [In French.] *Journal De Microscopie* 1, p. 395.

[13] Liebl, H., and R.F.K. Herzog. 1963. "Sputtering Ion Source for Solids." *Journal of Applied Physics* 34, no. 9, pp. 2893–96. doi: http://dx.doi.org/10.1063/1.1729826

[14] Slodzian, G. 1964. "Study of the Secondary Ion Emission Method of Analysis." [In French.] *Ann. Phys*. 9, p. 591.

[15] de Chambost, E. 2011. "A History of Cameca (1954–2009)." Chap. 1 in *Advances in Imaging and Electron Physics*, Vol. 167, 2–113. Elsevier. doi: http://dx.doi.org/10.1016/b978-0-12-385985-3.00001-8

[16] Benninghoven, A. 1969. "Analysis of Sub-Monolayers on Silver by Secondary Ion Emission." Physica Status Solidi 34, no. 2, pp. K169–71. doi: http://dx.doi.org/10.1002/pssb.19690340267

[17] Liebl, H. 1967. "Ion Microprobe Mass Analyzer." *Journal of Applied Physics* 38, no. 13, pp. 5277–83. doi: http://dx.doi.org/10.1063/1.1709314

[18] Andersen, C.A., and J.R. Hinthorne. 1972. "Ion Microprobe Mass Analyzer." *Science* 175, no. 4024, pp. 853–60. doi: http://dx.doi.org/10.1126/science.175.4024.853

[19] Clement, S., W. Compston, and G. Newstead. 1977. "Design of a Large, High Resolution Ion Microprobe." shrimp.anu.edu.au

[20] Cherepin, V.T. 1972. "Mass Spectral Microscopy—A New Method for Investigation of Solids." *Visn. Akad. Nauk. Ukr. SSR*, p.17.

[21] Maul, J., F. Schulz, and K. Wittmaack. 1972. "Determination of Implantation Profiles in Solids by Secondary Ion Mass Spectrometry." *Physics Letters A* 41, no. 2, pp. 177–78. doi: http://dx.doi.org/10.1016/0375-9601(72)91101-2

[22] Wittmaack, K., J. Maul., and F. Schultz. 1974. "A Versatile in-Depth Analyzer." *Proceedings of the 6th International Conference on Electron and Ion Beam Science and Technology*, ed. R. Backish, p. 164. The Electrochemical Society, Princeton.

[23] Liebl, H. 1974. "Quadrupole Secondary Ion Mass Spectrometry Apparatus with Enhanced Transmission." *International Journal of Mass Spectrometry and Ion Physics* 15, no. 1, pp. 116–19. doi: http://dx.doi.org/10.1016/0020-7381(74)80092-6

[24] Liebl, H. 1977. "Quadrupole Mass Filters in SIMS." *Adv. Mass Spectrom.* 7, p. 418.

[25] Magee, C.W, W.L. Harrington, and R.E. Honig. 1978. "Secondary Ion Quadrupole Mass Spectrometer for Depth Profiling—Design and Performance Evaluation." *Review of Scientific Instruments* 49 no. 4, pp. 477–85. doi: http://dx.doi.org/10.1063/1.1135438

[26] Poschenrieder, W.P. 1972. "Multiple-focusing Time-of-Flight Mass Spectrometers, Part II. TOFMS with Equal Energy Acceleration." *International Journal of Mass Spectrometry and Ion Physics* 9, no. 4, pp. 357–73. doi: http://dx.doi.org/10.1016/0020-7381(72)80020-2

[27] Niehuis, E. 1992. "Time-of-flight SIMS." In *Secondary Ion Mass Spectrometry, SIMS VIII*, eds. A. Benninghoven, K.T.F. Janssen, J. Tumpner, H.W. Werner, 269. Chichester, United Kingdom: Wiley.

[28] Steffens, P., E. Niehuis, T. Friese, D. Greifendorf, and A. Benninghoven. 1984. "A New Time-of-flight Instrument for SIMS and Its Application to Organic Compounds." In *Secondary Ion Mass Spectrometry SIMS IV*, eds. A. Benninghoven, J. Okano, R. Shimizu, H.W. Werner, 404–08. Berlin, Germany: Springer.

[29] Schueler, B., P. Sander, and D.A. Reed. 1990. "A New Time-of-flight Secondary Ion Microscope." In *Secondary Ion Mass Spectrometry SIMS VII*, eds. A. Benninghoven, C.A. Evans, K.D. McKeegan, H.A. Stroms, H.W, Werner, 851. Chichester, United Kingdom: Wiley.

[30] von Ardenne, M. 1956. *Tabellen der Electronen-physik, Ionenphysik, und Ubermikroscopie*, Vol. I. Berlin: VEB Deutscher Verlag der Wissenschaften.

[31] Storms, H.A., K.F. Brown, and J.D. Stein. 1977. "Evaluation of a Cesium Positive Ion Source for Secondary Ion Mass Spectrometry." *Analytical Chemistry* 49, no. 13, pp. 2023–30. doi: http://dx.doi.org/10.1021/ac50021a034

[32] Levi-Setti, R., G. Crow, and Y.L. Wang. 1986. "Imaging SIMS at 20nm Lateral Resolution: Exploratory Research Applications." In *Secondary Ion Mass*

Spectrometry SIMS V, eds. A. Benninghoven, R.J. Colton, D.S. Simons, and H.W. Werner, 132–38. Berlin, Germany: Springer.

[33] Krohn, V.E, and G.R. Ringo. 1975. "Ion Source of High Brightness Using Liquid Metal." *Applied Physics Letters* 27, no. 9, 479–81. doi: http://dx.doi.org/10.1063/1.88540

[34] Rudenauer, F.G. 1984. "Liquid Metal Ion Sources for Scanning SIMS." In *Secondary Ion Mass Spectrometry, SIMS IV*, eds. A. Benninghoven, J. Okano, R. Shimizu, and H.W. Werner, 133–37. Berlin, Germany: Springer.

[35] Orloff, J. 2008. *Handbook of Charged Particle Optics*, 29. CRC Press.

[36] Gillen, G., and S. Roberson. 1998. "Preliminary Evaluation of an SF_5^+ Polyatomic Primary Ion Beam for Analysis of Organic Thin Films by Secondary Ion Mass Spectrometry." *Rapid Communications in Mass Spectrometry* 12, no. 19, pp. 1303–12. doi: http://dx.doi.org/10.1002/(sici)1097-0231(19981015)12:19%3C1303::aid-rcm330%3E3.0.co;2–7

[37] Weibel, D., S. Wong, N. Lockyer, P. Blenkinsopp, R. Hill, and J.C. Vickerman. 2003. "A C_{60} Primary Ion Beam System for Time of Flight Secondary Ion Mass Spectrometry: Its Development and Secondary Ion Yield Characteristics." *Analytical Chemistry* 75, no. 7, pp. 1754–64. doi: http://dx.doi.org/10.1021/ac026338o

[38] Suzuki, M., M. Nojima, M. Fujii, T. Seki, and J. Matsuo. 2014. "Mass Analysis by Ar-GCIB-Dynamic SIMS for Organic Materials." *Surface and Interface Analysis* 47, no. 12, p. 295–97. doi: http://dx.doi.org/10.1002/sia.5705

[39] Benninghoven, A. 2011. "The Development of SIMS and International SIMS Conferences: A Personal Retrospective View." *Surface and Interface Analysis* 43, no. 1–2, pp. 2–11. doi: http://dx.doi.org/10.1002/sia.3688

[40] Benninghoven, A., C.A. Evans, R.A. Powell, R. Shimizu, and H.A. Storms, eds. 1979. *Secondary Ion Masfs Spectrometry SIMS II*. Berlin, Germany: Springer Verlag.

[41] Benninghoven, A., J. Giber, J. Laszlo, M. Riedel, H.W. Werner, eds. 1982. *Secondary Ion Mass Spectrometry, SIMS III*. Berlin, Germany: Springer Verlag.

[42] Benninghoven, A., J. Okano, R. Shimizu, H.W. Werner, eds. 1984. *Secondary Ion Mass Spectrometry, SIMS IV*. Berlin, Germany: Springer Verlag.

[43] Benninghoven, A., R.J. Colton, D.S. Simons, and H.W. Werner, eds. 1986. *Secondary Ion Mass Spectrometry, SIMS V*. Berlin, Germany: Springer Verlag.

[44] Benninghoven, A., A.M. Huber, H.W. Werner, eds. 1988. *Secondary Ion Mass Spectrometry, SIMS VI*. Chichester, United Kingdom: Wiley.

[45] Benninghoven, A., C.A. Evans, K.D. McKeegan, H.A. Storms, and H.W. Werner, eds. 1990. *Secondary Ion Mass Spectrometry, SIMS VII*. Chichester, United Kingdom: Wiley.

[46] Benninghoven, A., K.T.F. Janssen, J. Tumpner, and H.W. Werner, eds. 1992. *Secondary Ion Mass Spectrometry, SIMS VIII*. Chichester, United Kingdom: Wiley.

[47] Benninghoven, A., Y. Nihei, R. Shimizu, and H.W. Werner, eds. 1994. *Secondary Ion Mass Spectrometry, SIMS IX*. Chichester, United Kingdom: Wiley.

[48] Benninghoven, A., B. Hagenhoff, and H.W. Werner, eds. 1997. *Secondary Ion Mass Spectrometry, SIMS X*. Chichester, United Kingdom: Wiley.

[49] Gillen, G., R. Lareau, J. Bennett, and F. Stevie, eds. 1998. *Secondary Ion Mass Spectrometry, SIMS XI*. Chichester, United Kingdom: Wiley.

[50] Benninghoven, A., P. Bertrand, H-N. Migeon, and H.W. Werner, eds. 2000. *Secondary Ion Mass Spectrometry, SIMS XII*. Amsterdam, Netherlands: Elsevier.

[51] Applied Surface Science 2003. Vol. 203–204, p. 1–879

[52] Applied Surface Science 2004. Vol. 231–232, p. 1–980

[53] Applied Surface Science 2006. Vol. 252, p. 6403–7326

[54] Applied Surface Science 2008. Vol. 255, p. 803–1624

[55] Surface and Interface Analysis 2011. Vol. 43, p. 1–676

[56] Surface and Interface Analysis 2013. Vol. 45, p. 1–600

[57] Surface and Interface Analysis 2014. Vol. 46, p. 1–411

[58] Heinrich, K.F.J., and D.E. Newbury, eds. 1975. "Secondary Ion Mass Spectrometry." NBS Special Publication 427, U. S. Department of Commerce, Washington, DC.

[59] Benninghoven, A., F.G. Rudenauer, and H.W. Werner. 1987. *Secondary Ion Mass Spectrometry: Basic Concepts, Instrumental Aspects, Applications, and Trends*. New York: Wiley.

[60] Vickerman, J.C., A. Brown, and N.M. Reed, eds. 1989. *Secondary Ion Mass Spectrometry—Principles and Applications*. Oxford, United Kingdom: Oxford University Press.

[61] Wilson, R.G., F.A. Stevie, and C.W. Magee. 1989. *Secondary Ion Mass Spectrometry—A Practical Handbook for Depth Profiling and Bulk Impurity Analysis*. New York: Wiley.

[62] Bentz B.L., and W. Odom, eds. 1995. "Secondary Ion Mass Spectrometry." *International Journal of Mass Spectrometry and Ion Processes*, 143. Amsterdam, Netherlands: Elsevier.

[63] Vickerman, J.C., and D. Briggs. 2001. *ToF-SIMS: Surface Analysis by Mass Spectrometry.* Chichester, United Kingdom: IM Publications/Manchester, United Kingdom: SurfaceSpectra.

[64] van der Heide, P. 2014. *Secondary Ion Mass Spectrometry: An Introduction to Principles and Practices*. New York: Wiley.

[65] McHugh, J.A. 1975. "Secondary Ion Mass Spectrometry." In *Methods of Surface Analysis*, ed. A.W. Czanderna, 223. Amsterdam, Netherlands: Elsevier.

[66] Blaise, G. 1976. "Fundamental Aspects of Ion Microanalysis." In *Material Characterization Using Ion Beams*, eds. J.P. Thomas, and A. Cachard, 143. London, United Kingdom: Plenum Press.

[67] Werner, H.W. 1978. "Introduction to Secondary Ion Mass Spectrometry." In *Electron and Ion Spectroscopy of Solids*, eds. L. Fiermans, J. Vennik, and W. Dekeyser, 324. New York: Plenum Press.
[68] Williams, P. 1983. "Secondary Ion Mass Spectrometry." In *Applied Atomic Collision Physics*, ed. S. Datz, 327. New York: Academic Press.
[69] Feldman, L.C., and J.W. Mayer. 1985. "Sputter Depth Profiles and Secondary Ion Mass Spectrometry." In *Fundamentals of Surface and Thin Film Analysis*, eds. L.C. Feldman, and J.W. Mayer, 69. New York: North-Holland.
[70] Pantano, C.G. 1986. "Secondary Ion Mass Spectroscopy." In *Metals Handbook Ninth Edition,* Vol. 10—Materials Characterization, ed. R.E. Whan, 610. American Society for Metals, Materials Park.
[71] Chu, P.K. 1992. "Dynamic Secondary Ion Mass Spectrometry." In *Encyclopedia of Materials Characterization—Surfaces, Interfaces, and Thin Films*, eds. C.R. Brundle, C.A. Evans, Jr. and S. Wilson, 532. Boston, MA: Butterworth-Heinemann.
[72] American Society for Mass Spectrometry (ASMS) www.asms.org
[73] www.simsworkshop.org
[74] SIMS Europe. 2014. www.sims-europe.eu
[75] www.simssociety.org
[76] Wilson, R.G., F.A. Stevie, and C.W. Magee. 1989. *Secondary Ion Mass Spectrometry*, I-8, 9. New York: Wiley.

CHAPTER 2

SIMS TECHNIQUE

2.1 INTERACTION OF IONS WITH MATTER

An ion striking the surface of a sample gives rise to many secondary species. As shown in Figure 2.1, these species include electrons, x-rays, neutrals, and positive and negative secondary ions. Most of the ejected species are neutral atoms or molecules. For secondary ion mass spectrometry (SIMS) the species of interest are the secondary ions because they can be extracted and mass analyzed.

2.2 SPUTTERING PROCESS

The basis of SIMS is the sputtering process. Ions are used for sputtering since electrons have very limited sputtering capability. The difference in mass between an electron and an O_2^+ ion is 58,000, which is approximately the difference in mass between a pellet for a BB gun (0.2 g) and an 88 mm artillery shell (9 kg). As illustrated in Figure 2.2, a bombarding ion strikes the sample surface, loses charge at impact, and penetrates the sample surface. The energy of the bombarding species is dissipated in a collision cascade. The incident species comes to rest within the sample at an average depth that matches the projected range of an ion implanted atom. Some of the atoms in the collision cascade provide sufficient energy close enough to the surface to remove atoms or molecules from the sample. These ejected or sputtered species, some of which are ionized, leave the surface with an energy distribution with a most probable energy of less than 10 eV and the neutral species have line-of-sight trajectories. Figure 2.3 shows a schematic drawing of the energy distribution of the sputtered species, most of which are neutrals [1]. The secondary positive and negative ions are of interest for the SIMS technique. Other

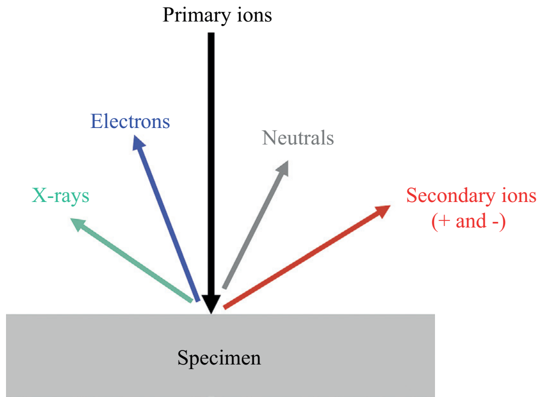

Figure 2.1. Interaction of ions with matter.

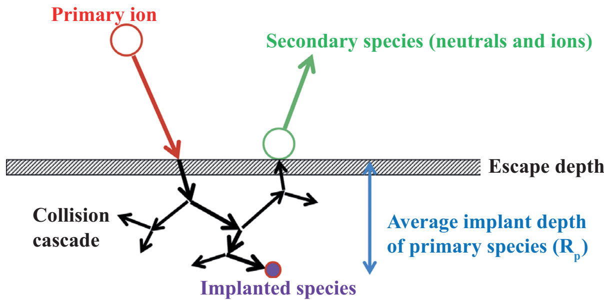

- **Primary ion penetrates surface, loses energy through collision cascade**
- **Primary atom implanted into solid**
- **Secondary species (neutrals and ions) leave surface at low energy**
- **Escape depth of sputtered species only first few monolayers**

Figure 2.2. SIMS process.

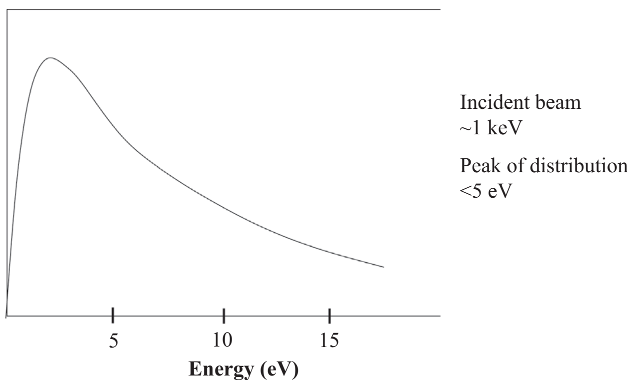

Figure 2.3. Energy distribution of sputtered particles.

species (secondary electrons, photons) are also emitted, but they do not significantly affect the secondary ion yield, with the possible exception of charging effects on insulating samples due to the loss of secondary electrons. Most of the sputtered species arise from the first monolayer [2]. The lifetime of a single cascade event is 10^{-11} to 10^{-13} s and the extent of the cascade is approximately 10 nm, which represents the ultimate lateral resolution of the technique.

Two simulation methods have been very useful to aid in understanding sputtering. One is the Transport of Ions in Matter (TRIM) Monte Carlo simulation for ion implantation [3] and the other is the molecular dynamics sputtering simulation typified by the work of Barbara Garrison [4]. The TRIM simulation program is available to anyone and can generate an array of informative plots, particularly the depth distribution of an ion implanted species. The software is capable of generating simulations for the implantation of any element into a wide range of substrates. Figure 2.4 shows TRIM calculations for boron implanted into silicon at two energies. The 50 keV boron implant has a projected range of 173 nm while the 10 keV projected range is 42 nm. Note that the SIMS process is very similar to the ion implantation process used in the semiconductor processing industry. In fact, the SIMS primary beam has been used to implant a known quantity of a species for later analysis as a standard [5, 6].

The Garrison group has long been known for the generation of three-dimensional sputtering simulations. The simulations range from bombardment of a material with an atomic ion, such as Ar^+ into rhodium, to bombardment with large molecular ions, such as C_{60}^+. Many of the

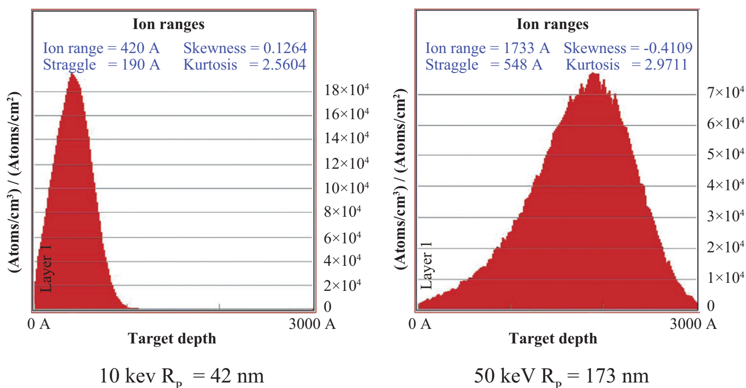

Figure 2.4. TRIM simulation at two impact energies.
Source: www.srim.org

simulations are available on the Garrison website [4]. Figure 2.5 shows a simulation of Ar^+ into rhodium [7]. Figure 2.6 shows an example of starting conditions for SF_5^+ bombardment of biphenyl molecules on Si and Cu substrates [8]. It can be inferred that the sputtering rate for silicon is less than that for copper because the density of atoms in the near-surface region is lower for silicon and fewer interactions near the surface will occur. Figure 2.7 shows C_{60}^+ bombardment of silver compared with Ga^+ bombardment [9].

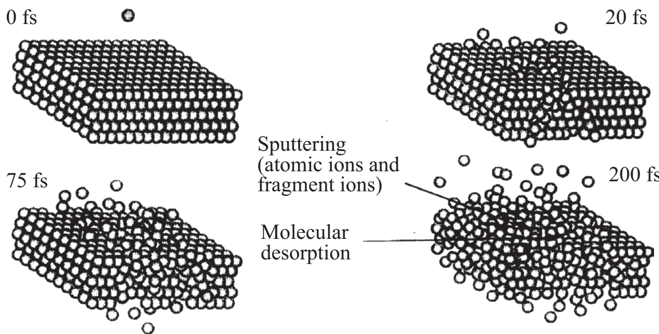

Collision cascade from impact of one Ar^+ at 25 keV on Rh crystal

Figure 2.5. Simulation of particle surface interaction.
Source: Reproduced with permission from R. Webb, University of Surrey [7].

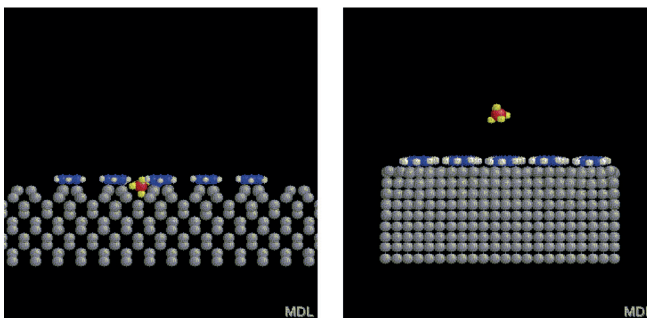

SF_5^+ on biphenyl molecules on Si substrate
SF_5 penetrates Si

SF_5^+ on biphenyl molecules on Cu substrate
SF_5 breaks up at surface

Figure 2.6. Sputtering simulations for SF_5^+.
Source: Reproduced with permission from K. Krantzman, College of Charleston [8].

2.3 SPUTTERING YIELD

The sputtering yield or number of atoms sputtered per incident ion has been measured as a function of incident ion parameters. Figure 2.8 shows the sputtering yield as a function of primary ion energy for Ar^+ and Ne^+

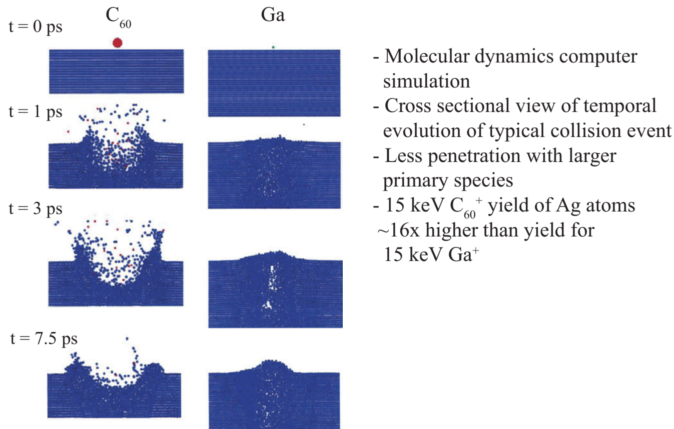

Figure 2.7. Sputtering simulation of C_{60}^+ versus Ga^+ on Ag(111).
Source: Reprinted with permission from Analytical Chemistry, Copyright 2003 by the American Chemical Society [9].

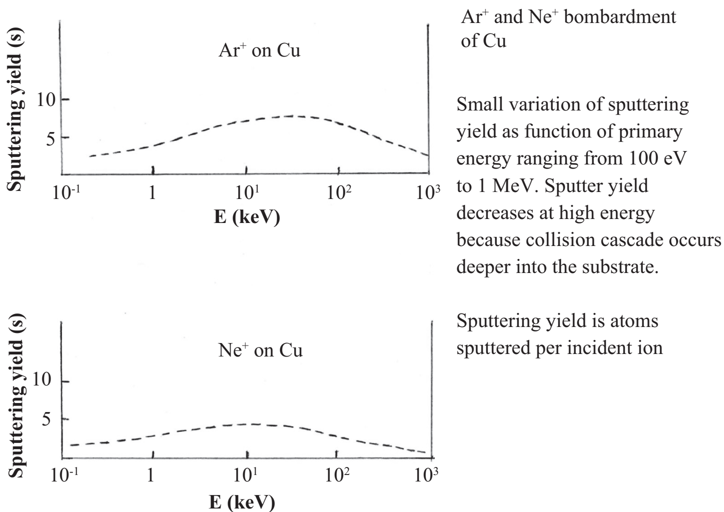

Figure 2.8. Sputtering yield versus primary energy.
Source: Sigmund [10], Reprinted with permission from Physical Review, Copyright 1969 by the American Physical Society.

bombardment of copper [10]. The sputtering yield does not change significantly with energy, but does show a peak at about 30 keV for Ar^+ and 15 keV for Ne^+. The peak can be explained by the deeper penetration of the bombarding species at high energy and hence less energy imparted to the surface to remove atoms. The energy available to surface atoms continues to decrease with increasing bombardment energy. At low energy the impact of the ion is diminished, there is less energy available to remove surface atoms, and the sputtering yield is reduced. Figure 2.9 shows sputtering yield versus incident energy for species most commonly used in SIMS [11–17]. Sputtering yield can be increased significantly for some materials with the use of cluster beam sources, such as C_{60} [18]. Figure 2.10 shows

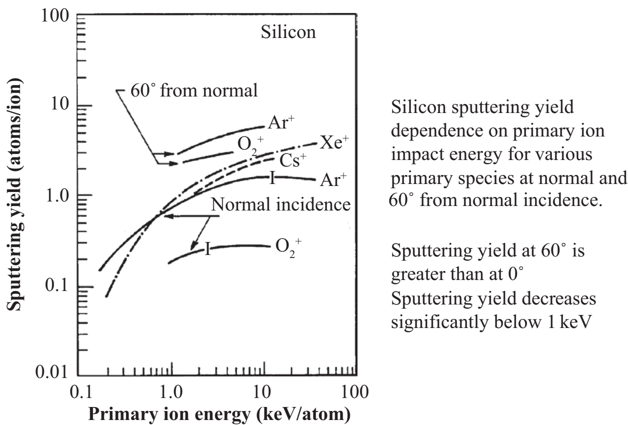

Figure 2.9. Sputtering yield versus primary energy.
Source: Morgan et al. [11]; Zalm [12]; Wittmaack [13–16].

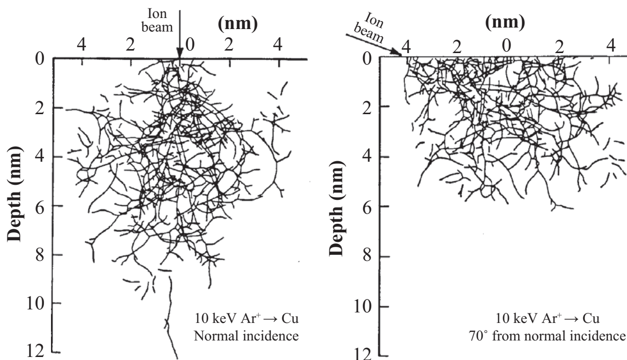

Figure 2.10. Penetration versus incidence angle.
Source: Wilson, Stevie, and Magee [19].

Monte Carlo simulations of the collision cascade at two different angles of incidence [19]. The normal incidence case shows a deeper distribution with fewer collisions next to the surface compared with the 70º incidence distribution that has more collisions near the surface. It is evident that the off-normal incidence case has a higher sputtering yield and the implanted atoms are closer to the surface. Figure 2.11 shows the same figure but with an overlay of a Gaussian summation of the implanted species and the projected range of the implant. Figure 2.12 is a schematic drawing that shows the relationship of sputtering yield with angle of incidence. This

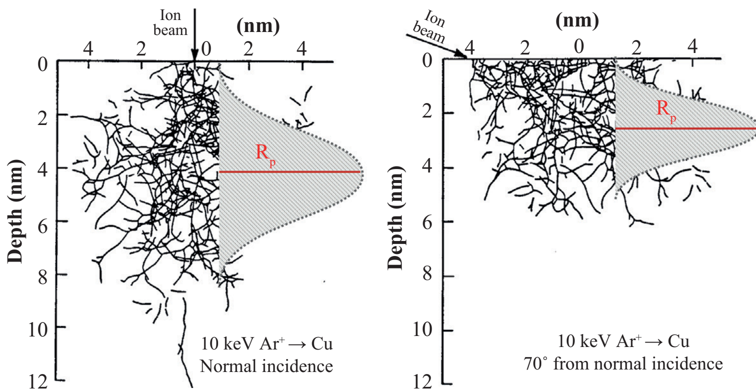

Figure 2.11. Distribution of implanted species.
Source: Wilson, Stevie, and Magee [19].

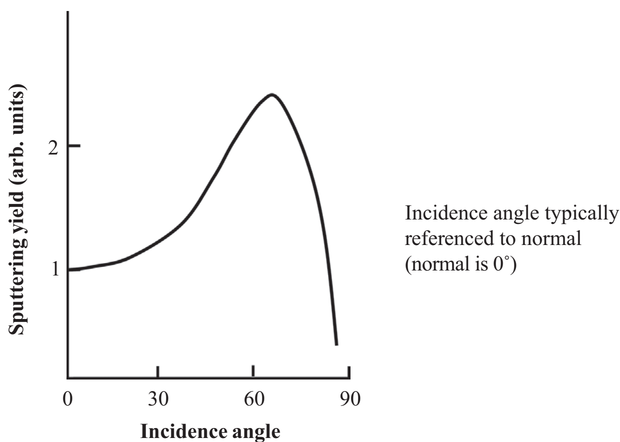

Figure 2.12. Sputtering yield versus incidence angle.

relationship has been found to be similar for O_2^+ bombardment of several matrixes, such as Ge, Si, and GaAs [20, 21]. All three substrates show significant increase in sputtering rate as the angle of incidence is increased from normal incidence to 60º from normal. Sputtering yield increases with the angle of incidence until about 70º from normal [22]. Note that in SIMS the convention is to specify the angle of incidence as the deviation from normal, i.e., normal incidence is zero degrees. Figure 2.13 helps summarize the results for energy and the angle of incidence with simulations for boron implanted at different energies (1, 3, 5 keV) and incidence angles (0°, 30°, 60º) from normal. The angular distribution of sputtered species is not uniform [23–25]. Figure 2.14 shows a schematic drawing of sputtered species for a sputtering beam of approximately 5 keV at 60º incidence.

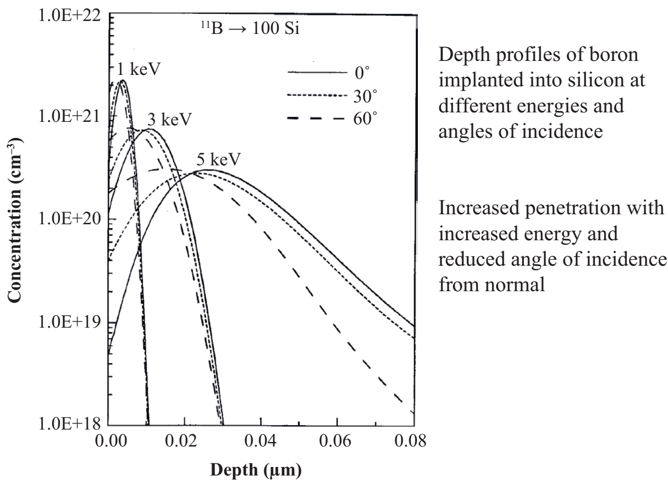

Figure 2.13. Penetration depth versus energy and incidence angle.

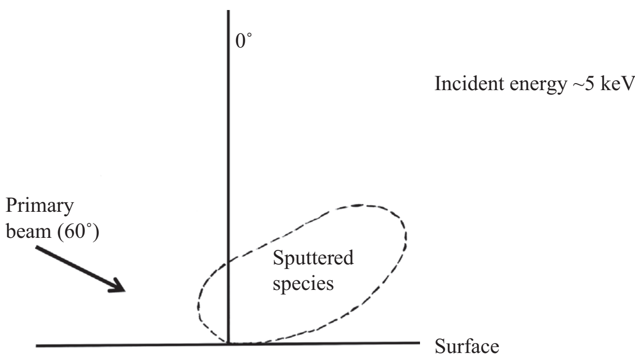

Figure 2.14. Angular distribution of sputtered material.

This figure illustrates the importance of detector location with respect to the primary beam incidence angle.

It is also important to understand the relationship between the sputtering yield and the bombarding and target species [26]. Figure 2.15 schematically shows the relationship of the sputtering yield with the atomic number of the bombarding ion. The shape of the curve is continuous with a low sputtering yield for low atomic number, but only a gradual increase is seen above atomic number 30. The situation is quite different for the target element. Figure 2.16 shows that the sputtering yield

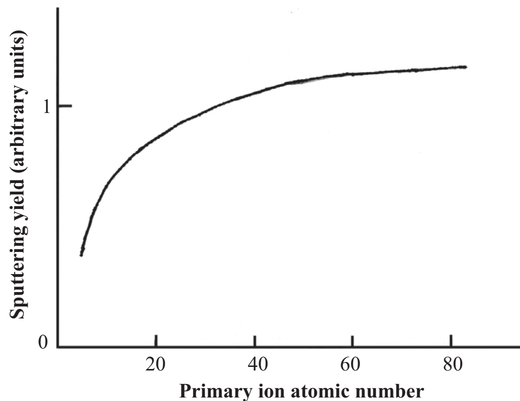

Figure 2.15. Sputtering yield versus primary ion atomic number.

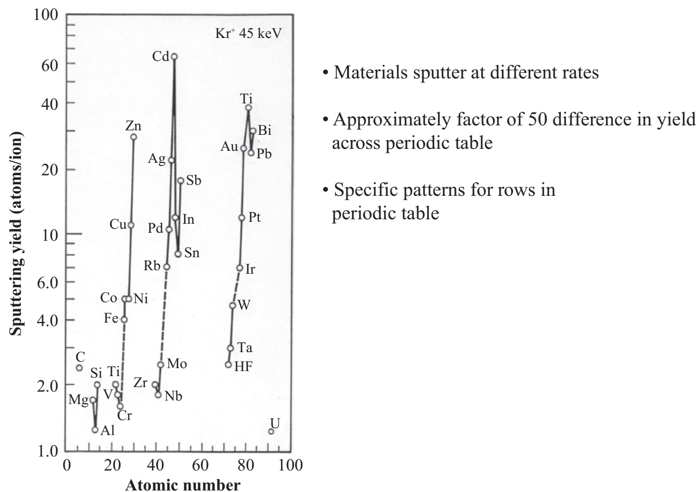

Figure 2.16. Sputtering yield versus target atomic number. *Source*: Wilson and Brewer [27], reprinted with permission from John Wiley and Sons.

varies dramatically over the periodic table and there is a general relationship between increasing sputtering rate and increasing atomic number for a row in the table [27]. The difference in sputtering rates for different elements (and different compounds) results in the need for corrections in the depth scale for the analysis of multilayer structures. For Kr^+ at 45 keV, zinc sputters at approximately a factor of seven faster than iron and a depth profile through zinc-coated steel would require a significant depth axis correction when converting sputtering time to depth.

2.4 PREFERENTIAL SPUTTERING

The sputtering of a matrix with more than one component can result in a nonstoichiometric removal of the components [28]. This is especially true if there is a significant difference in mass between the components. For example, in the analysis of tantalum silicide ($TaSi_2$) with O_2^+ bombardment, the tantalum is more difficult to remove than the silicon, and at an interface between $TaSi_2$ and another layer, the tantalum will show poorer depth resolution than the silicon. This effect can also be noted for isotopes, especially of low mass elements. For example, the analysis of lithium isotopes, ^6Li and ^7Li, has shown that the initial flux of sputtered species is enriched in the lighter isotope [29]. This isotope effect has implications for isotope ratio measurements.

2.5 SECONDARY ION YIELD

Both positive and negative secondary ions can be formed. We know that the positive secondary ion yields are related to ionization potential and the negative secondary ion yields are related to electron affinity. There are many possible ionization methods (electron impact, ion or atom impact, photoionization, surface ionization, charge transfer, thermal ionization) and the actual method of ionization in SIMS is still not completely understood [30]. Certain aspects of the ionization can be described. For bombardment using rare gases such as Ar^+ and Xe^+, the secondary ion yield is significantly lower than that for bombardment using reactive species such as oxygen or cesium. The secondary ion yield is affected by the chemical environment of the substrate. The presence of reactive species such as oxygen or cesium at the specimen surface enhances secondary ion yields for positive and negative ions, respectively [5, 31]. Oxygen is understood to enhance positive secondary ions because the surface is first oxidized

and then metal oxide bonds are broken. The use of cesium reduces the work function, which affects the ability to add an electron and increase negative secondary ion formation. The work function is the difference in energy between an electron in the vacuum with no kinetic energy (only electrostatic energy) and an electron at the Fermi level inside the solid. Electron affinity is the energy gained in taking an electron at rest just outside an atom and placing it in a vacant orbit. The change from Fermi level to electron affinity level indicates the formation of a negative ion. The amount of cesium on the surface can be affected by bombardment conditions (angle of incidence, energy, sputtering rate).

The secondary ion yield (fraction of sputtered atoms that are ionized) is also dependent on primary beam energy and angle of incidence. Figure 2.17 shows that changes in secondary ion yield do not vary significantly over the energy range 2 to 12 keV [11–17]. However, Figure 2.18 shows that both positive and negative secondary ion yields decrease dramatically as incidence angle is varied from 0° to 60º from normal [14, 20]. This is the opposite of the sputtering yield versus incidence angle plot shown in Figure 2.12. As a result, analyses are typically conducted with the angle of incidence between 0° and 60º to balance the sputtering yield and secondary ion yield.

Some of the models for secondary ion emission:

- Bond-breaking model [32–34]
- Electron-tunneling model [35, 36]

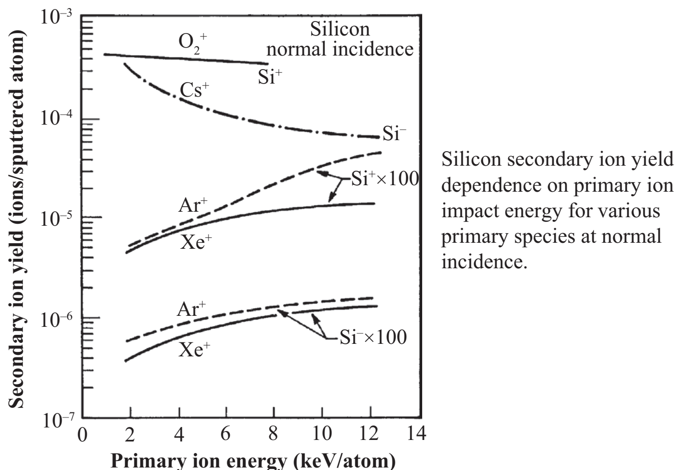

Figure 2.17. Secondary ion yield versus primary energy.
Source: Morgan et al. [11]; Zalm [12]; Wittmaack [13–16].

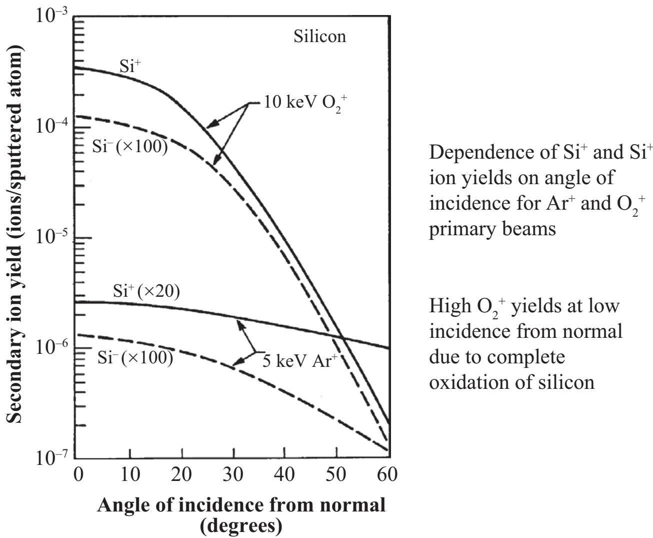

Figure 2.18. Secondary ion yield versus incidence angle.
Source: Wittmaack [14, 20].

- Local thermal equilibrium (LTE) model [37–39]
- Work function model [40]
- Surface-polarization model [41]
- Surface-excitation model [42]

An accurate model can provide a better understanding of the ionization process and simplify SIMS quantification. Initially, SIMS analysis was regarded as a semiquantitative technique that could provide only comparative information between samples. Some of the models were able to provide results within a factor of two or three, but this was not sufficiently accurate for many applications. The ion implantation method presented in Chapter 6 can routinely provide results within 10 to 20 percent of the actual value, and silicon dopant measurements within 1 percent can be achieved based on standards from National Institute for Standards and Technology.

2.6 OXYGEN FLOOD (OXYGEN LEAK, OXYGEN BACKFILL)

For O_2^+ bombardment, the amount of oxygen available to oxidize the surface is maximized at normal incidence and can totally oxidize the surface

for moderate sputtering rates. At nonnormal incidence, the oxidation of the surface is not complete. Enhancement with oxygen flood (oxygen leak, oxygen backfill) has often been used to increase the amount of oxygen present at the surface. This is accomplished with the addition of a nozzle close to the sample surface. Oxygen is inlet through the nozzle at a rate sufficient to aid the oxidation process. The background pressure in the analysis chamber will increase and limit the amount of gas that can be used. If the analysis chamber pressure is too high then the mean free path of ions in the gas will be too short to conduct the analysis. The increase in secondary ion yield can be very significant. For 4 keV Ar^+ bombardment of silicon at normal incidence, $^{28}Si^+$ increased by at least three orders of magnitude when oxygen partial pressure was increased from 10^{-6} Pa to 10^{-4} Pa [43]. Figure 2.19 shows the result of using oxygen flood on an ion implant of arsenic through a 50 nm SiO_2 layer on silicon [44, 45]. The analysis was made using O_2^+, and the higher oxygen concentration in the oxide resulted in a secondary ion yield enhancement, which is evidenced by a discontinuity at the oxide/Si interface. When oxygen flood was added to the O_2^+ primary beam, the oxygen concentration at the surface was sufficient throughout the profile to remove the yield difference between oxide and silicon. The depth profile then showed a constant matrix intensity and no discontinuity in the arsenic profile. However, the addition of an oxygen flood can affect the sputtering rate, which would require a depth scale correction.

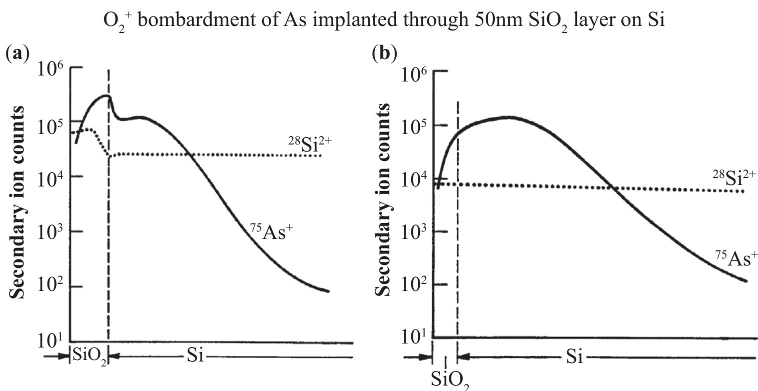

Figure 2.19. O_2^+ and oxygen flood remove matrix effect. (a) Yield enhancement in SiO_2 and discontinuity at interface and (b) added oxygen flood removed yield difference between SiO_2 and Si.
Source: Stingeder et al. [44]; Wilson, Stevie, and Magee [45].

2.7 MATRIX EFFECTS

Secondary ion yields for a given element can vary with the matrix. Studies of the important combination of silicon and germanium in semiconductor technology show the importance of this effect [46, 47]. The example just discussed for arsenic with oxygen flood displayed the difference in secondary ion yield between SiO_2 and silicon, and some yield change is almost always evident for an oxide layer on a nonoxidized substrate. Ion implantation of samples in oxide and substrate can be used to illustrate and resolve a matrix effect. Figure 2.20 shows separate implants of ^{31}P in silicon and SiO_2 and indicates a higher secondary ion yield for ^{31}P in SiO_2 compared with silicon. Figure 2.21a shows a depth profile for ^{31}P through a $SiO_2/Si/SiO_2/Si$ structure and appears to show phosphorus peaks at the interfaces of the SiO_2 layers with the silicon layer. If we plot the phosphorus profile referenced to phosphorus in silicon, as shown in Figure 2.21b, and plot phosphorus referenced to SiO_2 as shown in Figure 2.21c, the peaks still appear but the phosphorus profiles are different because of the yield difference between the oxide and silicon. Now if we plot phosphorus in silicon as shown by the dashed line in Figure 2.21c, then the composite profile referenced to the ion yield for the respective matrixes shows no peaks at the interfaces and a phosphorus concentration much higher in the silicon layer than in the oxide layers.

A similar result can occur for a material such as a silicide that contains an element that does not oxidize readily. Figure 2.22a shows a depth profile of PtSi/Si analyzed with an O_2^+ primary beam [48]. Even though platinum does not oxidize readily, PtSi contains silicon, which does oxidize easily. The result is a uniform platinum signal in the PtSi. Figure 2.22b, also obtained using O_2^+, shows an apparent peak at the interface of a layer

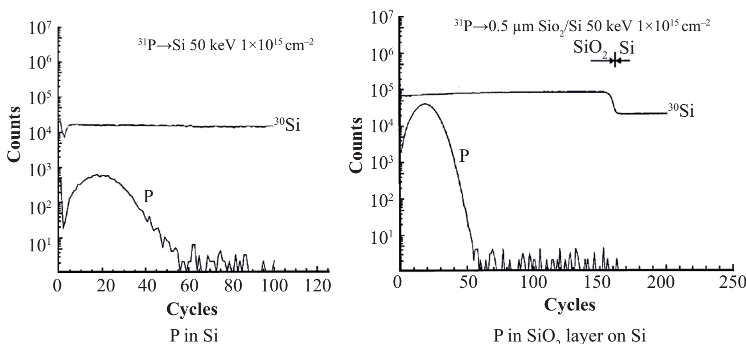

Figure 2.20. Matrix effect: P in Si versus SiO_2.

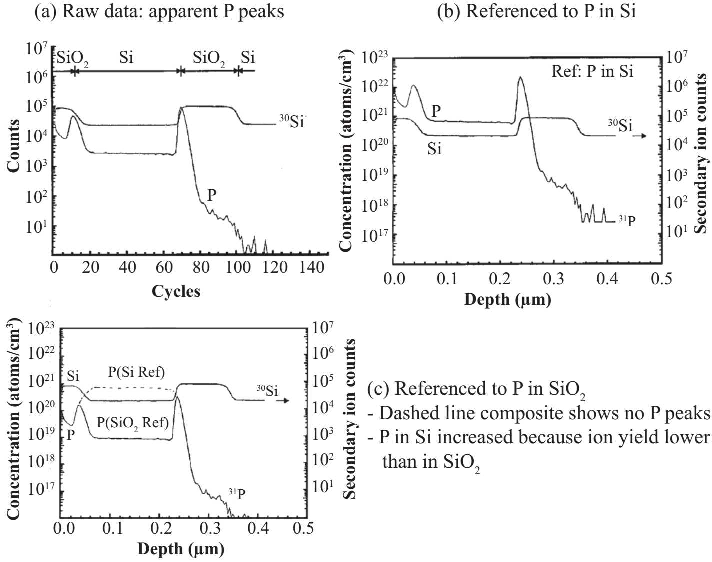

Figure 2.21. Matrix effect: P in Si versus SiO_2. (a) Raw data: apparent P peaks, (b) referenced to P in Si , and (c) referenced to P in SiO_2.

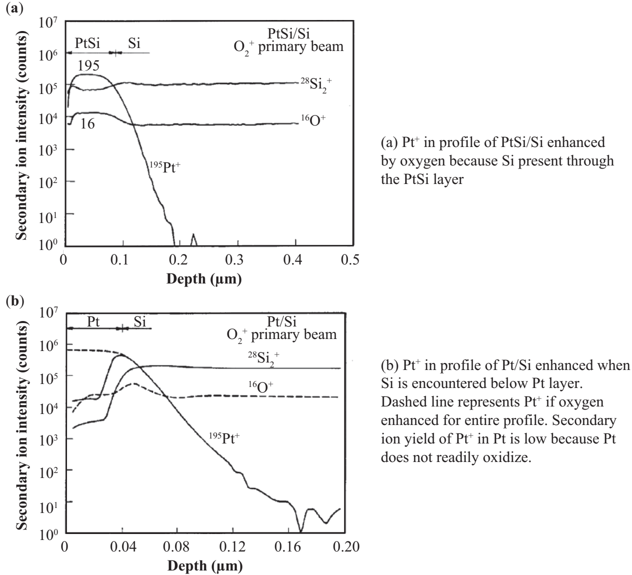

Figure 2.22. Matrix effect and yield enhancement for Pt analysis. (a) Pt^+ in profile of PtSi/Si is enhanced by oxygen because Si is present through the PtSi layer and (b) Pt^+ in profile of Pt/Si is enhanced when Si is encountered below the Pt layer.
Source: Wilson, Stevie, and Magee [48].

of Pt/Si. The peak occurs because the yield for platinum is low, but as the interface between platinum and silicon is reached, the silicon oxidizes and increases the secondary ion yield and shows the apparent increase in platinum.

REFERENCES

[1] Oechsner, H. 1970. "Energy Distributions Observed in Sputtering of Solids by Ion Bombardment." [In German.] *Z. Phys*. 238, p. 433.

[2] Burnett, J.W., J.P. Biersack, D.M. Gruen, B. Jorgensen, A.R. Krauss, M.J. Pellin, E.L. Schweitzer, J.T. Yates, Jr., and C.E. Young. 1988. "Depth of Origin of Sputtered Atoms: Experimental and Theoretical Study of Cu/Rh(0001)." *Journal of Vacuum Science & Technology* A6, p. 2064.

[3] Ziegler, J. TRIM Transport of Ions in Matter. www.srim.org

[4] Barbara Garrison website at The Pennsylvania State University (galilei.chem.psu.edu)

[5] Wittmaack, K. 1981. "Oxygen Concentration Dependence of Secondary Ion Yield Enhancement." *Surface Science* 112, p. 168.

[6] Lareau, R.T., and P. Williams. 1985. "In Situ Ion Implantation for Quantitative SIMS Analysis." In *Materials Research Society Symposium Proceedings*, eds. W. Katz and P. Williams, 48: 273.

[7] Webb, R., R. Smith, E. Dawnkaski, B. Garrison, and N. Winograd. 1993. "The Simulation of Energetic Particle Collisions with Solids—A Visual Representation." *International Video Journal of Engineering Research* 3, p. 63.

[8] Townes, J.A., A.K. White, E.N. Wiggins, K.D. Krantzman, B.J. Garrison, N. Winograd. 1999. "Mechanism for Increased Yield with SF_5^+ Projectiles in Organic SIMS: The Substrate Effect." *The Journal of Physical Chemistry A* 103, 24, pp. 4587–89. doi: http://dx.doi.org/10.1021/jp9907138

[9] Postawa, Z., B. Czerwinski, M. Szewczyk, E.J. Smiley, N. Winograd, B.J. Garrison. 2003. "Enhancement of Sputtering Yields Due to C_{60} versus Ga Bombardment of Ag {111} as Explored by Molecular Dynamics Simulations." *Analytical Chemistry* 75, no. 17, pp. 4402–07. doi: http://dx.doi.org/10.1021/ac034387a

[10] Sigmund, P. 1969. "Theory of Sputtering. I. Sputtering Yield of Amorphous and Polycrystalline Targets." *Physical Review* 184, no. 2, pp. 383–416. doi: http://dx.doi.org/10.1103/physrev.184.383

[11] Morgan, A.E., H.A.M. de Grefte, N. Warmoltz, H.W. Werner, and H.J. Tolle. 1981. "The Influence of Bombardment Conditions upon the Sputtering and Secondary Ion Yields of Silicon." *Applications of Surface Science* 7, no. 4, pp. 372–92. doi: http://dx.doi.org/10.1016/0378-5963(81)90084-2

[12] Zalm, P.C. 1983. "Energy Dependence of the Sputtering Yield of Silicon Bombarded with Neon, Argon, Krypton, and Xenon Ions." *Journal of Applied Physics* 54, no. 5, pp. 2660–66. doi: http://dx.doi.org/10.1063/1.332340

[13] Wittmaack, K. 1981. "Implications in the Use of Reactive Ion Bombardment for Secondary Ion Yield Enhancement." *Applications of Surface Science* 9, no. 1–4, pp. 315–34. doi: http://dx.doi.org/10.1016/0378-5963(81)90045-3

[14] Wittmaack, K. 1984. "Angular Dependence of Secondary Ion Emission from Silicon Bombarded with Inert Gas Ions." *Nuclear Instruments and Methods in Physics Research Section B: Beam Interactions with Materials and Atoms* 2, no. 1–3, pp. 674–78. doi: http://dx.doi.org/10.1016/0168-583x(84)90290-8

[15] Wittmaack, K. 1983. "Secondary Ion Yield Variations Due to Cesium Implantation in Silicon." *Surface Science* 126, no. 1–3, pp. 573–80. doi: http://dx.doi.org/10.1016/0039-6028(83)90760-4

[16] Wittmaack, K. 1985. "Influence of the Impact Angle on the Depth Resolution and the Sensitivity in SIMS Depth Profiling Using a Cesium Ion Beam." *Journal of Vacuum Science & Technology A* 3, no. 3, pp. 1350–54. doi: http://dx.doi.org/10.1116/1.572775.

[17] Wilson, R.G., F.A. Stevie, and C.W. Magee. 1989. *Secondary Ion Mass Spectrometry*, 1.2–4. New York: Wiley.

[18] Wucher, A. 2006. "Molecular Secondary Ion Formation under Cluster Bombardment: A Fundamental Review." *Applied Surface Science* 252, no. 19, pp. 6482–89. doi: http://dx.doi.org/10.1016/j.apsusc.2006.02.070

[19] Wilson, R.G., F.A. Stevie, and C.W. Magee. 1989. *Secondary Ion Mass Spectrometry*, 2.1–5. New York: Wiley.

[20] Wittmaack, K. 1983. "The Effect of the Angle of Incidence on Secondary Ion Yields of Oxygen-Bombarded Solids." *Nuclear Instruments and Methods in Physics Research* 218, no. 1–3, pp. 307–11. doi: http://dx.doi.org/10.1016/0167-5087(83)90996-1

[21] Wilson, R.G., F.A. Stevie, and C.W. Magee. 1989. *Secondary Ion Mass Spectrometry*, 1.3–3. New York: Wiley.

[22] Oechsner, H. 1973. "Investigations of Polycrystalline Metal Surfaces Sputtered with Angled Ion Beams in the 1 keV Energy Range." *Z. Physik* 262: 37. doi: htttp://dx.doi.org//10.1007/BF01402280

[23] Kerkow, H., and M. Trapp. 1974. "Secondary Ion Emission During Bombardment of Copper and Aluminum Single Crystals with Alkali Ions." *International Journal of Mass Spectrometry and Ion Physics* 13, no. 2, pp. 113–22. doi: http://dx.doi.org/10.1016/0020-7381(74)80016-1

[24] Winograd, N., B.J. Garrison, D.E. Harrison. 1978. "Angular Distributions of Ejected Particles from Ion-Bombarded Clean and Reacted Single-Crystal Surfaces." *Physical Review Letters* 41, no.16, p. 1120–23. doi: http://dx.doi.org/10.1103/physrevlett.41.1120

[25] Gurmin, B.M., Y.A. Ryzhof, and I.I. Shkarban. 1969. "Angular Distributions of Atoms Sputtered from Polycrystalline Targets by Ions of Inert Gases." *Bull. Acad. Sci. USSR Phys. Ser., USA* 33: 752.

[26] Oechsner, H. 1975. "Sputtering—A Review of Some Recent Experimental and Theoretical Aspects." *Applied Physics* 8, no. 3, pp. 185–98. doi; http://dx.doi.org/10.1007/bf00896610

[27] Wilson, R.G., and G.R. Brewer. 1973. *Ion Beams: With Applications to Ion Implantation*, 317. New York: Wiley.

[28] Barcz, A., M. Bugajski, M. Croset, and L.M. Mercandalli. 1983. "Stoichiometry Changes in III-V Compounds Under Ion Bombardment." *Nuclear Instruments and Methods in Physics Research* 209–210, p. 621–27. doi: http://dx.doi.org/10.1016/0167-5087(83)90858-x

[29] Gnaser, H., and I.D. Hutcheon. 1988. "Preferential Emission of Lighter Isotopes in the Initial Stage of Sputtering." *Surface Science* 195, no. 3, pp. 499–512. doi: http://dx.doi.org/10.1016/0039-6028(88)90356-1

[30] Wittmaack , K. 2013. "Unraveling the Secrets of Cs Controlled Secondary Ion Formation: Evidence of the Dominance of Site Specific Surface Chemistry, Alloying and Ionic Bonding." *Surface Science Reports* 68, no. 1, pp. 108–230. doi: http://dx.doi.org/10.1016/j.surfrep.2012.11.001

[31] Yu, M.L. 1986. "Chemical Enhancement Effects in SIMS Analysis." *Nuclear Instruments and Methods in Physics Research Section B* 15, no. 1–6, pp. 151–58. doi: http://dx.doi.org/10.1016/0168-583x(86)90273-9

[32] Hennequin, J-F, G. Blaise, and G. Slodzian. 1969. "Origin of Multi-Charged Secondary Ions Produced by Ionic Bombardment of a Metal." [In French.] *Compt. Rend. Acad. Sci.* B263: 1246.

[33] Mann, K., and M.L. Yu. 1986. "Origin of the Chemical Enhancement of Positive Secondary Ion Yield in SIMS." In *Secondary Ion Mass Spectrometry, SIMS V*, eds. A. Benninghoven, R.J. Colton, D.S. Simons, and H.W. Werner, 26. Berlin, Germany: Springer-Verlag.

[34] Yu, M.L., and K. Mann. 1986. "Bond Breaking and the Ionization of Sputtered Atoms." *Physical Review Letters* 57, no. 12, pp. 1476–79. doi: http://dx.doi.org/10.1103/physrevlett.57.1476

[35] Yu, M.L. 1978. "Work-function Dependence of Negative-Ion Production During Sputtering." *Physical Review Letters* 40, no. 9, pp. 574–77. doi: http://dx.doi.org/10.1103/physrevlett.40.574

[36] Yu, M.L, and N.D. Lang. 1986. "Mechanisms of Atomic Emission During Sputtering." *Nuclear Instruments and Methods in Physics Research Section B* 14, no. 4–6, pp. 403–13. doi: http://dx.doi.org/10.1016/0168-583x(86)90135-7

[37] Andersen, C.A., and J.R. Hinthorne. 1973. "Thermodynamic Approach to the Quantitative Interpretation of Sputtered Ion Mass Spectra." *Analytical Chemistry* 45, no. 8, pp. 1421–38.doi: http://dx.doi.org/10.1021/ac60330a034

[38] Andersen, C.A. 1975. "A Critical Discussion of the Local Thermal Equilibrium Model for the Quantitative Correction of Sputtered Ion Intensities." In *Secondary Ion Mass Spectrometry*, eds. K.F.J. Heinrich, and D.E. Newbury, 79. Washington, DC: NBS.

[39] Simons, D.S., J.E. Baker, and C.A. Evans, Jr. 1976. "Evaluation of the Local Thermal Equilibrium Model for Quantitative Secondary Ion Mass Spectrometric Analysis." *Analytical Chemistry* 48, no. 9, pp. 1341–48. doi: http://dx.doi.org/10.1021/ac50003a021

[40] Yu, M.L. 1983. "Effect of Surface Chemistry and Work Function in Secondary Ion Mass Spectrometry." *Journal of Vacuum Science & Technology A* 1, no. 2, p. 500. doi: http://dx.doi.org/10.1116/1.571915

[41] Williams, P., and C.A. Evans Jr. 1978. "Anomalous Enhancement of Negative Sputtered Ion Emission by Oxygen." *Surface Science* 78, no. 2, pp. 324–38. doi: http://dx.doi.org/10.1016/0039-6028(78)90084-5

[42] Williams, P. 1979. "The Sputtering Process and Sputtered Ion Emission." *Surface Science* 90, no. 2, pp. 588–634. doi: http://dx.doi.org/10.1016/0039-6028(79)90363-7

[43] Wittmaack, K. 1980. "Aspects of Quantitative Secondary Ion Mass Spectrometry." *Nuclear Instruments and Methods* 168, no. 1–3, pp. 343–56. doi: http://dx.doi.org/10.1016/0029-554x(80)91275-6

[44] Stingeder, G., M. Grasserbauer, E. Guerrero, H. Potzl, and R. Tielert. 1983. "Quantitative Distribution Analysis of Dopant Elements in Silicon with SIMS for the Improvement of Process Modeling." *Fresenius Zeitschrift fur Analytische Chemie* 314, no. 3, pp. 304–08. doi: http://dx.doi.org/10.1007/bf00516826

[45] Wilson, R.G., F.A. Stevie, and C.W. Magee. 1989. *Secondary Ion Mass Spectrometry*, 2.3–5. New York: Wiley.

[46] Gillen, G., J.M. Phelps, R.W. Nelson, P. Williams, and S.M. Hues. 1989. "Secondary Ion Yield Matrix Effects in SIMS Depth Profiles of Si/Ge Multilayers." *Surface and Interface Analysis* 14, no. 11, pp. 771–80. doi: http://dx.doi.org/10.1002/sia.740141114

[47] Jackman, J.A., L. Dignard-Bailey, R.S. Storey, C. MacPherson, S. Rolfe, L. Van Der Zwan, and T.E. Jackman. 1990. "Matrix Effects in SIMS Depth Profiles of SiGe Superlattices." *Nuclear Instruments and Methods in Physics Research Section B* 45, no. 1–4, pp. 592–96. doi: http://dx.doi.org/10.1016/0168-583x(90)90907-c

[48] Wilson, R.G., F.A. Stevie, and C.W. Magee. 1989. *Secondary Ion Mass Spectrometry*, 4.4–10. New York: Wiley.

CHAPTER 3

Analysis Parameters

Secondary ion mass spectrometry (SIMS) is a technique where the details matter. There are a number of parameters that need to be considered for primary beam, secondary species, and analyzer. This section discusses how to optimize these parameters in order to obtain the desired SIMS data.

3.1 PARAMETERS OF INTEREST FOR DEPTH PROFILING

The primary beam polarity, species, energy, current, and angle of incidence
Raster and detected area
Secondary beam polarity, species, energy distribution
Mass resolution

3.2 PRIMARY BEAM POLARITY AND SPECIES

When the SIMS technique began to blossom in the 1970s, it became quickly apparent that positive secondary ion yields for materials such as metals showed a dramatic increase in secondary ion yield in the native oxide compared with the bulk metal [1]. Table 3.1 shows that positive secondary ion yields were typically higher by a factor of 10 to 100 or more in the oxide. This caused issues in depth profiling of many materials with rare gas beams as there was a large change in secondary ion yield in the profile and poor secondary ion yields in the matrix. One conclusion from these data was to perform the analysis using an oxygen beam. With a duoplasmatron source (described in Chapter 4, instrumentation) a positive oxygen beam could be obtained with high current density. It was noted

Table 3.1. Absolute positive secondary ion yields

M (element)	S_M^+ (clean surface)	S_M^+ (oxygen-covered surface)
Mg	0.01	0.9
Al	0.007	0.7
Ti	0.0013	0.4
V	0.001	0.3
Cr	0.0012	1.2
Mn	0.0006	0.3
Fe	0.0015	0.35
Ni	0.0006	0.045
Cu	0.0003	0.007
Sr	0.0002	0.16
Nb	0.0006	0.05
Mo	0.00065	0.4
Ba	0.0002	0.03
Ta	0.00007	0.02
W	0.00009	0.035
Si	0.0084	0.58
Ge	0.0044	0.02

Source: Benninghoven [1].

Ar^+ 3 keV, 70º incidence

Most elements show greater than × 10 increase for oxygen covered surface compared with clean surface

Try analysis using O_2^+

that the species from the positive beam contained significant amounts of both O^+ and O_2^+ but the latter was more intense by about a factor of 10. For this reason O_2^+ is almost universally used. Another advantage of the use of O_2^+ is that the energy of the beam is split over the two oxygen atoms and that reduces the impact energy for each atom by a factor of two and results in shallower penetration into the sample. As will be shown in Chapter 5 (depth profiling) lower energy provides better depth resolution. A mass filter in the primary column prior to bombardment of the sample can separate the two oxygen ion species (monomer and dimer).

Good secondary ion yields for many elements, especially the electropositive ones, were obtained using O_2^+, but there were many elements, such as the halides, that had very poor positive secondary ion yields and weak negative secondary ion yields. A study of these elements, which had high electronegativity, showed that Cs^+ could lower the work function and significantly improve negative secondary ion yields [2].

These early studies resulted in the selection of O_2^+ and Cs^+ as the typical beams for depth profiling of inorganic materials. These two species provide complementary secondary ion yield enhancement over the periodic table. Figures 3.1 and 3.2 show relative sensitivity factors (RSFs) plotted versus atomic number in a silicon matrix for the two beams [3]. RSFs are obtained from analysis of standards and reflect the difference in sensitivity for different elements. The RSFs are inversely proportional to secondary ion yields so a low RSF equates to a high secondary ion yield. It is readily apparent that species such as the halides have poor positive secondary ion yields with O_2^+ but have the highest negative secondary ion yields with Cs^+ bombardment. An example of the variation of secondary

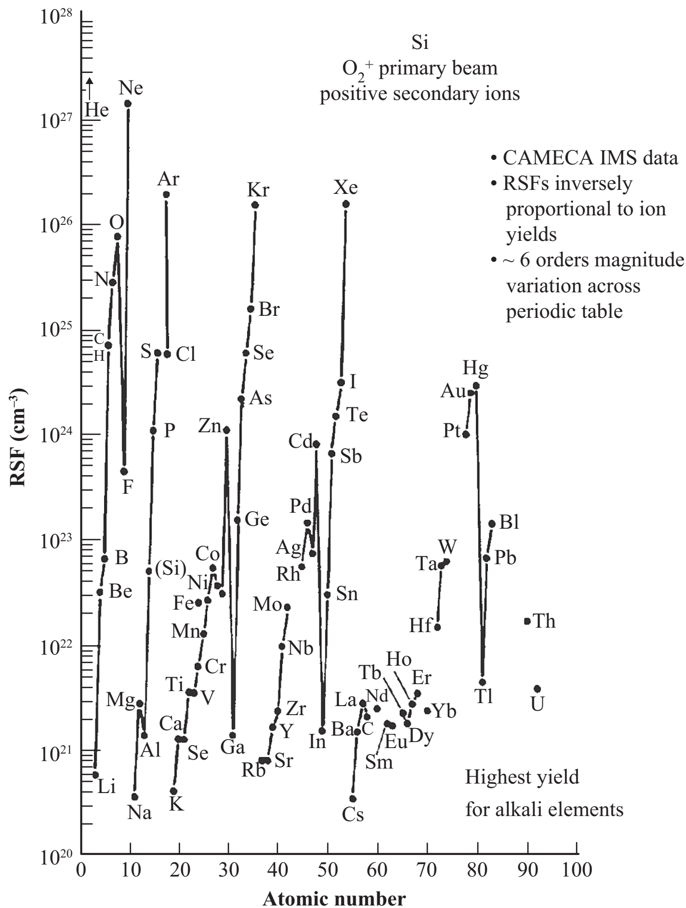

Figure 3.1. Positive secondary ion yields for O_2^+ impact on Si. *Source*: Wilson, Stevie, and Magee [14].

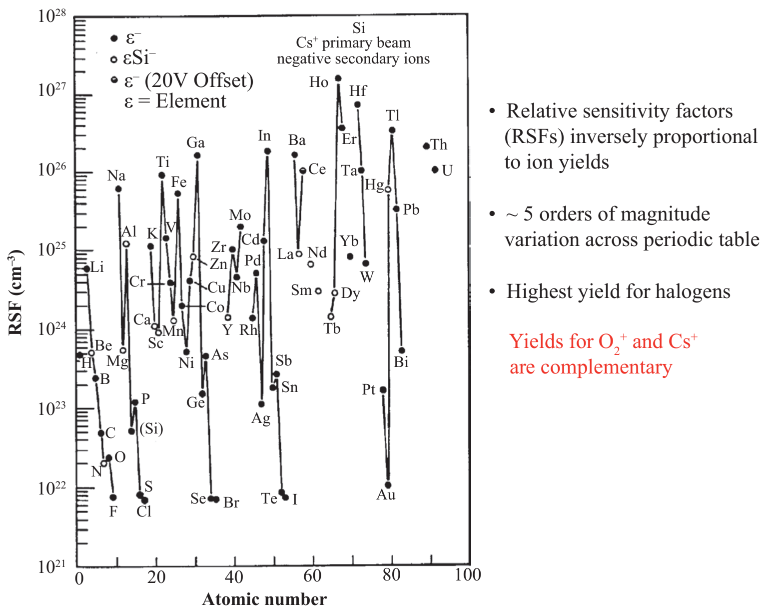

Figure 3.2. Negative secondary ion yields for Cs^+ impact on Si.
Source: Wilson, Stevie, and Magee [14].

ion yield with primary ion species was noted in the analysis of GaAs with an argon ion beam [4]. Approximately a factor of 1000 higher secondary ion yield was obtained for Ga^+ compared with As^+, and this matches fairly well with the difference expected as shown in the RSF plot of Figure 3.1. If polarities are reversed, then As^- was larger than Ga^- by nearly the same factor. These differences in secondary ion yield are important to understand. In a mass spectrum, one might expect that two peaks of equal intensity would imply that equal amounts of the species were present. However, if the ions detected are Ga^+ and As^+, the arsenic concentration may be about 1,000 times higher than the Ga concentration.

Some elements do not have good secondary ion yields for O_2^+ or Cs^+ bombardment. These elements, particularly zinc, cadmium, and the rare gas elements, have shown improved yields with cesium cluster ions. In this mode, the bombarding species is Cs^+ but secondary positive molecular ions are detected. The molecular ions of interest contain a cesium atom and the atom of interest. Figure 3.3 shows the relative cesium cluster ion yields for a number of elements in a plot of RSF versus atomic number [3].

The optimum choice of primary beam for analysis of a particular element is summarized in periodic table format in Figure 3.4 [5]. The figure has been modified from the original source to contain uranium, which is

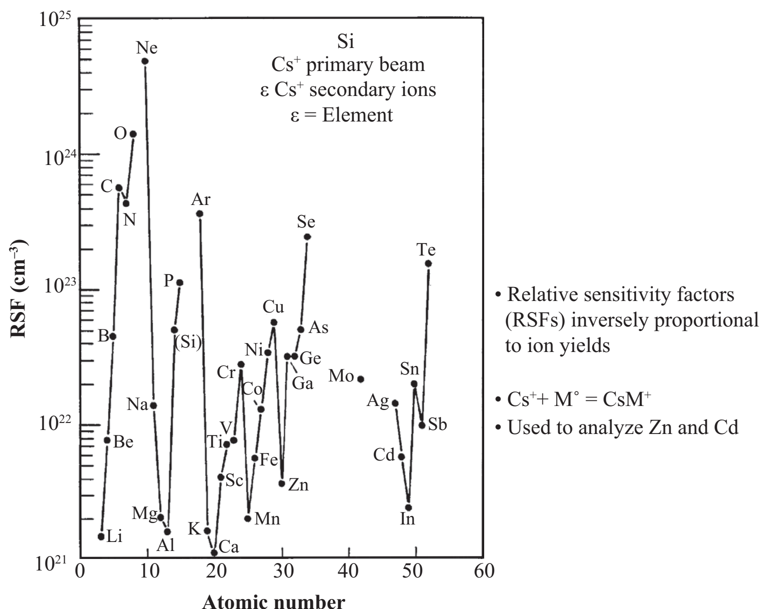

Figure 3.3. Positive secondary Cs-molecular ion yields for Cs^+ bombardment of Si.
Source: Wilson, Stevie, and Magee [14].

best detected with an O_2^+ primary beam. Note that O_2^+ bombardment and detection of negative secondary ions is rarely used except in cases where a Cs^+ source is not available. The elements in white have no stable isotopes.

The choices for primary beam species have expanded, especially for the TOF-SIMS instruments. There has been a progression of primary species with increasing mass coupled with increased overall secondary ion intensity and increased yield at high mass. This was noted beginning with the use of Xe^+ instead of Ar^+ [6]. Similar improvements were noted for comparisons such as Ga^+ versus In^+ and In^+ versus C_{60}^+ [7]. The list includes Ar^+, Xe^+, Ga^+, SF_5^+, Au^+, Au_3^+, Bi^+, Bi_3^+, C_{60}^+, and gas cluster sources such as Ar_{2500}^+. This progression to higher mass species has not ended as other species, such as charged droplets, are under investigation [8, 9].

3.3 SECONDARY ION POLARITY AND SPECIES

The secondary ion mass spectrum contains more species than just atomic ions. Table 3.2 shows the species detected in the secondary ion mass spectrum from 0 to 110 Da for analysis of aluminum using an Ar^+ primary

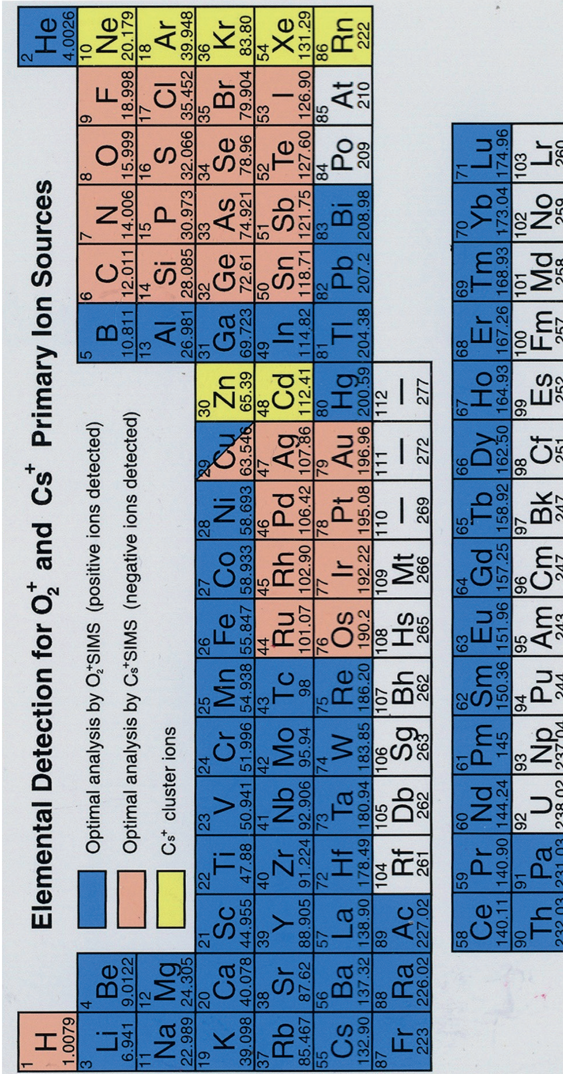

Figure 3.4. Periodic table summary of optimum primary beam choices.
Source: Reproduced with permission from Evans Analytical Group, www.eag.com

beam [10]. One might expect to see just Al^+ but polymeric ions Al_2^+, Al_3^+, and Al_4^+ are present as well as multiply charged species Al^{2+} and Al^{3+}. For a simple monoisotopic material, we have at least six ions detected. If we extended the mass range, we would expect to detect aluminum polymeric ions greater than Al_4^+. When a reactive beam such as O_2^+ is used, then not only do we observe the types of ions noted for Ar^+ bombardment but we also observe combinations of the primary species and the analysis material. If the material has multiple isotopes then the result can be the species tabulated in Table 3.3 where silicon is bombarded with O_2^+, and species

Table 3.2. Secondary ion species for Ar^+ bombardment of Al

Species	Mass/charge (Da)
Al^{3+}	9
Al^{2+}	13.5
Al^+	27
Al_2^+	54
Al_3^+	81
Al_4^+	108

Table 3.3. Secondary ion species for O_2^+ bombardment of Si

Species	Mass/charge (Da)
Si^{2+}	14, 14.5, 15
$^{16}O^+$	16
Si^+	28–30
$^{16}O_2^+$	32
SiO^+	44–46
Si_2^+	56–60
SiO_2^+	60–62
Si_2O^+	72–76
Si_3^+	84–90
$Si_2O_2^+$	88–92
Si_3O^+	100–106
$Si_2O_3^+$	104–108
$Si_3O_2^+$	116–122
$Si_3O_3^+$	132–138

Oxygen isotopes 17 and 18 are not included

such as Si_2O^+ can have a high secondary ion yield [11]. There are peaks at many of the masses in the range shown. One can have a multielement sample with a mass spectrum that has a peak at almost every mass. If we add less than 3 percent of a high yielding species to a matrix, such as aluminum added to GaN, and analyze positive secondary ions, then it is possible to detect not just Al^+, but molecular ions such as Al_2^+, $GaAl^+$, and Ga_2Al^+. This result clearly adds to the complexity of the mass spectrum as displayed in Figure 3.5 [12].

The choice of primary and secondary species and polarity is made simultaneously. The results summarized in the periodic table display of Figure 3.4 were determined by analysis of a large number of samples from multiple matrixes [3, 5, 13]. Each matrix had on the order of 50 elements implanted, and atomic and molecular secondary ions were monitored for each element analyzed. The determining factor was usually the set of analysis conditions that achieved the best detection limit. Examples of the results are shown in figures 3.6 and 3.7 [14]. Figure 3.6 displays depth profiles for indium in silicon obtained with O_2^+ and Cs^+ primary beams. The best detection limit for Cs^+ is the molecular ion $InSi^-$ but the result with O_2^+ and detection of In^+ is significantly better. Molecular ions are frequently advantageous to monitor. Figure 3.7(a) shows that for O_2^+ bombardment of dysprosium in GaAs, the best detection limit was obtained with a molecular ion that contained the element of interest and the primary beam species. Figure 3.7(b) indicates that the best detection limit obtained for Cs^+ bombardment of germanium in InP was obtained with a molecular ion that contained the element of interest and a matrix element.

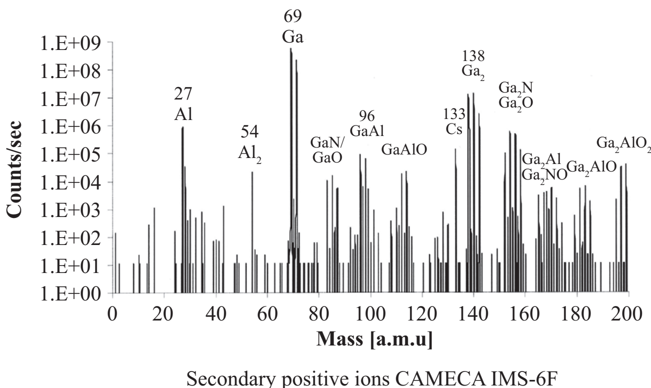

Figure 3.5. AlGaN mass spectrum, 2.8% Al, O_2^+ bombardment. *Source*: C. Gu, North Carolina State University [12].

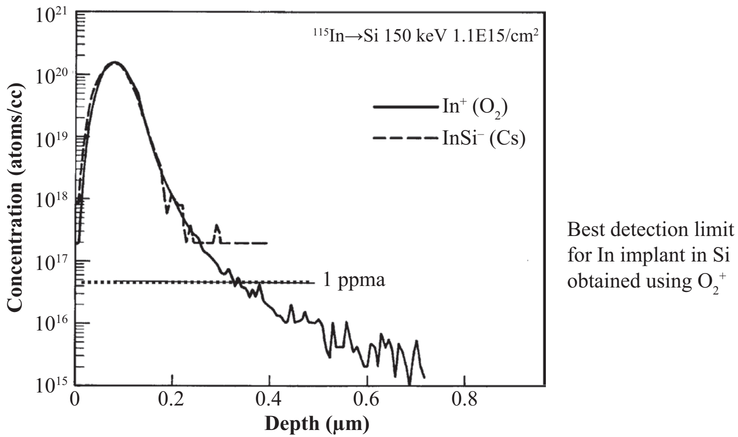

Figure 3.6. Choice of primary beam for detection limit.

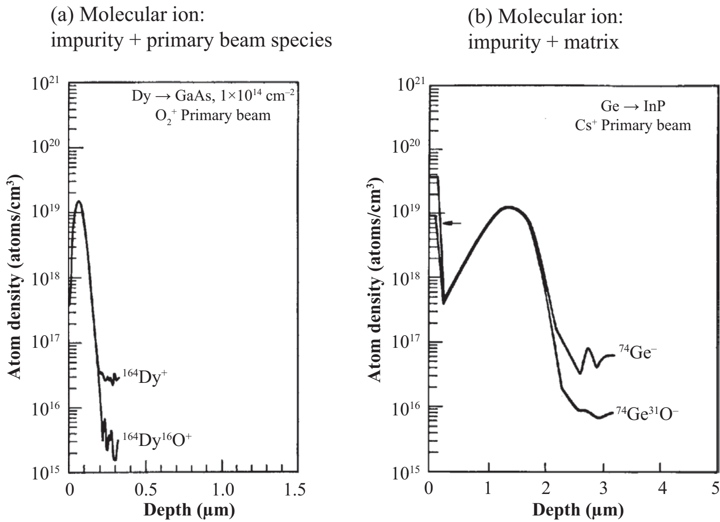

Figure 3.7. Choice of secondary species: Molecular ions. (a) Impurity + primary beam species, (b) impurity + matrix.
Source: Wilson, Stevie, and Magee [14].

3.4 PRIMARY BEAM ENERGY

Besides the choice of species, the primary beam energy is an important parameter. Beam focusing usually improves with increased beam voltage and would provide better lateral resolution images. However, the higher

the primary energy, the deeper the ion beam penetration and mixing region. This mixing affects the location of the atoms removed and can degrade depth resolution. Depth resolution will be discussed in detail in Chapter 5. Sputter yields are energy dependent so primary beam energy is also an important consideration for analysis time.

3.5 PRIMARY BEAM ANGLE OF INCIDENCE

Primary beam angle of incidence is significant for several considerations. Sputtering yield, secondary ion yield, and penetration into sample (depth resolution) are significantly affected by angle of incidence. As was displayed in figures 2.10 and 2.11, an angle of incidence that is more oblique will result in less penetration and higher sputtering rate. The angle of incidence can also affect the cesium concentration when a Cs^+ primary beam is used [15].

For instruments such as the magnetic sector where primary beam and sample are usually at high voltage, the sample voltage can alter the trajectory of the primary ions and the angle of incidence. For the CAMECA IMS series instruments, the mechanical angle of incidence is 30° from normal. For a positive primary voltage of 10 keV and a positive sample voltage of 4.5 keV (conditions for analysis of positive secondary ions), the actual angle of incidence is 42° from normal for older IMS instruments, as shown in Figure 3.8 [16]. For more recent IMS instruments, O_2^+

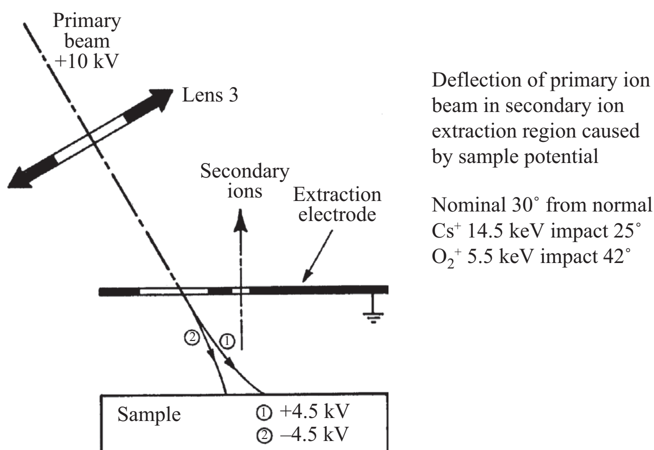

Figure 3.8. Angle of incidence dependence on sample voltage. *Source*: CAMECA instruments early IMS series operating manual, reproduced with permission from CAMECA.

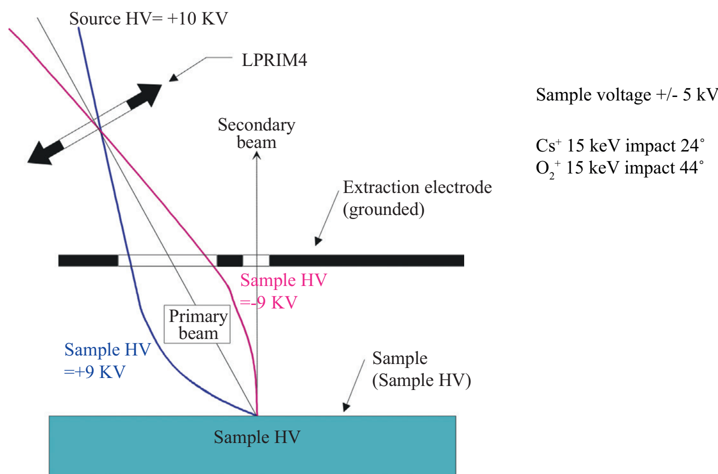

Figure 3.9. Angle of incidence dependence on sample voltage. *Source*: CAMECA instruments, IMS 7F users guide, reproduced with permission from CAMECA.

bombardment at 10 keV and 5 keV sample voltage will be at 44° from normal as shown in Figure 3.9.

3.6 PRIMARY BEAM CURRENT, RASTER SIZE

Changes in primary beam current and raster size permit variation of the sputtering rate. The choice depends on the sample and the rate of analysis desired.

3.7 SECONDARY BEAM ENERGY DISTRIBUTION—VOLTAGE OFFSET

In Chapter 2 it was noted that the peak of the secondary ion energy distribution was less than 10 eV. However, the secondary ion energy distribution does vary with the species detected. The atomic ion has a much broader energy distribution than molecular ions [17] as displayed schematically in Figure 3.10. The higher energy component can be used to reduce the complexity of the mass spectrum [18]. Figure 3.11 shows how voltage offset can be used to limit collection of ions in the high energy portion of the secondary ion distribution [16]. The figure shows the procedure for a CAMECA IMS series instrument where the sample

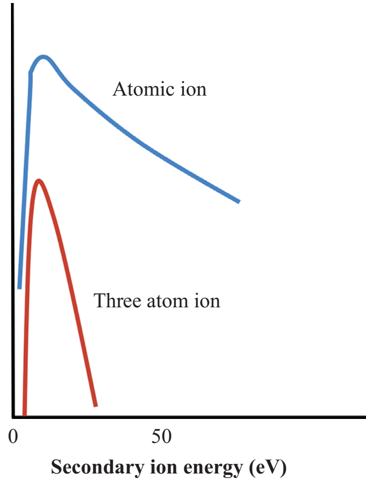

Figure 3.10. Secondary ion energy distribution.

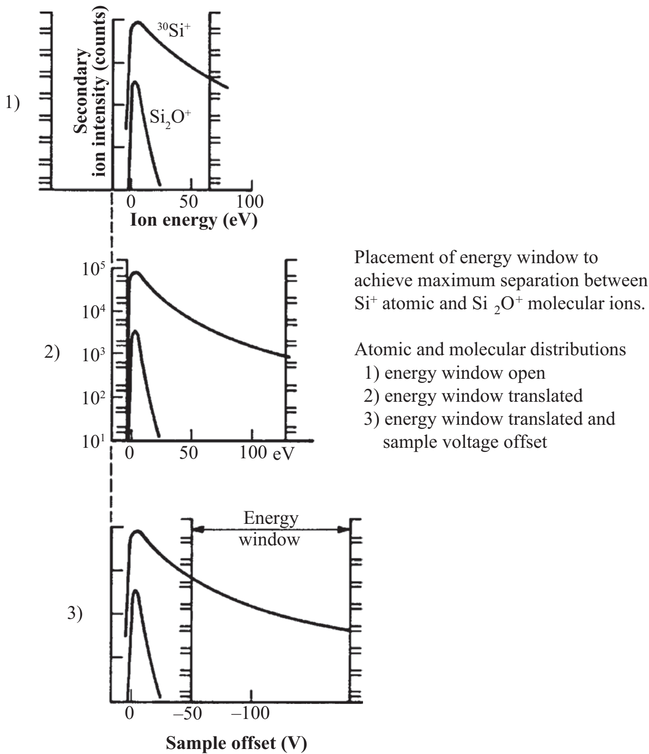

Figure 3.11. Voltage offset.
Source: CAMECA instruments IMS series operating manual, reproduced with permission from CAMECA.

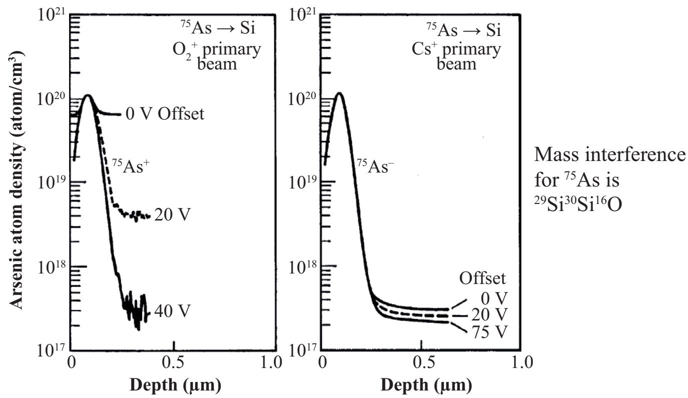

Figure 3.12. Voltage offset.
Source: Wilson, Stevie, and Magee [14].

voltage is offset, but the offset method can also be applied to a quadrupole instrument. The voltage offset method does not provide adequate separation between an atomic ion and a two-atom ion, but works well for separation between an atomic ion and any ion that contains at least three atoms. Figure 3.12 shows voltage offset applied to analysis of a ^{75}As implant in silicon where the mass interference is $^{29}Si^{30}Si^{16}O$ [19]. The voltage offset provides a significant improvement in detection limit for arsenic analyzed with an O_2^+ primary beam. However, the offset method did not result in significant improvement for analysis with a Cs^+ primary beam because there was much less oxygen present to provide the mass interference.

Figure 3.13 shows the effect of voltage offset on a mass spectrum [20]. InSb was analyzed using an O_2^+ primary beam and without offset, and as shown in Figure 3.13 (a), there are a number of molecular ions present. With voltage offset applied as shown in Figure 3.13 (b), the only ions that remain are the atomic ions and the molecular ions that contain two atoms.

It is not always possible to know in advance the amount of offset to be used. The larger the number of atoms in the molecular ion, the easier it is to achieve separation from the atomic ion. The typical approach is to profile the atomic ion with multiple offset voltages applied in the same profile and use the offset that obtains the best detection limit. Note that the absolute signal from the atomic ion is reduced by this method, but the signal to background is improved.

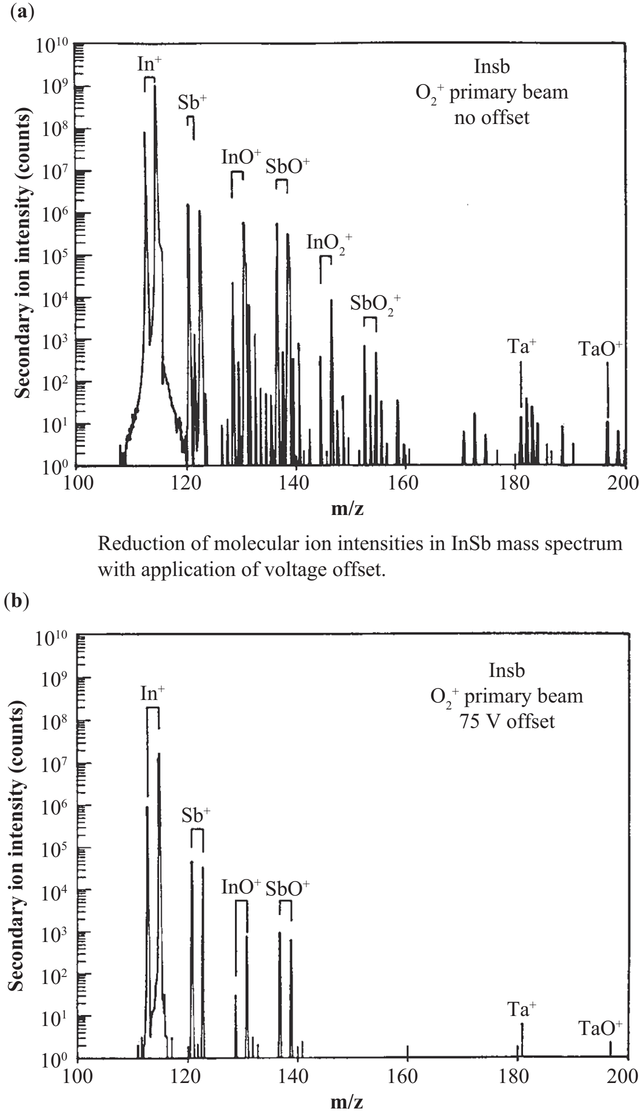

Figure 3.13. Voltage offset on mass spectrum.
Source: Wilson, Stevie, and Magee [14].

3.8 MASS INTERFERENCES, MASS RESOLUTION

Mass interferences affect the ability to accurately measure the species of interest. Mass interferences occur when two species have the same nominal mass, for example, ^{28}Si and $^{12}C^{16}O$ both occur at mass 28. However,

the atomic masses are not exactly the same because of differences in the nuclear binding energies that hold the protons and neutrons together in the nucleus. If we use exact masses, ^{28}Si has mass 27.977 and $^{12}C^{16}O$ has mass 27.995 for 0.018 atomic mass unit difference. Even though this difference is small, SIMS instruments with magnetic sector or time-of-flight analyzers can separate the two species. The mass resolution required to resolve the two is defined as the mass of interest divided by the difference in mass between the two interfering species ($M/\Delta M$) and in this case would be 28/0.018 or 1556. More than one mass interference can be present at the same nominal mass. The species N_2 and C_2H_4 also occur at mass 28. Table 3.4 shows the resolution required to separate some common mass interferences.

Figure 3.14 shows a representation of two species at the same nominal mass in a mass spectrum for different mass resolution conditions. Figure 3.14 (a) shows complete separation and Figure 3.14 (b) shows

Table 3.4. Common mass interferences

Species	Mass	Mass interference	Mass	ΔM	M/ΔM
^{14}N	14.003	$^{12}C^{1}H_2$	14.016	0.013	1077
^{16}O	15.995	$^{12}C^{1}H_4$	16.032	0.037	432
^{27}Al	26.982	$^{12}C_2{}^{1}H_3$	27.024	0.042	643
^{28}Si	27.977	$^{12}C^{16}O$	27.995	0.018	1556
^{28}Si	27.997	$^{14}N_2$	28.031	0.034	824
^{28}Si	27.997	$^{12}C_2{}^{1}H_4$	28.032	0.035	800
^{31}P	30.974	$^{30}Si^{1}H$	30.982	0.008	3875
^{40}Ar	39.962	^{40}Ca	39.963	0.0002	190476
^{46}Ti	45.953	$^{30}Si^{16}O$	45.969	0.016	2875
^{48}Ti	47.948	$^{12}C_4$	48.000	0.052	923
^{48}Ti	47.948	$^{30}Si^{18}O$	47.973	0.025	1920
^{56}Fe	55.935	$^{28}Si_2$	55.954	0.019	2947
^{63}Cu	62.930	$^{35}Cl^{28}Si$	62.946	0.016	3938
^{70}Ge	69.924	$^{28}Si_2{}^{14}N$	69.957	0.033	2121
^{72}Ge	71.922	$^{28}Si_2{}^{16}O$	71.949	0.027	2667
^{74}Ge	73.921	$^{30}Si_2{}^{14}N$	73.951	0.03	2467
^{75}As	74.922	$^{29}Si^{30}Si^{16}O$	74.945	0.023	3261
^{75}As	74.922	$^{74}Ge^{1}H$	74.929	0.007	10714

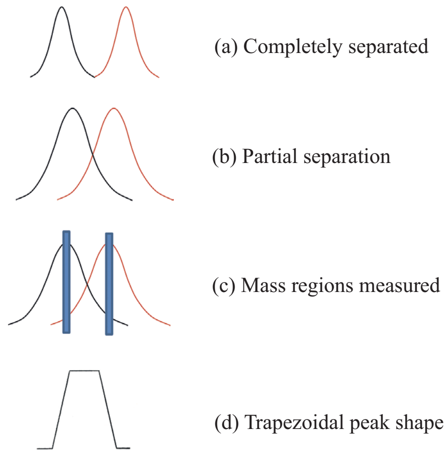

Figure 3.14. Mass resolution. (a) Completely separated, (b) partial separation, (c) mass regions measured, (d) trapezoidal peak shape.

partial separation. Separation requires some criterion, such as full width at half maximum, or 50 percent valley. The 50 percent valley definition refers to the valley height in the sum of the two peaks of equal intensity relative to the peak intensities. Figure 3.14 (c) shows the portions of the mass spectrum that might actually be monitored in a high mass resolution depth profile for the two peaks with the slit settings arranged as shown. The entrance and exit slits are adjusted to provide the mass resolution desired. As indicated in Figure 3.14 (d) the peak shape can be trapezoidal, especially at higher mass for magnetic sector instruments. This is a desirable condition because the mass region actually monitored can be located on a flat topped peak and a small variation in mass stability will not affect the accuracy of the measurement. A flat topped peak is typically achieved when the entrance slit of a magnetic sector mass spectrometer is considerably narrower than the exit slit.

Note that when mass resolution is increased, transmission of secondary ions is decreased. Thus there is a practical limit to the mass resolution that can be achieved using a particular instrument. Some mass interferences require a mass resolution that exceeds the capability of the instrument. For example, ^{75}As in a germanium matrix can have mass interference from $^{74}Ge^{1}H$. The difference is only 0.007 amu and the mass resolution required is 10714, which may be obtained on a magnetic sector instrument but only if the species of interest has sufficient intensity.

Mass interferences are very common in SIMS [21, 22]. Table 3.3 shows many molecular ions detected for the bombardment of silicon with

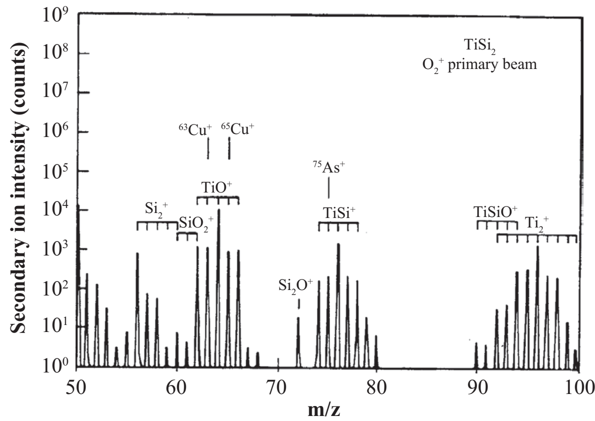

Mass spectrum of $TiSi_2$ from m/z 50 to 100. Numerous mass interferences present because of Ti and Si isotopes and low mass of matrix species.

Figure 3.15. Mass interferences.
Source: Wilson, Stevie, and Magee [14].

O_2^+. Figure 3.15 shows the mass range 50 to 100 for analysis of $TiSi_2$ using an O_2^+ primary beam. There are many peaks present because we have combinations of the ^{16}O primary beam species, three isotopes for silicon, and five isotopes for titanium. Two elements of frequent interest are copper and arsenic. As shown in Figure 3.15, the ^{63}Cu isotope has interference from $^{16}O^{47}Ti^+$ and the ^{65}Cu isotope has interference from $^{16}O^{49}Ti^+$, so use of a different isotope would not help [23]. The ^{63}Cu mass interference requires mass resolution of 3706 and the ^{65}Cu mass interference requires 4333, so the mass 63 isotope would be preferred for analysis and it has higher natural abundance than the mass 65 isotope. For ^{75}As, there is interference from two molecular ions, $^{28}Si^{47}Ti^+$ and $^{29}Si^{49}Ti^+$, and both require mass resolution of 10714, which would be difficult to obtain. Figure 3.16 shows a high resolution mass spectrum for mass 28 to 31 for a silicon substrate using an O_2^+ primary beam [23]. If hydrogen is present, and this should be expected for polycrystalline silicon, then the dopant ^{31}P will have significant interference from $^{30}Si^1H$ and $^{29}Si^1H_2$ as shown in the figure. Figure 3.17 shows how the detection limit for ^{31}P would be improved from use of high mass resolution and a Cs^+ primary beam, which produces much higher secondary ion yield for ^{31}P than an O_2^+ primary beam [24].

Some mass interferences can be difficult to detect. Copper has two isotopes and the lower mass isotope has higher intensity. Figure 3.18 shows analysis of copper in a SiO_2 layer on silicon. Chlorine has often

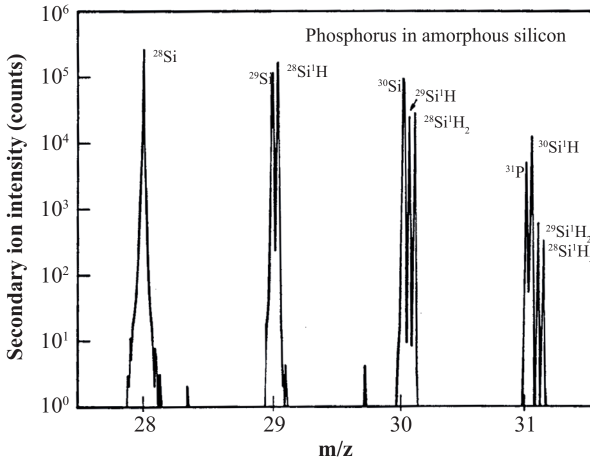

High mass resolution spectrum of P in amorphous Si analyzed using O_2^+ primary beam. High H content causes strong mass interferences.

Figure 3.16. High mass resolution separates mass interferences in Si.
Source: Wilson, Stevie, and Magee [14].

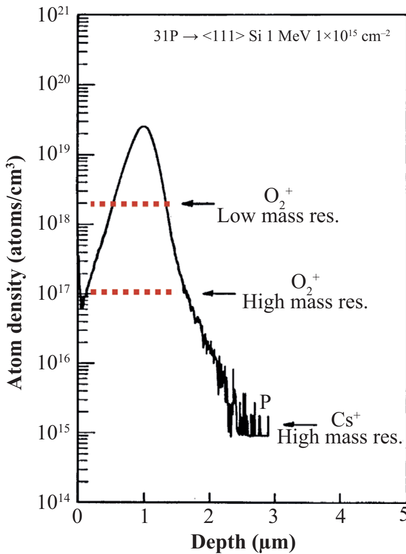

Depth profile of P in Si for Cs^+ bombardment and high mass resolution. Detection limits shown by arrows for Cs^+ and for O_2^+ bombardment at low and high mass resolution.

Figure 3.17. High mass resolution.
Source: Wilson, Stevie, and Magee [14].

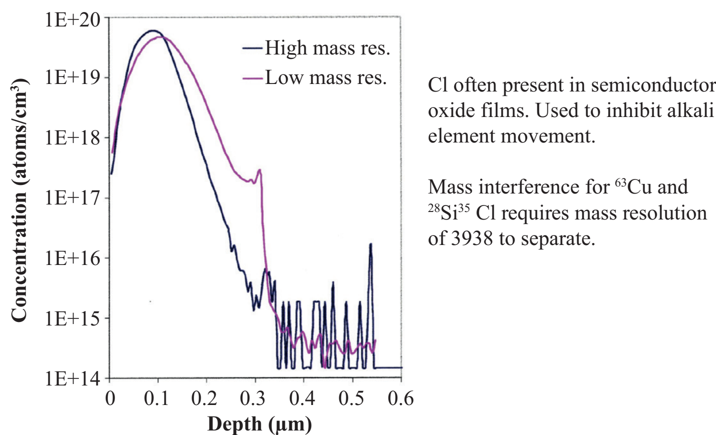

Figure 3.18. Mass interference for Cu in 0.3 µm SiO_2 film on Si.

been added to SiO_2 layers in silicon semiconductor technology in order to reduce the mobility of alkali elements that can degrade the insulating properties of the oxide. Chlorine also has two isotopes, with the lower mass isotope at higher intensity and the ratio of lower mass isotope to higher mass isotope similar to that for copper (3.1 for chlorine and 2.2 for copper). The mass interferences of $^{28}Si^{35}Cl$ with ^{63}Cu and $^{28}Si^{37}Cl$ with ^{65}Cu will therefore have a similar pattern, and for positive secondary ions, $SiCl^+$ has higher secondary ion yield than Cl^+. This means that in a mass spectrum, one may easily detect peaks at mass 63 and 65 and assume they are due entirely to copper because there would be very low chlorine ion yield. Figure 3.18 shows the analysis of ^{63}Cu at low and high mass resolution and indicates how the mass interference might affect the result if not removed.

Information from ion implanted samples can help in determining a mass interference. This information may be useful when high mass resolution cannot be applied or is not available. For example, from O_2^+ analysis of a sodium implant in silicon, it can be determined that the count level for $^{23}Na^{16}O^+$ is 0.002 relative to $^{23}Na^+$. For analysis of $^{39}K^+$, one can determine the amount of $^{23}Na^{16}O^+$ that would be present by multiplying 0.002 times the $^{23}Na^+$ count level.

High mass resolution is not the only method to separate mass interferences. Alternative methods to high mass resolution are the use of different primary beam, molecular ions, other isotopes, or voltage offset. The approach to separate a mass interference can be summarized as

follows: identify the interference, check for other isotopes, determine if voltage offset can be used, and decide which primary beam is best to avoid the interference. If it is necessary to use high mass resolution, determine the mass resolution required, and adjust settings on the instrument to obtain that resolution.

REFERENCES

[1] Benninghoven, A. 1976. "Surface Analysis by Means of Ion Beams." *Critical Reviews in Solid State Sciences* 6, no. 3, pp. 291–316. doi: http://dx.doi.org/10.1080/10408437608243561.

[2] Storms, H.A., K.F. Brown, and J.D. Stein. 1977. "Evaluation of a Cesium Positive Ion Source for Secondary Ion Mass Spectrometry." *Analytical Chemistry* 49, no. 13, pp. 2023–30. doi: http://dx.doi.org/10.1021/ac50021a034.

[3] Wilson, R.G, F.A. Stevie, and C.W. Magee. 1989. *Secondary Ion Mass Spectrometry*, Appendix E. New York: Wiley.

[4] Magee, C.W. 1981. "Secondary Ion Mass Spectrometry and Its Relation to High-Energy Ion Beam Analysis Techniques." *Nuclear Instruments and Methods in Physics Research* 191, no. 1–3, pp. 297–307. doi: http://dx.doi.org/10.1016/0029-554x(81)91019-3

[5] Evans Analytical Group. www.eag.com

[6] Campana, J.E., M.M. Ross, S.L. Rose, J.R. Wyatt, and R.J. Colton. 1983. "Mass Spectrometry of Secondary Ions: Polymers, Plasticizers, and Polycyclic Aromatic Hydrocarbons." In *Ion Formation from Organic Solids*, ed. A. Benninghoven, Vol. 25, Springer Series in Chemical Physics, 144. Berlin, Germany: Springer Verlag.

[7] Xu, J., S. Ostrowski, C. Szakal, A.G. Ewing, and N. Winograd. 2003. "ToF-SIMS Imaging with Cluster Ion Beams." *Applied Surface Science* 231–232, pp. 159–163.doi: http://dx.doi.org/10.1016/j.apsusc.2004.03.104

[8] Fujiwara, Y., N. Saito, H. Nonaka, T. Nakanaga, and S. Ichimura. 2011. "Characteristics of a Charged-Droplet Beam Generated by Vacuum Electrospray of an Ionic Liquid." *Chemical Physics Letters* 501, no. 4–6, pp. 335–39. doi: http://dx.doi.org/10.1016/j.cplett.2010.11.067

[9] Yamada, I. 2014. "Historical Milestones and Future Prospects of Cluster Ion Beam Technology." *Applied Surface Science* 310, pp. 77–88. doi: http://dx.doi.org/10.1016/j.apsusc.2014.03.147

[10] Werner, H.W. 1978. "Introduction to Secondary Ion Mass Spectrometry (SIMS)." In *Electron and Ion Spectroscopy of Solids*, eds. L. Fiermans, J. Vennik, and W. Dekeyser, 324. New York: Plenum Press.

[11] Pantano, C.G. 1986. "Secondary Ion Mass Spectroscopy." In *Metals Handbook Ninth Edition,* Vol. 10—Materials Characterization, ed. R.E. Whan, 610. American Society for Metals, Metals Park.

[12] Chunzhi, G. 2005. *SIMS Quantification of Matrix and Impurity Species in III-Nitride Alloys* [ProQuest Dissertations and Theses; Thesis (Ph.D.)]. North Carolina State University, Vol. 67–06, Section B, p. 3385, 198.

[13] Wilson, R.G, and S.W. Novak. 1988. "Systematics of SIMS Relative Sensitivity Factors versus Electron Affinity and Ionization Potential for Si, Ge, GaAs, GaP, InP, and HgCdTe Determined from Implant Calibration Standards for about 50 Elements." In *Secondary Ion Mass Spectrometry, SIMS VI*, eds. A. Benninghoven, A.M. Huber, H.W. Werner, 57. Chichester, United Kingdom: Wiley.

[14] Wilson, R.G., F.A. Stevie, and C.W. Magee. 1989. *Secondary Ion Mass Spectrometry*, 1.6–10. New York: Wiley.

[15] Wittmaack, K. 1985. "Influence of the Impact Angle on the Depth Resolution and the Sensitivity in SIMS Depth Profiling Using a Cesium Beam." *Journal of Vacuum Science & Technology A* 3, no. 3, p. 1350. doi: http://dx.doi.org/10.1116/1.572775

[16] CAMECA Instruments IMS Series Operating Manuals.

[17] Wittmaack, K. 1979. "On the Mechanism of Cluster Emission in Sputtering." *Physics Letters A* 69, no. 5, 322–25. doi: http://dx.doi.org/10.1016/0375-9601(79)90421-3

[18] McIntyre, N.S., W.J. Chauvin, J.B. Metson, and G.M. Bancroft. 1984. "Suppression of Molecular Ions in Secondary Ion Mass Spectra." *Le Journal de Physique Colloques* 45 no. C2, pp. C2-143 to C2-146. doi: http://dx.doi.org/10.1051/jphyscol:1984232

[19] Wilson, R.G., F.A. Stevie, and C.W. Magee. 1989. *Secondary Ion Mass Spectrometry*, 1.8–5. New York: Wiley.

[20] Wilson, R.G, F.A. Stevie, and C.W. Magee. 1989. *Secondary Ion Mass Spectrometry*, 1.8–7. New York p: Wiley.

[21] Colby, B.N., and C.A. Evans, Jr. 1973. "Spectral Interferences in Secondary Ion Mass Spectrometry." *Applied Spectroscopy* 27, no. 4, pp. 274–79. doi: http://dx.doi.org/10.1366/000370273774333515

[22] Bakale, D.K, R.N. Colby, and C.A. Evans, Jr. 1975. "High Mass Resolution Ion Microprobe Mass Spectrometry of Complex Matrices." *Analytical Chemistry* 47, no. 9, pp. 1532–37. doi: http://dx.doi.org/10.1021/ac60359a037

[23] Wilson, R.G, F.A. Stevie, and C.W. Magee. 1989. *Secondary Ion Mass Spectrometry*, 2.11–6. New York p: Wiley.

[24] Wilson, R.G., F.A. Stevie, and C.W. Magee. 1989. *Secondary Ion Mass Spectrometry*, 2.11–7. New York p: Wiley.

CHAPTER 4

INSTRUMENTATION

4.1 VACUUM SYSTEM

Analytical instruments involving charged particle beams require a vacuum environment so that ions can move freely in the chamber and the adsorption of residual gas species on the sample surface is reduced. The mean free path of a charged or neutral species in a vacuum chamber is the average distance the species can travel without colliding with another particle. As the pressure in the volume of interest is increased, the probability of a collision that will change the intended trajectory of the ion increases and the mean free path decreases. The mean free path for air at room temperature can be expressed by

$$\lambda = \text{constant}/P = 5 \times 10^{-3}/P \qquad (4.1)$$

where P is the pressure in Torr and λ has dimension of cm

At 1×10^{-6} Torr the density is 3.25×10^{10} molecules/cm^3 and the mean free path is 51 m. A typical secondary ion mass spectrometry (SIMS) magnetic sector or time-of-flight (TOF) instrument has a path length of about 2 m. At 1×10^{-9} Torr the density is 3.25×10^{7} molecules/cm^3 and the mean free path increases to 51 km.

An important concept concerning vacuum construction and safety is the pressure differential across the vacuum chamber wall. The difference is the pressure exerted by the atmosphere, which is 14.7 lb/in^2 (10.1 n/cm^2). For example, the force on a six inch (15.2 cm) diameter surface is 415 lb (1846 n). This helps explain why vacuum systems are built of sturdy materials, such as stainless steel. The AVS has publications on vacuum technology and safety that can be consulted for additional information [1, 2].

Another vacuum consideration is the adsorption onto the sample of residual gas species (H, C, N, O) present in the vacuum system. This can

cause problems with detection limits for these species. For example, if the sticking coefficient is one (every atom that lands is adsorbed on the surface), then at 1×10^{-6} Torr one monolayer is adsorbed every second. It would be necessary to achieve a background pressure of at least 10^{-8} Torr to have 100 seconds to do the analysis. The sticking coefficient is usually less than one, but low analysis chamber vacuum is important for surface analysis and typical analysis pressures are in the 10^{-10} Torr range.

SIMS instruments have employed almost every type of vacuum pump to achieve the desired vacuum. Most modern systems use turbo molecular pumps and dry fore pumps (scroll pumps) where high gas loads are expected, such as for sample introduction, and ion pumps for the analysis chamber. If oxygen flood is used in the analysis chamber, then turbo molecular pumps will be used instead of ion pumps. The dry fore pumps contain no oil and eliminate contamination due to oil back streaming. Titanium sublimators are used to reduce background gases, particularly H, which is the dominant gas at ultrahigh vacuum. If residual gas species (H, O, C, N) are to be analyzed, then dry or oil-free pumping solutions (ion pump, Ti sublimator, cryo-pump) will be preferred.

4.2 OVERALL INSTRUMENT

Figure 4.1 shows a block diagram of a SIMS instrument. One or more primary beam sources are coupled to an ion column. The ion column focuses the primary beam and provides the raster. The beam interacts with the specimen in the sample chamber. In the secondary ion column the secondary ions are extracted and energy and mass are analyzed before the ions are detected. Multiple detectors are used to accommodate the wide dynamic range for SIMS and a computer controls the operation of the system.

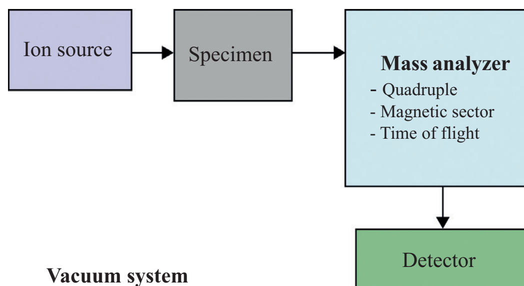

Figure 4.1. SIMS instrument block diagram.

4.3 ION SOURCES

The most common primary ion beams are O_2^+ and Cs^+ because the chemical effects that occur when these ions bombard the sample surface enhance positive and negative secondary ion yields, respectively. Other sources have been developed, especially to provide very shallow penetration for the analysis of regions close to the surface. For example, use of SF_6 to provide a SF_5^+ ion beam reduces the interaction zone to achieve optimal penetration when compared with Ga^+, and C_{60}^+ has even shallower penetration.

A commonly used source for ionization of gas species is the duoplasmatron, which is an arc discharge ion source. Figure 4.2 shows the construction of the duoplasmatron, which has an anode, a cathode, an intermediate electrode and a coil [3]. The intermediate electrode and coil are used to reduce the beam diameter and are the origin of the name of the source. The duoplasmatron provides a high ionization efficiency (>80%), low energy spread (~30 eV), and high current density 100 mA/cm^2). Many different gaseous species have been used (Ar, Xe, O_2, N_2, SF_6). Negative ions can be obtained by using the edge of the plasma instead of the center. O^- is often used for the analysis of minerals because the negative primary beam aids in charge neutralization. Note that the cathode (typically nickel construction) oxidizes over time and, as the oxide powder builds up, the duoplasmatron performance will be degraded so that maximum current will be reduced and the plasma that generates the primary current will not be as well defined. The anode, cathode, and intermediate electrode need to be cleaned at regular intervals to remove the oxide.

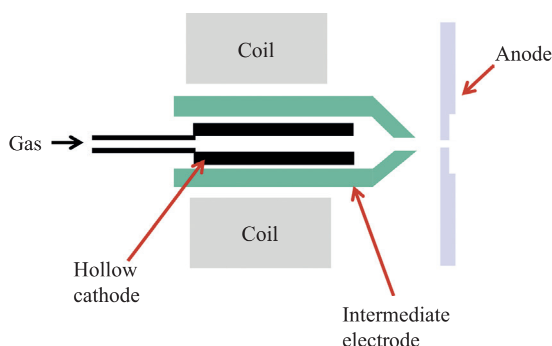

Figure 4.2. Duoplasmatron.

Radio frequency (RF) plasma sources have now been adapted to SIMS instruments and can be used with oxygen. Both Oregon Physics and Orsay Physics (TESCAN) have sources available. Very small beam size can be achieved (46 nm at 0.86 pA), with brightness at least 10 times more than the duoplasmatron.

Thermal ionization cesium sources consist of a reservoir to contain the cesium or cesium compound (cesium carbonate, Cs_2CO_3, is currently being used on CAMECA microbeam sources) and a tungsten frit as shown in Figure 4.3 [4]. The reservoir is heated only enough to provide sufficient cesium vapor pressure (cesium kinetic energy about 4 eV) to the frit. The frit (4.7 eV work function) is kept at 1000°C. As cesium vapor strikes the frit, the work function acts to remove an electron and the cesium ion evaporates from the tungsten due to high temperature. Cesium leaving the frit is essentially completely ionized. An extraction voltage is used to direct the Cs^+ into the primary column. This extraction voltage must be present while the source generates cesium ions otherwise the cesium will coat the extraction lens. Subsequent cesium ions striking a cesium-coated surface produce a high number of secondary electrons that cause a leakage current to the source that can be high enough to prevent operation. Current density is approximately 5 mA/cm^2.

Liquid metal ion source (LMIS) is used for imaging and for TOF analysis. The LMIS uses gallium almost universally for focused ion beam (FIB) instruments, but other sources, such as bismuth or composites

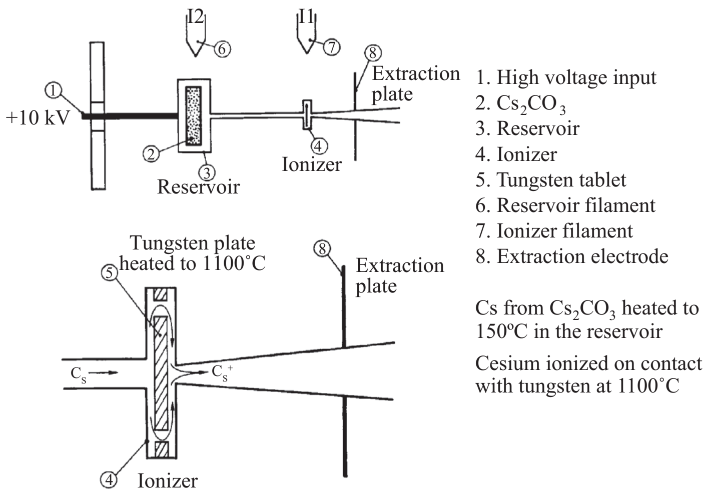

Figure 4.3. Cesium microbeam source.
Source: CAMECA instruments, reproduced with permission from CAMECA.

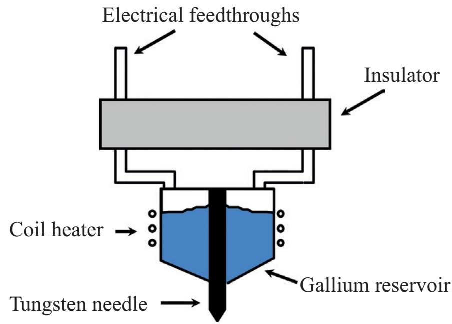

Figure 4.4. Liquid metal ion source (LMIS).

(gold–beryllium), are used in TOF-SIMS instruments. For the gallium source a gallium droplet is heated and gallium flows to wet a tungsten needle, as shown in Figure 4.4. The field differential at the tip is very high (~10^8 V/cm) and gallium ions are extracted by field ionization. The gallium flow and high electric field cause the formation of an elongated conical shape (Taylor cone) [5]. The LMIS column on commercially available FIB instruments can provide <10 nm diameter beams. The vacuum requirement in the tip region is similar to that for field emission electron sources.

C_{60} is a large molecule that does not penetrate significantly into the sample compared with Ga^+. The energy of the incident ion is transferred to the top few monolayers and generates high sputtering yield and minimal damage. This source helps provide high molecular ion yields for many TOF-SIMS analyses of organic materials. However, at low energies the C_{60} sputtering yield for silicon decreases to the point where deposition occurs instead of sputtering [6]. The source generates C_{60}^+ ions by vaporizing a powder and then ionization with low energy electron impact. At 10 to 20 keV, a current of 2 nA can be achieved [7].

A recent addition to the array of SIMS sources is the argon cluster beam. Ar clusters form as a result of a cooling process when a jet of high pressure gas expands into a vacuum. The cluster is ionized by electron bombardment. Sources can provide clusters from two to over 2000 atoms selected by Wien filter. Beam energy can be 5 to 20 keV. For Ar_{1700} and voltage to provide 2 eV/atom, the impact on the sample is low and high secondary ion yields can be achieved with reduced damage to the specimen. Water cluster sources with as many as 1,000 H_2O molecules in one cluster have shown promise as the latest advance in cluster beams [8].

Table 4.1 summarizes the properties of the ion sources in common use.

Table 4.1. Properties of SIMS sources

Type	Beam species	Beam diameter	Current density
Duoplasmatron	O_2^+, O^-, Ar^+, SF_5^+	500 nm	100 mA/cm^2
Thermal ionization	Cs^+	200 nm	5 mA/cm^2
LMIS	Ga^+	5–7 nm	1 A/cm^2
MIIS (Au-Ge)	Au^+, Au_2^+, Au_3^+	50 nm	
	Bi_3^{2+}	60 nm	
Electron impact	C_{60}^+	200 nm	
RF plasma	O_2^+	50 nm	>1 A/cm^2

4.4 PRIMARY ION COLUMN

The source is just the first component in the ion column [9] as shown in Figure 4.5. A mass separator is used to select the species of interest, such as O_2^+, and reject unwanted species such as O^+ and contaminants. The beam is then focused with electrostatic lenses and apertures and rastered over the analysis location.

4.5 SAMPLE CHAMBER AND SAMPLE

The sample chamber is designed to permit the sample to be moved so that the region of interest can be bombarded by the ion beam. Electron gun and oxygen flood sources are often used and are located in this chamber. If available, a rotation capability for the sample holder can help minimize topography formation due to nonuniform sputtering of the sample (see Chapter 5).

Electron sources for charge neutralization would normally have condenser and objective lenses. Different voltage ranges are used on different instruments and information on analysis of insulators is provided in Chapter 8.

4.5.1 SAMPLE REQUIREMENTS

The sample requirements for SIMS analysis can be summarized as vacuum compatible and sized to fit the sample holder. If a sample is outgassing or if it contains pockets or occlusions of a gas or liquid, it can seriously impact

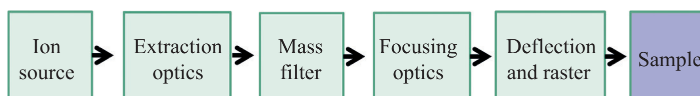

Typical sources are duoplasmatron for O_2^+ and surface ionization for Cs^+.
Extraction optics provide beam extraction, preliminary focusing, acceleration.
Ions are mass separated, focused, and rastered.

Figure 4.5. Primary ion column components.

the vacuum level in the instrument, which will affect static SIMS results and the ability to analyze gas elements such as oxygen and carbon. If it is necessary to analyze a sample that may have volatile components, the analysis time must be very limited or the sample can be cooled to reduce the vapor pressure. Powder samples present special problems. If particles are allowed to freely move in the analysis chamber, major damage can occur because particles can block an aperture or short an electrode. Virtually all SIMS instruments can accommodate a sample that is 1 cm × 1 cm × a few mm thick. The surface should be flat if good depth resolution and uniform extraction of secondary ions are desired. Since SIMS analyses are usually obtained from areas less than 500 µm × 500 µm, the samples are often less than 1 cm × 1 cm. However, sample chambers have been constructed to handle 300 mm diameter wafers for instruments of all three analyzer types (magnetic sector, TOF, and quadrupole).

4.6 SECONDARY ION COLUMN AND MASS ANALYZERS

The secondary ion column also has multiple components. Secondary ion extraction and transfer optics are designed to optimize the number of secondary ions that can be obtained from the analysis region. There are three types of analyzers used in SIMS: magnetic sector, quadrupole, and TOF. Each analyzer provides different capabilities but all separate ions by their mass to charge ratio. The quadrupole uses a set of RF and DC electric fields, the magnetic sector an electromagnet, and the TOF a flight tube.

4.6.1 QUADRUPOLE

Ions are injected at low energy (~25 eV) into a quadrupole analyzer comprised of four closely spaced circular rods with RF and DC voltages applied to pairs of rods [10]. As shown in Figure 4.6, one pair has

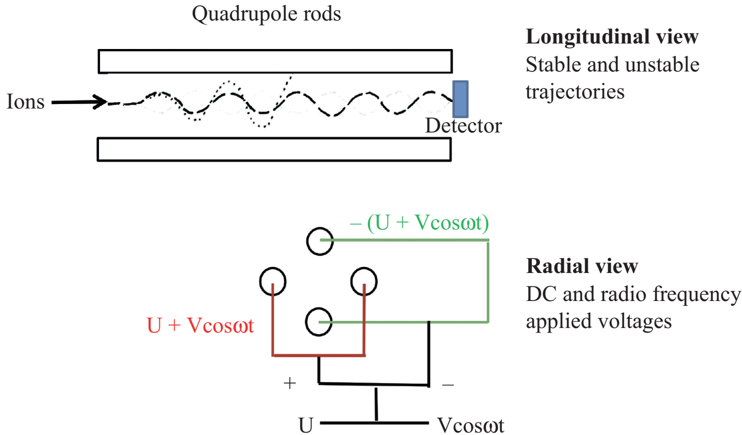

Figure 4.6. Quadrupole analyzer.

U+Vcos(ωt) and the other –(U+Vcos(ωt)), where U is a DC voltage and Vcos(ωt) an RF voltage. The RF voltages for one pair of rods are 180° out of phase with the RF voltages applied to the other pair. For a given RF and DC voltage combination, ions with a specific mass to charge ratio will undergo stable oscillations and pass through the quadrupole. All other ions will have unstable oscillations and will hit the rods. As the voltages are scanned, a mass spectrum can be obtained. The alternating frequency and the ratio between alternating and DC voltages remain constant. The larger the rods, the better the performance will be in terms of transmission and mass resolution. Rods on the order of 1 cm diameter with 20 cm or longer length are used for SIMS analyzers, but much smaller assemblies are often used for residual gas analysis where the mass range may be less than 100 amu.

This analyzer is easy to use and has fast mass switching. It is possible to analyze positive and negative secondary ions in the same depth profile. Because the injection voltage is low, it is possible to use very low energy primary beams, which provide good depth resolution. The open geometry permits optimum positioning of an electron gun, which permits good charge neutralization.

One mass is transmitted at a time. Mass resolution and mass range are limited. This analyzer has transmission about a factor of 50 lower than other analyzers and transmission drops off more rapidly at high mass. The energy band pass is limited to ~10 eV and secondary ions are more susceptible to charging effects.

4.6.2 MAGNETIC SECTOR

Magnetic sector SIMS instruments use an electrostatic sector coupled with a magnetic sector to provide a double focusing instrument as shown in Figure 4.7. The electrostatic sector provides energy dispersion and the magnetic sector mass dispersion as shown in the trajectories for three different energies in Figure 4.8 [11]. The separation of mass to charge ratio is accomplished using the relationships of:

potential energy of an ion is equal to kinetic energy after acceleration

$$qV = \frac{1}{2} mv^2 \tag{4.2}$$

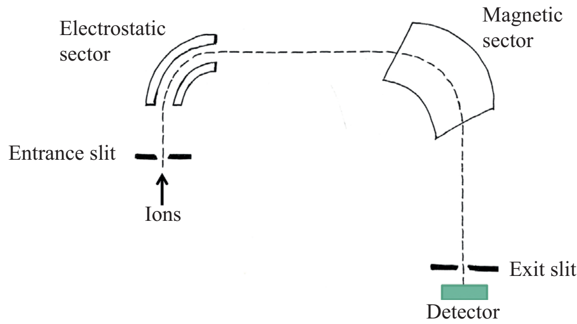

Figure 4.7. Double focusing magnetic sector analyzer.

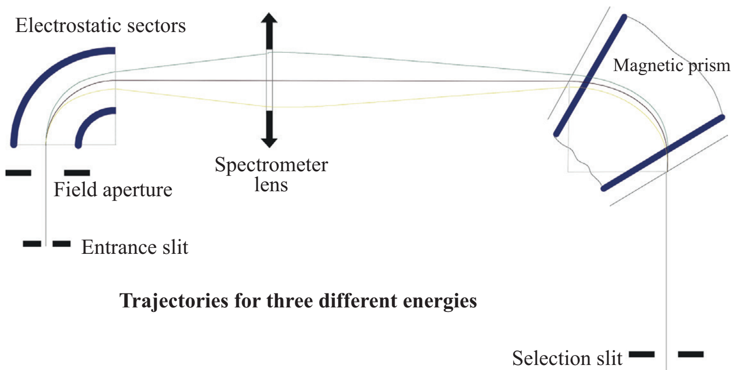

Figure 4.8. Ion trajectories for magnetic sector.
Source: CAMECA-IMS 6f user guide (1996), reproduced with permission from CAMECA.

in a magnetic field, centripetal force is equal to centrifugal force

$$Bqv = mv^2/R \tag{4.3}$$

with result

$$m/q = B^2r^2/2V \tag{4.4}$$

where m/q is the mass to charge ratio, B is the magnetic field, V is the accelerating voltage of a secondary ion, r is the radius of curvature for the ion to pass through the magnetic field.

For constant r and V, the mass range of interest is scanned by varying the magnetic field.

The magnetic sector analyzer provides high mass resolution (10,000 to 25,000) and has the best sensitivity of all the analyzers. Transmission is high and the energy acceptance is large (~120 eV). High quality optical gating is employed to reduce crater edge effects that can degrade depth resolution and detection limit. Entrance and exit slits are adjusted to vary mass resolution.

Magnetic sector analyzers are typically large and expensive instruments. The ions to be analyzed in a depth profile must be selected before starting the profile. The analyzer has relatively slow mass switching. The extraction field is high with a small gap, which makes it difficult to employ a low energy primary beam.

Schematic drawings of the CAMECA IMS-7F and NanoSIMS50L instruments are shown in figures 4.9 and 4.10 [12]. Magnetic sectors have been primarily used for depth profiling of inorganics; however, the high lateral resolution of the NanoSIMS50 series of instruments has also been applied to the analysis of a number of organic materials. Specially designed instruments have been made, especially for the analysis of geological samples or meteorites where measurement of the isotopic abundance is very important. For these instruments, multiple detectors are arranged so that all the isotopes of the same element are detected at the same time. Current examples are the IMS 1280-HR from CAMECA [13] (www.cameca.com) and the Shrimp II from Australian Scientific Instruments [14] (shrimp.anu.edu.au).

There are two imaging strategies: ion microscope, where spatial resolution is determined by stigmatic optics, and ion microprobe, where spatial resolution is determined by size of the primary beam.

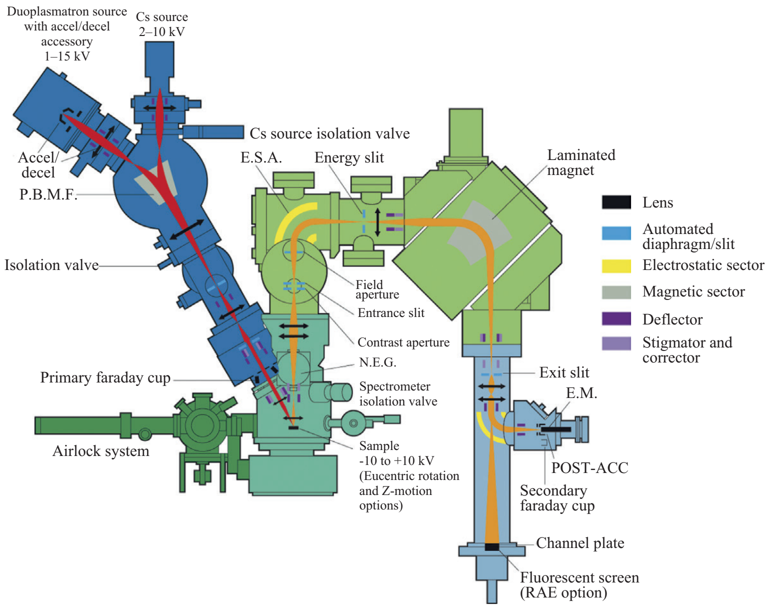

Figure 4.9. CAMECA IMS 7f magnetic sector analyzer.
Source: CAMECA instruments, reproduced with permission from CAMECA.

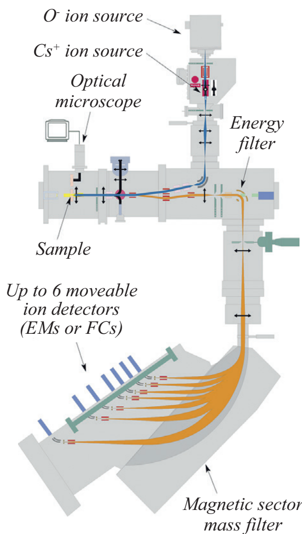

Short working distance lens allows small primary ion beam size and optimum secondary ion extraction

Simultaneous detection of up to 7 ion species maximizes sample usage and accuracy of signal ratios

Primary ion impact energy 16 keV

Depth resolution ~ 10–20 nm

Requires Cs^+ for negative ions (50 nm) and O^- for positive ions (50 nm)

Figure 4.10. CAMECA NanoSIMS 50L magnetic sector analyzer.
Source: CAMECA instruments, reproduced with permission from CAMECA.

Because the magnetic sector sample is held at a high potential in order to inject ions into the secondary column, the primary ion beam will be deflected as it approaches the sample and the angle of incidence will be altered. On the CAMECA IMS series of instruments, the nominal incidence angle is 30° from normal. For a positive primary beam and sample voltage, the beam will be slightly repelled and the angle of incidence will be higher (about 42° from normal for 10 keV beam and 4.5 kV sample). For positive primary and negative secondary voltages, the beam will be attracted to the sample and the angle of incidence will be less than 30° from normal [15].

It is useful to calculate some of the parameters for primary and secondary beams using a magnetic sector (CAMECA IMS-3f) with sample at 4500 V and detection of positive secondary ions. For a 10 keV 150 nA O_2^+ primary beam rastered over a 200 µm × 200 µm area on a silicon substrate, the O_2^+ velocity is

$$\begin{aligned}(2qV/m)^{1/2} &= (2 \times 1.6 \times 10^{-19} \text{ coul} \times 10000 \text{ V}/(32 \times 1.67 \times 10^{-27} \text{ kg}))^{1/2} \\ &= 2.45 \times 10^5 \text{ m/s} \qquad (4.5)\end{aligned}$$

and flight time for primary column is 1.12 m/(2.45 × 10^5 m/s) = 4.6 µs

The O_2^+ current density is 150 nA/(200 µm × 200 µm) = 0.38 mA/cm^2

The O_2^+ flux is 0.38 × 10^{-3} coul/s/cm^2/1.6 × 10^{-19} coul/ion = 2.3 × 10^{15} ions/cm^2s

For the 200 µm × 200 µm area, this is 9.2 × 10^{11} ions/s.

For the secondary ions, with 150 nA primary beam on silicon, 10 to 20 nA total secondary ions can be measured before entry into the electrostatic analyzer.

The $^{28}Si^+$ velocity is 1.75 × 10^5 m/s

$^{28}Si^+$ flight time for secondary column is 1.72 m/1.75 × 10^5 m/s = 9.8 µs

The material removed from 1 µm deep crater has a volume of 4 × 10^{-8} cm^3, and with silicon density of 5 × 10^{22} atoms/cm^3 or 2.33 g/cm^3, the silicon removed = density/volume = 2 × 10^{15} atoms = 93 ng

For a detected area of 60 µm diameter, the volume = 2.83 × 10^{-9} cm^{-3} (ratio of detected volume to crater volume is 1/14) and the silicon removed is 1.4 × 10^{14} atoms or 6.6 ng

By comparison, for a Ga^+ LMIS,

$$1 \text{ nA } Ga^+ \times (1 \text{ ion}/1.6 \times 10^{-19} \text{ coul}) = 6.25 \times 10^9 \text{ ions/s} \qquad (4.6)$$

The Ga^+ current density over a 5 µm × 5 µm area is 4 mA/cm^2.

4.6.3 TIME OF FLIGHT

TOF instruments operate by pulsing the primary beam onto the specimen [16]. The analyzer uses the difference in flight time for secondary ions through a field free drift region (typically ~2 m long) to separate ions of different masses as shown in Figure 4.11. All secondary ions have kinetic energy equal to the potential energy of an ion in an electric field

$$\tfrac{1}{2}mv^2 = qV \tag{4.7}$$

where q is the charge on the ion, V is the extraction voltage, m is the ion mass and v is the ion velocity

$$v = d/t$$

where d is the length of the drift tube and t is the time to traverse that distance

Flight time can then be expressed by

$$t = d(m/2qV)^{1/2} \tag{4.8}$$

so that flight time is proportional to the square root of mass

For the same kinetic energy, ions of lighter mass will reach the detector faster than ions of heavier mass. For a 1000 Da ion, 2.0 m flight path, and 2 kV extraction voltage, the flight time would be

$$t = 2.0\ \text{m}[(1000\ \text{Da})\ (1.67 \times 10^{-27}\ \text{kg/Da})/((2)(1.6 \times 10^{-19}\ \text{coul})(2000\ \text{V}))]^{1/2}$$
$$= 102\ \mu\text{s}$$

The pulsing of the primary beam and the cycle time can be varied. Common values are 1 through 10 ns for the primary beam pulse width and

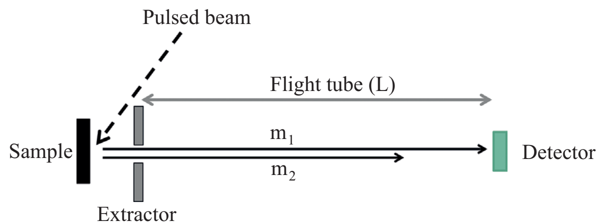

Figure 4.11. Time of flight analyzer.

a duty cycle (beam on/beam off) of 10^{-3} to 10^{-5}. Since the duty cycle is low, the sputtering rate will be much slower than an instrument that uses a continuous primary beam. If a second ion beam is used to sputter the specimen during the off time of the cycle, the sputtering rate can be much higher. An example of a timing diagram is shown in Figure 4.12. An electron beam can also be applied between analysis pulses in order to provide charge neutralization. LMISs have lateral resolution less than 10 nm but with a pulsed beam the lateral resolution is closer to 100 nm. An example of a reflectron based instrument (ION-TOF) is shown in Figure 4.13 and an electrostatic sector (Physical Electronics) in Figure 4.14.

Parallel detection of all masses permits retrospective analysis. This instrument has high transmission (10 to 90%) and high mass resolution (>10,000). In addition, it has a high mass range, theoretically unlimited

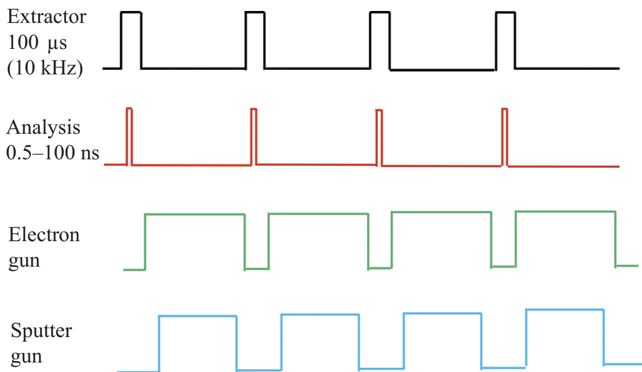

Figure 4.12. TOF-SIMS timing diagram.

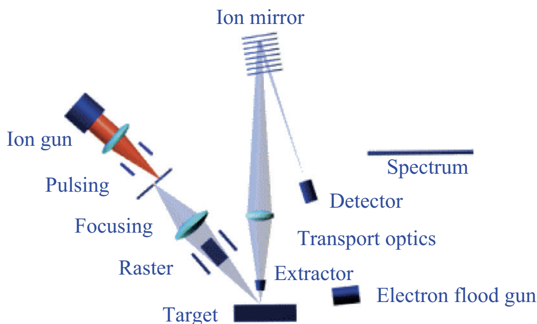

Figure 4.13. TOF-SIMS reflectron analyzer.
Source: ION TOF, reproduced with permission.

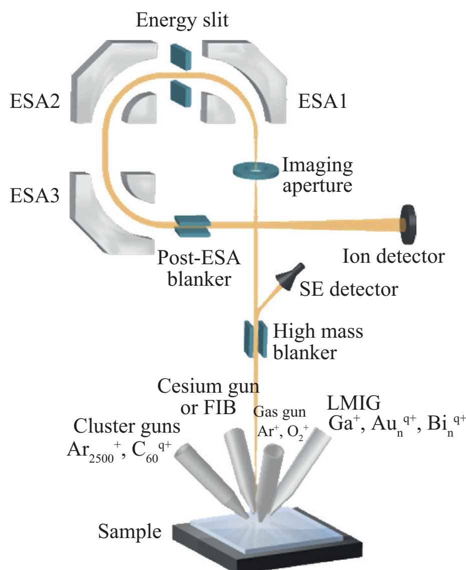

Figure 4.14. TOF-SIMS electrostatic analyzer. *Source*: Physical electronics PHI nano TOF II reproduced with permission.

with relatively simple mass calibration. TOF-SIMS is ideal for analysis of organic or inorganic surfaces and the pulsed electron method works well for insulators.

Operation requires a pulsed primary beam. If additional ion and electron sources are used, they must also be pulsed. Ions are extracted with high field and small gap similar to the magnetic sector. Ion sources that use elements with more than one isotope, such as gallium, must be monoisotopic.

Properties of the three types of mass analyzers are summarized in Table 4.2. Even though mass resolution is limited, the quadrupole provides good depth resolution because it can easily operate at low impact energy. The magnetic sector can analyze with high primary current and has the best sensitivity. The TOF has the best transmission and can most easily obtain high mass resolution.

4.7 DETECTORS

To cover the range of secondary ion intensities, more than one secondary ion detector is required. Several detectors have been used [17, 18] but

Table 4.2. Comparison of mass analyzers

Type	Resolution	Mass range	Transmission	Mass detection	Relative sensitivity
Quad	<1000	<1000	0.01–0.1	sequential	1
Magnet	10000	>1000	0.1–0.5	sequential	50
TOF	10000	>1000	0.5–0.9	parallel	10000

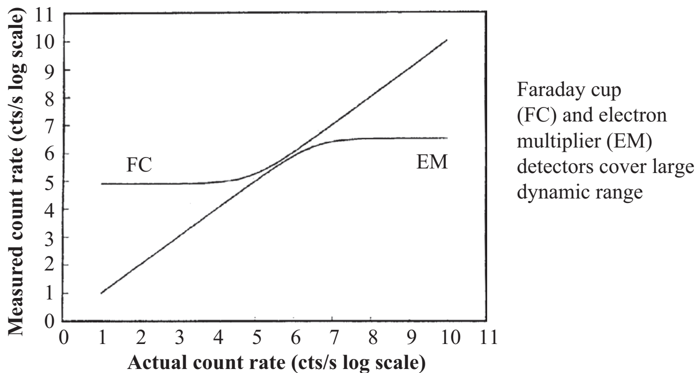

Theoretical response of electron multiplier and Faraday cup detectors. Electron multiplier dead time assumed to be 300 ns and offset of Faraday cup detector equivalent to 8×10^4 cts/sec

Figure 4.15. Faraday cup and electron multiplier responses.

Faraday cup and electron multiplier are most often paired. Figure 4.15 shows how the two detectors can measure secondary ion currents over a dynamic range that can exceed nine orders of magnitude. The electron multiplier is subject to dead time issues for high current rates [19]. The Faraday cup is used for higher ion currents and the electron multiplier for count rates down to zero. The performance of the multiplier is remarkable since it provides a gain of $\sim 10^8$.

4.8 FOCUSED ION BEAM SIMS (FIB-SIMS)

The combination of a FIB primary source with the detection of secondary ions is referred to as FIB-SIMS and provides the opportunity to acquire elemental information from a very small region. This high lateral resolution has been exploited for some time, particularly by the Levi-Setti

group at University of Chicago [20]. The FIB utilizes the LMIS described earlier in this chapter, and sources of this type with beam diameter less than 10 nm are commercially available. The secondary ion yields from the gallium LMIS are similar to those for an argon primary beam, which are about a factor of 50 to 100 less than for an oxygen primary beam. However, with yield enhancement from an oxygen leak or oxygen or cesium beams, FIB-SIMS has the potential to provide isotope-specific elemental and impurity microanalyses to the parts per thousand range and below. Plasma ion sources and scaled down TOF-SIMS analyzer offer new possibilities for small area analysis. Initial results with a xenon plasma source on a TESCAN instrument show ppm detectability for lithium, sodium, and potassium without enhancement by oxygen [21], and use of an oxygen plasma source should provide higher secondary ion yields.

4.9 COMPUTERS AND DATA MANIPULATION

Computers are used to control the instrument and reduce and transmit data. Automatic operation and three-dimensional analysis are possible. The amount of memory required for a high resolution mass spectrum or image depth profile using TOF-SIMS is no longer an issue with the availability of inexpensive terabyte storage.

Some data processing is relatively simple and provides conversion of sputtering time to depth and count rate to concentration. However, interpretation and reduction of TOF-SIMS data can require days of time for hours of analyses.

4.10 RELATED INSTRUMENTS

For many species sputtered, the ionization probability is low and most of the sputtered species are neutrals. High ion yields can be obtained by ionizing the neutral species ejected during sputtering with lasers, electrons, or plasmas. This approach is called postionization or sputtered neutral mass spectrometry and can provide better detection limits with potentially fewer matrix related ion yield variations than the instruments that collect just secondary ions. For example, if 25 percent of the sputtered atoms are present in the laser beam zone and 100 percent ionization can be obtained, then with 50 percent transmission a useful yield of 10 percent can be achieved. Useful yield is defined as the number of ions detected relative to the number of atoms present in the analysis area. However,

the actual result for many elements is similar to that for traditional SIMS instruments and without a clear advantage, the postionization instruments have had limited success [22–29].

REFERENCES

[1] AVS website www.avs.org

[2] O'Hanlon, J.F. 1980. *A User's Guide to Vacuum Technology*. New York: John Wiley & Sons.

[3] Werner, H.W. 1978 "Introduction to Secondary Ion Mass Spectrometry (SIMS)." In *Electron and Ion Spectroscopy of Solids*, eds. L. Fiermans, J. Vennik, and W. Dekeyser, 324. New York: Plenum Press.

[4] CAMECA Instruments. 1996. *Microbeam Cesium Source Principle, IMS 6-F User's Guide*, pp. 1–65

[5] Kingham, D.R., and L.W. Swanson. 1984. "Shape of a Liquid Metal Ion Source." *Applied Physics A* 34, no. 2, p. 123–32. doi: http://dx.doi.org/10.1007/bf00614764

[6] Gillen, G., J. Batteas, C.A. Michaels, P. Chi, J. Small, E. Windsor, A. Fahey, J. Verkouteren, and K.J. Kim. 2006. "Depth Profiling Using C_{60}^{+} SIMS—Deposition and Topography Development During Bombardment of Silicon." *Applied Surface Science* 252, no. 19, pp. 6521–25. doi: http://dx.doi.org/10.1016/j.apsusc.2006.02.234

[7] Weibel, D., S. Wong, N. Lockyer, P. Blenkinsopp, R. Hill, and J.C. Vickerman. 2003. "A C_{60} primary Ion Beam System for Time of Flight Secondary Ion Mass Spectrometry: Its Development and Secondary Ion Yield Characteristics." *Analytical Chemistry* 75, no. 7, pp. 1754–64. doi: http://dx.doi.org/10.1021/ac026338o

[8] Sheraz nee Rabbani, S., A. Barber, I. Berrueta Razo, J.S. Fletcher, N.P. Lockyer, and J.C. Vickerman. 2014. "Prospect of Increasing Secondary Ion Yields in ToF-SIMS Using Water Cluster Primary Ion Beams." *Surface and Interface Analysis* 46, S1, pp. 51–53. doi: http://dx.doi.org/10.1002/sia.5606

[9] Morgan, A.E. 1989. "SIMS." In *Characterization of Semiconductor Materials, Principles, and Methods, Vol. 1*, ed. G.E. McGuire, 48. Park Ridge, NJ: Noyes Publications.

[10] Vickerman, J.C., A. Brown, N.M. Reed, eds. 1989. *Secondary Ion Mass Spectrometry—Principles and Applications*. Oxford, United Kingdom: Oxford University Press.

[11] CAMECA-IMS 6f user guide. 1996. *Mass Spectrometer*, I-16, Fig. 2.12.

[12] Hillion, F., B. Daigne, F. Girard, and G. Slodzian. 1994. "A New High Performance Instrument: The CAMECA NanoSIMS 50." In *Secondary Ion Mass Spectrometry, SIMS IX*, eds. A. Benninghoven, Y. Nihei, R. Shimizu, and H.W. Werner, 254. Chichester, United Kingdom: Wiley.

[13] CAMECA Instruments website www.cameca.com

[14] Australian Scientific Instruments website shrimp.anu.edu.au

[15] Meuris, M., P. De Bisschop, J.F. Leclair, and W. Vandervorst. 1989. "Determination of the Angle of Incidence in a Cameca IMS-4f SIMS Instrument." *Surface and Interface Analysis* 14, no. 11, pp. 739–43. doi: http://dx.doi.org/10.1002/sia.740141110

[16] Vickerman, J., and D. Briggs, eds. 2001. *ToF-SIMS—Surface Analysis by Mass Spectrometry*. Chichester, United Kingdom: IM Publications.

[17] Wiza, J.L. 1979. "Microchannel Plate Detectors." *Nuclear Instruments and Methods* 162, no. 1–3, pp. 587–601. doi: http://dx.doi.org/10.1016/0029-554x(79)90734-1

[18] Daly, N.R. 1960. "Scintillation Type Mass Spectrometer Ion Detector." *Review of Scientific Instruments* 31, no. 3, p. 264. doi: http://dx.doi.org/10.1063/1.1716953

[19] Fahey, A.J. 1998. "Measurements of Dead Time and Characterization of Ion Counting Systems for Mass Spectrometry." *Review of Scientific Instruments* 69, no. 3, p. 1282. doi: http://dx.doi.org/10.1063/1.1148796

[20] Levi-Setti, R, Y. Wang, and G. Crow. 1984. "High Spatial Resolution SIMS with the UC-HRL Scanning Ion Microprobe." *Le Journal de Physique Colloques* 45, no. C9, pp. C9-197 to C9-205. doi: http://dx.doi.org/10.1051/jphyscol:1984933

[21] Stevie, F.A., L. Sedlacek, P. Babor, J. Jiruse, E. Principe, and K. Klosova. 2014. "FIB-SIMS Quantification using TOF-SIMS with Ar and Xe Plasma Sources." *Surface and Interface Analysis* 46, S1, pp. 285–87. doi: http://dx.doi.org/10.1002/sia.5483

[22] Oechsner, H., and W. Gerhard. 1972. "A Method for Surface Analysis by Sputtered Neutrals." *Physics Letters A* 40, no. 3, pp. 211–12. doi: http://dx.doi.org/10.1016/0375-9601(72)90660-3

[23] Lipinsky, D., R. Jede, O. Ganshow, and A. Benninghoven. 1985. "Performance of a New Ion Optics for Quasisimultaneous Secondary Ion, Secondary Neutral, and Residual Gas Mass Spectrometry." *Journal of Vacuum Science & Technology A: Vacuum, Surfaces, and Films* 3, no. 5, p. 2007–17. doi: http://dx.doi.org/10.1116/1.572917

[24] Williams, P., and L.A. Streit. 1986. "Quantitative Analysis Using Sputtered Neutrals in a Secondary Ion Microanalyser." *Nuclear Instruments and Methods in Physics Research Section B* 15, no. 1–6, pp. 159–64. doi: http://dx.doi.org/10.1016/0168-583x(86)90274-0

[25] Parks, J.E. 1990. "Surface Analysis Using Resonance Ionization Spectroscopy." In *Lasers and Mass Spectrometry*, ed. D.M. Lubman, 37. New York: Oxford University Press.

[26] Mackay, S.G., and C.H. Becker. 1992. "Surface Analysis by Laser Ionization." In *Encyclopedia of Materials Characterization—Surfaces, Interfaces, Thin Films*, eds. C.R. Brundle, C.A. Evans, Jr., S. Wilson, 559. Boston, MA: Butterworth-Heinemann.

[27] Downey, S.W., A.B. Emerson, and R.F. Kopf. 1992. "Quantitative Depth Profiling Resonance Ionization Mass Spectrometry of GaAs/AlGaAs heterojunction Bipolar Transistors." *Journal of Vacuum Science & Technology B* 10, no. 1, p. 385. doi: http://dx.doi.org/10.1116/1.586363

[28] Arlinghaus, H.F., M.T. Spaar, N. Thonnard, A.W. McMahon, T. Tanigaki, H. Shichi, and P.H. Holloway. 1993. "Quantitative and Sensitive Profiling of Dopants and Impurities in Semiconductors Using Sputter-Initialed Resonance Ion Spectroscopy." *Journal of Vacuum Science & Technology A* 11, no. 4, p. 2317 .doi: http://dx.doi.org/10.1116/1.578369

[29] Downey, S.W., A.B. Emerson, G.E. Georgiou, J. Bevk, R.C. Kistler, N. Moriya, D.C. Jacobsen, and M.L. Wise. 1995. "Depth Profiling of Dopants in Thin Gate Oxides in Complementary Metal Oxide-Semiconductor Structures by Resonance Ion Mass Spectrometry." *Journal of Vacuum Science & Technology B* 13, no. 2, p. 167. doi: http://dx.doi.org/10.1116/1.587993

CHAPTER 5

DEPTH PROFILING (DYNAMIC SIMS)

The surface of a sample is important but subsurface information is often desired. One may want to investigate a buried layer or an interface between a layer and substrate. This requires a controlled removal of material. Electrons have very limited sputtering capability and laser ablation lacks uniformity of removal. Sputtering with an ion beam is typically used because the beam of ions can be precisely controlled. Secondary ion mass spectrometry (SIMS) is one of the preferred profiling techniques because of depth resolution and sensitivity [1–5]. All SIMS analyzer types can be used to obtain depth profiles, and this chapter provides details on this type of analysis.

5.1 RASTER AND GATE

SIMS depth profiling provides composition versus depth information. A depth profile is normally achieved with a selection of the species of interest that are monitored as a crater is sputtered. The data are plotted as intensity of species versus sputtering time and this can be converted to concentration versus depth as shown in Chapter 6, Quantification. This is a destructive technique but the amount of material removed is quite small. With magnetic sector and quadrupole instruments, one has to make the decision in advance as to which species will be monitored. For TOF-SIMS, all masses are recorded at each data point so it is possible to retrospectively determine the depth profile for a species that was not preselected.

Dynamic SIMS is the incidence of ions with enough density to remove more than the surface monolayer. The depth profiling mode can achieve high sensitivity coupled with excellent depth resolution.

Important parameters to control in order to obtain good depth resolution are the raster and gate [6]. Figure 5.1 shows a diagram of a profile through a layer [7]. The crater bottom is flat, but the sidewalls of the crater are sloped. If secondary ions are detected from the entire sputtered region, then even though the layer has been removed from the center of the crater, the layer will continue to be sputtered at the edge of the crater. Therefore, detection of all ions from the crater will provide poor depth resolution. If a gate is applied to reduce the area of detection, then only ions from the gated region would be detected. A comparison of the depth resolution for the two scenarios is shown in the same figure. The profile that is gated is more representative of the actual layer in the sample.

The gating method varies for the instrument used. For the CAMECA IMS series of magnetic sector instruments, the gating in a depth profile is determined by placing a field aperture in the ion optic column. This aperture is variable in size and determines the circular region at the center of the crater from which the secondary ions are collected. For example, for a CAMECA IMS-6F, a field aperture size of 750 µm diameter at an imaged field of 150 µm will provide a detected region of 60 µm diameter.

For most quadrupole instruments, the gating is electronically determined. The detector is gated on only when the primary beam is resident within the desired detected region. The quality of gating is dependent on the diameter of the primary beam. As shown in Figure 5.2, if the primary

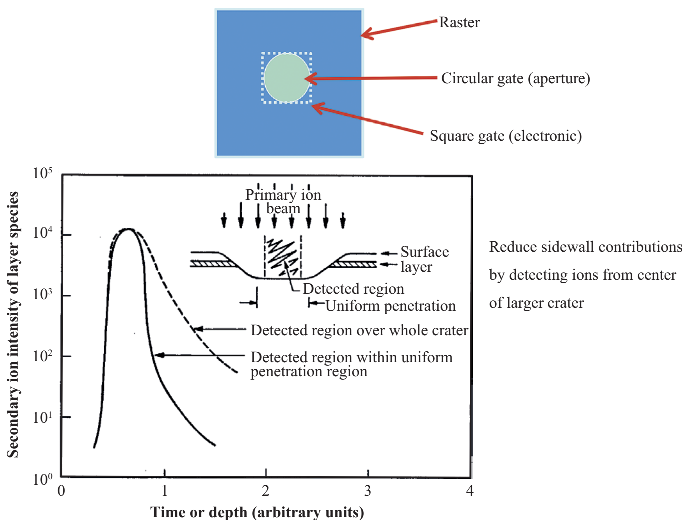

Figure 5.1. Raster and gate relationship with depth profile shape. *Source*: Wilson, Stevie, and Magee [7].

- Crater size will be raster chosen plus beam diameter
- For electronic gating, detected area is beam diameter added to gated length and width

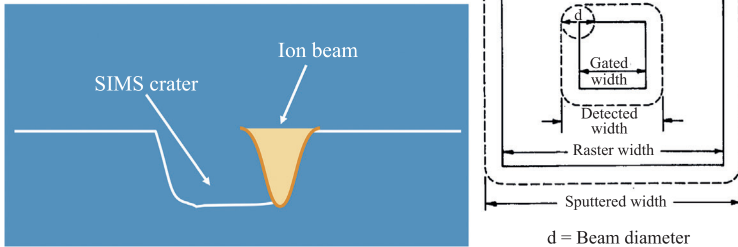

Figure 5.2. Beam diameter effect on raster and gate.
Source: Wilson, Stevie, and Magee [8].

beam is large, then even when the center of the beam is just inside the gated region, secondary ions generated from the part of the beam outside the desired detected area will also be detected [8]. Some quadrupole instruments also use a field aperture to improve gating.

For TOF-SIMS, depth profiles are achieved with the use of two beams, one to sputter the specimen and one to perform the analysis of the crater surface at regular intervals. Each pixel contains a mass spectrum and the region of interest can be selected after the profile is complete in order to optimize the detected region.

5.2 DEPTH RESOLUTION

Parameters of interest in a depth profile are depth resolution, dynamic range, detection limit, and peak concentration as illustrated in the depth profile of an ion implant shown in Figure 5.3.

Depth resolution is the ability to discriminate atoms at one depth of the sample from atoms in the region immediately below. Good depth resolution is one of the most significant capabilities of SIMS and is dependent on a number of factors:

- Crater shape
- Choice of raster and gate
- Penetration depth of primary beam. Less penetration means less ion beam mixing of the atoms in the sample and better depth resolution.

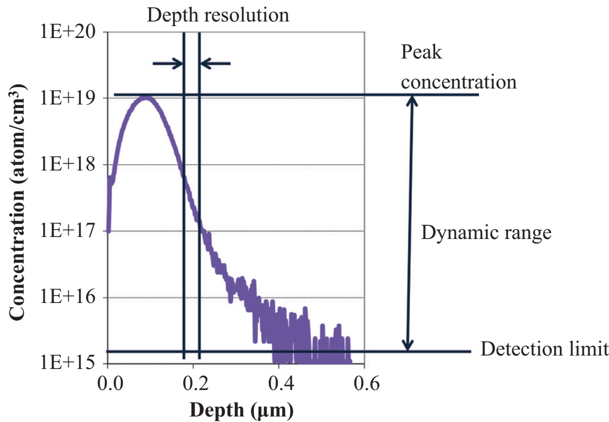

Figure 5.3. Depth profile characteristics.
Source: F. Stevie, Analytical instrumentation facility, North Carolina State University.

- Knock-on due to head-on collisions with sample atoms.
- Uniformity of removal of material in the crater. This is determined by the quality of raster electronics and by sputtering characteristics of the material. Some materials do not sputter uniformly.
- Depth of analysis—Depth resolution generally degrades with depth.
- Mobility of certain elements. Some elements, such as Na, Li, and K in insulators, are mobile when an electric field is applied (see Chapter 8 on insulator analysis).

Knock-on and nonuniform removal are diagrammed in Figure 5.4. Proper choice of raster and gate reduces contributions from sidewalls and the surface. Nonuniform sputtering and movement of an atom into a region below its initial location (ion beam mixing, knock-on) [9] will be discussed in more detail later in this chapter.

The raster to gate ratio can be optimized by keeping the detected area constant and varying the raster size. In Figure 5.5, profile B obtained with a raster near the size of the detected area shows a significantly deeper profile than profile A obtained with a raster length and width about three times the diameter of the detected area [8]. Figure 5.6 shows a more detailed study on another instrument and indicates that the minimum raster size without significant distortion is about 100 µm × 100 µm for a 63 µm detected area. It is important to understand the scale of the crater depth relative to the raster. Figure 5.7 shows the actual scale for a 250 nm deep crater and the distorted scale, which is normally shown by the display from a diamond stylus profilometer used to measure the crater depth. For very shallow

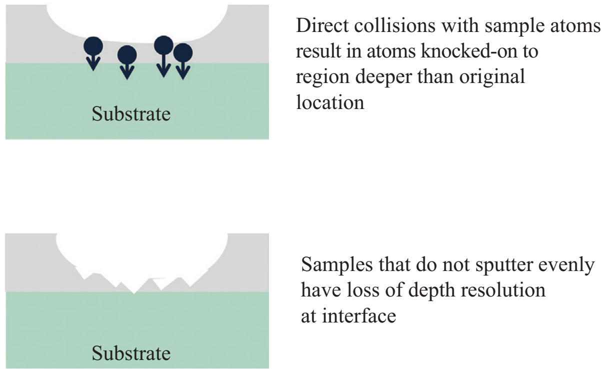

Figure 5.4. Knock-on and nonuniform sputtering.

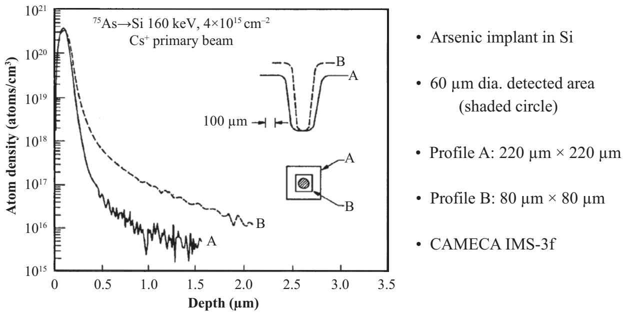

Profile A has larger raster to gate ratio and is more accurate
Profile B illustrates the distortion introduced by a raster that is insufficient to reject sidewall contributions.

Figure 5.5. Detected area versus raster size.
Source: Wilson, Stevie, and Magee [8].

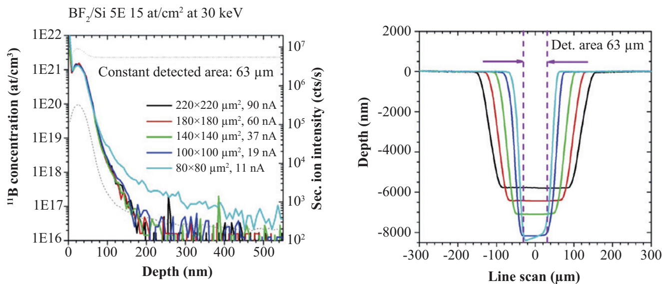

Profile does not show distortion until raster reduced to 80 μm for 63 μm diameter detected area
Data obtained with CAMECA SC-Ultra

Figure 5.6. Detected area versus raster size.
Source: Damiano Giubertoni, FBK, reproduced with permission.

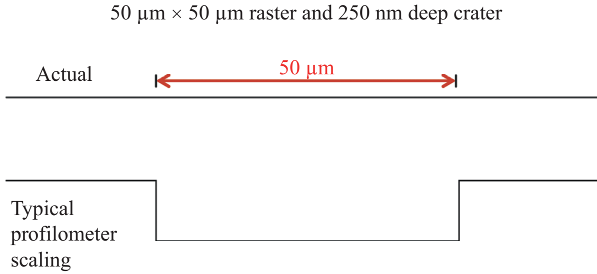

Figure 5.7. Crater perspective.

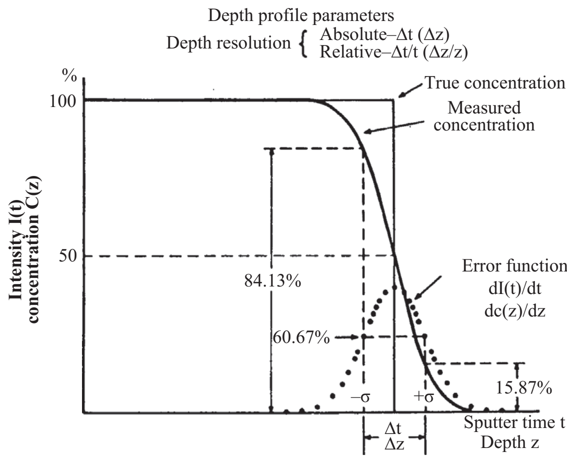

- Error function is derivative of interface curve
- +/- sigma points correspond to 84% and 16% of max intensity

Figure 5.8. Depth profile parameters for interface.
Source: Wilson, Stevie, and Magee [10].

profiles, it may be possible to use a smaller raster and not have significant edge effects. Proper sizing of the raster to detected area is important to optimize depth resolution.

Because of the variety of sample types, more than one metric is used to measure depth resolution. For an interface, this parameter can be given by the depth interval over which the signal decreases from 84 percent to 16 percent of maximum (±σ) as illustrated in Figure 5.8 [10]. Another term commonly used is decay length in nm/decade. This is the depth for a signal to drop by one order of magnitude. There may be separate designations for leading and trailing edges of a layer interface. The leading edge will usually have a smaller value because this marks the onset

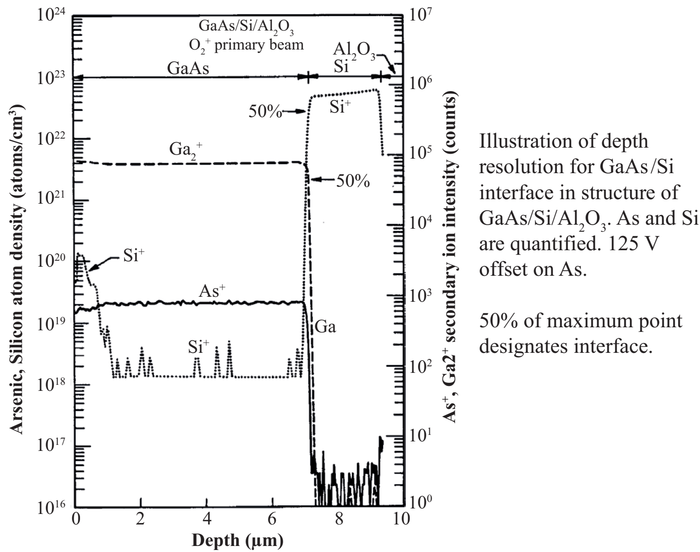

Figure 5.9. Interface location.
Source: Wilson, Stevie, and Magee [11].

of the layer and is less affected by knock-on than the trailing edge. Note that in interpretation of the data, the location of the interface should be at 50 percent of maximum signal intensity as shown in Figure 5.9 [11]. Yet another designation is the depth required to decrease the signal to 1/e of maximum and this is expressed as λ. An example of the nm/decade and λ depth resolution calculations is shown in Figure 5.10. This profile was obtained using TOF-SIMS to analyze a very shallow boron implant. For the analysis of layers intended to be very thin or even one monolayer, the resolution is often expressed as full width at half maximum (FWHM), which is shown for beryllium in GaAs in Figure 5.11 [12].

5.2.1 PRE-EQUILIBRIUM REGION

Because the incident ion has some energy, it will penetrate the surface and implant into the specimen. For depth profiles, until the specimen is sputtered to the most probable depth (projected range) of the implanted primary beam, the concentration of the primary species in the specimen is not uniform. This depth is called the pre-equilibrium zone and quantification in this region is difficult. Figure 5.12 shows a schematic drawing of a depth profile of oxygen using an oxygen primary beam and the variation

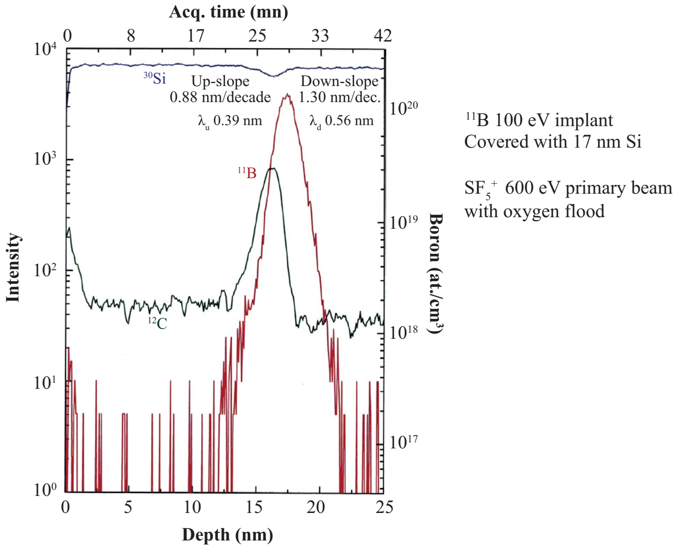

Figure 5.10. TOF-SIMS depth resolution.
Source: ON TOF TOF-SIMS IV, reproduced with permission.

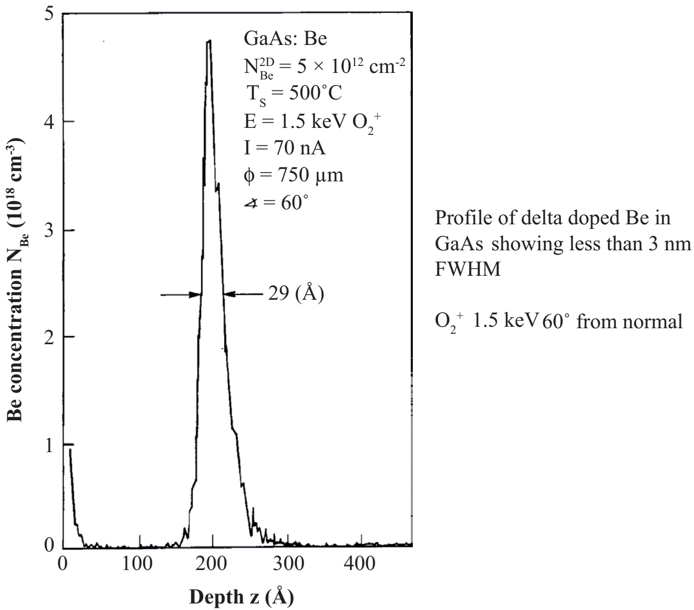

Figure 5.11. Depth resolution for delta layer.
Source: Stevie [12], reprinted with permission from American Institute of Physics copyright 1992, American Vacuum Society.

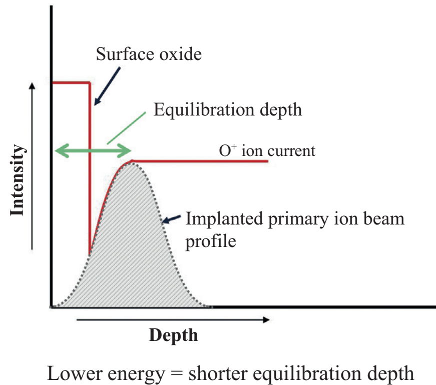

Figure 5.12. Surface equilibration region.

in oxygen concentration between the surface oxide, the depth required to reach oxygen equilibration (pre-equilibrium region), and the rest of the profile where equilibrium has been achieved. For bombardment of silicon at normal incidence with 8 keV O_2^+, the ion dose required to reach equilibrium for $^{30}Si^+$ and $^{16}O^+$ signals was 6×10^{16} ions/cm^2 [13]. The measured transition widths are approximately twice the average penetration of the primary beam species [14]. The oxygen concentration variation in the surface and near-surface region will affect the composition of the matrix and the sputtering rate of the material, so adjustment of the depth scale may be necessary [15].

The pre-equilibrium region can be reduced by decreasing the penetration depth of the primary beam. This can be accomplished by the use of a primary beam with lower energy, higher mass, or more grazing incidence angle. Many authors have investigated the effects of these parameters on depth resolution [16–23]. The effect of primary energy on the profile shape is shown in Figure 5.13, where reducing the primary beam energy improves the depth resolution of the profile [18]. The difference in the profiles is due to knock-on of atoms during the analysis. Knock-on occurs when an atom from the beam has a collision with an atom in the sample that causes the sample atom to be pushed deeper into the sample. This atom will be removed later in the depth profile but will appear to have originated from a location deeper than the original site. Figure 5.14 shows the analysis of a shallow ion implant of antimony in silicon. In this case the primary energy and incidence angle were optimized and the result on the as implanted and annealed profiles is a dramatic reduction in antimony depth. Figure 5.15 shows a table of beam energy and incidence angle conditions for a CAMECA IMS-6F and the penetration range for

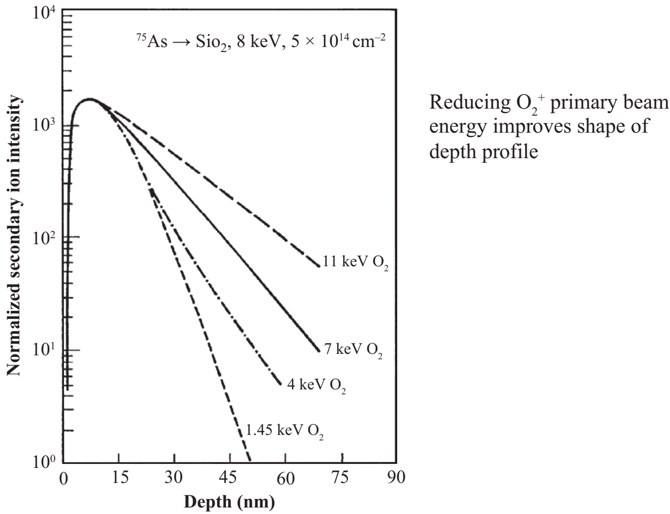

Figure 5.13. Knock-on variation with primary energy.
Source: Vandervorst et al [18].

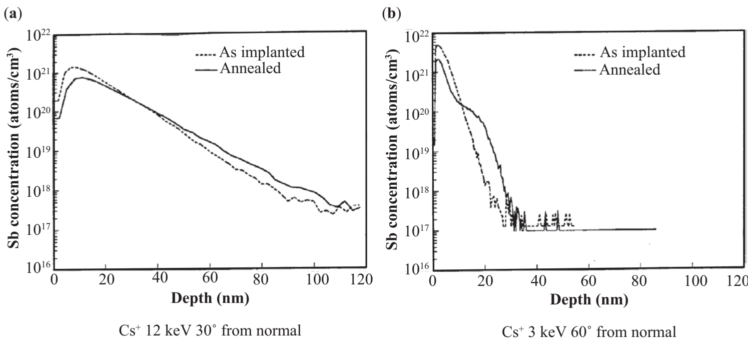

Figure 5.14. Effect of primary beam energy and incidence angle on Sb depth profile in Si.
Source: Luftman, AT&T Bell Laboratories, Sample from B. G. park.

those conditions in GaN, along with Transport of Ions in Matter (TRIM) simulations of three of the bombardment conditions [24]. The penetration range is expressed as the most probable range of ion penetration plus the straggle of that distribution. All distributions were calculated using TRIM [25].

Note that for many instruments the incidence angle is fixed so that the only practical choice to reduce the pre-equilibrium region for a given primary beam is to lower the energy. The sputtering rate also decreases

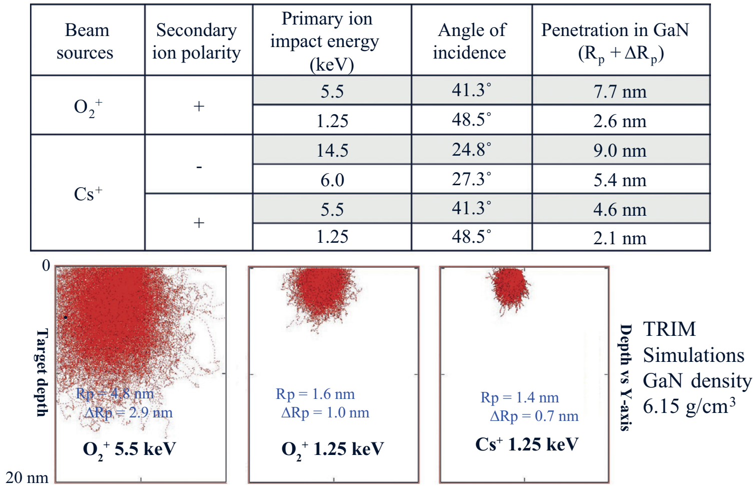

Beam sources	Secondary ion polarity	Primary ion impact energy (keV)	Angle of incidence	Penetration in GaN ($R_p + \Delta R_p$)
O_2^+	+	5.5	41.3°	7.7 nm
		1.25	48.5°	2.6 nm
Cs^+	-	14.5	24.8°	9.0 nm
		6.0	27.3°	5.4 nm
	+	5.5	41.3°	4.6 nm
		1.25	48.5°	2.1 nm

Figure 5.15. Penetration in GaN for CAMECA IMS-6F analyses.
Source: C. Gu, North Carolina State University [24].

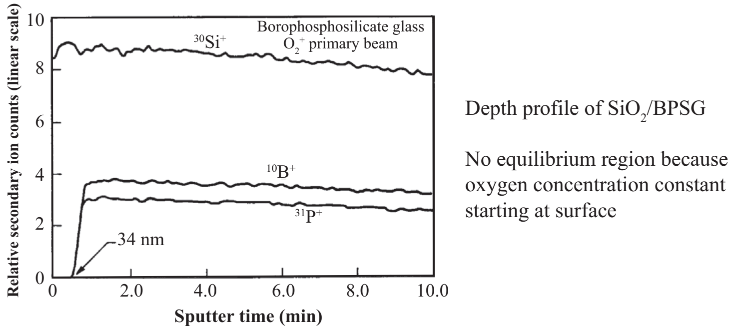

Figure 5.16. Absence of equilibration region in SiO_2.
Source: Wilson, Stevie, and Magee [26].

rapidly as the incident energy drops below 1 keV, so there is a practical limit to the reduction in ion energy.

If the concentration of the primary species is already maximized in the sample, for example analysis of silicon oxide using O_2^+, then the species monitored will be uniform starting at the surface. The enhancement effect of oxygen is not further increased by the additional oxygen from the primary beam. Figure 5.16 shows a depth profile using O_2^+ of a silicon oxide layer on borophosphosilicate glass [26]. The goal was to measure the thickness of the oxide. Since the oxygen enhancement of secondary ion yield is at maximum starting at the surface of the sample, there is no

equilibration depth. Other approaches are the use of a normal incidence O_2^+ primary beam, which can completely oxidize certain materials, such as silicon, or with oxygen flood (oxygen leak, oxygen backfill), which provides additional oxygen to the specimen surface through a nozzle close to the sample surface, as discussed in Chapter 2.

Because of the pre-equilibrium zone, quantitative analysis of species at the surface or near surface can be very difficult. In addition, adsorption of gaseous species on the surface can complicate the analysis. One method that can sometimes be used to improve this type of analysis is to cap the surface region with another layer [27–29]. The surface is protected and the pre-equilibrium zone is passed by the time the layer of interest is reached in the depth profile. Figure 5.17 shows how a capping method was used to study the origin of boron on a silicon surface [30]. The source of the boron was confirmed by the use of a cap layer to preserve the surface of interest. Boron was detected at the surface covered by the cap layer when the surface was exposed to clean room air between depositions, and not detected when the second layer was deposited without air exposure. The primary boron source was found to be the borosilicate filters used in clean room air filters. The cap layer must be the same matrix as the surface of interest. The cap should also be flat and incur no significant sample heating during deposition.

5.2.2 ULTRA-SHALLOW ANALYSES

The drive to reduce device size in the semiconductor industry resulted in the requirement to analyze dopant profiles in silicon with total profile depth less than 50 nm. The information close to the surface is of high importance, which meant shrinking the pre-equilibrium region to the shortest distance possible to obtain the best depth resolution. This demand resulted in an extensive body of work by many researchers and is referred to as ultra-shallow analysis [31–42]. A series of meetings (International Workshop on the Measurement, Characterization, and Modeling of Ultra-Shallow Doping Profiles in Semiconductors) was dedicated to this topic.

Some of the issues that were encountered were pre-equilibrium effects, variation in sputtering rate due to oxide formation, surface roughening during bombardment, surface oxide, analysis time, and validation of implanted dose [43]. Even at the lowest bombardment energy used, there will always be a pre-equilibrium region unless a cap layer, as described previously, is used. However, it is very difficult to place a thin cap layer

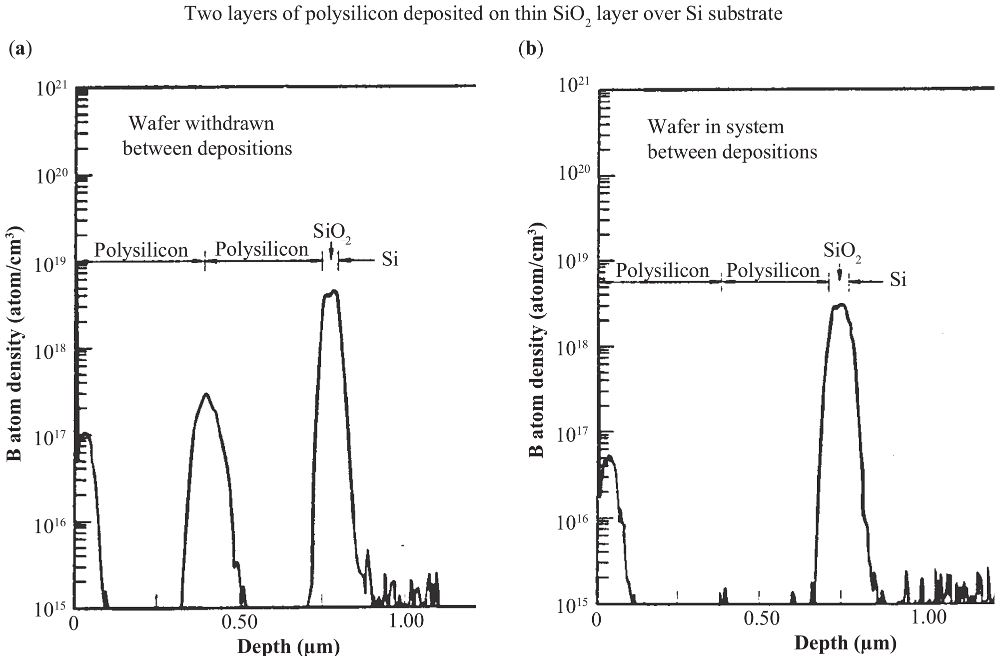

Figure 5.17. Cap layer to improve surface analysis. (a) Sample withdrawn from deposition system into clean room between depositions. (b) Wafer left in system between depositions.
Source: Stevie et al. [30], reprinted with permission from American Institute of Physics, copyright 1991, American Vacuum Society.

without contamination or oxidation of the surface and this method is often not available. With O_2^+ at 100 eV and 40° from normal incidence on silicon, the projected range and straggle are 0.7 nm and 0.4 nm, respectively. We have to recognize that the typical size of one atom is 0.2 nm and the theoretical depth resolution limit is approximately 0.3 nm [44]. A value of 0.39 nm for λ has been achieved using SF_5^+ at 600 eV and 52° from normal incidence (see Figure 5.10).

Bombardment of a silicon surface with oxygen at low energy has the complication that the surface composition changes from surface oxide to pre-equilibrium oxygen concentration to equilibrium concentration. There is a difference in sputtering rate for these regions that is negligible for a 500 nm deep profile but significant for one less than 50 nm. The oxygen bombardment actually causes a swelling or expansion of the silicon at the start of the profile and this requires a sputtering rate correction to calibrate the depth axis [15].

Some analysis conditions produced roughening of the surface and loss of depth resolution. This topic will be discussed in more detail later in this chapter. As a result, certain bombardment angles were avoided to optimize the analysis.

The sputtering rate drops rapidly below 500 eV, and from 250 eV to 100 eV there is about an order of magnitude decrease in sputtering rate for 36° from normal incidence [45]. Oxidation of silicon is nearly complete with 150 eV O_2^+ bombardment [46]. For low energy and normal incidence, the sputtering rate becomes a significant issue. Alignment and focusing of the primary beam is also problematic at very low energy, and this presents a limitation on the minimum area that can be analyzed.

Validation of the implanted dose was achieved by the use of techniques that did not involve sputtering of the surface, such as elastic recoil detection analysis and medium energy ion scattering [38]. X-ray photoelectron spectroscopy (XPS) can also provide information on the concentration at and near the surface for high dose implants.

Several methods were devised and similar results could be obtained with the approaches detailed as shown in Figure 5.18. Two approaches often used were to analyze at normal incidence without oxygen flood or backfill and to analyze at 45 to 60° from normal incidence with oxygen flood. Figure 5.18 shows examples of normal incidence analysis and two conditions for oblique analysis with similar profiles obtained. Figure 5.19 shows that small differences in dopant penetration could be detected for a profile that covers less than 15 nm, but the first 2 nm had uncertain quantification because of the pre-equilibration region. Ultra-shallow phosphorus and arsenic depth profiles have been obtained using Cs^+ at low energy, such

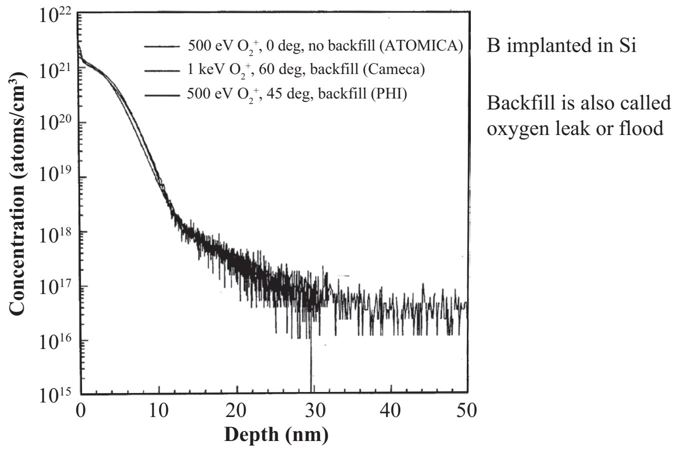

Figure 5.18. Ultra-shallow analysis approaches.
Source: Bennett, SEMATECH, reproduced with permission.

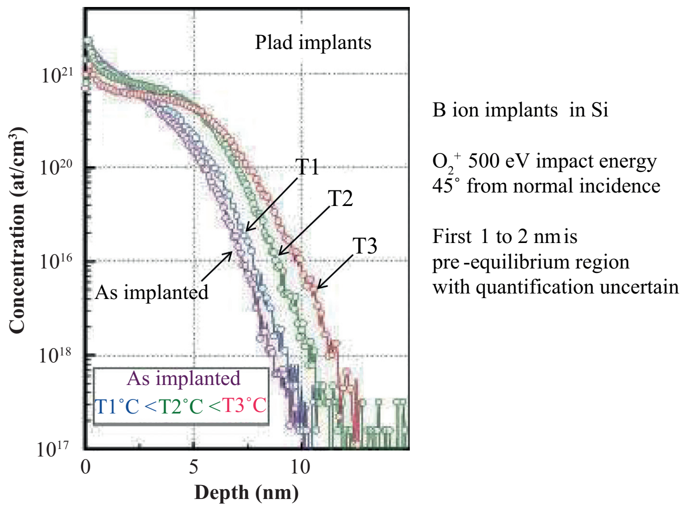

Figure 5.19. Ultra-shallow implant technology.
Source: CAMECA instruments reproduced with permission from CAMECA.

as 1 keV. Since Cs^+ is significantly more massive than O_2^+ and penetrates less into the substrate for the same energy, the Cs^+ energy may not have to be as low as that for O_2^+ to achieve the desired resolution. Figure 5.20 shows the analysis of a 3 kV arsenic implant using Cs^+ at as low as

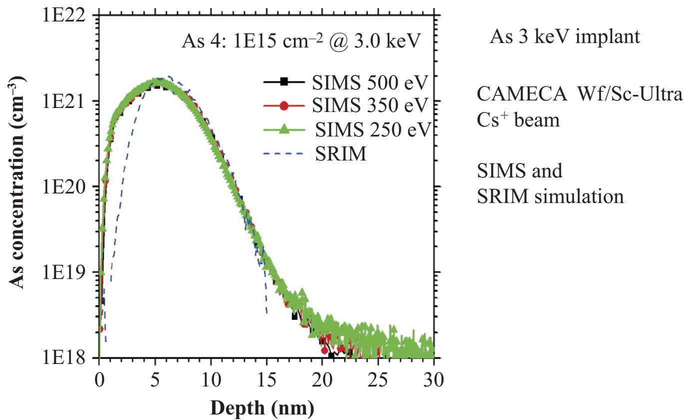

Figure 5.20. Arsenic ultra-shallow analyses.
Source: Giubertoni, et al. [47].

250 eV [47]. For Cs^+ at 250 eV and 40° from normal incidence in silicon, the projected range and straggle are 0.18 nm and 0.05 nm, respectively.

5.3 SPUTTERING RATE

The sputtering rate determines the analysis time for the depth profile. Sputtering rate is varied by changing the raster size or primary beam current. Note that for a multilayer sample, one should expect the sputtering rate to be different for each layer. Detection limit is usually improved by an increase in the sputtering rate. Usually the fastest analysis is desired but one must consider the data density required. If the sputtering rate is too high then information may be lost, especially at an interface.

5.4 NONUNIFORM SPUTTERING, SAMPLE ROTATION

Any crater nonuniformity will result in degraded depth resolution [48]. Ion bombardment can cause nonuniform sputtering, even for crystalline materials. Polycrystalline samples, such as metals, expose grains at varied angles to the ion beam. When the atoms in a grain are aligned with the beam, the beam penetrates further and there is less sputtering than when the atoms are misaligned to the beam. As a result the misaligned grains erode faster and leave a nonuniform surface that causes loss of depth resolution.

Development of microtopography during bombardment can be observed optically. The bottom of the crater will become darker with sputtering because the rough surface scatters the light used for observation. After analysis, the three instruments used to measure roughness, in order of increasing sensitivity, are stylus profilometer, scanning electron microscope (SEM), and atomic force microscope (AFM).

Several authors noted topography changes under ion bombardment even for single crystal specimens [49–52]. As shown in Figure 5.21, for single crystal silicon, depth profiles at 5.5 keV O_2^+ and 42° from normal showed a change in matrix intensity at about 3 μm into the sample. SEM micrographs of a sample after sputtering to depths before, during, and after the intensity change showed development of ripple formation correlated with the change in ion intensity [53]. The change in Si intensity was not observed when a Cs^+ primary beam was used. The origin of the ripples has been of interest and can degrade depth resolution even for shallow profiles [54, 55]. The atomic arrangement of the target material appears to determine the nature of the roughened surface [56].

Reduction of roughening due to ion bombardment can be mitigated by the choice of primary species, energy and angle of incidence, and by sample rotation during analysis. Figure 5.22 shows that roughness is significantly higher at bombarding angles in the range of 50 to 65° from normal for O_2^+ bombardment of silicon [54]. For this reason, analysis in the range 40 to 50° would be a better choice. One of the best options for removal of microtopography due to sputtering is rotation of the sample

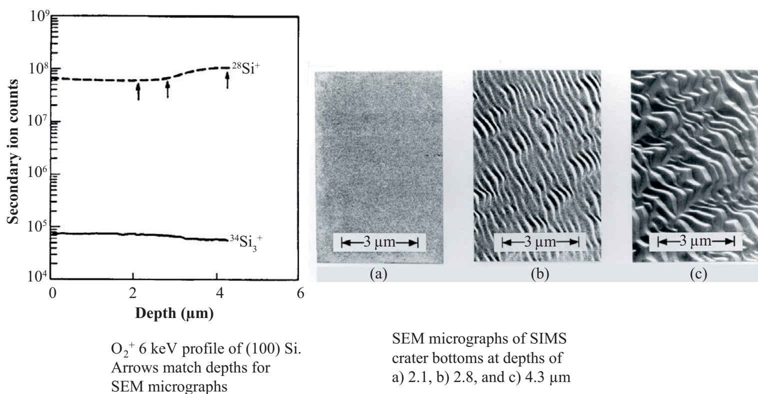

Figure 5.21. Sputter induced roughness on crystalline Si.
Source: Stevie, Kahora, Simons, and Chi [53], reprinted with permission from American Institute of Physics, copyright 1988, American Vacuum Society.

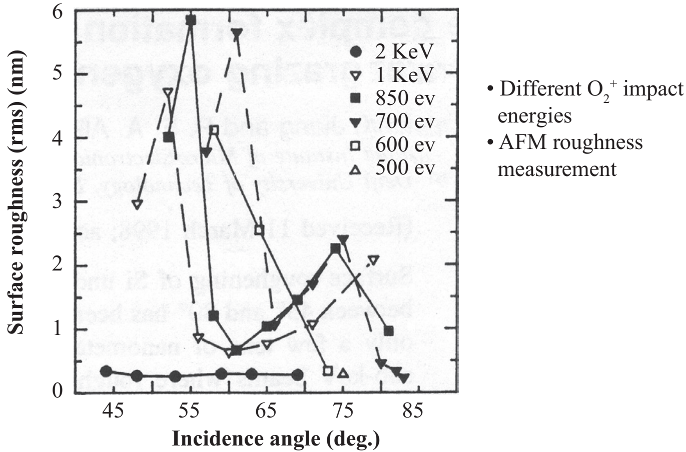

Figure 5.22. RMS roughness vs. incidence angle.
Source: Jiang and Alkemade [54], reprinted with permission from Applied Physics Letters, copyright 1998, AIP Publishing LLC.

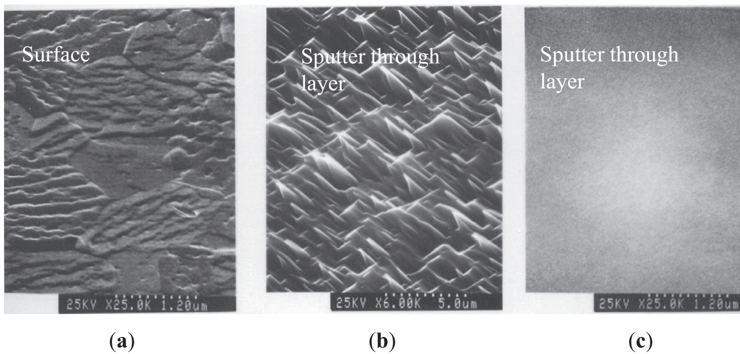

Figure 5.23. Sample rotation during ion bombardment of Al. SEM micrographs of (a) aluminum surface, (b) bottom of crater sputtered through 1 μm aluminum layer into underlying silicon without rotation and (c) with rotation.
Source: Stevie and Moore [60].

during analysis. This is also referred to as Zalar rotation [57]. Several authors showed the improvement in depth resolution for SIMS depth profiles with sample rotation [58–63]. Figure 5.23 shows SEM micrographs of the surface of an aluminum layer and after sputtering through the 1 μm layer with and without sample rotation [60]. The crater bottom is quite

rough without rotation but no features can be observed with rotation. The impact of the rotation on depth resolution is illustrated in Figure 5.24, which shows SIMS depth profiles in the same aluminum layer with and without sample rotation. With sample rotation the boron at the interface is clearly defined and it can be observed that silicon from the Al–Si–Cu layer

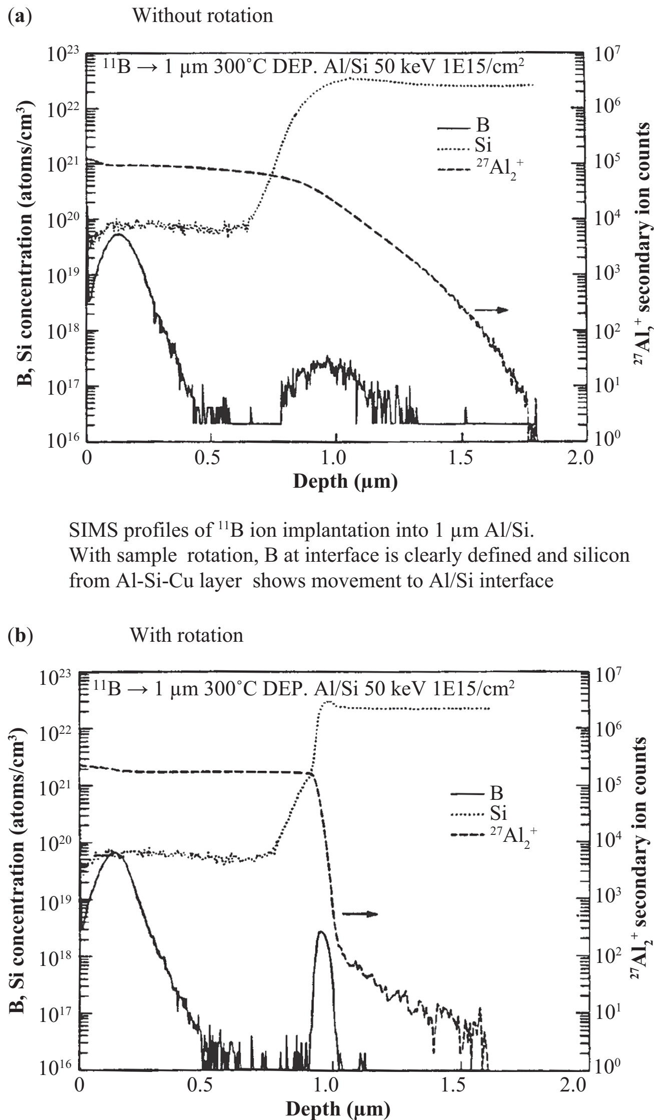

Figure 5.24. Sample rotation during ion bombardment of Al. *Source*: Stevie and Moore [60].

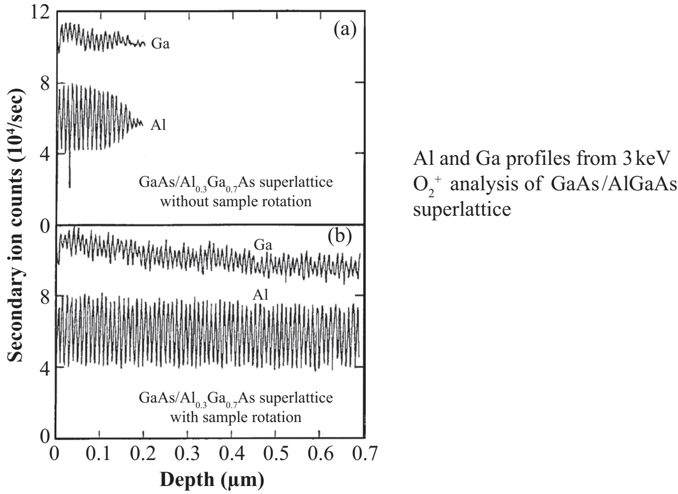

Figure 5.25. Sample rotation for multilayer analysis. (a) Without rotation, (b) with rotation.
Source: Cirlin, et al. [58], reproduced with permission from American Institute of Physics, copyright 1990, American Vacuum Society.

shows movement to the Al/Si interface. Figure 5.25 shows the analysis of alternating layers of GaAs/AlGaAs. Without rotation, one can identify about 17 layer pairs. With rotation, many more layer pairs are distinguished without apparent loss of depth resolution [59].

Note that roughening of the sample may occur as a result of adding oxygen flood [55]. This can impact the depth resolution in an ultra-shallow profile but can be mitigated with the choice of primary angle of incidence.

5.5 DETECTION LIMIT, DYNAMIC RANGE, MEMORY EFFECT

SIMS is a mass spectrometric technique and has the capability to provide data over a concentration range from 100 percent to ppm to ppb. By comparison, commonly used techniques such as Auger electron spectroscopy (AES) and XPS are limited to three orders of magnitude dynamic range (see Chapter 1). The detection limit is an important parameter for depth profiling. Ion implantation is a method used to place elements into a substrate with control of depth and concentration. This method is used extensively in semiconductor wafer processing, especially to insert dopants such as boron, phosphorus, and arsenic into silicon substrates.

Ion implantation has proven to be very useful in SIMS depth profiling. With ion implants, it is possible not only to quantify the species of interest but also to measure the detection limit. Figure 5.26 shows an implant of potassium in silicon and a detection limit of 10 ppta for potassium [64]. Potassium has very high secondary ion yield for O_2^+ bombardment, and a high yield is important to achieve a good detection limit. Figure 5.27

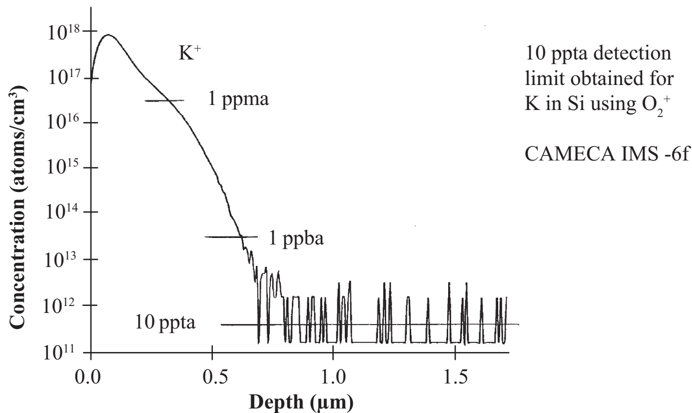

Figure 5.26. K detection limit in Si.
Source: Stevie, Wilson, McKinley, and Hitzman [64], reprinted with permission from John Wiley and Sons.

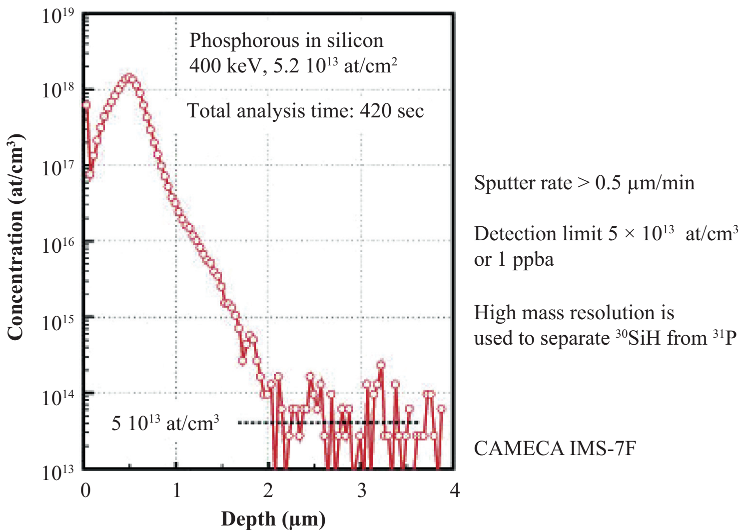

Figure 5.27. P detection limit in Si.
Source: CAMECA instruments, reproduced with permission from CAMECA.

shows an excellent detection limit of 5×10^{13} atoms/cm^3 for phosphorus in silicon. This is notable since high mass resolution was required to separate ^{31}P from $^{30}Si^{1}H$ mass interference.

One cannot simultaneously optimize detection limit and depth resolution. The best detection limit is achieved with high sputtering rate and large detected area, which provides higher count rate. The high sputtering rate is achieved with high primary voltage and current. The best depth resolution is obtained at low impact energy, which results in less penetration into the sample, and low sputtering rate and small detected area. The small area minimizes the effect of variations on the sample surface.

A limiting factor for detection limit in an ion implant has been the sidewalls of the crater. An analysis made on a specimen where the surrounding material was removed showed an extended dynamic range. It may be possible to improve the dynamic range with sample preparation [65]. Sidewall contributions can be mitigated by the use of a specimen that has been pretreated to provide a mesa structure. The mesa is obtained by sputtering a trench around the region of interest. This can be accomplished with a focused ion beam (FIB) instrument or with an ion beam available on the analysis instrument. The mesa sample is analyzed by placing the raster in the trench. With this approach, there are no crater walls and no contributions to background from the walls. This method may provide as much as an order of magnitude improvement in the dynamic range. Figure 5.28 shows a comparison of depth profiles with and without mesa structure [66]. Mesas were prepared over a range of 100 μm × 100 μm to 200 μm × 200 μm within a raster range of 400 μm × 400 μm to 700 μm ×

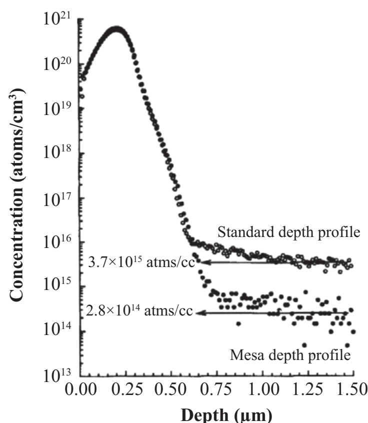

Comparison of standard and mesa SIMS depth profiles of ^{11}B ion implant into Si at 5 keV and 1×10^{16} atoms/cm^2

Figure 5.28. Mesa analysis to reduce sidewall contributions.
Source: Gillen [66], reprinted with permission from John Wiley and Sons.

700 µm. A dynamic range of almost six orders of magnitude has been achieved for boron implanted in silicon [67]. In this study, neutral sputtering was suppressed by insertion of a bend in the primary beam near the sample. The use of background subtraction can additionally improve this range.

Previously analyzed samples can affect the detection limit for a subsequent analysis. For the magnetic sector instrument the close proximity of the sample and immersion lens cover plate permits resputtering of material previously analyzed. Figure 5.29 displays the magnetic sector geometry and indicates the sequence where a material is sputtered, a new material is then inserted and analyzed, and material from the first sample is sputtered off of instrument components and onto the second sample and then detected during analysis. This would appear to be a low probability event, but it does occur at about one part in 10^4 to 10^5 below the matrix density of the material of interest [68, 69]. Since the SIMS dynamic range can exceed that value, the contaminant will be detected. For example, prior analysis of InP will put significant amounts of phosphorus into the sample chamber. Subsequent analysis for phosphorus in silicon will show background phosphorus due to the InP starting at approximately 5×10^{18} to 5×10^{17} atoms/cm^3. This memory effect can be reduced by sputtering the new material for sufficient time to coat the instrument surfaces.

The quadrupole instrument has a much more open geometry as shown in Figure 5.30 and memory effect background is less than that for magnetic sector but can be present [70]. The TOF-SIMS has close proximity elements similar to the magnetic sector, but low sputtering rate and low counts reduce this effect.

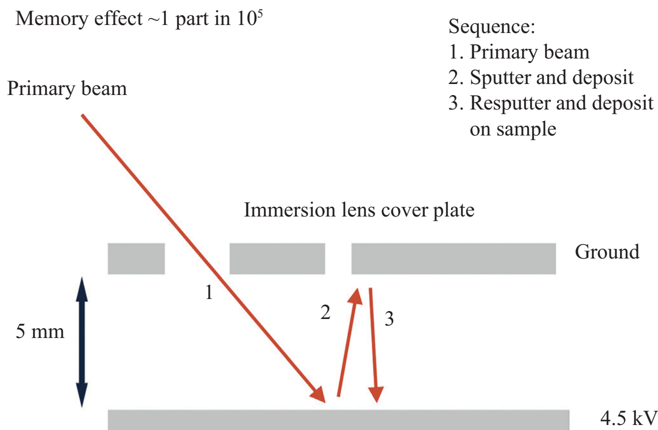

Figure 5.29. Magnetic sector geometry.

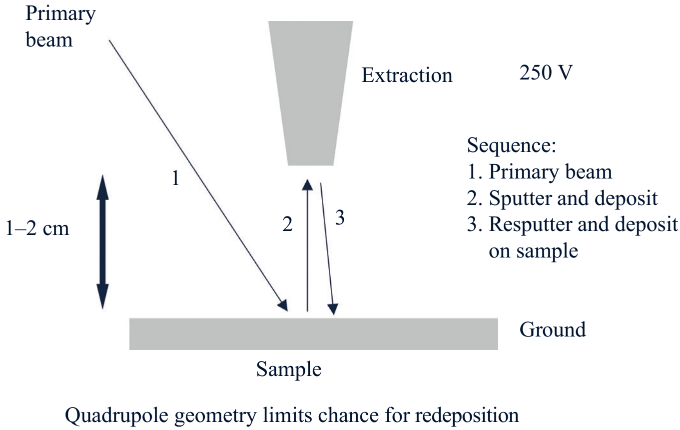

Figure 5.30. Quadrupole geometry.

5.6 COUNT RATE SATURATION—DETECTOR DEAD TIME

SIMS data are often obtained with a high sputtering rate and the detected count rates can be high enough to affect the linearity of the response of an electron multiplier and even a Faraday cup. As count rates are increased, an electron multiplier reaches a level where dead time affects the count rate. The output becomes more nonlinear as the input count rate increases. A typical electron multiplier may have the ability to measure 3×10^6 counts/s with only small count losses due to detector dead time [71]. It is important to understand that for a given raster and gate, the count rate during the gated time is not the average count rate shown on the detector but the count rate shown times the ratio of the rastered to detected area. This high instantaneous count rate can easily be 20 times the measured rate as shown in Figure 5.31 [72]. Count rate saturation can be overlooked. Figure 5.32 shows that for a depth profile of an ion implant, which is displayed on a logarithmic scale, it may not be obvious that profile B has a significant error compared with profile A [73]. This effect can occur for all three types of analyzers. Figure 5.33 shows silicon mass spectra obtained with two gating settings. Both spectra show an incorrect ratio for ^{28}Si and ^{30}Si [74]. In cases where high count rates may be an issue, it is useful to monitor more than one matrix isotope in a depth profile. One can check the isotope ratio for correct value and use the lower intensity isotope for analysis if needed. For this reason, analysis of a silicon matrix species is often made with ^{30}Si instead of ^{28}Si.

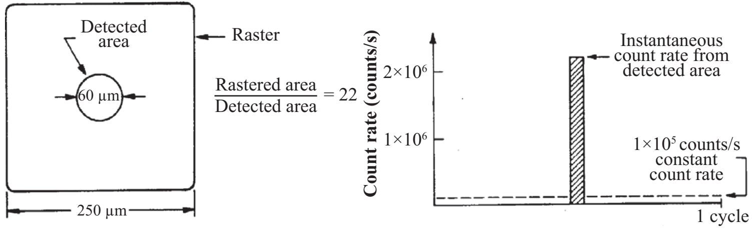

- Determine gated or detected area to rastered area ratio to convert measured constant count rate to instantaneous count rate.
- Instantaneous count rate is measured count rate times ratio of rastered area to detected area.

Figure 5.31. Dead time issues (count rate saturation).
Source: Wilson, Stevie, and Magee [72].

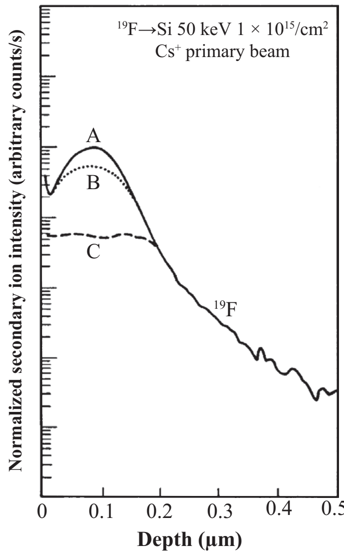

- Depth profiles of fluorine in Si with different count rates. Instantaneous counts are higher.
- The profiles are adjusted to show effect of different levels of count rate saturation on profile shape
- Expect 10% loss for multiplier receiving 4×10^6 cts/sec

Count rate at implant peak (counts/s):

	Average	Instantaneous
A.	1×10^5	2×10^6
B.	6×10^5	1.2×10^7
C.	1×10^6	2×10^7

Figure 5.32. Count rate saturation.
Source: Wilson, Stevie, and Magee [73].

5.7 SMALL AREA ANALYSIS

The amount of material analyzed in a SIMS depth profile is microscopic. Figure 5.34 helps illustrate the dimensions. For a sample size of 1 cm × 1 cm, a sputtered crater of 100 μm × 100 μm, analysis area 30 μm in

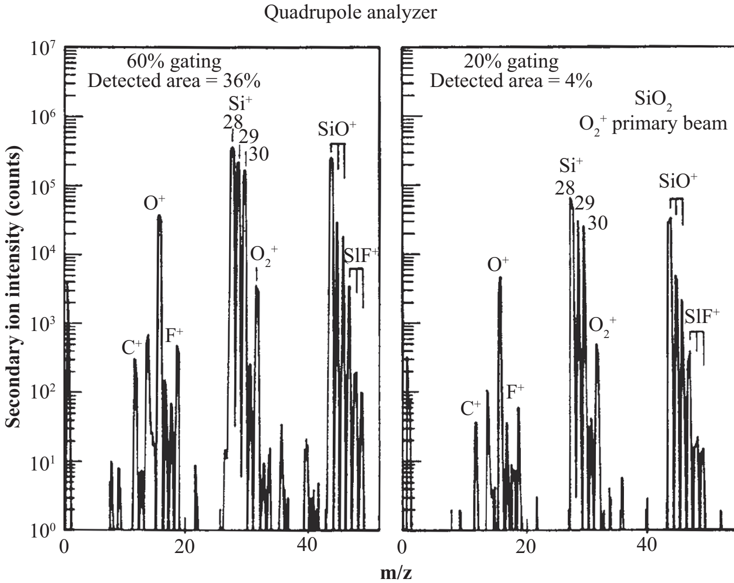

Figure 5.33. Count rate saturation.
Source: Wilson, Stevie, and Magee [74].

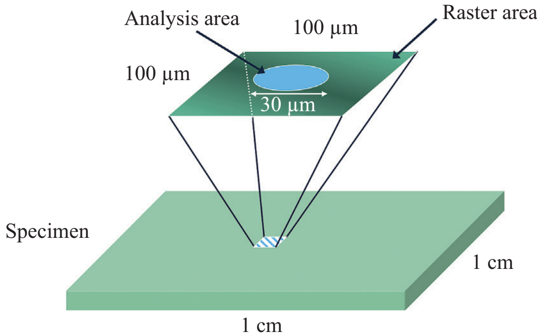

Figure 5.34. Analysis region.

diameter, and a 1 μm deep crater, the analysis volume is 7.1×10^{-10} cm^3. For a silicon matrix, the amount sampled is:

$$\text{Silicon density} \times \text{analysis volume} = 5 \times 10^{22} \text{ atoms/cm}^3 \times 7.1 \times 10^{-10} \text{ cm}^3$$
$$= 3.6 \times 10^{13} \text{ atoms} \times 28 \text{ g}/6.02 \times 10^{23} \text{ atoms}$$
$$= 1.7 \text{ ng}$$

This is a very small value and supports the need to obtain more than one analysis per sample.

Depth profiling is designed to provide good sensitivity and depth resolution by rastering an ion beam to sputter over a region and then detecting ions from a small area at the center of the raster. Small areas can be analyzed, but at a sacrifice of sensitivity and depth resolution. As the detected region is reduced, fewer atoms are available for analysis.

Useful yield is the ratio of ions detected to number of atoms present and a number of 0.1 percent might be expected for boron in silicon under O_2^+ bombardment. For silicon with density 5×10^{22} atoms/cm^3 and 10^{15} atoms/cm^2 in one monolayer, a 100 nm × 100 nm detected area has only 1×10^5 atoms in one monolayer. For a sputtering rate of 1 nm/s (or approximately 5 monolayers/s), we have 5×10^5 atoms/s. With a useful yield of 0.1 percent and a detection capability of 2 ions/s, the detection limit would be only 2×10^{20} atoms/cm^3 or 0.4 percent atomic. If useful yield is increased to 1 percent, the detection limit improves to 2×10^{19} atoms /cm^3, which is only marginally better than that for AES. This shows that there is a crossover point between SIMS and AES for sensitivity as the analysis region is decreased.

There is a practical limit to the analysis area. With modern SIMS instrumentation, it is usually fairly routine to perform a SIMS analysis on a region at least 100 μm × 100 μm in size. The detected area would typically be about 30 μm in the center of a raster over that area. As the analysis size is decreased, it becomes more difficult to align and conduct the analysis and the number of atoms available is reduced so the detection limit will not be as low [75].

For samples such as semiconductor wafers, the device features are less than 100 nm and are much smaller than the typical SIMS analysis detected area. Surface topography distorts profiles obtained from a small area [76], and even though some studies have been made in on-chip areas [77], the size of the features precludes direct SIMS analysis. One approach has been to design dedicated SIMS analysis patterns in the space between the chips and these have been in use for some time [78–80]. The size of the pattern is constrained to be on the order of 100 μm in one dimension but can be longer in the other dimension, so that rectangular or square patterns can be available. The advantage of the rectangular pattern is that there is enough space to sputter for alignment and analysis on the same structure. Since the semiconductor wafer has a high degree of repetition, patterns may be available across the wafer so that analyses can be made that test one area of the wafer versus another. Layers of interest can be deposited on SIMS patterns at the same time the layers are deposited on the rest of the wafer to produce semiconductor devices. This approach provides a duplicate of the small transistor structures, but on a scale that can be easily

analyzed with SIMS. Figure 5.35 shows an example of a SIMS pattern layout on a semiconductor wafer. Figure 5.36 shows a diagram of complementary metal oxide semiconductor structures with analysis sites of interest marked with arrows. Figure 5.37 shows two profiles obtained from dedicated SIMS analysis areas for those sites on a 0.35 μm technology wafer. PTOX refers to PTHINOX, which represents the p type source and drain profile. NCHAN refers to n type channel and shows doping of the polycrystalline silicon and the gate oxide in the channel region. It might also include a silicide over the polycrystalline silicon. Detection limits at or below 1×10^{16} atoms/cm^3 could be obtained for boron, phosphorus, and arsenic dopant elements. For larger chips, some on-chip patterns have been designed and utilized.

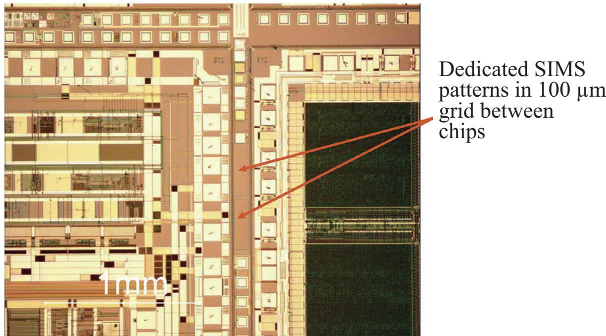

Figure 5.35. SIMS patterns on silicon patterned wafers.
Source: F. Stevie, AT&T Bell Laboratories.

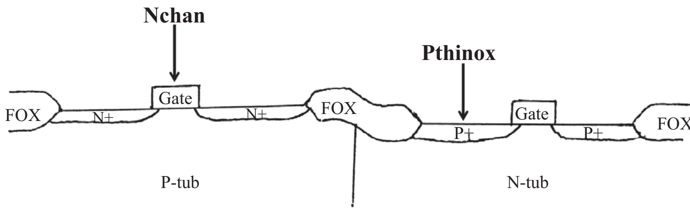

Fox – Field oxide
Gate oxide present under gate

Figure 5.36. 0.35 μm technology CMOS analysis sites.

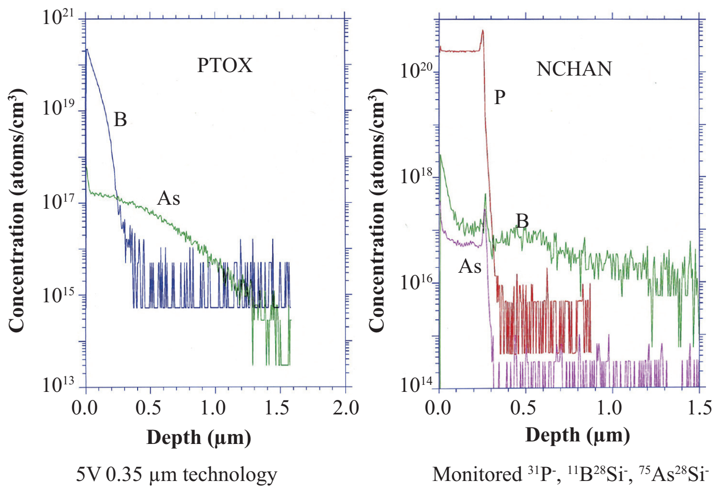

Figure 5.37. Dopant profiles from SIMS test areas.
Source: F. Stevie, AT&T Bell Laboratories.

5.8 NONUNIFORM DISTRIBUTION

For a depth profile, the secondary ions detected represent a lateral average over the detected region. If the species of interest is laterally nonuniform on the surface or at any depth, the detected species will sum those nonuniform regions (often due to particles) and the surrounding area. Figure 5.38 shows a schematic drawing of a region where the species of interest is nonuniform. Figure 5.39 shows a SIMS depth profile and a transmission electron microscopy micrograph of an annealed chromium ion implant region containing microscale nonuniformities at a depth just past the projected range of the original ion implant. The small chromium concentrations average to the same value for a relatively large detected area. If the nonuniformities are small and evenly distributed, multiple depth profiles will provide similar results. Figure 5.40(a) shows a profile typical for a region with a large particle. The shape of the profile usually shows a sharp drop in concentration until the particle has been sputtered away [81]. Figure 5.40(b) shows a boron profile in silicon with a dynamic range not as large as expected. A repeat analysis taken adjacent to the first measurement shows the anticipated profile. The difference was due to a boron particle. A simple way to check for nonuniformities is to take a second depth profile. It is almost impossible for two depth profiles to be identical if the sample has large particulates or a significant nonuniform

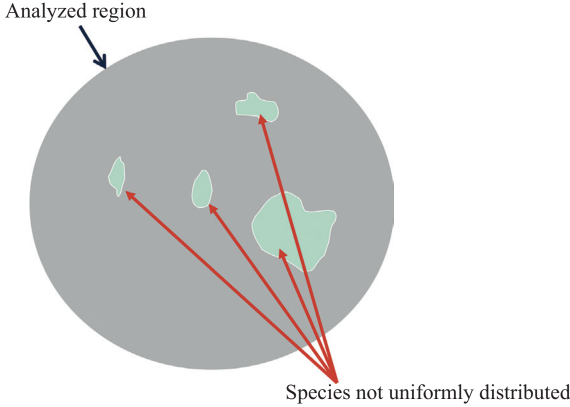

Figure 5.38. Nonuniform distribution.

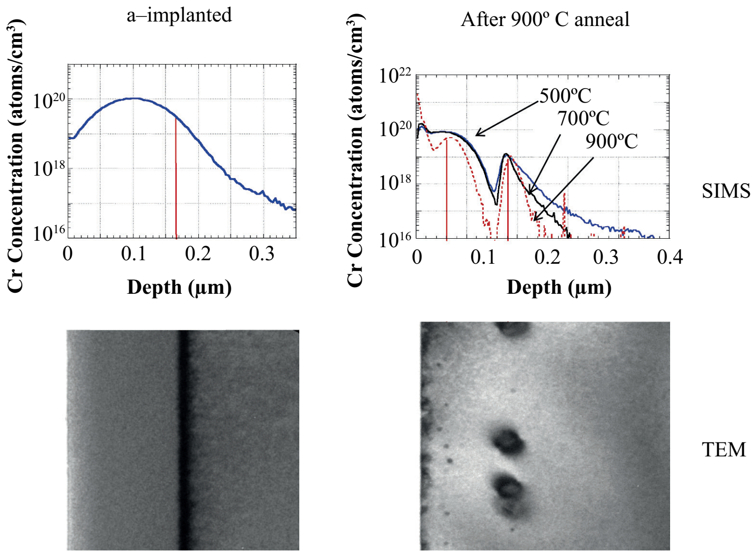

Figure 5.39. Nonuniform distribution—diffusion of implanted Cr in Si. *Source*: H. Francois Saint Cyr and F. Stevie, University of Central Florida.

distribution of an element. Another approach is to obtain a secondary ion image of each species at each measurement. This image depth profile can be examined after the analysis has been completed and selected regions chosen to eliminate the contributions of nonuniform regions.

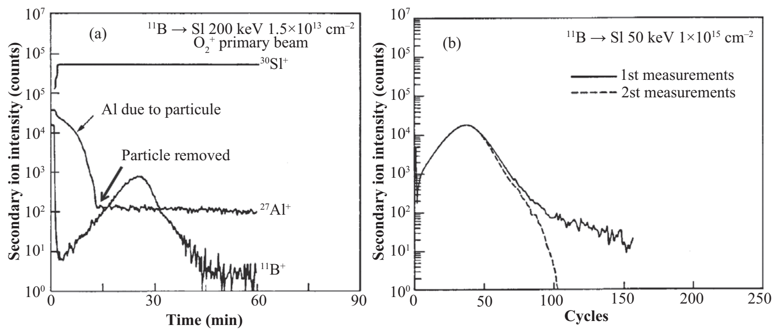

Figure 5.40. Particulates or nonuniform distributions. (a) Depth profile of B implant in Si. Profile shape of Al particle shown. (b) Distortion of first profile due to localized B source, second profile adjacent to first.
Source: Wilson, Stevie, and Magee [81].

5.9 IMAGE DEPTH PROFILE—LATERAL RESOLUTION

As noted, an image depth profile is a preferred way to obtain SIMS data because it is possible to do retrospective analysis. With this capability, nonuniform regions can be removed during data reduction to obtain a profile more representative of the material. The signal can also be maximized by observation of the signal that can be included near crater edges where it might otherwise be rejected [82, 83]. Figure 5.41 shows an image depth profile of FIB implants of gallium into silicon [84]. The result can be displayed in a three-dimensional figure, and in this case, because the implant dose is known, the gallium can be quantified. Note that the interaction region for an ion that bombards the surface of a sample is on the order of 10 nm in diameter and sets a practical limit for lateral resolution.

5.10 MOVEMENT OF SPECIES DUE TO CHEMICAL EFFECT

Movement of certain species is possible due to chemical effects. Gibbsian segregation is the tendency of one species in a multielement solid to increase concentration at the surface because the chemical potential is lower than the rest of the solid. A strong chemical gradient can be produced at the surface by adsorption of oxygen [85]. Use of an oxygen primary

Images normalized to matrix ion species
RSFs used to convert per pixel secondary ion intensity to atom density
Impurity density in atoms/cm^3 = $I_i/_m \times$ RSF
where I_i = impurity isotope intensity (counts/s)
I_m = matrix isotope intensity (counts/s)

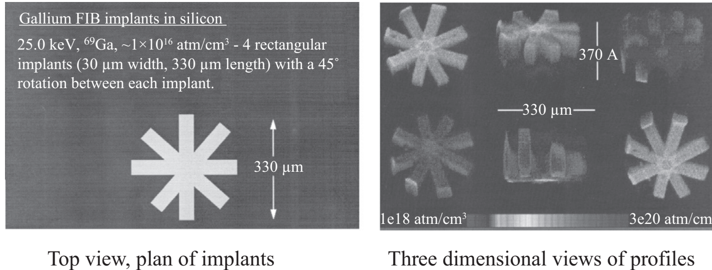

Top view, plan of implants — Three dimensional views of profiles

Figure 5.41. Quantitative 3-D image depth profiling.
Source: Gillen and Myklebust [84], reprinted with permission from John Wiley and Sons.

beam can produce a similar effect, referred to as ion beam induced segregation. If copper implanted in silicon is analyzed at normal incidence, total oxidation of the silicon occurs during the depth profile. The primary beam generated electric field across that oxide layer can cause the copper to move away from the oxide/silicon interface and an implant shape will be severely distorted [86–90]. In this case bombardment at less oxidizing angle of incidence, such as 64° from normal, will provide a more accurate profile. This effect has also been observed for silver and cesium [91].

REFERENCES

[1] Zinner, E. 1980. "Depth Profiling by Secondary Ion Mass Spectrometry." *Scanning* 3, no. 2, pp. 57–78. doi: http://dx.doi.org/10.1002/sca.4950030202

[2] Magee, C.W., and R.E. Honig. 1982. "Depth Profiling by SIMS—Depth Resolution, Dynamic Range and Sensitivity." *Surface and Interface Analysis* 4, no. 2, pp. 35–41. doi: http://dx.doi.org/10.1002/sia.740040202

[3] Wittmaack, K. 1982. "Depth Profiling by Means of SIMS: Recent Progress and Current Problems." *Radiation Effects* 63, no. 1–4, pp. 205–18. doi: http://dx.doi.org/10.1080/00337578208222841

[4] Hofmann, S. 1991. "Compositional Depth Profiling by Sputtering." *Progress in Surface Science* 36, no. 1, 35–87. doi: http://dx.doi.org/10.1016/0079-6816(91)90013-t

[5] Chu, P.K. 1992. "Dynamic Secondary Ion Mass Spectrometry." In *Encyclopedia of Materials Characterization—Surfaces, Interfaces, and Thin Films*, eds. C.R. Brundle, C.A. Evans, Jr., and S. Wilson, 532. Boston, MA: Butterworth-Heinemann.

[6] Wittmaack, K. 1977. "Raster Scanning Depth Profiling of Layer Structures." *Applied Physics* 12, no. 2, pp. 149–56. doi: http://dx.doi.org/10.1007/bf00896140

[7] Wilson, R.G., F.A. Stevie, and C.W. Magee. 1989. *Secondary Ion Mass Spectrometry*, I–9. New York: Wiley.

[8] Wilson, R.G., F.A. Stevie, and C.W. Magee. 1989. *Secondary Ion Mass Spectrometry*, 1.5–2. New York: Wiley.

[9] Pantano, C.G. 1986. *SIMS*, *Metals Handbook Ninth Edition*, Vol. 10, ed. R.E. Whan, 610. American Society for Metals, Metals Park.

[10] Wilson, R.G., F.A. Stevie, and C.W. Magee. 1989. *Secondary Ion Mass Spectrometry*, 2.1–8. New York: Wiley.

[11] Wilson, R.G., F.A. Stevie, and C.W. Magee. 1989. *Secondary Ion Mass Spectrometry*, 2.1–7. New York: Wiley.

[12] Stevie, F.A. 1992. "Secondary Ion Mass Spectrometry Analysis Strategy for Shallow Junctions on Test And Product Silicon Wafers." *Journal of Vacuum Science & Technology B* 10, no. 1, 323. doi: http://dx.doi.org/10.1116/1.586353

[13] Wittmaack, K. 1980. "Aspects of Quantitative Secondary Ion Mass Spectrometry." *Nuclear Instruments and Methods* 168, no. 1–3, 343–56. doi: http://dx.doi.org/10.1016/0029-554x(80)91275-6

[14] Jiang, Z. X, and P.F.A. Alkemade. 1999. "The Surface Transient in Si for SIMS with Oblique Low-Energy O_2^+ Beams." *Surface and Interface Analysis* 27, no. 3, pp. 125–31. doi: http://dx.doi.org/10.1002/(sici)1096-9918(199903)27:3%3C125::aid-sia490%3E3.0.co;2-8

[15] Wittmaack, K. 1996. "Sputtering Yield Changes, Surface Movement and Apparent Profile Shifts in SIMS Depth Analyses of Silicon Using Oxygen Primary Ions." *Surface and Interface Analysis* 24, no. 6, pp. 389–98. doi: http://dx.doi.org/10.1002/(sici)1096-9918(199606)24:6%3C389::aid-sia135%3E3.0.co;2-l

[16] Williams, P., and J.E. Baker. 1981. "Implantation and Ion Beam Mixing in Thin Film Analysis." *Nuclear Instruments and Methods* 182–183, pp. 15–24. doi: http://dx.doi.org/10.1016/0029-554x(81)90667-4

[17] Wittmaack, K. 1984. "Beam-Induced Broadening Effects in Sputter Depth Profiling." *Vacuum* 34, no. 1–2, pp. 119–37. doi: http://dx.doi.org/10.1016/0042-207x(84)90115-5

[18] Vandervorst, W., H.E. Maes, and R.F. DeKeersmaecker. 1984. "Secondary Ion Mass Spectrometry: Depth Profiling of Shallow As Implants in Silicon and Silicon Dioxide." *Journal of Applied Physics* 56, no. 5, p. 1425. doi: http://dx.doi.org/10.1063/1.334142

[19] Lidzbarski, E., and J.D. Brown. 1986. “Selective Sputtering and Ion Beam Mixing Effects on SIMS Depth Profiles.” In *Secondary Ion Mass Spectrometry, SIMS V*, eds. A. Benninghoven, R.J. Colton, D.S. Simons, and H.W. Werner, 306. Berlin, Germany: Springer-Verlag.

[20] Clegg, J.B. 1987. “Depth Profiling of Shallow Arsenic Implants in Silicon using SIMS.” *Surface and Interface Analysis* 10, no. 7, 332–37. doi: http://dx.doi.org/10.1002/sia.740100704

[21] McPhail, D.S., E.A. Clark, J.B. Clegg, M.G. Dowsett, J.P. Gold, G.D.T. Spiller, and D. Sykes. 1988. “The Depth Resolution of Secondary Ion Mass Spectrometers: A Critical Evaluation.” *Scanning Microscopy* 2, no. 2, pp. 639–52.

[22] Clegg, J.B., and R.B. Beall. 1989. “Measurement of Narrow Si Dopant Distributions in GaAs by SIMS.” *Surface and Interface Analysis* 14, no. 6–7, pp. 307–14. doi: http://dx.doi.org/10.1002/sia.740140607

[23] Meuris, M., W. Vandervorst, P. De Bisschop, and D. Avau. 1989. “Mass and Energy Dependence of Depth Resolution in Secondary-Ion Mass Spectrometry Experiments with Iodine, Oxygen, and Cesium Beams on AlGaAs Multilayer Structures.” *Applied Physics Letters* 54, no. 16, p. 1531. doi: http://dx.doi.org/10.1063/1.101341

[24] Chunzhi Gu. 2006. *SIMS Quantification of Matrix and Impurity Species in III-Nitride Alloys* [dissertation]. North Carolina State University http://www.lib.ncsu.edu/resolver/1840.16/4640

[25] www.srim.org

[26] Wilson, R.G, F.A. Stevie, and C.W. Magee. 1989. *Secondary Ion Mass Spectrometry*, 2.4–6. New York: Wiley.

[27] Corcoran, S.F., and S.B. Felch. 1992. “Evaluation of Polyencapsulation, Oxygen Leak, and Low Energy Ion Bombardment in the Reduction of Secondary Ion Mass Spectrometry Surface Ion Yield Transients.” *Journal of Vacuum Science & Technology B* 10, no. 1, pp. 342–47. doi: http://dx.doi.org/10.1116/1.586356

[28] Ng, C.M., A.T.S. Wee, C.H.A. Huan, N. Yakoviev, and A. See. 2002. “Evaluation of the Silicon Capping Technique in SIMS.” *Surface and Interface Analysis* 33no. 9, pp. 735–41. doi: http://dx.doi.org/10.1002/sia.1443

[29] Miwa, S. 2004. “a-Si Capping SIMS for Shallow Dopant Profiles.” *Applied Surface Science* 231–232, pp. 658–62. doi: http://dx.doi.org/10.1016/j.apsusc.2004.03.138

[30] Stevie, F.A., E.P. Martin, Jr., P.M. Kahora, J.T. Cargo, A.K. Nanda, A.S. Harrus, A.J. Muller, and H.W. Krautter. 1991. “Boron Contamination of Surfaces in Silicon Microelectronics Processing: Characterization and Causes.” *Journal of Vacuum Science & Technology A* 9, no. 5, pp. 2813–16. doi: http://dx.doi.org/10.1116/1.577206

[31] Zalm, P.C. 1995. “Ultra Shallow Doping Profiling with SIMS.” *Reports on Progress in Physics* 58, no. 10, pp. 1321–74. doi: http://dx.doi.org/10.1088/0034-4885/58/10/004

[32] Dowsett, M.G. 2003. "Depth Profiling Using Ultra-Low-Energy Secondary Ion Mass Spectrometry." *Applied Surface Science* 203–204, pp. 5–12. doi: http://dx.doi.org/10.1016/s0169-4332(02)00630-x

[33] Alkemade, P.F.A., Z.X. Jiang, C.C.G. Visser, and S. Radelaar. 1998. "Ultra-high Depth Resolution Secondary Ion Mass Spectrometry with Sub-keV Grazing O_2^+ Beams." *Journal of Vacuum Science & Technology B* 16, no. 1, p. 373. doi: http://dx.doi.org/10.1116/1.589813

[34] Jiang, Z.X., and P.F.A. Alkemade. 1998. "Secondary Ion Mass Spectrometry and Atomic Force Spectroscopy Studies of Surface Roughening, Erosion Rate Change and Depth Resolution in Si During 1 keV 60° O_2^+ Bombardment with Oxygen Flooding." *Journal of Vacuum Science & Technology B* 16, no. 4, p. 1971. doi: http://dx.doi.org/10.1116/1.590116

[35] Ronsheim, P.A.,K.L. Lee, S.B. Patel, and M. Schuhmacher. 1998. "A Comparison of Normal Incidence versus Oblique Incidence with an Oxygen Flood for Sub 10 nm Depth Profiles of Boron in Silicon." In *Secondary Ion Mass Spectrometry, SIMS XI*, eds. G. Gillen, R. Lareau, J. Bennett, and F. Stevie, 301. Chichester, United Kingdom: Wiley.

[36] Iltgen,K., O. Brox, and A. Benninghoven. 1998. "Ultra Shallow Depth Profiling by TOF-SIMS: Investigation of the Transient Region." In *Secondary Ion Mass Spectrometry, SIMS XI*, eds. G. Gillen, R. Lareau, J. Bennett, and F. Stevie, 305. Chichester, United Kingdom: Wiley.

[37] Lee, J.J., T. Neil, L. Wu, S. Collins, and D. Sieloff. 1998. "Depth Profiling of Ultra-Shallow B Implants Using a Cameca IMS-6F." In *Secondary Ion Mass Spectrometry, SIMS XI*, eds. G. Gillen, R. Lareau, J. Bennett, and F. Stevie, 309. Chichester, United Kingdom: Wiley.

[38] Giubertoni, D., M. Bersani, M. Barozzi, S. Pederzoli, E. Iacob, J.A. van den Berg, and M. Werner. 2006. "Comparison Between the SIMS and MEIS Techniques for the Characterization of Ultra Shallow Arsenic Implants." *Applied Surface Science* 252, no. 19, pp. 7214–17.doi: http://dx.doi.org/10.1016/j.apsusc.2006.02.137

[39] Kataoka, Y., and T. Itani. 2007. "Ultrashallow Depth Profiling Using SIMS and Ion Scattering Spectroscopy." *Surface and Interface Analysis* 39, no. 10, pp. 826–31. doi: http://dx.doi.org/10.1002/sia.2597

[40] Vandervorst, W. 2008. "Semiconductor Profiling with Sub-nm Resolution: Challenges and Solutions." *Applied Surface Science* 255, no. 4, pp. 805–12. doi: http://dx.doi.org/10.1016/j.apsusc.2008.05.090

[41] Honicke, P., B. Beckhoff, M. Kolbe, D. Giubertoni, J. van den Berg, and G. Pepponi. 2010. "Depth Profile Characterization of Ultra Shallow Junction Implants." *Analytical and Bioanalytical Chemistry* 396, no. 8, pp. 2825–32. doi: http://dx.doi.org/10.1007/s00216-009-3266-y

[42] Mohacsi, I., P. Petrik. M. Fried, T. Lohner, J.A. van den Berg, M.A. Reading, D. Giubertoni, M. Barozzi, and A. Parisini. 2011. "Characterisation of Ultra-Shallow Disorder Profiles and Dielectric Functions in Ion Implanted Si." *Thin Solid Films* 519, no. 9, pp. 2847–51. doi: http://dx.doi.org/10.1016/j.tsf.2010.12.076

[43] Liu, R., and A.T.S. Wee. 2004. "Sub-keV Secondary Ion Mass Spectrometry Depth Profiling: Comparison of Sample Rotation and Oxygen Flooding." *Applied Surface Science* 231–232, pp. 653–57. doi: http://dx.doi.org/10.1016/j.apsusc.2004.03.136

[44] Hoffman, S. 2000. "Ultimate Depth Resolution and Profile Reconstruction in Sputter Profiling with AES and SIMS." *Surface and Interface Analysis* 30, no. 1, pp. 228–36. doi: http://dx.doi.org/10.1002/1096-9918(200008)30:1%3C228::aid-sia821%3E3.3.co;2-5

[45] Merkulov, A., P. Peres, S. Choi, F. Desse, and M. Schuhmacher. 2010. "Advanced SIMS Quantification in the First Few nm of B, P and As Ultrashallow Implants." *Surface and Interface Analysis* 43, no. 1–2, pp. 522–24. doi: http://dx.doi.org/10.1002/sia.3459

[46] Juhel, M., F. Laugier, D. Delille, C. Wyon, L. F. Tz. Kwakman, and M. Hopstaken. 2006. "SIMS Depth Profiling of Boron Ultra Shallow Junctions Using Oblique O_2^+ Beams Down to 150eV." *Allied Surface Science* 252, no. 19, pp. 7211–13. doi: http://dx.doi.org/10.1016/j.apsusc.2006.02.242

[47] Giubertoni, D., G. Pepponi, B. Beckhoff, P. Hoenicke, S. Gennaro, F. Meirer, D. Ingerie, G. Steinhauser, M. Fried, P. Petrik, A. Parisini, M.A. Reading, C. Streli, J.A. van den Berg, and M. Bersani. 2009. "Multi-Technique Characterization of Arsenic Ultra Shallow Junctions in Silicon within the ANNA Consortium." In *Frontiers of Characterization and Metrology for Nanoelectronics*, AIP, ed. D.G. Seiler et al., p. 45

[48] McPhail, D.S., M.G. Dowsett, and E.H.C. Parker. 1986. "Loss of Depth resolution with Depth in Secondary Ion Mass Spectrometry (SIMS) Due to Variations in Ion Dose Density Across the Rastered Area." *Vacuum* 36, no. 11–12, pp. 997–1000. doi: http://dx.doi.org/10.1016/0042-207x(86)90154-5

[49] Robinson, R.S., and S.M. Rossnagel. 1982. "Ion-Beam-Induced Topography and Surface Diffusion." *Journal of Vacuum Science and Technology* 21, no. 3, p. 790. doi: http://dx.doi.org/10.1116/1.571826

[50] Robinson, R.S., and S.M. Rossnagel. 1984. "Diffusion Processes in Bombardment-Induced Surface Topography." In *Ion Bombardment Modification of Surfaces*, eds. O. Auciello, and R. Kelly, 299. Amsterdam, Netherlands: Elsevier.

[51] Duncan, S., R. Smith, D.E. Sykes, and J.M. Walls. 1984. "Surface Morphology of Si(100), GaAs(100) and InP(100) Following O_2^+ and Cs^+ Ion Bombardment." *Vacuum* 34, no. 1–2, pp. 145–151. doi: http://dx.doi.org/10.1016/0042-207x(84)90117-9

[52] Bradley, R.M., and J.M.E. Harper. 1988. "Theory of Ripple Topography Induced by Ion Bombardment." *Journal of Vacuum Science & Technology A* 6, no. 4, p. 2390. doi: http://dx.doi.org/10.1116/1.575561

[53] Stevie, F.A, P.M. Kahora, D.S. Simons, and P. Chi. 1988. "Secondary Ion Yield Changes in Si and GaAs Due to Topography Changes During O_2^+

or Cs^+ Ion Bombardment." *Journal of Vacuum Science & Technology A* 6, no. 1, p. 76. doi: http://dx.doi.org/10.1116/1.574972

[54] Jiang, Z.X., and P.F.A. Alkemade. 1998. "The Complex Formation of Ripples During Depth Profiling of Si with Low Energy, Grazing Oxygen Beams." *Applied Physics Letters* 73, no. 3, p. 315. doi: http://dx.doi.org/10.1063/1.121819

[55] Jiang, Z.X., and P.F.A. Alkemade .1998. "Erosion Rate Change and Surface Roughening in Si During Oblique O_2^+ Bombardment with Oxygen Flooding." In *Secondary Ion Mass Spectrometry, SIMS XI*, eds. G. Gillen, R. Lareau, J. Bennett, and F. Stevie, 431. Chichester, United Kingdom: Wiley.

[56] Prenitzer, B.I., L.A. Giannuzzi, B.W. Kempshall, J.M. McKinley, and F.A. Stevie. 2000. "Microstructural Evaluation of SIMS Crater Roughening." In *Secondary Ion Mass Spectrometry, SIMS 12*, eds. A. Benninghoven, P. Bertrand, H. –N. Migeon, and H.W. Werner, 77. Amsterdam, Netherlands: Elsevier.

[57] Zalar, A. 1985. "Improved Depth Resolution by Sample Rotation During Auger Electron Spectroscopy Depth Profiling." *Thin Solid Films* 124, no. 3–4, pp. 223–30. doi: http://dx.doi.org/10.1016/0040-6090(85)90269-x

[58] Cirlin, E.-H., J.J. Vajo, T.C. Hasenberg, and R.J. Hauenstein. 1990. "High Resolution Secondary Ion Mass Spectrometry Depth Profiling Using Continuous Sample Rotation and Its Application to Superlattice and Delta-Doped Sample Analysis." *Journal of Vacuum Science & Technology A* 8, no. 6, pp. 4101. doi: http://dx.doi.org/10.1116/1.576447

[59] Cirlin, E.-H, J.J. Vajo, R.E. Doty, and T.C. Hasenberg. 1991. "Ion-Induced Topography, Depth Resolution, and Ion Yield During Secondary Ion Mass Spectrometry Depth Profiling of a GAAs/AlGaAs superlattice: Effects of Sample Rotation." *Journal of Vacuum Science & Technology A* 9, no. 3, p. 1395. doi: http://dx.doi.org/10.1116/1.577634

[60] Stevie, F.A., and J.L. Moore. 1992. "Application of Sample Rotation to Secondary Ion Mass Spectrometry Depth Profiling of Aluminum Metallization." *Surface and Interface Analysis* 18, no. 2, pp. 147–52. doi: http://dx.doi.org/10.1002/sia.740180215

[61] Hofmann, S., A. Zalar, E. –H. Cirlin, J.J. Vajo, H.J. Mathieu, and P. Panjan. 1993. "Interlaboratory Comparison of the Depth Resolution in Sputter Depth Profiling of Ni/Cr Multilayers with and without Sample Rotation Using AES, XPS and SIMS." *Surface and Interface Analysis* 20, no. 8, pp. 621–26. doi: http://dx.doi.org/10.1002/sia.740200803

[62] Stevie, F.A., J.L. Moore, S.M. Merchant, C.A. Bollinger, and E.A. Dein. 1994. "Secondary Ion Mass Spectrometry Analysis of a Three-Level Metal Structure Using Sample Rotation." *Journal of Vacuum Science & Technology A* 12, no. 4, pp. 2363. doi: http://dx.doi.org/10.1116/1.579215

[63] Hofmann, S., and A. Zalar. 1994. "Depth Profiling with Sample Rotation: Capabilities and Limitations." *Surface and Interface Analysis* 21, no. 5, pp. 304–09. doi: http://dx.doi.org/10.1002/sia.740210507

[64] Stevie, F.A., R.G. Wilson, J.M. McKinley, and C.J. Hitzman. 1998. "Multiple Element Ion Implants for Metal Contamination Analysis in Semiconductor Technology." In *Secondary Ion Mass Spectrometry, SIMS XI*, eds. G. Gillen, R. Lareau, J. Bennett, and F. Stevie, 983. Chichester, United Kingdom: Wiley.

[65] von Criegern, R., I. Weitzel, H. Zeininger, and R. Lange-Giesler. 1990. "Optimization of the Dynamic Range of SIMS Depth Profiles by Sample Preparation." *Surface and Interface Analysis* 15, no. 7, pp. 415–21. doi: http://dx.doi.org/10.1002/sia.740150704

[66] Gillen, G. 1992. "High Dynamic Range SIMS Depth Profiling on In Situ Ion-beam-generated Mesas Using the Ion Microscope." *Surface and Interface Analysis* 18, no. 11, pp. 777–80. doi: http://dx.doi.org/10.1002/sia.740181107

[67] Wittmaack, K., and J.B. Clegg. 1980. "Dynamic Range of 10^6 in Depth Profiling Using Secondary-Ion Mass Spectrometry." *Applied Physics Letters* 37, no. 3, p. 285. doi: http://dx.doi.org/10.1063/1.91908

[68] Deline, V. 1983. "Instrumental Cross-Contamination in the CAMECA IMS-3F Secondary Ion Microscope." *Nuclear Instruments and Methods in Physics Research* 218, no. 13, pp. 316–18. doi: http://dx.doi.org/10.1016/0167-5087(83)90998-5

[69] Blackmore, G.W., S.J. Courtney, J. Geiss, S.J.C. Irvine, and S. Haq. 1988. "The Measurement of Gallium in Epitaxial Cd_x $Hg_{1-x}Te$ Grown on GaAs Substrate." In *Secondary Ion Mass Spectrometry, SIMS VI*, eds. A. Benninghoven, A.M. Huber, and H.W. Werner, 311. New York p: Wiley.

[70] Clegg, J.B. 1986. "Memory Effects in Qudrupole SIMS." In *Secondary Ion Mass Spectrometry, SIMS V*, eds. A. Benninghoven, R.J. Colton, D.S. Simons, and H.W. Werner, 112. Berlin, Germany: Springer-Verlag.

[71] Kurz, E.A. 1979. "Channel Electron Multipliers." *American Laboratory* 11, p. 67.

[72] Wilson, R.G., F.A. Stevie, and C.W. Magee, 1989. *Secondary Ion Mass Spectrometry*, 2.9–3. New York: Wiley.

[73] Wilson, R.G., F.A. Stevie, and C.W. Magee. 1989. *Secondary Ion Mass Spectrometry*, 2.9–5. New York: Wiley.

[74] Wilson, R.G., F.A. Stevie, and C.W. Magee. 1989. *Secondary Ion Mass Spectrometry*, 2.9–4. New York: Wiley.

[75] Meuris, M., P. De Bisschop, and W. Vandervorst. 1993. "Quantitative Study of Background Signals from Crater Edges and Surroundings in Depth Profiling of Small Areas with Secondary Ion Mass Spectrometry." *Surface and Interface Analysis* 20, no. 3, pp. 206–14. doi: http://dx.doi.org/10.1002/sia.740200304

[76] Walker, A.J., M.T. Borchert, C.J. Vriezema, and P.C. Zalm. 1990. "Influence of Surface Topography on Depth Profiles Obtained with Secondary-Ion Mass Spectrometry." *Applied Physics Letters* 57, no. 22, p. 2371. doi: http://dx.doi.org/10.1063/1.103874

[77] von Criegern, R., H. Zeininger, and S. Rohl. 1988. "The 4 Megabit DRAM Trench Wall Analysis—A Challenge for SIMS." In *Secondary Ion Mass Spectrometry, SIMS VI,* eds. A. Benninghoven, A.M. Huber, and H.W. Werner, 419. Chichester, United Kingdom: Wiley.

[78] Drum, C.M., and F.A. Stevie. 1984. "Determination of Junction Defect Densities and Determination by SIMS of Impurity Properties Using Bipolar SIC Test Structures." *Journal of the Electrochemical Society Extended Abstracts* 84–2, p. 673.

[79] Stevie, F.A., G.W. Cochran, P.M. Kahora, W.A. Russell, N. Linde, D.M. Wroge, A.M. Garcia, and M. Geva. 1992. "Test Structures for Secondary Ion Mass Spectrometry Analysis of Patterned Silicon Wafers." *Journal of Vacuum Science & Technology A: Vacuum, Surfaces, and Films* 10, no. 4, p. 2880. doi: http://dx.doi.org/10.1116/1.577724

[80] Harris, W.C., H.E. Smith, A.J. Pelillo, and J.L. Beagle. 1992. "Secondary Ion Mass Spectrometry Test Structures for Analyses of Semiconductor Product Wafers." *Journal of Vacuum Science & Technology A: Vacuum, Surfaces, and Films* 10, no. 4, p. 2887. doi: http://dx.doi.org/10.1116/1.577725

[81] Wilson, R.G., F.A. Stevie, and C.W. Magee. 1989. *Secondary Ion Mass Spectrometry*, 2.5–2. New York: Wiley.

[82] Patkin, A.J., and G.H. Morrison. 1982. "Secondary Ion Mass Spectrometric Image Depth Profiling for Three-Dimensional Elemental Analysis." *Analytical Chemistry* 54, no. 1, 2–5. doi: http://dx.doi.org/10.1021/ac00238a005

[83] Daiser, S.M., C. Scholze, and J.L. Maul. 1988. "The Checkerboard Technique: An Essential Progress in SIMS Data Acquisition and Evaluation." *Nuclear Instruments and Methods in Physics Research Section B: Beam Interactions with Materials and Atoms* 35, no. 3–4, pp. 544–49. doi: http://dx.doi.org/10.1016/0168-583x(88)90328-x

[84] Gillen, G., and R.L. Myklebust. 1992. "Quantitative Three-Dimensional SIMS Imaging Using the Ion Microscope." In *Secondary Ion Mass Spectrometry, SIMS VIII*, eds. A. Benninghoven, K.T.F. Janssen, J. Tumpner, and H.W. Werner, 509. Chichester, United Kingdom: Wiley.

[85] Hues, S.M., and P. Williams. 1986. "Oxygen-Induced Segregation Effects in Sputter Depth-Profiling." *Nuclear Instruments and Methods in Physics Research Section B: Beam Interactions with Materials and Atoms*15, no. 1–6, pp. 206–209. doi: http://dx.doi.org/10.1016/0168-583x(86)90286-7

[86] Boudewijn, P.R., H.W.P. Ackerboom, and M.N.C. Kempeners. 1984. "Profile Distortion in SIMS." *Spectrochimica Acta Part B: Atomic Spectroscopy* 39, no. 12, pp. 1567–71. doi: http://dx.doi.org/10.1016/0584-8547(84)80184-6

[87] Deline, V.R., W. Reuter, and R. Kelly. 1986. "Gibbsian Segregation During the Depth Profiling of Copper in Silicon." In *Secondary Ion Mass Spectrometry, SIMS V*, eds. A. Benninghoven, R.J. Colton, D.S. Simons, and H.W. Werner, 299. Berlin, Germany: Springer-Verlag.

[88] Boudewijn, P.R., and C.J. Vriezema. 1988. "Segregation Effects During SIMS Analysis of Cu-Implanted Si." In *Secondary Ion Mass Spectrometry, SIMS VI*, eds. A. Benninghoven, and A.M. Huber, and H.W. Werner, .499. Chichester, United Kingdom: Wiley.

[89] Homma, Y., and T. Maruo. 1989. "Comparison of Beam-Induced Profile Broadening Effects of Gallium and Copper in Oxygen-Bombarded Silicon." *Surface and Interface Analysis* 14, no. 11, 725–29. doi: http://dx.doi.org/10.1002/sia.740141108

[90] Vriezama, C.J., K.T.F. Janssen, G.M. Fontijn, and P.C. Zalm. 1990. "Field Induced Impurity Migration During SIMS Depth Profiling." In *Secondary Ion Mass Spectrometry, SIMS VII*, eds. A. Benninghoven, C.A. Evans, K.D. McKeegan, H.A. Storms, and H.W. Werner, 619. Chichester, United Kingdom: Wiley.

[91] Vriezema, C.J., and P.C. Zalm. 1991. "Impurity Migration During SIMS Depth Profiling." *Surface and Interface Analysis* 17, no. 12, pp. 875–87. doi: http://dx.doi.org/10.1002/sia.740171207

CHAPTER 6

QUANTIFICATION

6.1 NEED FOR SECONDARY STANDARDS

For elemental analysis, the first question asked is “What elements are present?” and the second question is “How much?” The secondary ion mass spectrometry (SIMS) technique is not self-quantitative and requires secondary standards. As was shown in Chapter 2, secondary ion yields can vary over five to six orders of magnitude for the periodic table and can also vary from matrix to matrix. Therefore one cannot reliably estimate quantity based on relative intensities. Other techniques used for elemental analysis, such as Auger electron spectroscopy (AES) or x-ray photoelectron spectroscopy (XPS), show most elements with about a factor of 20 variation in sensitivity. The secondary ion emission models discussed in Chapter 2 did provide methods to estimate quantitative data but the results were not sufficiently accurate. More accurate results could be obtained by the use of ion implanted or bulk doped standards [1, 2].

6.2 DEPTH PROFILE QUANTIFICATION—RELATIVE SENSITIVITY FACTORS

Relative sensitivity factors (RSFs) derived from ion implanted or bulk doped samples have been widely used for SIMS depth profile quantification. The RSF converts secondary ion intensity to concentration:

$$\rho_i = (I_i/I_m)(RSF) \tag{6.1}$$

where ρ_i is the impurity concentration (atomic density) in atoms/cm^3

I_i is the impurity isotope secondary ion intensity in counts/s

I_m is the matrix isotope secondary ion intensity in counts/s

RSF has units of atoms/cm^3, and the RSF of the matrix element is equal to the atomic density of the matrix (for example, the RSF for silicon in a silicon matrix is 5×10^{22} atoms/cm^3).

The RSF calculation for a depth profile of an ion implanted standard is relatively simple. Most of the information is obtained from the depth profile.

$$RSF = (\Phi C I_m t)/(z I_s) \tag{6.2}$$

where Φ is the implanted dose (fluence, areal density) in atoms/cm^2

C is the number of data cycles

I_m is the matrix isotope secondary ion intensity in counts/s

t is the count time/cycle for species of interest (usually 1s)

z is the depth of crater in cm

I_s is the summation of secondary ion intensity of species of interest in counts

The calculation has two important assumptions: Implanted dose is correct (or, for a bulk standard, dopant concentration is correct) and sputtering rate (crater depth/analysis time) is uniform.

If it is possible to subtract a background count rate from the profile, then the RSF equation becomes

$$RSF = (\Phi C I_m t)/(z I_s - z I_b C) \tag{6.3}$$

where I_b is the background secondary ion intensity in counts/s

Note that the background count rate may be subtracted in the analysis of an ion implanted standard but this approach can be questionable for the sample of interest that might contain a constant low level of impurity.

Accurate SIMS quantification of an element in a matrix can be obtained with ion implanted standards. A depth profile of an ion implanted sample provides not only quantification but also sensitivity in the form of a detection limit. Figure 6.1(a) shows a raw data depth profile for ion implanted ^{58}Ni in silicon in the form of counts versus time or data cycles. One cycle is one measurement of secondary ion counts on each species. Figure 6.1(b) shows the reduced data plot of the same data in the form of concentration or atomic density versus depth. The concentration is determined by knowledge of the implanted dose and calculation of RSF. The conversion to concentration is made on a point-by-point basis using Equation (6.1). The depth axis was converted by measurement of the crater depth. If a uniform sputtering rate is achieved in a homogeneous

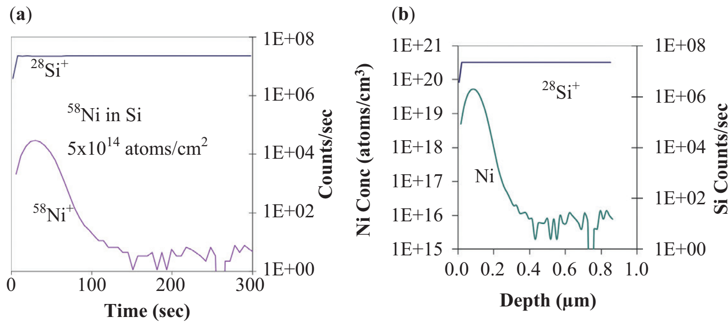

- Raw data in counts versus time
- Convert to reduced data in concentration versus depth

Figure 6.1. Conversion of raw to reduced data. (a) Raw data. (b) Reduced data.
Source: F. Stevie, Analytical Instrumentation Facility, North Carolina State University.

material, scaling of the depth axis will be linear. For multilayer structures, the sputtering rate will not be uniform and corrections are required for each layer.

The crater depth is normally measured after the analysis using a diamond stylus profilometer. These instruments are specified with less than 1 percent error and can measure features less than 20 nm in depth. The performance of these instruments is remarkable since repeatability can be 1 nm, which is equivalent to only five atomic layers. Optical measurements of crater depth can be obtained during the analysis without removing the sample from the instrument. However, this method is difficult to calibrate for multilayer samples.

Small variations in height over a sample holder can affect extraction of secondary ion species, particularly for instruments such as a magnetic sector where 4500 V extraction is often used over a distance of 4.5 mm. Normalization to a matrix species is used to account for differences due to different sample holder positions and sample holders. Figure 6.2 shows three normalization methods: measurement of matrix species at the end of profile, average matrix intensity, and point-by-point reference to a matrix profile. The point-by-point method has the advantage of correcting for small variations that can occur within a single depth profile as well as between profiles.

Note that where an unknown sample has been measured and quantified, it is possible to determine the equivalent dose. In this case Equation (6.2) is used to solve for dose, Φ. This calculation is commonly

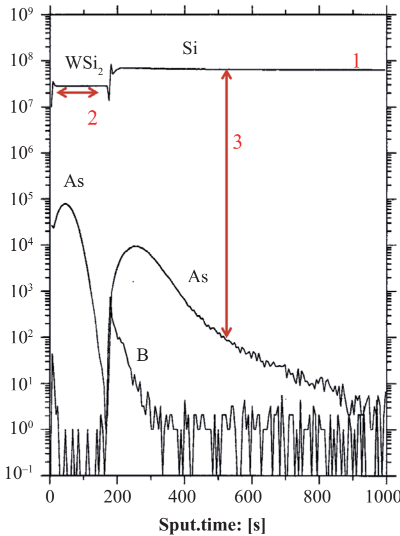

WSi_2/Si with As implanted in layer and substrate

Measure matrix species to accommodate analysis variations due to factors such as sample position on holder

Three methods
1. Measurement at end of profile
2. Average over region of interest
3. Point by point

Figure 6.2. Normalization.
Source: F. Stevie AT&T Bell Laboratories.

performed for checks on ion implantation and for analyses of alkali element contamination in insulators (see Chapter 8).

6.3 ION IMPLANTED STANDARDS

The typical method for quantification of SIMS depth profiles has been the use of ion implantation, by which the element of interest can be placed in the matrix under study. The dose of the ion implant is obtained from the ion implanter and allows an accurate determination of concentration in the sample. The success of this approach is perhaps demonstrated by the amount of RSF data from ion implants accumulated by various researchers. Tables of RSF values can be found in the literature [3–18].

The quantification sequence for the element of interest is:

- Obtain ion implant of the element in the same matrix as the material of interest
- Depth profile through the implanted region of the standard
- Calculate RSF (and determine detection limit)
- Use RSF to quantify element in depth profile of the material under study

Even though an ion implant is required for each species quantified, the use of ion implanted standards has great versatility and has dominated quantification of depth profiles. There are several reasons for this:

- All elements and isotopes can be implanted
- Depth can be varied with implant energy
- Peak concentration can be varied with dose
- All substrates and structures can be implanted
- Multiple elements can be implanted into a single substrate
- Detection limit can be calculated

The variation of implant energy, dose, and detection limit on an ion implant profile is illustrated in Figure 6.3, which displays an ion implant of ^{24}Mg in GaN. It is possible to implant multiple elements in the same sample. This provides several RSFs from one analysis. Figure 6.4 shows depth profiles of boron, phosphorus, and arsenic implants in silicon and permits quantification of all three dopants.

The implant standard can be made for one isotope and the RSF generated can be applied to the measurement of another isotope in the sample by applying a correction for the isotopic abundance. This is necessary when ^{10}B is used (this is the isotope chosen by National Institute for Standards and Technology (NIST) to develop a boron standard) to quantify a profile that contains only ^{11}B. The simplest approach is to calculate the RSF for all the isotopes and then determine the ^{11}B RSF.

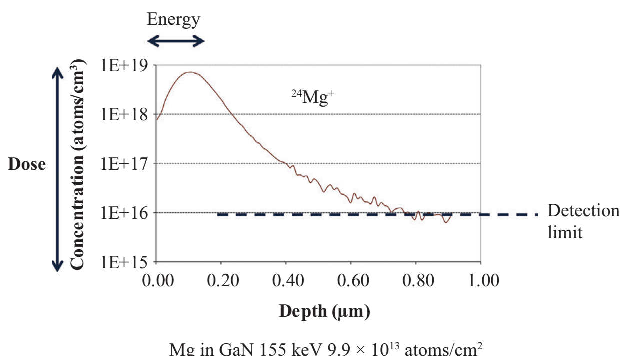

Figure 6.3. Versatility of ion implanted standards.
Source: F. Stevie, Analytical Instrumentation Facility, North Carolina State University.

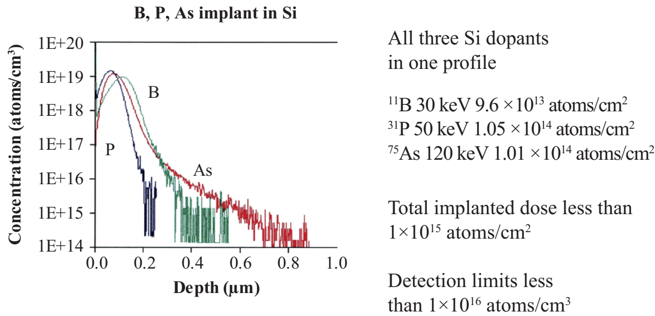

Figure 6.4. Multiple implants in the same sample.
Source: F. Stevie, Analytical Instrumentation Facility, North Carolina State University.

For samples where the species of interest is not implanted and contains normal isotopic abundance, then the RSF for all isotopes would be used to determine total concentration of the element in the sample.

For calculations where it is necessary to convert from atomic percent to weight percent:

For a two-component (x,y) material, the weight percent of x is

$$wt\%_x = (at\%_x)\ (atomic\ wt_x)\ (100\%)/((at\%_x)(at\ wt_x) + (at\%_y)\ (at\ wt_y)) \tag{6.4}$$

6.3.1 EXISTING STANDARDS

There are only three traceable standards, which are the dopant species boron, arsenic and phosphorus in a silicon matrix. They are certified reference materials (standard reference material [SRM] 2137 for ^{10}B, SRM 2134 for ^{75}As, SRM 2133 for ^{31}P) available through NIST [19, 20]. All three standards are based on ion implantation of the dopant with approximately 1×10^{15} atoms/cm^2 dose and have been extensively verified by other analytical methods. Figure 6.5 shows a SIMS depth profile for arsenic in SRM 2134.

Some standards, particularly in silicon, can be obtained from a major analytical company [21]. However, most standards in use were created to quantify specific elements for the matrix of interest.

6.3.2 CREATION OF STANDARDS

Preparation of ion implanted standards does require some work to ensure that the desired standard is obtained. Normally the most intense isotope is

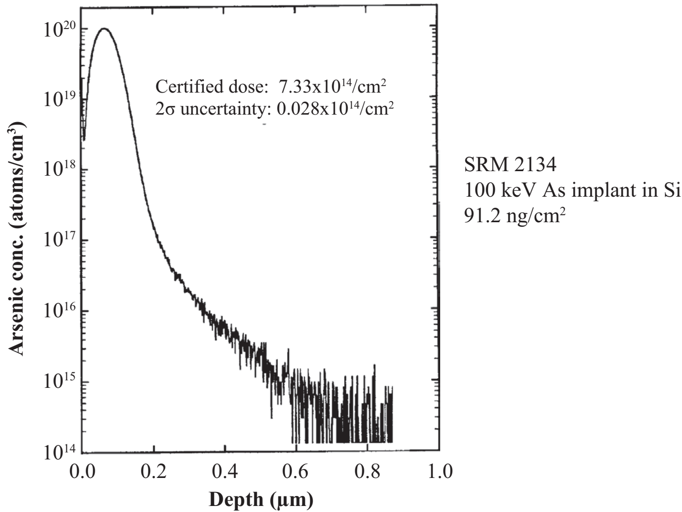

Figure 6.5. NIST standard reference material for As in Si. *Source*: Evans East [21], reproduced with permission from Evans analytical group.

chosen but a check should be made for possible mass interferences. Most implanters use relatively low mass resolution so one should avoid possible mass interferences by selection of another isotope if possible [22]. For example, implantation of ^{28}Si can have $^{12}C^{16}O$ mass interference and ^{29}Si may be a better choice. When multiple species are implanted the selection of species should avoid mass interferences with each other. For example, if ^{11}B and ^{27}Al are implanted together, then there is possible mass interference of ^{27}Al from $^{11}B^{16}O$. Multiple species are often grouped to match the primary beam used for analysis. For example, hydrogen, carbon, nitrogen, and oxygen are commonly implanted together because they all have best secondary ion yields with Cs^+ bombardment.

The depth can be varied with implant energy and should be matched if possible with the expected depth of the analysis. If the implant is too deep, it may take too long to sputter if low energy analysis conditions are used. If the depth is too shallow, then the projected range, R_p, may be too close to the surface. As a result the implant peak may not be well defined and could be difficult to quantify because it would lie within the equilibration depth discussed in Chapter 5. Residual gas species such as hydrogen, carbon, nitrogen, and oxygen should be implanted deep enough to achieve separation of the implant peak from possible contamination at the surface.

Since the SIMS instrument is essentially an ion implanter with attached mass analyzer, it is possible to use the SIMS instrument to obtain some standards. Since many instruments have a mass analyzer on the

primary column, a beam of ions, such as oxygen or carbon, can be used to expose a region of the sample for a specific amount of time and ion current. This will provide a known dose of that species [23, 24].

If you are implanting into a thin layer, care must be taken to ensure that enough of the implant is in the layer to make an accurate quantification. For thin layers it will be difficult to determine the detection limit. Transport of Ions in Matter (TRIM) [25] can be used to determine the projected range and straggle for the implant. Note that most implants in (100) silicon are made at 7° from normal incidence to minimize channeling. Figure 6.6(a) shows an example of too low implant energy [26]. Since tin has a relatively high mass compared with boron, phosphorus, and arsenic dopants in silicon and since InP has a higher density than a matrix such as silicon, the energy chosen for the implant was insufficient to place the peak well below the surface. As a result it would be problematic to use this implant for quantification. Figure 6.6(b) shows an implant energy that was too high to keep the beryllium from penetrating beyond the SiO_2 layer. The beryllium in the silicon does not have the same yield enhancement as the beryllium in the oxide and use of this implant for quantification is compromised. Figure 6.7 shows iron implanted at the same energy and dose into three different substrates [27]. The penetration range of iron is quite different for the three matrixes and reflects differences in matrix density.

Proper choice of implant dose is also very important. Where possible the implant dose for the standard should produce a peak concentration

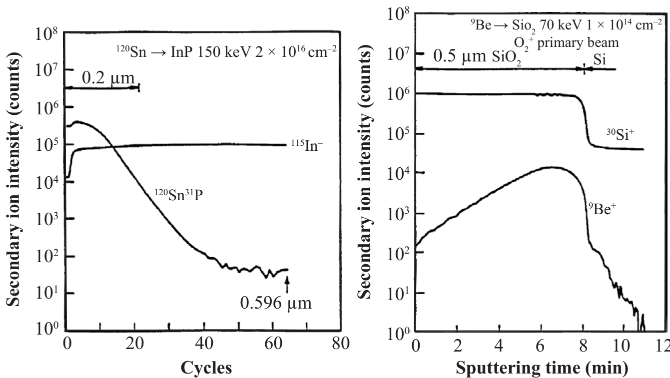

Figure 6.6. Implant energy considerations. (a) Implant energy too low for Sn → InP. Dose error near surface. (b) Implant energy too high for Be → SiO_2 layer on Si, much of the Be is beyond the SiO_2. *Source*: Wilson, Stevie, and Magee [26].

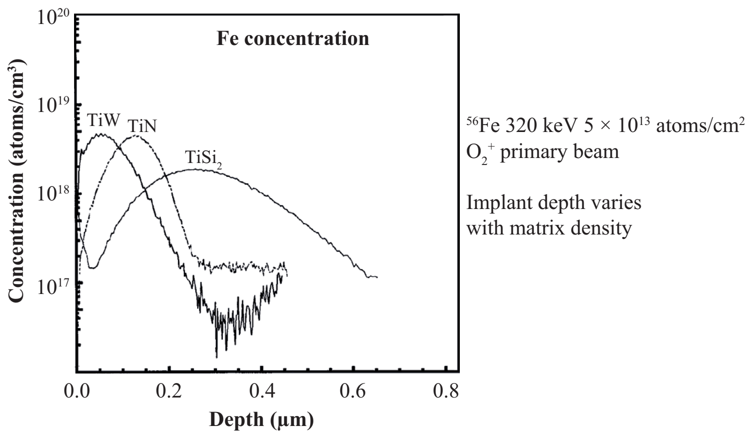

Figure 6.7. Fe depth profiles in TiW, TiN, and $TiSi_2$.
Source: Lux, Stevie, Kahora, Wilson, and Cochran [27], reprinted with permission from American Institute of Physics, copyright 1993, American Vacuum Society.

that is matched with the expected concentration in the sample of interest. If the dose is too high, then it may be necessary to use different analysis conditions for the standard and the sample. For example, a high count rate on the standard might require a Faraday cup measurement when the sample of interest is measured with an electron multiplier. If the implant dose is too low then the profile can be affected by contaminants in the sample. A typical dose for SIMS standards is 1×10^{14} to 1×10^{15} atoms/cm^2, which will provide a peak concentration of approximately 1×10^{19} to 1×10^{20} atoms/cm^3.

When samples are sent for ion implantation, it is often worthwhile to include other matrixes. Since the ion implant beam will place the same dose into every sample, additional standards can be acquired at the same time. There are several companies that will provide implantation services and they can be found with an internet search. If the ion implanter has the capability to rotate the sample during implantation, this will help provide a uniform distribution across the sample.

It is necessary to verify the dose and check the isotopic distribution. The implanted dose is based on a measurement of collected charge and is not an absolute measurement for the species of interest. The mass resolution of the implanter may not be sufficient to remove interferences. If the sample is an insulator, sample charging can affect the measured dose.

If the element is at a mass that exceeds that of the matrix, then analysis using Rutherford backscattering spectrometry (RBS) can verify the dose of the element present in the sample. For low atomic number elements, a cross check of dose can be difficult and the best method is often comparison with other standards. For this reason, it is suggested to always implant a piece of silicon with the material of interest. Implants in silicon are probably the easiest to obtain and can be used to verify the dose. For implants of Si, the GaAs matrix is a reasonable choice because Si is a dopant in this material and this standard should not be too difficult to obtain. The isotopic distribution can be verified with a SIMS profile. Figure 6.8 shows a depth profile of an ion implant of molybdenum in silicon [28]. The intent was to implant only ^{98}Mo. However, some of the dose was implanted into ^{96}Mo and ^{97}Mo. The results of the SIMS profile were applied to the total dose and the correct dose could then be calculated.

Multiple elements can be implanted into one substrate as shown in Figure 6.4 for boron, phosphorus, and arsenic in silicon. If the total implanted dose is too high then the implanted species will be at matrix levels and accuracy will be affected. The total dose should not exceed 2×10^{16} atoms/cm^2, which would have a peak concentration of approximately 4 percent atomic in silicon. Note that even a relatively low implanted dose may amorphize a crystalline substrate. If several elements are to be implanted, it can be advantageous to implant one that will amorphize the

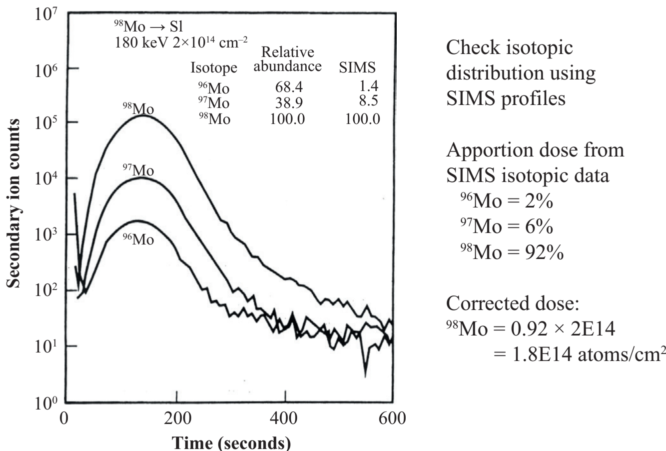

Figure 6.8. Isotope check.
Source: Stevie, Wilson, Simons, Current, Zalm [28], reprinted with permission from American Institute of Physics, copyright 1994, American Vacuum Society.

material first, followed by the others. This will minimize channeling of the second and subsequent implants and provide a shallower distribution.

Peak concentration can be estimated from the implanted dose. Because the implant shape is roughly Gaussian, the concentration profile can be approximated by

$$n(x) = n_0 \exp(-(x - R_p)^2/2\Delta R_p^{\,2}) \quad (6.5)$$

where $n_0 = \Phi/(\sqrt{(2\pi)}\,\Delta R_p)$ or approximately $0.4\,\Phi/\Delta R_p$

Φ = dose

ΔR_p = straggle

For typical $\Delta R_p = 0.01$ to $0.1\,\mu m$

$n(R_p) = 0.4\,\Phi/(0.1 \text{ to } 1 \times 10^{-4}\text{ cm})$

$= 0.4 \times 10^5 \text{ to } 4 \times 10^5\,\Phi\text{ cm}^{-3}$

For P implanted in Si at 100 keV, $\Delta R_p = 0.04\,\mu m = 0.04 \times 10^{-4}$ cm

$n(R_p) = 0.4\,\Phi/0.04 \times 10^{-4} = 1 \times 10^5\,\Phi\text{ cm}^{-3}$

For example, the ^{24}Mg implant in Figure 6.3 has an implanted dose of approximately 1×10^{14} atoms/cm^2. The peak concentration should be $\sim 10^5 \times$ dose or $\sim 1 \times 10^{19}$ atoms/cm^3 and this is what is observed. This approximation becomes less accurate when the implant is very shallow or very deep.

6.4 BULK STANDARDS

Bulk standards can be quite useful. A bulk standard can be obtained with a substrate that is uniformly doped during fabrication. For example, in silicon technology, the silicon boule is made with a constant concentration of a dopant to provide a p-type or n-type material. Figure 6.9 shows analysis comparison of bulk and implanted standards for B in silicon. Bulk standards provide constant concentration with depth.

Calculation of RSF for a bulk doped sample is made by rearrangement of Equation 6.1:

$$RSF = \rho_i(I_m/I_i) \quad (6.6)$$

and in this case the concentration is known.

Layers can also be uniformly doped and be used as a standard. Even though the substrate does not contain the element of interest, as long as the concentration is uniform and can be verified by some method, the layer would be suitable as a standard.

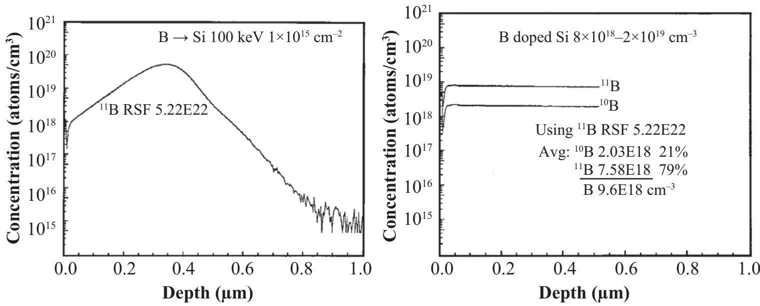

Implanted standard usually contains only one isotope

Bulk doped standard usually contains all isotopes at natural abundances

Figure 6.9. Comparison of implant and bulk standards for B in Si. *Source*: F. Stevie AT&T Bell Laboratories.

One characteristic of bulk doped standards is that the RSF can be determined quickly by sputtering until the secondary ion yield is constant and there is no need to measure the crater depth. This can be very useful for quantification of elements at or near the surface. The number of elements available is limited and may be difficult to obtain other than boron, phosphorus, and arsenic in a silicon substrate or boron and phosphorus in SiO_2 when borophosphosilicate glass is used.

6.5 MATRIX AND TRACE QUANTIFICATION

Counts versus concentration should be linear for SIMS quantification from the ppt level up to at least 1 percent atomic at which the trace species must be treated as a matrix element and can affect secondary ion yields [1]. Figure 6.10 shows an ion implant where peak concentration is at 10 percent atomic [29]. It can be observed that in the implant peak region the silicon matrix signal decreases. This is shown on a logarithmic scale and would be even more evident on a linear plot.

SIMS is used to quantify more for trace than for matrix levels. It is preferred to use other techniques such as AES or energy dispersive spectroscopy for higher levels. However, SIMS can also be used for high concentration measurements with proper standards.

Layers of SiGe at various germanium fractions are used extensively in semiconductor fabrication. Since the germanium is a matrix species, it is necessary to account for matrix effects. In order to provide a calibration

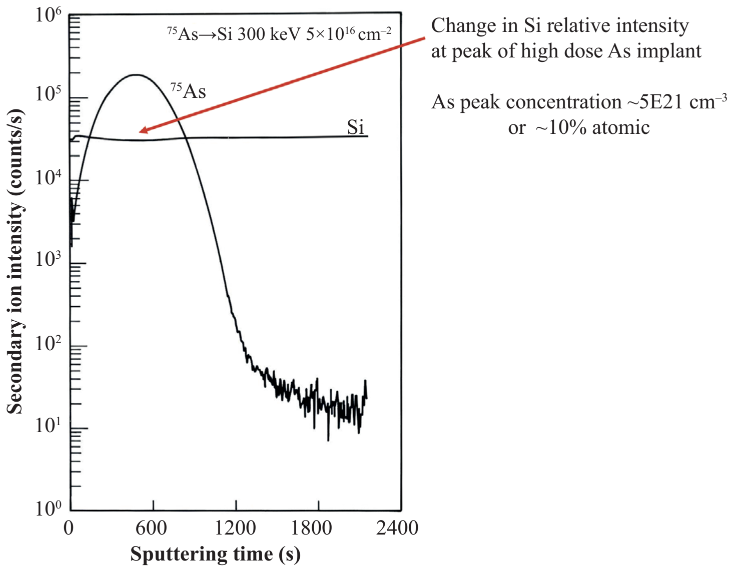

Figure 6.10. Nonlinear region.
Source: Wilson, Stevie, Magee [29].

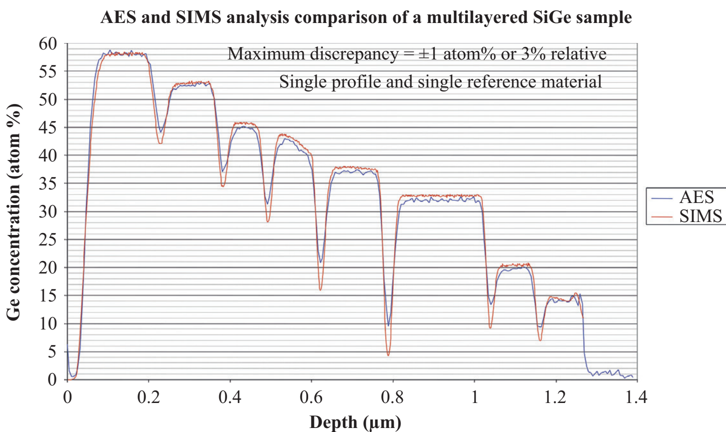

Figure 6.11. Analysis of SiGe matrix elements.
Source: C. Magee, Evans analytical group, reproduced with permission from Evans analytical group.

curve, it is necessary to analyze samples of Si_xGe_{1-x} for a range of x values. This can be achieved with one sample as shown in the multilayer analysis of Figure 6.11 [21, 30]. The secondary ion yield can be affected by the SiGe variations and accurate quantification requires implants of the

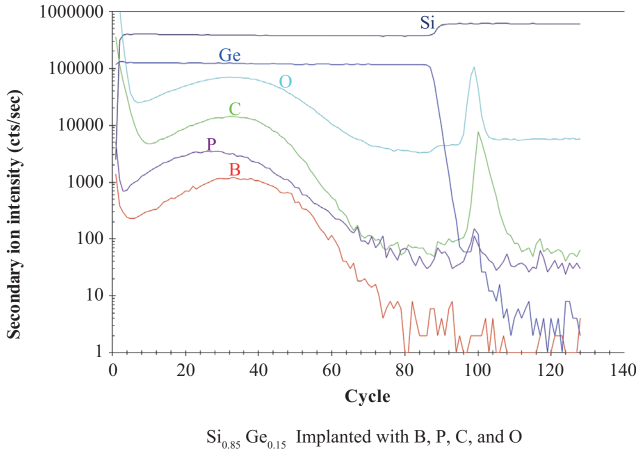

Figure 6.12. Analysis of SiGe impurity elements.
Source: C. Magee, Evans analytical group, reproduced with permission from Evans analytical group.

species of interest. An example of boron, phosphorus, carbon, and oxygen impurity quantification in SiGe is shown in Figure 6.12. These implants were made into all of the x values for Si_xGe_{1-x} used in the calibration curve. Proper matrix and trace quantification as displayed in these two figures requires significant effort but is necessary for accurate measurements.

If a layer standard is made with a constant concentration, it is helpful if it can be at least 100 nm thick to avoid any variations at the start and end of the layer formation or deposition.

6.6 USEFUL YIELD

Useful yield (τ) can be described as the ratio of secondary ion counts detected to the number of atoms that were present in the detected area of the sample. For an ion implant,

$$\tau = \Sigma I_i / (\Phi\ A) \tag{6.7}$$

where ΣI_i = sum of detected counts

Φ = implant dose in atoms/cm^2

A = detected area in cm^2

Since the useful yield incorporates the transmission and detection capability of the instrument, it can be used to compare the performance

of different instruments. Useful yields for CAMECA IMS-f series instruments have been reported for varied instrument conditions [31].

6.7 PRECISION AND ACCURACY

With the assumption that the dose of an ion implanted standard is accurate, typical depth profile measurements are quoted to be within 10 to 20 percent of true value for concentration and within 5 to 10 percent for depth. Compared with some analytical techniques, this accuracy may not seem that notable, but it is actually very useful since it is valid over many orders of magnitude of concentration. With careful work, it is possible to have dose repeatability of less than 5 percent [32] and this has been achieved for all three analyzer types. This quality of work is routinely accomplished where it is necessary to analyze semiconductor dopant dose for product wafers. The dose is a critical parameter for the semiconductor processing industry.

An example of precision or reproducibility is provided in Figure 6.13, which shows depth profiles from multiple analyses of the NIST boron standard obtained with a magnetic sector analyzer [19]. The results are so similar that they are indistinguishable. This quality of data permits very accurate results, such as peak depth and concentration, to be obtained. As noted above, the measurement of dose is especially of interest when the

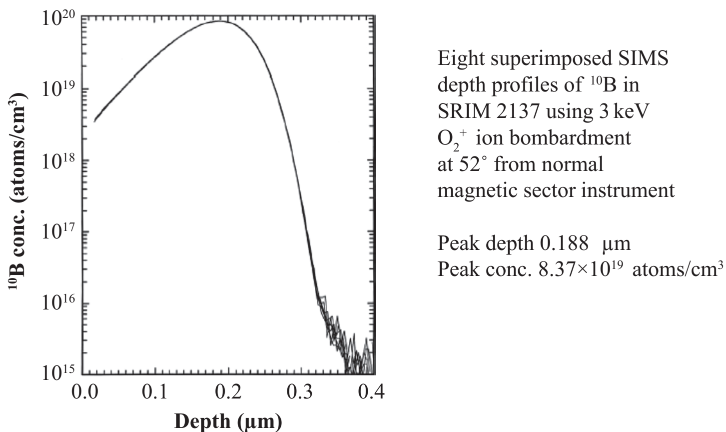

Figure 6.13. Precision (reproducibility).
Source: Simons et al. [19], reproduced with permission from American Institute of Physics, copyright 2007, American Vacuum Society.

species is a dopant. Figure 6.14 shows less than 1 percent relative standard deviation for a set of 18 measurements of a 5 keV ^{11}B implant obtained with a quadrupole instrument. Figure 6.15 shows excellent dosimetry accuracy obtained for a 1 keV ^{11}B implant, also with a quadrupole instrument. This figure indicates that dosimetry measurement can be precise and

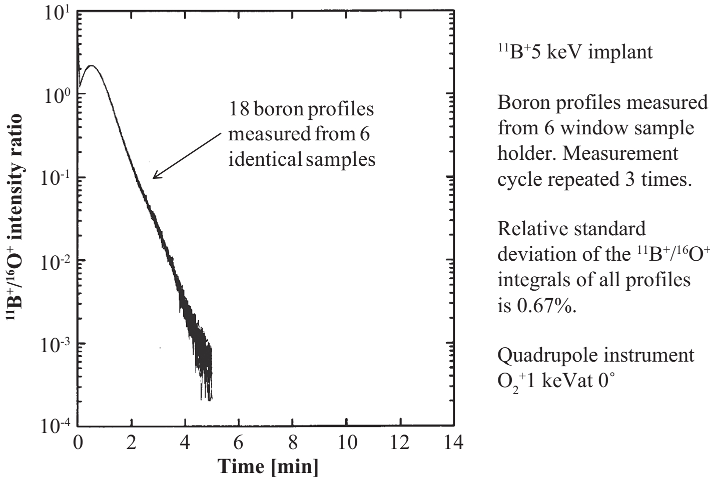

Figure 6.14. Dose precision (reproducibility).
Source: CAMECA quadrupole instruments, reproduced with permission from CAMECA.

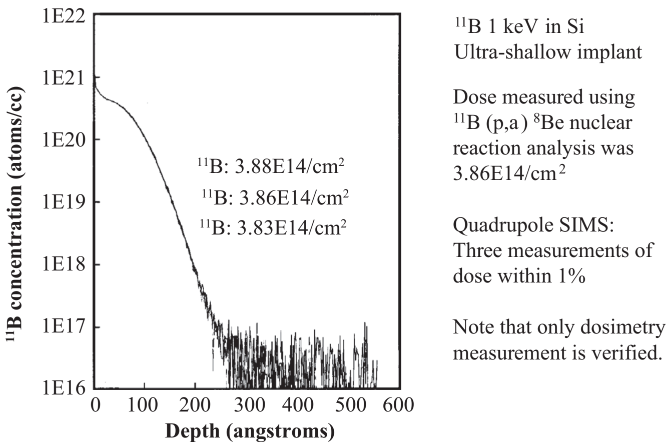

Figure 6.15. Precision (reproducibility) and accuracy.
Source: Evans analytical group, reproduced with permission from Evans analytical group.

accurate using a NIST SRM and nuclear reaction analysis, but this is not a guarantee that the profile shape is correct [33].

Isotope fractionation can occur. It is possible that not all isotopes of a particular element will be detected with the same sensitivity. The heavier isotopes are often underrepresented [34–36]. This is important for isotope abundance measurements and for transferring RSFs from one isotope to another, for example ^{10}B to ^{11}B.

6.8 QUANTIFICATION IN MULTIPLE MATRIXES—CESIUM CLUSTER IONS

Chapter 2 indicated that secondary ion yields can vary with the matrix. Many technologies use multiple layers in their products. Not just semiconductors but items as common as bathroom fixtures and projector lamps often have layers with very different composition and properties. Conductors, semiconductors, insulators, metals, and ceramics can be adjacent. Since SIMS has excellent depth profiling capability it is important to address the quantification of a profile through multiple layers, each of which may contain multiple matrix elements. It would appear that so many standards would be needed that quantification would be almost impossible. For a multilayer sample with layers where composition may not be well established, SIMS should not be the first technique to be used. Depth profiling with a technique such as AES would establish the matrix composition for the layers and then SIMS could be of much more use. SIMS also is best suited for trace analysis. If there were two or three elements of importance, then quantification in a multilayer system can be established if a set of samples can be obtained that have each layer of interest as the top layer. All those samples can be implanted at the same time to obtain the standards desired.

The use of cesium cluster ions (MCs^+, where M is the element of interest) can provide a reduced matrix effect [37, 38]. This approach is also called cesium attachment. The secondary ion formation for bombardment with Cs^+ and detection of cesium molecular ions is different from that for detection of negative secondary ions. The cluster ions offer the possibility of trace element detection but for some species show direct correlation with matrix concentration. Figure 6.16 shows a profile of a sample with layers that contain varying concentrations of InGaAsP [39]. The species $CsZn^+$ shows the trace concentration for the dopant Zn, but $CsIn^+$, $CsGa^+$, $CsAs^+$, CsP^+ show accurate atomic fractions for indium, gallium, arsenic, and phosphorus, respectively.

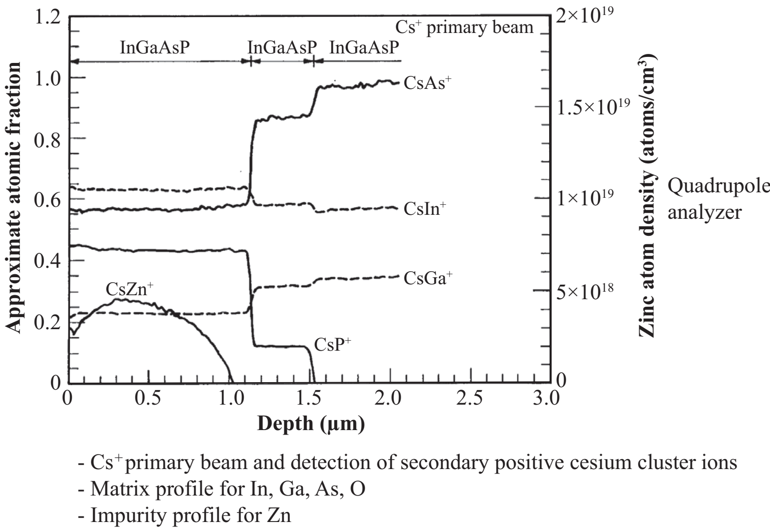

- Cs^+ primary beam and detection of secondary positive cesium cluster ions
- Matrix profile for In, Ga, As, O
- Impurity profile for Zn

Figure 6.16. Matrix and impurity element quantification.
Source: Wilson, Stevie, and Magee [39].

Cesium cluster ions have shown increased usage for analysis of rare gases and elements such as zinc and cadmium that have moderate secondary ion yields with O_2^+ or Cs^+ bombardment [40–44]. A cesium neutral beam has also been successfully employed to enhance secondary ion yields, particularly for MCs^+, with the use of any other beam for analysis [45]. Note that low energy (less than 500 eV) cesium bombardment has the potential to have so much cesium implanted in the material that the cesium cluster ion yields may be affected.

6.9 STATIC SIMS QUANTIFICATION

Static SIMS can provide an analysis of only a fraction of the top monolayer by limiting the dose in atoms/cm^2 to be significantly less than one atomic layer (1×10^{15} atoms/cm^2 for silicon). It is possible to achieve some measure of quantification starting at the surface. Ion implantation provides a simple approach to quantify a depth profile; however, the implant is not well defined at the surface. The peak concentration of an ion implant can be accurately determined. If the implant is made through a removable layer that has the thickness of the implant projected range, then when the

layer is removed we have a known surface concentration [46]. Figure 6.17 schematically displays this approach and analyses have demonstrated this method [47]. Measurements have been made primarily using TOF-SIMS and an example of that data is shown in Table 6.1.

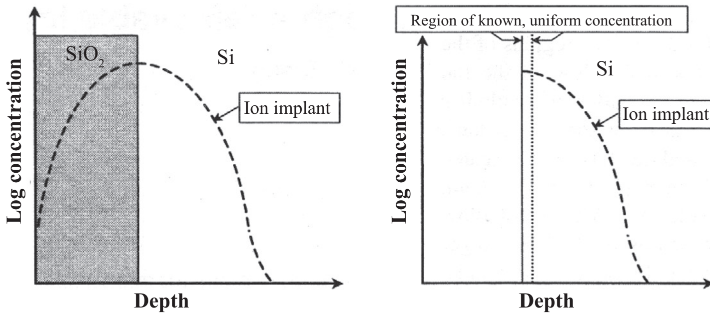

Figure 6.17. Implant through removable layer.
Source: Stevie et al. [46], reproduced with permission from American Institute of Physics, copyright 2000, American Vacuum Society.

Table 6.1. TOF-SIMS of implants through SiO_2

Quantified with existing standards					
Species	**Energy (keV)**	**Total dose (at/cm²)**	**Calc dose 1 nm**	**Meas dose 1 nm**	
^{31}P	74.5	1E14	1E12	9.1E11	**0.1 µm SiO_2 layer removed**
^{75}As	160	1E14	1E12	1.0E12	
^{24}Mg	56	1E14	1E12	8.6E11	
^{27}Al	62	1E14	1E12	6.9E11	**Results within factor of 2 for 11 elements**
^{39}K	96	1E14	1E12	1.2E12	
^{58}Ni	141	1E14	1E12	5.6E11	
^{40}Ca	100	1E14	1E12	6.8E11	
^{59}Co	137	1E14	1E12	7.2E11	
^{48}Ti	110	1E14	1E12	6.3E11	
^{56}Fe	131	1E14	1E12	8.9E11	
^{63}Cu	147	1E14	1E12	1.7E12	

Source: Reich et al. [47]

For materials such as organics, quantification can be established from a set of samples analyzed using techniques such as XPS to obtain a calibration curve and then analyzed with SIMS [48].

6.10 RSF RELATIONSHIP WITH IONIZATION POTENTIAL AND ELECTRON AFFINITY

In Chapter 2 it was noted that secondary ion yields varied widely across the periodic table. Figure 6.18 shows a compilation of positive secondary ion RSF data for 80 elements implanted into a silicon matrix, and it is evident that variations of five orders of magnitude can be noted between elements [10, 16, 49]. However, if positive secondary ion yields are plotted versus ionization potential, as shown in Figure 6.19, systematic trends are observed [50]. Most of the elements lie on a single line. This figure shows similar results for eight matrixes, which include conductors, insulators, and semiconductors. With implants into only three elements (as shown by the circles in this figure), it would be possible to determine the slope of the line and provide some measure of quantification to the other elements. A reasonable estimate is that those other elements would be accurate to about a factor of three.

Similarly, if negative secondary ion yields are plotted versus electron affinity as shown in Figure 6.20, systematic trends are also observed [51]. As was noted for the positive secondary ions, the trends are similar for the eight matrixes shown. This indicates that the results are relatively independent of the material analyzed [4, 8, 14, 49].

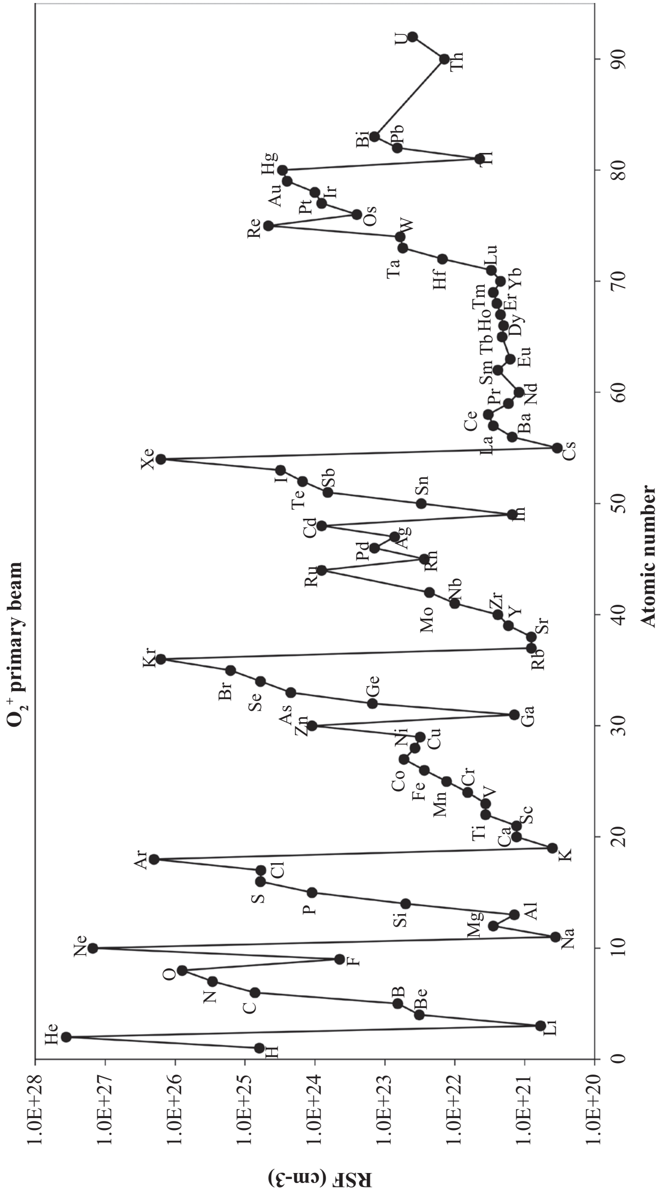

Figure 6.18. Positive secondary ion yields for 80 elements in Si.
Source: Wilson, Stevie, and Magee [49]; Stevie and Wilson [10]; Wilson, Stevie, Chryssoulis, Irwin [16].

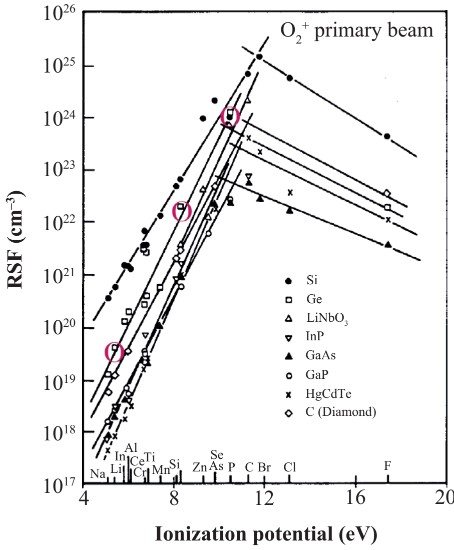

- O_2^+ bombardment positive secondary ion RSFs vs. ionization potential for 8 matrixes
- Same pattern observed for all 8 matrixes
- Implant 3 elements to define major line

Figure 6.19. RSF patterns for secondary positive ions. *Source*: Wilson, Stevie, and Magee [50].

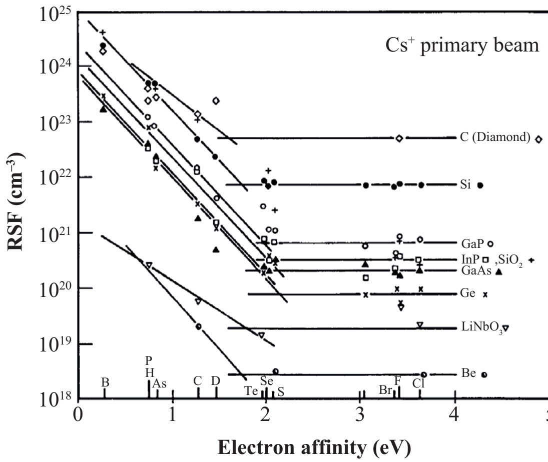

Cs^+ bombardment negative secondary ion RSFs vs. electron affinity for 8 matrixes

Same pattern observed for all 8 matrixes

Figure 6.20. RSF patterns for secondary negative ions. *Source*: Wilson, Stevie, and Magee [51].

REFERENCES

[1] Williams, P. 1985. "Secondary Ion Mass Spectrometry." *Annual Review of Materials Science* 15, pp. 517–48. doi: 10.1146/annurev.ms.15.080185.002505

[2] Williams, P. 1988. "Aspects of Quantitative Analysis Using Secondary Ion Microanalysers." In *Secondary Ion Mass Spectrometry, SIMS VI*, eds. A. Benninghoven, A.M. Huber, and H.W. Werner, 261. Chichester, United Kingdom: Wiley.

[3] Leta, D.P., and G.H. Morrison. 1980. "Ion Implanted Standards for Secondary Ion Mass Spectrometric Determination of the 1A–7A Group Elements in Semiconducting Matrices." *Analytical Chemistry* 52, no. 3, pp. 514–19. doi: http://dx.doi.org/10.1021/ac50053a032

[4] Wilson, R.G., and S.W. Novak. 1988. "Systematics of SIMS Relative Sensitivity Factors versus Electron Affinity and Ionization Potential for Si, Ge, GaAs, GaP, InP, and HgCdTe Determined from Implant Calibration Standards for About 50 Elements." In *Secondary Ion Mass Spectrometry, SIMS VI*, eds. A. Benninghoven, A.M. Huber, and H.W. Werner, 57. Chichester, United Kingdom: Wiley.

[5] Stevie, F.A., P.M. Kahora, S. Singh, L. Kroko. 1988. "Atomic and Molecular Relative Secondary Ion Yields of 46 Elements in Si for O_2^+ and Cs^+ Bombardment." In *Secondary Ion Mass Spectrometry, SIMS VI*, eds. A. Benninghoven, A.M. Huber, and H.W. Werner, 319. Chichester, United Kingdom: Wiley.

[6] Wilson, R.G., 1988. "Secondary Ion Mass Spectrometry Sensitivity Factors versus Ionization Potential and Electron Affinity for Many Elements in HgCdTe and CdTe Using Oxygen and Cesium Ion Beams." *Journal of Applied Physics* 63, no. 10, p. 5121. doi: http://dx.doi.org/10.1063/1.340413

[7] Wilson, R.G., F.A. Stevie, and C.W. Magee. 1989. *Secondary Ion Mass Spectrometry*, Appendix E. New York: Wiley.

[8] Wilson, R.G., and S.W. Novak. 1991. "Systematics of Secondary-Ion Mass Spectrometry Relative Sensitivity Factors versus Electron Affinity and Ionization Potential for a Variety of Matrixes Determined from Implanted Standards of More Than 70 Elements." *Journal of Applied Physics* 69, no. 1, p. 466. doi: http://dx.doi.org/10.1063/1.347687

[9] Wilson, R.G. 1990. "Oxygen and Cesium SIMS of Rare Earth and Low Electron Affinity (<0.2 eV) Elements Implanted in Semiconductors and Their Electron Affinities Estimated form SIMS Measurements." In *Secondary Ion Mass Spectrometry, SIMS VII,* eds. A. Benninghoven, C.A. Evans, K.D. McKeegan, H.A. Storms, and H.W. Werner, 131. Chichester, United Kingdom: Wiley.

[10] Stevie, F.A., and R.G. Wilson. 1991. "Relative Sensitivity Factors for Positive Atomic and Molecular Ions Sputtered from Si and GaAs." *Journal of Vacuum Science & Technology A* 9, no. 6, p. 3064. doi: http://dx.doi.org/10.1116/1.577174

[11] Wilson, R.G., C.L. Kirschbaum, G.E. Lux, S.P. Smith, and C.J. Hitzman. 1992. "SIMS Depth Profiling and Relative Sensitivity Factors and Systematics for More Than 50 Elements from H to U Implanted in Insulators (SiO_2, Si_3N_4, UO_2, ZnSe, diamond)." In *Secondary Ion Mass Spectrometry, SIMS VIII,* eds. A. Benninghoven, K.T.F. Janssen, and J. Tumpner, 151. Chichester, United Kingdom: Wiley.

[12] Wilson, R.G., F.A. Stevie, and P.M. Kahora. 1992. "SIMS Depth Profiling and Relative Sensitivity Factors And Systematics for More Than 50 Elements from H to U Implanted in Metal Matrixes (Be, Al, Ti, Ni, W, and Au)." In *Secondary Ion Mass Spectrometry, SIMS VIII*, eds. A. Benninghoven, K.T.F. Janssen, and J. Tumpner, 487. Chichester, United Kingdom: Wiley.

[13] Wilson, R.G., F.A. Stevie, G.E. Lux, C.L. Kirschbaum, S. Frank, and J. Pallix. 1992. "Depth Profiles, Projected Ranges, and Secondary Ion Mass Spectrometry Relative Sensitivity Factors for More Than 50 Elements from Hydrogen to Uranium Implanted into Metals." *Surface and Coatings Technology* 51, no. 1–3, pp. 358–63. doi: http://dx.doi.org/10.1016/0257-8972(92)90264-b

[14] Wilson, R.G., G.E. Lux, and C.L. Kirschbaum. 1993. "Depth Profiling and Secondary Ion Mass Spectrometry Relative Sensitivity Factors and Systematics for Polymers/Organics." *Journal of Applied Physics* 73, no. 5, p. 2524. doi: http://dx.doi.org/10.1063/1.353084

[15] Satoh, H., M. Owari, and Y. Nihei. 1993. "Relative Sensitivity Factors for Submicron Secondary Ion Mass Spectrometry with Gallium Primary Ion Beam." *Japanese Journal of Applied Physics* 32, part 1, no. 8, pp. 3616–20. doi: http://dx.doi.org/10.1143/jjap.32.3616

[16] Wilson, R.G., F.A. Stevie, S.L. Chryssoulis, and R.B. Irwin. 1994. "Secondary Ion Mass Spectrometry Relative Sensitivity Factors for Ru, Rh, Pr, Eu, Tm, Lu, Re, Os, and Ir." *Journal of Vacuum Science & Technology A* 12, no. 4, p. 2415. doi: http://dx.doi.org/10.1116/1.579224

[17] Wilson, R.G. 1995. "SIMS Quantification in Si, GaAs, and Diamond—An Update." *International Journal of Mass Spectrometry and Ion Processes* 143, pp. 43–49. doi: http://dx.doi.org/10.1016/0168-1176(94)04136-u

[18] Parks, C.C. 2001. "Comparative Ion Yields by Secondary Ion Mass Spectrometry from Microelectronic Films." *Journal of Vacuum Science & Technology A* 19, no. 4, p. 1134. doi: http://dx.doi.org/10.1116/1.1361037

[19] Simons, D.S., R.G. Downing, G.P. Lamaze, R.M. Lindstrom, R.R. Greenburg, R.L. Paul, S.B. Schiller, and W.F. Guthrie. 2007. "Development of Certified Reference Materials of Ion-Implanted Dopants in Silicon for Calibration of Secondary Ion Mass Spectrometers." *Vacuum Science & Technology B* 25, no. 4, p. 1365. doi: http://dx.doi.org/10.1116/1.2759937

[20] National Institute of Standards and Technology (NIST) www.nist.gov

[21] Evans Analytical Group (EAG). www.eag.com

[22] Meuris, M., W. Vandervorst, H.E. Maes. 1988. "Investigation of Cross Contamination During Si-Implantation in GaAs with SIMS." *Surface and Interface Analysis* 12, no. 6, pp. 339–343. doi: http://dx.doi.org/10.1002/sia.740120604

[23] Lareau, R.T., and P. Williams. 1985. "In Situ Ion Implantation for Quantitative SIMS Analysis." *Materials Research Society Symposium Proceedings* 48, p. 373. doi: http://dx.doi.org/10.1557/proc-48-273

[24] Smith, H.E., and G.H. Morrison. 1985. "On-Line Implantation for Quantification in Secondary Ion Mass Spectrometry: Determination of Trace Carbon in Thin Layers of Silicon." *Analytical Chemistry* 57, no. 13, pp. 2663–68. doi: http://dx.doi.org/10.1021/ac00290a052

[25] Transport of ions in matter www.srim.org

[26] Wilson, R.G., F.A. Stevie, and C.W. Magee. 1989. *Secondary Ion Mass Spectrometry*, 3.2–10. New York: Wiley.

[27] Lux, G.E., F.A. Stevie, P.M. Kahora, R.G. Wilson, and G.W. Cochran. 1993. "Secondary Ion Mass Spectrometry Quantification of Elements in $TiSi_2$, TiN, and TiW Matrixes." *Journal of Vacuum Science & Technology A* 11, no. 4, p. 2373. doi: http://dx.doi.org/10.1116/1.578336

[28] Stevie, F.A., R.G. Wilson, D.S. Simons, M.I. Current, and P.C. Zalm. 1994. "A Review of SIMS Characterization of Contamination Associated with Ion Implantation." *Journal of Vacuum Science & Technology B* 12, no. 4, p. 2263. doi: http://dx.doi.org/10.1116/1.587753

[29] Wilson, R.G., F.A. Stevie, and C.W. Magee. 1989. *Secondary Ion Mass Spectrometry*, 3.2–8. New York: Wiley.

[30] Denker, M.S., T. Buyuklimanli, and J.T. Mayer. 2000. "SIMS Depth Profiling of SiGe Structures Using Both Oxygen and Cesium Primary Ion Bombardment: A Comparison." In *Secondary Ion Mass Spectrometry, SIMS XII*, eds. A. Benninghoven, P. Bertrand, H.-N. Migeon, and H.W. Werner, 639. Amsterdam, Netherlands: Elsevier.

[31] Hervig, R.L., F.K. Mazdab, P. Wiolliams, Y. Guan, G.R. Huss, and L.A. Leshin. 2006. "Useful Ion Yields for Cameca IMS 3f and 6f SIMS: Limits on Quantitative Analysis." *Chemical Geology* 227, 1–2, pp. 83–99. doi: http://dx.doi.org/10.1016/j.chemgeo.2005.09.008

[32] Simons, D.S. 1994. "Quantification in SIMS—Considerations of Uncertainty in Depth Profile Measurements." In *Secondary Ion Mass Spectrometry, SIMS IX*, eds. A. Benninghoven, Y. Nihei, R. Shimizu, and H.W. Werner, 140. Chichester, United Kingdom: Wiley.

[33] Buyuklimanli, T.H., C.W. Magee, J.W. Marino, and S.R. Walther. 2006. "Near-Surface Secondary-Ion-Mass-Spectrometry Analyses of Plasma-Based B Ion Implants in Si." *Journal of Vacuum Science & Technology B* 24, no. 1, p. 408. doi: http://dx.doi.org/10.1116/1.2163879

[34] Slodzian, G. 1982. "Dependence of Ionization Yields upon Elemental Composition: Isotopic Variations." In *Secondary Ion Mass Spectrometry, SIMS III*, eds. A. Benninghoven, J. Giber, J. Laszlo, M. Riedel, and H.W. Werner, 115. Berlin, Germany: Springer-Verlag.

[35] Schwarz, S.A. 1987. "Measurements of the Secondary Ion Mass Spectrometry Isotope Effect." *Journal of Vacuum Science & Technology A* 5, no. 3, p. 308. doi: http://dx.doi.org/10.1116/1.574151

[36] Deloule, E., M. Chaussidon, and P. Alle. 1992. "Instrumental Limitations for Isotope Measurements with a CAMECA Ims-3f Ion Microprobe: Examples of H, B, S, and Sr." *Chemical Geology:* Isotope *Geoscience section* 101, no. 1–2, pp. 187–192. doi: http://dx.doi.org/10.1016/0009-2541(92)90217-s

[37] Gao, Y. 1988. "A New Secondary Ion Mass Spectrometry Technique for III-V Semiconductor Compounds Using the Molecular Ions CsM^+." *Journal of Applied Physics* 64, no. 7, p. 3760. doi: http://dx.doi.org/10.1063/1.341381

[38] Magee, C.W., W.L. Harrington, and E.M. Botnik. 1990. "On the Use of CsX^+ Cluster Ions for Major Element Depth Profiling in Secondary Ion Mass Spectrometry." *International Journal of Mass Spectrometry and Ion Processes* 103, no. 1, pp. 45–56. doi: http://dx.doi.org/10.1016/0168-1176(90)80015-u

[39] Wilson, R.G., F.A. Stevie, and C.W. Magee. 1989. *Secondary Ion Mass Spectrometry*, 4.8–4. New York: Wiley.

[40] Gnaser, H., and H. Oechsner. 1991. "Novel Detection Scheme for the Analysis of Hydrogen and Helium by Secondary Ion Mass Spectrometry." *Surface and Interface Analysis* 17, no. 9, pp. 646–49. doi: http://dx.doi.org/10.1002/sia.740170906

[41] K. Wittmaack (1992) "Basic requirements for quantitative SIMS analysis using cesium bombardment and detection of MCs^+ secondary ions." *Nuclear Instruments and Methods in Physics Research Section B* 64, no. 1–4, pp. 621–25. doi: http://dx.doi.org/10.1016/0168-583x(92)95545-3

[42] Gnaser, H., and H. Oechsner. 1994. "Emission of MCs^+ Secondary Ions from Semiconductors by Caesium Bombardment." *Surface and Interface Analysis* 21, no. 4, pp. 257–60. doi: http://dx.doi.org/10.1002/sia.740210408

[43] Gnaser, H. 1994. "Improved Quantification in Secondary-Ion Mass Spectrometry Detecting MCs^+ Molecular Ions." *Journal of Vacuum Science & Technology A* 12, no. 2, p. 452. doi: http://dx.doi.org/10.1116/1.579262

[44] Gnaser, H., and H. Oechsner. 1994. "The Influence of Polarizability on the Emission of Sputtered Molecular Ions." *Surface Science Letters* 302, no. 1–9, pp. L289–92. doi: http://dx.doi.org/10.1016/0039-6028(94)91090-1

[45] Wirtz, T., H.-N. Migeon. 2004. "Optimization of SIMS Analyses Performed in the MCs_x^+ Mode by Using an In Situ Deposition of Cs." *Applied Surface Science* 231–232, pp. 743–48. doi: http://dx.doi.org/10.1016/j.apsusc.2004.03.044

[46] Stevie, F.A., R.F. Roberts, J.M. McKinley, M.A. Decker, C.N. Granger, R. Santiesteban, and C.J. Hitzman. 2000. "Surface Quantification by Ion Implantation Through a Removable Layer." *Journal of Vacuum Science & Technology B* 18, no. 1, p. 483. doi: http://dx.doi.org/10.1116/1.591216

[47] Reich, D.F., B.W. Schueler, F.A. Stevie, J.M. McKinley, and C.N. Granger. 2000. "TOF-SIMS Analysis of Surface Metal Standards Produced by Ion Implantation Through a Removable Layer." In *Secondary Ion Mass*

Spectrometry, SIMS XII, eds. A. Benninghoven, P. Bertrand, H-N. Migeon, and H.W. Werner, 425. Amsterdam, Netherlands: Elsevier.

[48] Galuska, A.A. 1994. "Surface Characterization of EVA Copolymers and Blends Using XPS and ToF-SIMS." *Surface and Interface Analysis* 21, no. 10, pp. 703–10. doi: http://dx.doi.org/10.1002/sia.740211005

[49] Wilson, R G., F.A. Stevie, and C.W. Magee. 1989. *Secondary Ion Mass Spectrometry*, 3.3–1. New York: Wiley.

[50] Wilson, R.G., F.A. Stevie, and C.W. Magee. 1989. *Secondary Ion Mass Spectrometry*, 3.3–5. New York: Wiley.

[51] Wilson, R.G., F.A. Stevie, and C.W. Magee. 1989. *Secondary Ion Mass Spectrometry*, 3.3–6. New York: Wiley.

CHAPTER 7

Surfaces, Interfaces, Multilayers, Bulk

7.1 SAMPLE CONSIDERATIONS

Secondary ion mass spectrometry (SIMS) analysis is primarily applied to solid samples, which need to be vacuum compatible. It is possible to use cryogenic sample holders to freeze samples that would otherwise have a high vapor pressure, but this capability is not available on most SIMS instrumentation. Sample cleanliness is very important and is critical for analysis of the surface. This means that attention must be paid to sample storage. Sample containers must not outgas, and Fluoroware and glass are good choices. Aluminum foil is typically very clean but may have an organic material on the surface. Plastic bags are laden with polydimethylsiloxane (PDMS), which is a mobile lubricant. Sample size must also be considered. Samples of approximately 1 cm × 1 cm and no more than a few mm thick provide easy sample handling for almost any analytical instrument. As sample size is decreased below a few mm per side, mounting can become a challenge. Many instruments are limited to about 25 mm diameter samples, but some have been constructed to handle 300 mm wafers. When the analysis region is reduced below 100 µm × 100 µm, more time is required to align the sample and the instrument. Samples should be flat if possible. Rough surfaces can be problematic for secondary ion extraction and depth resolution will be degraded.

7.2 SURFACE—STATIC SIMS

SIMS is a destructive analytical method. However, the technique can provide useful information before even the surface monolayer has been removed. The concept of static SIMS is to analyze secondary ions from

locations that have not experienced a sputtering event. Since a surface monolayer, using silicon as an example, contains about 10^{15} atoms/cm^2, the static SIMS limit has typically been stated as a primary ion dose of 10^{13} atoms/cm^2 or 1 percent of the surface area [1]. Note that a lower dose of 5×10^{12} atoms/cm^2 is considered the limit by some researchers. The ability to obtain information from the surface has proven to be of great value in the study of organic materials. A good vacuum is essential to this analysis to prevent the absorption of material on the surface of interest. Most samples can be analyzed with little or no sample preparation. Overlayers, such as insulators, may sometimes be removed with chemical etching before analysis to prevent sample charging.

Table 7.1 illustrates the differences between static and dynamic SIMS. For a static SIMS limit of 1×10^{13} ions/cm^2 in a silicon matrix,
1 nA beam into 1000 μm × 1000 μm raster,

1 nA/(1000 μm × 1000 μm) = 6.25×10^{11} ions/cm^2-s

48 s to reach static limit

For 10 pA beam we have 6.25×10^{9} ions/cm^2-s

4800 s to reach static limit

By comparison, for dynamic SIMS with 100 nA into 250 μm × 250 μm raster

100 nA/(250 μm × 250 μm) = 1×10^{15} ions/cm^2-s

Less than 1 s to exceed static limit

Static SIMS analysis is typically achieved by acquisition of positive and negative secondary ion mass spectra and interpretation of the ion patterns to identify the material under study. The fragmentation pattern will typically show many segments of the molecule under study but may

Table 7.1. Static vs. dynamic conditions

Parameter	Static	Dynamic
Residual pressure	10^{-10} Torr	10^{-7} Torr
Primary current density	10^{-3} - 10^{-1} μA/cm^2	10 - 10^{3} μA/cm^2
Analyzed area	10^{-1} - 10^{-2} cm^2	5×10^{-4} cm^2
Atomic layer erosion rate	10^{-5} - 10^{-3}/s	10^{-1} - 10/s
Primary current	1 nA	100 nA
Raster	1000 × 1000 μm^2	250 × 250 μm^2
Primary current density	<1 nA/cm^2	0.16 mA/cm^2
Sputtering rate	0.5 nm/hr	3.6 μm/hr
Atoms in Si monolayer	10^{15} atoms/cm^2 or 10^{7} atoms/μm^2	

not include the parent ion. Quadrupole instruments have often been used for static SIMS analysis because the mass range could be scanned quickly and the simplicity of the instrumentation is conducive to excellent vacuum levels. However, the quadrupole is limited when compared with TOF analyzers because the mass range is not as extensive and mass resolution is limited to less than 1,000, defined by M/ΔM, whereas several thousand is needed for most applications. The available magnetic sector instruments scan slowly and are not designed for mass analysis in the thousands of Daltons. TOF-SIMS is typically used for this analysis because this analyzer has the ability to provide parallel detection of all the secondary ion species and because these data can be obtained at high mass resolution over an extensive mass range. Figure 7.1 shows an example of TOF-SIMS analysis in static SIMS mode. The mass spectrum shown is for an adhesive film that is essentially completely covered with PDMS. PDMS is a silicon based organic polymer found as a very common contaminant. The chemical formula is $CH_3[Si(CH_3)_2O]_nSi(CH_3)_3$ and the major peaks in the figure correspond to fragments from this polymer. Chemical mapping can also be obtained on the TOF with lateral resolution less than 500 nm.

As discussed in Chapter 5, characterization of the surface and near-surface region in a depth profile is complicated by the pre-equilibrium region. Before the penetration depth of the primary beam is reached, the concentration of the beam species used to enhance secondary ion yields will not be constant [2]. Several approaches have been used to minimize this effect. One approach is to use a cap layer to cover the sample and then analyze with a depth profile. This was discussed in Chapter 5 and is illustrated in Figure 7.2, which shows how boron at the surface of an oxide layer can be identified and quantified with the deposition of another oxide layer [3]. The oxide layers were deposited using tetraethylorthosilicate. Other approaches to the study of surfaces with dynamic SIMS instruments include use of oxygen flood, low energy ion bombardment, and normalization to a matrix species [4–6].

7.3 INTERFACES

Interfaces are often of interest because the presence of contaminants can indicate a problem with a particular process or help provide an explanation for a layer adhesion problem. Mass spectra obtained at an interface (usually with TOF or quadrupole analyzers) can provide very important information. Figure 7.3 shows an example for an interface between a $MoSi_2$ film and a silicon substrate. The depth profile shows an accumulation of

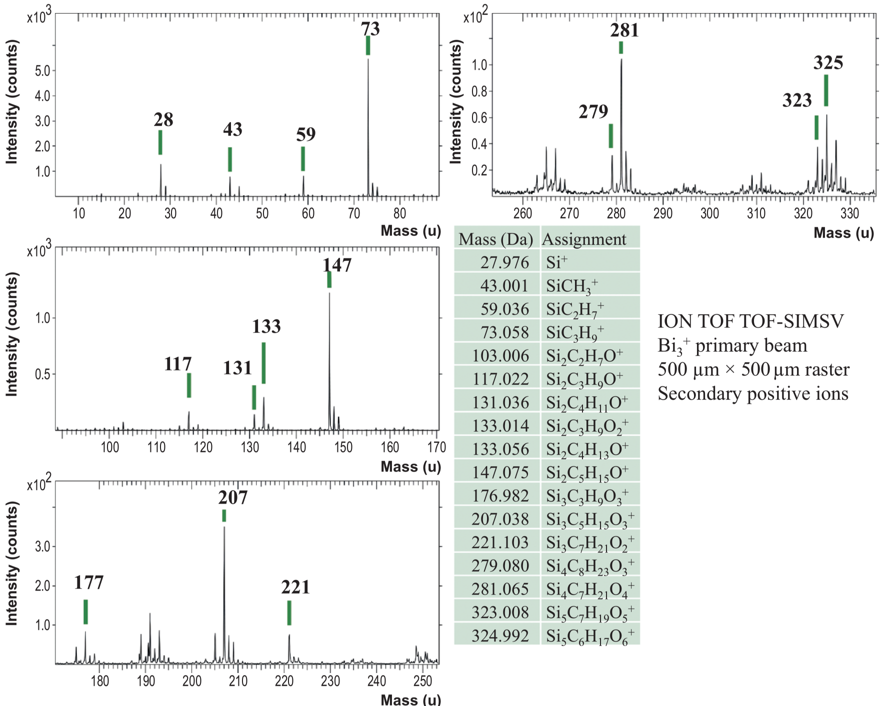

Mass (Da)	Assignment
27.976	Si^+
43.001	$SiCH_3^+$
59.036	$SiC_2H_7^+$
73.058	$SiC_3H_9^+$
103.006	$Si_2C_2H_7O^+$
117.022	$Si_2C_3H_9O^+$
131.036	$Si_2C_4H_{11}O^+$
133.014	$Si_2C_3H_9O_2^+$
133.056	$Si_2C_4H_{13}O^+$
147.075	$Si_2C_5H_{15}O^+$
176.982	$Si_3C_3H_9O_3^+$
207.038	$Si_3C_5H_{15}O_3^+$
221.103	$Si_3C_7H_{21}O_2^+$
279.080	$Si_4C_8H_{23}O_3^+$
281.065	$Si_4C_7H_{21}O_4^+$
323.008	$Si_5C_7H_{19}O_5^+$
324.992	$Si_5C_6H_{17}O_6^+$

Figure 7.1. Polydimethylsiloxane (PDMS).
Source: C. Zhou, Analytical Instrumentation Facility North Carolina State University.

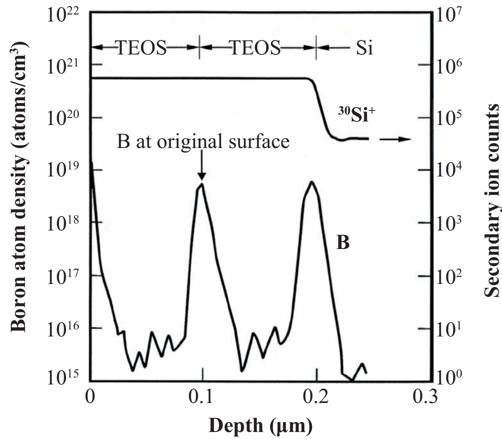

Oxide cap layer used to analyze B at surface of first oxide layer

Figure 7.2. Capping layer to analyze and quantify surface species.
Source: Stevie et al. [3], reproduced with permission from American Institute of Physics, copyright 1991, American Vacuum Society.

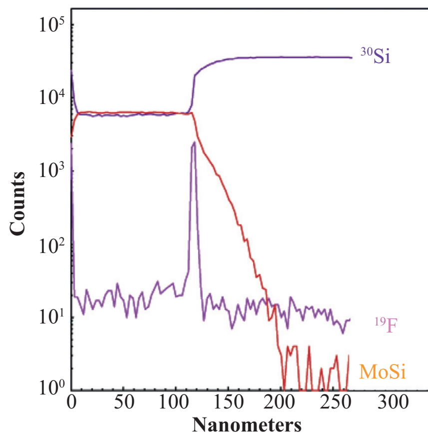

- TOF-SIMS depth profile of a thin $MoSi_2$ film on silicon
- Fluorine contaminant detected at film/substrate interface

Physical electronics
reproduced with permission

Figure 7.3. Contaminant at the interface between layers.
Source: Physical electronics, reproduced with permission.

fluorine at the interface. It is important to locate the interface correctly on a depth profile. Figure 7.4(a) shows the interface between a Si_3N_4 layer and a silicon substrate and appears to indicate the presence of aluminum at the interface between the layer and the substrate. The expanded x-axis in Figure 7.4(b) shows that the aluminum is located at the bottom of the Si_3N_4 layer and not at the interface.

Quantification at an interface can be difficult because the interface is often very thin and typically marks the proximity of two different matrixes, which can have very different secondary ion yields [7–9]. The sputtering rate of the two matrixes would also be expected to be different. Figure 7.5 shows a fluorine profile through a SiO_2 layer on silicon [10]. The fluorine profile has a discontinuity at the interface between the oxide and the substrate because the secondary ion yield for fluorine is higher in the oxide. The discontinuity can be removed if corrected for the difference in secondary ion yields between the oxide and the substrate.

Quantification of a thin interfacial layer at an interface between two layers of the same material can be achieved for species such as a thin oxide between polysilicon and a silicon substrate. In this case, depth resolution is not an advantage. Analysis under degraded depth resolution conditions will broaden the layer and quantification will be more accurate than for

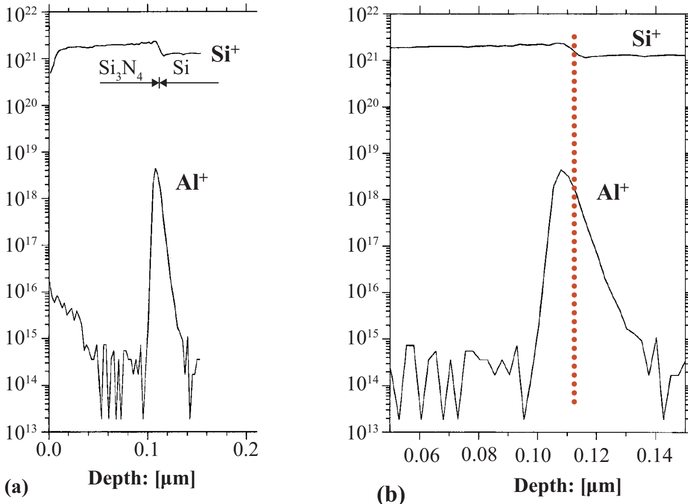

Figure 7.4. Interface region. (a) Possible Al at the interface, (b) Al is at the bottom of the Si_3N_4 layer, not at the interface.
Source: F. Stevie, Analytical Instrumentation Facility, North Carolina State University.

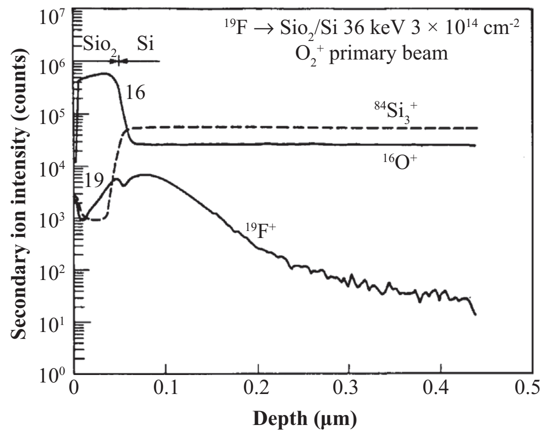

- F implant through 50 nm SiO_2 layer in Si
- SiO_2/Si interface shown by discontinuity in F^+ profile
- F^+ secondary ion yield higher in oxide

Figure 7.5. Quantification at the interface.
Source: Wilson, Stevie, and Magee [10].

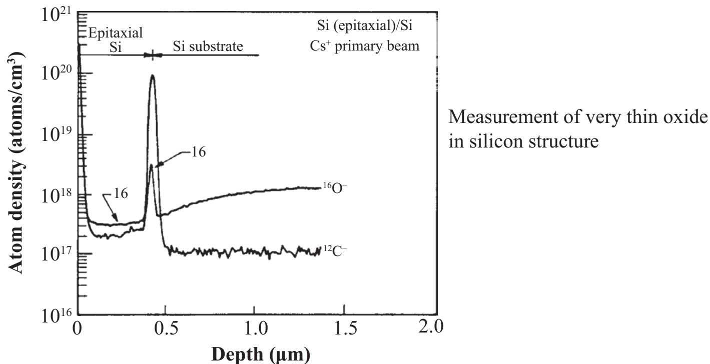

- Analyze with reduced depth resolution
- Calibrate with analysis of implant of oxygen in Si
- Determine equivalent dose for detected oxygen
- 1 monolayer Si = 1E15 atoms/cm^2
- 0.1 nm Si = 4.7E14 atoms/cm^2
- Example: 2.07E15 atoms/cm^2 oxygen = 0.44 nm

Figure 7.6. Quantification of contaminant at the interface.
Source: Wilson, Stevie, and Magee [10].

a high depth resolution analysis [11]. As shown in Figure 7.6, an oxide is present at the interface between polycrystalline silicon and the silicon substrate [10]. The oxide thickness can be calibrated with an ion implant

standard of oxygen in silicon. It is possible to determine an equivalent dose for the oxygen at the interface and convert to thickness [12]. As an example,

1 monolayer of Si = 1×10^{15} atoms/cm^2
0.1 nm of Si = 4.7×10^{14} atoms/cm^2
Measured 2.07×10^{15} atoms/cm^2 oxygen = 0.44 nm SiO_2 [13]

7.4 MULTILAYERS

Multilayers are samples where SIMS excels in terms of analytical value. A depth profile through a structure can show the entire history of a complicated process. Many samples, particularly semiconductors, are quite stable and can be used as a control sample for decades. Depth resolution is very important for multilayer analysis and good depth resolution can provide dramatic results. Figure 7.7 shows that 64 pairs of AlGaAs/GaAs layers could be resolved [14]. It is possible to evaluate the quality of each layer.

Quantification and sputtering rate issues become more complicated when many layers are present. If a species such as a dopant must be monitored in many layers, then standards must be obtained for each layer [15, 16]. As discussed in Chapter 6, if all the matrixes of interest can be

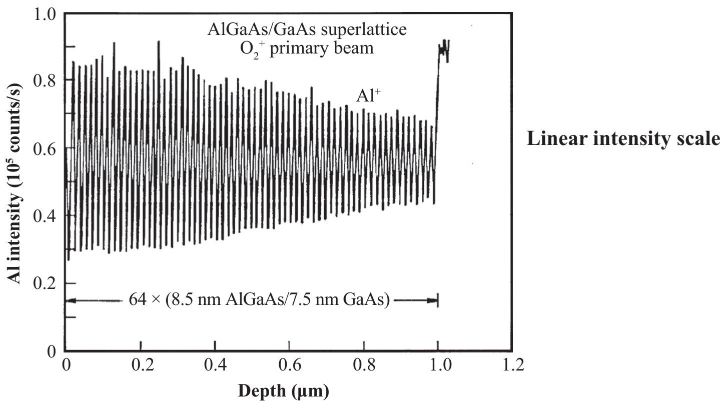

Figure 7.7. Multilayer analysis.
Source: Wilson, Stevie, and Magee [14].

accumulated, then they can all be implanted at one time. The sputter rate for each layer can be determined when the depth profiles on the standards are obtained.

7.5 BACK SIDE ANALYSIS

There are cases where analysis from the front of the sample is problematic. The region of interest may be buried under a thick layer that would degrade depth resolution if sputtered in a depth profile. It is difficult to obtain trace analysis of an element after sputtering through a high concentration of that same element. It is almost impossible to perform the analysis from the top of the sample to determine if a matrix species in a layer has diffused into a layer below. That problem is made even more difficult if the covering layer does not sputter evenly, such as would occur for a polycrystalline metal layer. The solution is to turn the sample over and remove enough material from the back to perform the analysis. The method is shown schematically in Figure 7.8. The sample is usually attached with epoxy on a holder that can be mounted on the polishing unit. Otherwise the thinned sample would break if removed. The sample is thinned with a series of gradually finer sized polishing media.

- Remove most of sample from back by polishing or etching
- Analyze from back side

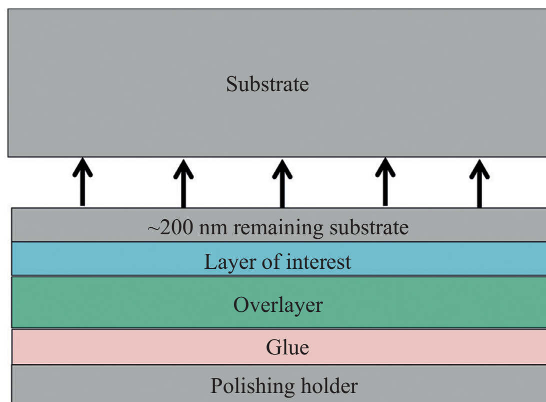

Figure 7.8. Back side analysis method.

An example of a polishing sequence for silicon:

- Polish with a series of diamond lapping films (15 μm to 1 μm) until ~3 μm thick
- Interference fringes observed under illumination of red light when the sample is a few micrometers thick provide a sensitive gauge of depth
- Polish with 1 μm diamond film until remaining silicon is ~0.5 μm
- Final polish performed with 0.02 μm colloidal silica and velvet cloth
- Entire procedure may require four hours of time.

After substrate removal, the resulting surface should be highly polished and parallel to the layer of interest. Roughness of less than a few nanometers has been achieved. If an overlayer is an insulator, it is important to provide a conductive path from the polished sample surface to the sample holder.

The initial back side analyses were made on GaAs- or InP-based materials and incorporated some polishing, but the final material removal was with a chemical etch [17–20]. Figure 7.9 shows good depth resolution with back side analysis of a sample that had metal contacts to GaAs [17].

Back side analysis has been applied to resolve issues in silicon semiconductor technology [21]. Diffusion of copper through barrier layers is

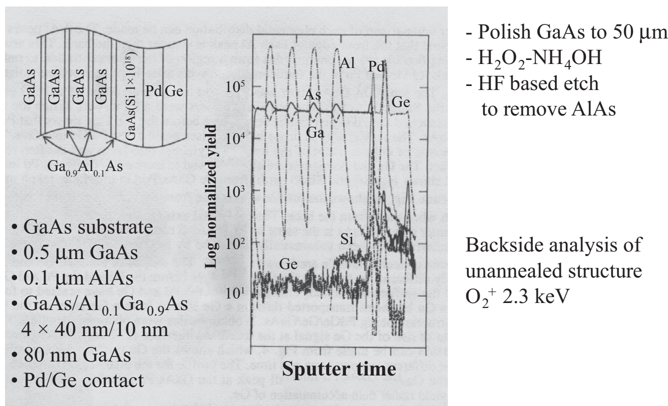

Figure 7.9. Back side analysis: metal contacts on GaAs.
Source: Palmstrom et al. [17], reprinted with permission from Cambridge University Press.

of particular interest and provided incentive for some of the polishing development [22]. Another major application is the analysis of high-k dielectric layers used to make an insulator layer, such as a gate oxide, thicker and easier to manufacture, yet having the same physical properties as a thinner layer. There were many issues such as diffusion of the high-k elements into adjacent layers and sputtering of high atomic number species that were resolved with back side analysis [23–26]. Figure 7.10 shows a front side analysis of hafnium silicate and exhibits poor depth resolution. Hafnium appears to be present in the silicon substrate but the lack of depth resolution makes this an uncertain conclusion. The interface between silicate and the substrate is not defined sufficiently to identify any possible interlayer. Figure 7.11 shows a back side analysis of the same $Hf_xSi_yO_2$ on silicon sample [25]. The hafnium is not present in the substrate, and the existence of an interlayer between the layer and the substrate is visible and was confirmed with TEM analysis. The depth resolution of the hafnium leading edge is 1.3 nm/decade.

Site-specific back side analyses can be obtained. For a substrate such as silicon, when the polishing has removed all but a few micrometers of substrate, the silicon becomes transparent and it is possible to make sure that the region of interest is in an area that is uniformly thin and to locate the analysis with the precision necessary [27]. The polishing process requires significant time and advanced training. Application of a milling machine used to deprocess semiconductor devices has shown success in the effort to make the substrate removal an automated procedure [28].

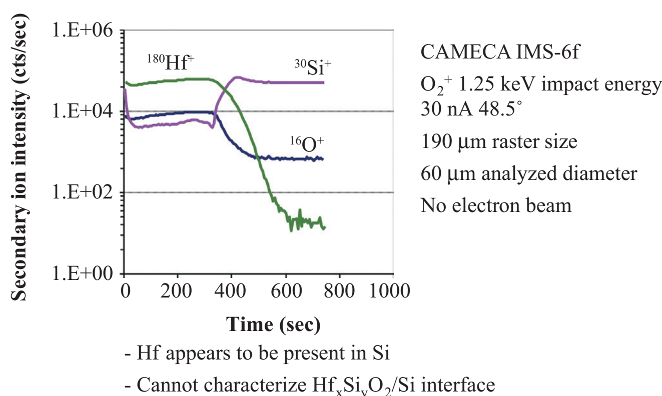

Figure 7.10. Front side analysis of 25 nm hafnium silicate. *Source*: Gu et al. [25], reprinted with permission from Applied Surface Science, copyright 2006, with permission from Elsevier.

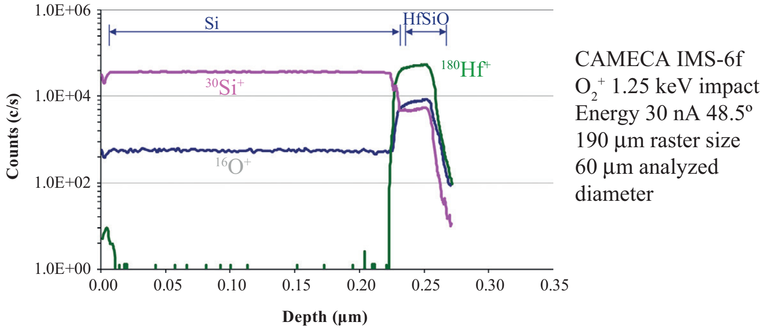

- Approximately 0.2 μm Si remains, 1.3 nm/decade for Hf leading edge
- Depth profile corrected for sputter rate
- Hf does not diffuse into Si
- Interlayer between silicate and substrate

Figure 7.11. Back side SIMS analysis of 25 nm $Hf_xSi_yO_2$.
Source: Gu et al. [25], reprinted with permission from Applied Surface Science, copyright 2006, with permission from Elsevier.

7.6 BULK ANALYSIS

Bulk analysis measurements for trace impurities can be made using SIMS depth profiling, but it is important to understand the sampling volume. As we saw in Chapter 5, for an analysis volume of 30 μm diameter and 1 μm deep, the amount of material removed in a silicon matrix is less than 2 ng. In order to have a valid analysis of the sample, it is common to obtain at least two measurements. Since depth resolution is not important, the measurements can be made with high primary beam current to analyze a larger volume. The result is a depth profile with degraded depth resolution. The data from the different locations are checked for differences. To avoid surface contamination, it is useful to sputter clean the sample by first sputtering with a larger raster and then making the analysis at the same location with a smaller raster. This method is useful if the impurities are uniformly distributed. For nonuniformly distributed species in a bulk material, another mass spectrometric technique, glow discharge mass spectrometry, uses a much larger sampling volume and would provide a more accurate result.

If a sufficient set of relative sensitivity factor (RSF) data can be obtained for a matrix, then it is possible to quantify the elements obtained in a mass spectrum as a bulk analysis. Figure 7.12 shows a mass spectrum of HgCdTe [29] obtained under analysis conditions for which RSFs were

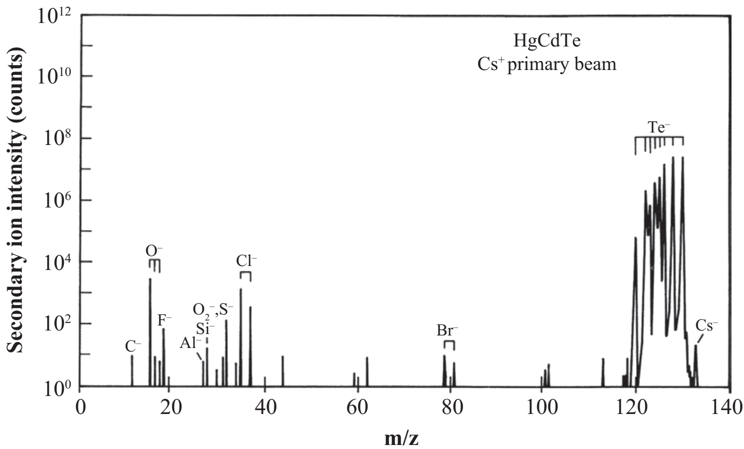

Figure 7.12. Bulk analysis of HgCdTe.
Source: Wilson, Stevie, and Magee [29].

Table 7.2. Calculation of atom densities in HgCdTe

Element	Raw intensity (counts/s)	RSF (cm^{-3})	Corrected intensity (counts/s)	Impurity/ Te ratio	Impurity/ Te (ppm or %)
C	9	1.1×10^{23}	60	5×10^{-7}	0.5
O	3000	2.4×10^{22}	4200	3.5×10^{-5}	35
F	70	7.2×10^{20}	29	2.4×10^{-8}	0.02
Al	7	2.6×10^{24}	1100	9×10^{-6}	9
Si	18	8.8×10^{23}	940	8×10^{-6}	8
Cl	2000	2.7×10^{20}	32	2.7×10^{-7}	0.3
Br	15	4.4×10^{20}	0.39	3.3×10^{-9}	0.003
Te	1.2×10^{8}	1.7×10^{22}	1.2×10^{8}	~1	~100%

Source: Cs^+ bombardment, negative secondary ions, CAMECA IMS-3f, 75V sample offset RSF values from Wilson [30].

available for the elements detected [30]. Table 7.2 shows how the calculation of concentration or atom density would be made for each element. The corrected intensity is obtained by applying the RSF values to the raw intensity.

REFERENCES

[1] Vickerman, J.C. 2001. "ToF-SIMS—An Overview." In *ToF-SIMS: Surface Analysis by Mass Spectrometry*, eds. J.C. Vickerman, and D. Briggs, 1. Chichester: IM Publications and SurfaceSpectra Limited.

[2] Wittmaack, K. 1975. "Pre-equilibrium Variation of the Secondary Ion Yield." *International Journal of Mass Spectrometry and Ion Physics* 17, no. 1, pp. 39–50. doi: http://dx.doi.org/10.1016/0020-7381(75)80005-2

[3] Stevie, F.A., E.P. Martin, Jr., P.M. Kahora, J.T. Cargo, A.K. Nanda, A.S. Harrus, A.J. Muller, and H.W. Krautter. 1991. "Boron Contamination of Surfaces in Silicon Microelectronics Processing: Characterization and Causes." *Journal of Vacuum Science & Technology A* 9, no. 5, pp. 2813. doi: http://dx.doi.org/10.1116/1.577206

[4] Vandervorst, W., F.R. Shepherd, J. Newman, B.F. Phillips, and J. Remmerie. 1985. "Surface Transient Behavior of the $^{30}Si^{+}$ Yield with Angle of Incidence and energy of an O_2^+ Primary Beam." *Journal of Vacuum Science & Technology A* 3, no. 3, p. 1359. doi: http://dx.doi.org/10.1116/1.572778

[5] Bryan, S.R., R.W. Linton, and D.P. Griffis. 1987. "Characterization and Removal of Ion Yield Transients in the Near Surface Region of Secondary Ion Mass Spectrometry Depth Profiles." *Journal of Vacuum Science & Technology A* 5, no. 1, p. 9. doi: http://dx.doi.org/10.1116/1.574825

[6] Corcoran, S., and S.B. Felch. 1992. "Evaluation of Polyencapsulation, Oxygen Leak, and Low Energy Ion Bombardment in the Reduction of Secondary Ion Mass Spectrometry Surface Ion Yield Transients." *Journal of Vacuum Science & Technology B* 10, no. 1, p. 342. doi: http://dx.doi.org/10.1116/1.586356

[7] Loxton, C.M., J.E. Baker, A.E. Morgan, and T.-Y.J. Chen. 1986. "SIMS Measurements of As at the SiO_2/Si Interface." In *Secondary Ion Mass Spectrometry, SIMS V*, eds. A. Benninghoven, R.J. Colton, D.S. Simons, and H.W. Werner, 291. Berlin, Germany: Springer.

[8] Morgan, A.E., and P. Maillot. 1988. "Dopant Depth Profiling at the SiO_2/Si Interface." In *Secondary Ion Mass Spectrometry, SIMS VI*, eds. by A. Benninghoven, A.M. Huber, and H.W. Werner, 709. Chichester, United Kingdom: Wiley.

[9] Williams, P. 1988. "Aspects of Quantitative Analysis Using Secondary Ion Microanalysers." In *Secondary Ion Mass Spectrometry, SIMS VI*, eds. A. Benninghoven, A.M. Huber, and H.W. Werner, 261. Chichester, United Kingdom: Wiley.

[10] Wilson, R.G., F.A. Stevie, C.W. Magee. 1989. *Secondary Ion Mass Spectrometry*, 4.4–7. New York: Wiley.

[11] Williams, P., and J.E. Baker. 1980. "Quantitative Analysis of Interfacial Impurities Using Secondary-Ion Mass Spectrometry." *Applied Physics Letters* 36, no. 10, p. 842. doi: http://dx.doi.org/10.1063/1.91343

[12] Jones, C.M., and J. Zhao. 2001. "Determination of Sub-2-nm SiO_2 Interlayer Thickness Using Secondary Ion Mass Spectrometry." *Surface and Interface Analysis* 31, no. 1, pp. 51–53. doi: http://dx.doi.org/10.1002/sia.952

[13] Miyamoto, T., E. Hayashi, N. Morita, N. Nagai, T. Hasegawa, M. Hatada, A. Karen, and A. Ishitani. 2000. "Quantification of Oxygen at the Interface Between Poly Silicon Film and the Silicon Interface." In *Secondary Ion Mass Spectrometry, SIMS XII*, eds. A. Benninghoven, P. Bertrand, H. –N. Migeon, and H.W. Werner, 377. Amsterdam, Netherlands: Elsevier.

[14] Wilson, R.G., F.A. Stevie, and C.W. Magee. 1989. *Secondary Ion Mass Spectrometry*, 4.5–3. New York: Wiley.

[15] Novak, S.W., and R.G. Wilson. 1988. "SIMS Measurements of Impurities and Dopants in AlGaAs Heterostructures." In *Secondary Ion Mass Spectrometry, SIMS VI*, eds. A. Benninghoven, A.M. Huber, and H.W. Werner, 303. Chichester, United Kingdom: Wiley.

[16] Corcoran, S.F., D.P. Griffis, and R.W. Linton. 1988. "Quantitative Depth Profiling of Multilayer Semiconductor Materials." In *Secondary Ion Mass Spectrometry, SIMS VI*, eds. A. Benninghoven, A.M. Huber, and H.W. Werner, 283. Chichester, United Kingdom: Wiley.

[17] Palmstrom, C.J., S.A. Schwarz, E.D. Marshall, E. Yablonovitch, J.P. Harbison, C.L. Schwartz, L. Florez, T.J. Gmitter, L.C. Wang, and S.S. Lau. 1988. "A High Depth Resolution Backside Secondary Ion Mass Spectrometry Technique Used for Studying Metal/GaAs Contacts." *Materials Research Society Symposium Proceedings* 126, p. 283. doi: http://dx.doi.org/10.1557/proc-126-283

[18] Lareau, R.T. 1988. "SIMS Back-Side Sputter Depth Profile Technique." In *Secondary Ion Mass Spectrometry, SIMS VI*, eds. A. Benninghoven, A.M. Huber, and H.W. Werner, 437. New York: Wiley.

[19] Schwarz, S.A., C.J. Palmstrom, C.L. Schwartz, T. Sands, L.G. Shantharama, E.D. Marshall, G.G. Han, S.S. Lau, L.H. Allen, and J.W. Mayer. 1990. "Backside Secondary Ion Mass Spectrometry Investigation of Ohmic and Schottky Contacts on GaAs." *Journal of Vacuum Science & Technology A* 8, no. 3, p. 2079. doi: http://dx.doi.org/10.1116/1.577006

[20] Schwarz, S.A., M.A.A. Pudens, T. Sands, T.J. Gmitter, R. Bhat, M. Koza, L.C. Wang, and S.S. Lau. 1992. "Backside Secondary Ion Mass Spectrometry Study of a Ge/Pd Ohmic Contact to InP." *Applied Physics Letters* 60, no. 9, p. 1123. doi: http://dx.doi.org/10.1063/1.106428

[21] Jackman, J.A., A. Kular, L. Weaver, D. Mayer, T.E. Jackman, and C. MacPherson. 1990. "Back-Side SIMS Profiles of Dopant Redistribution Under Silicide Films." *Surface and Interface Analysis* 15, no. 7, pp. 451–53. doi: http://dx.doi.org/10.1002/sia.740150710

[22] Gu, C., A. Pivovarov, R. Garcia, F. Stevie, D. Griffis, J. Moran, L. Kulig, and J.F. Richards. 2004. "Secondary Ion Mass Spectrometry Backside Analysis of Barrier Layers for Copper Diffusion." *Journal of Vacuum Science & Technology B* 22, no. 1, p. 350. doi: http://dx.doi.org/10.1116/1.1617278

[23] Vandervorst, W., J. Bennett, C. Huyghebaert, T. Conard, C. Gondran, H. De Witte. 2004. "On the Reliability of SIMS Depth Profiles Through HfO_2-Stacks." *Applied Surface Science* 231–232, pp. 569–573. doi: http://dx.doi.org/10.1016/j.apsusc.2004.03.102

[24] Sivasubramani, P., M.J. Kim, B.E. Gnade, R.M. Wallace, L.F. Edge, D.G. Schlom, H.S. Craft, and J.-P. Maria. 2005. "Outdiffusion of La and Al from Amorphous $LaAlO_3$ in Direct Contact with Si (001)." *Applied Physics Letters* 86, no. 20, p. 201901. doi: http://dx.doi.org/10.1063/1.1928316

[25] Gu, C., F.A. Stevie, R. Garcia, J. Bennett, and D.P. Griffis. 2006. "Back Side SIMS Analysis of Hafnium Silicate." *Applied Surface Science* 252, no. 19, p. 7179. doi: http://dx.doi.org/10.1016/j.apsusc.2006.02.099

[26] Hongo, C., M. Takenaka, Y. Kamimuta, M. Suzuki, and M. Koyama. 2004. "Backside-SIMS Profiling of Dopants in thin Hf Silicate Film." *Applied Surface Science* 231–232, pp. 594–97. doi: http://dx.doi.org/10.1016/j.apsusc.2004.03.118

[27] Gu, C., R. Garcia, A. Pivovarov, F. Stevie, and D. Griffis. 2004. "Site-specific SIMS Back Side Analysis." *Applied Surface Science* 231–232, pp. 663–67. doi: http://dx.doi.org/10.1016/j.apsusc.2004.03.140

[28] Stevie, F.A., R. Garcia, C. Richardson, and C. Zhou. 2014. "Back Side SIMS Analysis." *Surface and Interface Analysis* 46, no. S1, pp. 241–43. doi:http://dx.doi.org/10.1002/sia.5470

[29] Wilson, R.G., F.A. Stevie, and C.W. Magee. 1989. *Secondary Ion Mass Spectrometry*, 4.1–12. New York: Wiley.

[30] Wilson, R.G. 1988. "Secondary Ion Mass Spectrometry Sensitivity Factors versus Ionization Potential and Electron Affinity for Many Elements in HgCdTe and Cd Te Using Oxygen and Cesium Ion Beams." *Journal of Applied Physics* 63, no. 10, p. 5121. doi: http://dx.doi.org/10.1063/1.340413

CHAPTER 8

Insulators

8.1 SAMPLE CHARGING

Insulators represent a large segment of the materials of potential interest for surface analysis. However, since secondary ion mass spectrometry (SIMS) utilizes an ion beam for analysis, the application of this charged beam to an insulating material can cause a charge buildup on the surface of the insulator [1]. In general, the SIMS ion beam will cause the sample to charge positively because the primary beam is usually positive and the primary ion current is significantly larger than the secondary ion current. The ejection of secondary electrons from the sample surface also causes an increase in positive charge [2]. For positive secondary ions and a sample biased with positive voltage, the secondary electrons will be attracted to the sample and will not be a factor. However, for secondary negative ions and a sample biased negative, the secondary electrons can be a factor especially for Cs^+ bombardment, which can generate a high number of secondary electrons.

Positive sample charging is shown schematically in Figure 8.1. The amount of charge buildup can be sufficient to distort the extraction fields for the secondary ions and reduce or extinguish the detected secondary ion current. Figure 8.2 shows depth profiles for a fluorine implanted SiO_2 layer on silicon with and without charge neutralization. The depth profile without neutralization does not have a constant matrix signal in the insulating layer and has a fluorine distribution that is quite distorted from the expected Gaussian shape for the implanted fluorine as shown in the profile with charge neutralization. Charging of the sample can even reach the voltage required to cause electrical breakdown and result in an electrical discharge within the vacuum system. This discharge can produce significant damage to the sample and even damage the instrument. Figure 8.3 shows discharge tracks that occurred during analysis of a 1.3 μm layer of

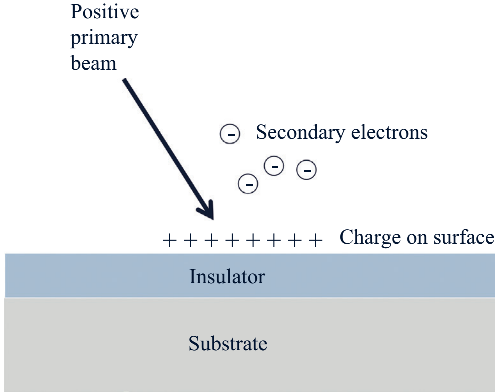

Figure 8.1. Positive primary beam and ejection of secondary electrons cause sample surface to charge positive.

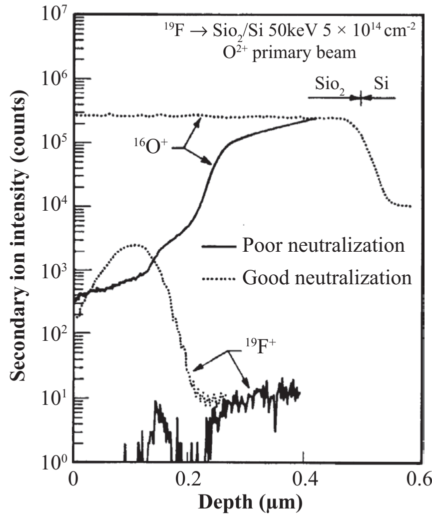

Figure 8.2. Depth profiles of F implanted into 500 nm SiO_2/Si with and without neutralizing electron beam.
Source: Wilson, Stevie, and Magee [3].

SiO_2 on silicon. The sample was analyzed using a cesium primary beam on a magnetic sector instrument with insufficient charge neutralization for secondary negative ion detection. Sample charging may not always be obvious. Figure 8.4 shows the analysis of a SiO_2 layer on Si with and

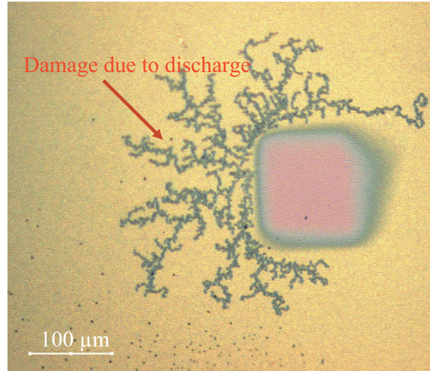

Figure 8.3. Discharge on sample due to Cs^+ bombardment of SiO_2 layer on Si.
Source: F. Stevie, Analytical Instrumentation Facility, North Carolina State University.

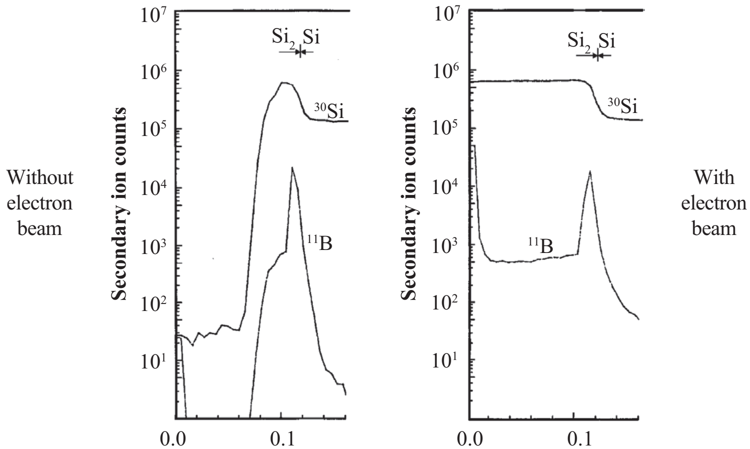

Figure 8.4. Analysis without electron beam appears to show additional layer at surface.
Source: F. Stevie, Analytical Instrumentation Facility, North Carolina State University.

without an electron beam. The analysis without the electron beam appears to show the presence of a layer with low boron and silicon concentration on top of a SiO_2 layer. The sample becomes conductive as the SiO_2/Si interface is approached, possibly due to penetration of positive primary ions into the conductive substrate. With charge neutralization, the

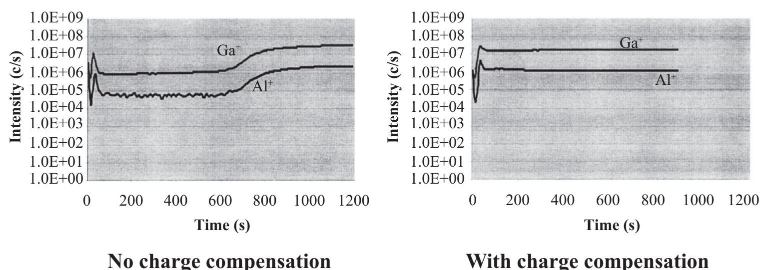

CAMECA IMS-6F
O_2^+ 1.25 kV impact energy (3 kV source 1.75 kV sample)
Electron 6.25 kV impact energy (–4.5 kV source 1.75 kV sample)

Figure 8.5. Sample charging on Au coated 2% Al in AlGaN.
Source: C. Gu, Analytical Instrumentation Facility, North Carolina State University.

intensities of the boron and silicon are restored to their correct levels and the presence of a single layer of SiO_2 is clear. Figure 8.5 shows the depth profiles of an AlGaN sample with and without neutralization, and the two matrix species monitored indicate that charging can result in a decreased but constant intensity over a certain depth. Especially with a new set of samples, it is recommended to try analyzing at least one sample with and without neutralization and check for a difference in profiles.

8.2 CHARGE COMPENSATION METHODS

Several methods have been devised to reduce sample charging. The sample can be coated with a conductive material, analyzed with a negative ion beam, or charge compensated with an electron beam [3] or even a laser [4].

A conductive coating provides a path for charge to leak away from the surface to the sample holder [5, 6]. The sample surface should have sufficient overall coating so that part of the coated surface is in direct contact with the sample holder. Typical coating materials are gold, gold–palladium, or carbon, but several other metals, such as chromium, have been used. Note that mass interferences from the coating material can be an issue. For this reason gold is often the material of choice because it is monoisotopic and occurs at a high mass. Carbon has the disadvantages of low mass and having more than one isotope. This means additional peaks from species such as carbon polymeric ions (C_2, C_3, …) can be present in

the mass spectrum and appear in the depth profile until all the C has been removed. Gold has the disadvantage in that a relatively thick layer may need to be deposited to produce a continuous film because gold does not deposit evenly. The coating is usually obtained by sputtering a layer on the sample using a plasma sputter coater. The thickness of any coating layer needs to be known and corrected for if the depth profiles require accurate depth scales. Another method is to place a conductive grid, such as copper, over the surface of the sample and analyze between the grid lines. The grid can be one used for transmission electron microscopy, which is 3 mm in diameter, and selected to provide a wide spacing between grid lines. This approach is successful for some samples but may be insufficient for a thick insulating layer or a material that is a bulk insulator.

The O^- approach uses the negatively charged primary beam to negate the tendency of the sample to charge positively [7]. The sample is usually coated with a conductor or covered with a mask or a conductive grid placed on the surface, with analyses made between the grid lines [8]. Use of a negatively charged beam, O^-, was successful for the analysis of a gold coated bulk insulator with the use of a magnetic sector instrument from Applied Research Laboratories [9]. The O^- primary beam is available on CAMECA magnetic sector instruments with a duoplasmatron and is provided by shifting the position of the cathode so that the negative species at the edge of the cathode predominate in the ion beam. This method uses the same duoplasmatron used to provide O_2^+ and has been successfully employed, particularly for the analysis of glasses or minerals [8, 10]. An example of this method for mineral analysis is shown in Figure 8.6, which is a study of silver in sphalerite. The samples were implanted with silver and the baseline for the two samples shows a significant difference in silver content. This method provides an in situ calibration of the bulk level of silver in the samples. Use of a conductive grid is shown in Figure 8.7, where a gold grid was placed on a bulk glass sample and 100 µm × 100 µm craters located between grid lines. The sample is lithium aluminum silicate (Zerodur), which is an inorganic nonporous material with crystalline and glass phases and has essentially no thermal expansion.

8.3 ELECTRON BEAM NEUTRALIZATION

The most common method employed for charge neutralization is the application of an electron beam coincident with the ion beam analysis region. Since the sample charges positively, the negative electrons provide

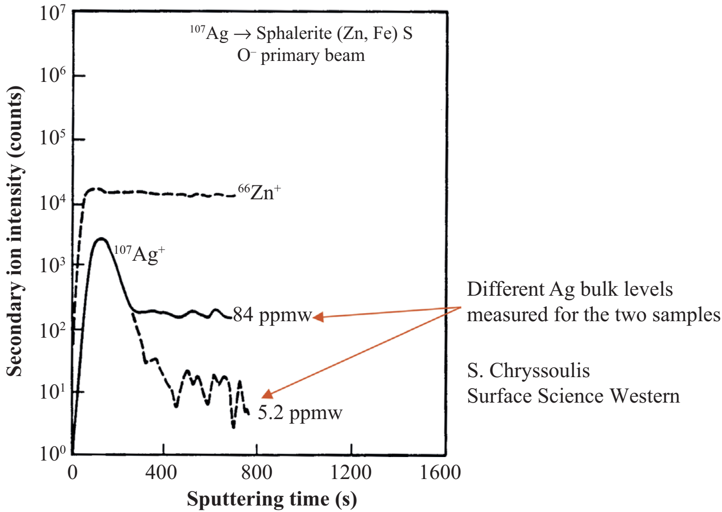

Figure 8.6. SIMS depth profiles of two samples of sphalerite bulk insulator using O^-.
Source: Wilson, Stevie, and Magee [3].

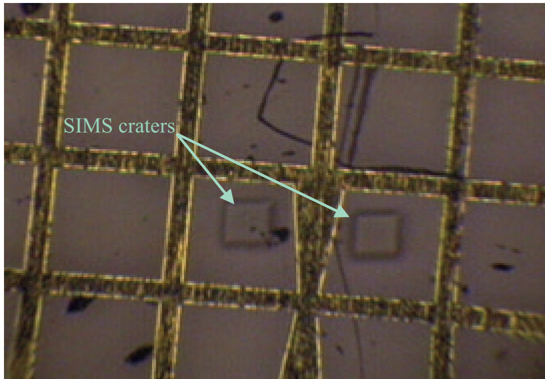

Sample covered with TEM grid
CAMECA IMS-6F analysis with $^{16}O^-$ at 50 nA 100 µm × 100 µm raster
and detection of positive secondary ions

Figure 8.7. SIMS craters from $^{16}O^-$ analysis of lithium aluminum silicate.
Source: F. Stevie, AT&T Bell Laboratories.

charge compensation. A wide range of electron energies and currents have been used as will be discussed later. A conductive coating is often applied to the surface to assist the electron beam in the removal of surface charge. The electron beam can generate secondary electrons, and Figure 8.8 shows

a generic plot of secondary electron emission versus electron energy. Electron energy for charge neutralization is usually chosen to be above or below the voltage range where total electron emission exceeds incident electron current. The peak may be as high as 5 to 20 times the incident electrons [11].

The interaction of an electron beam with an insulator causes formation of electron hole pairs that can make that region conductive by electron beam induced conductivity (EBIC) (Figure 8.9). If the insulator is a thin layer on a conducting substrate, then use of an electron beam with sufficient energy to penetrate the layer allows EBIC to provide a conductive

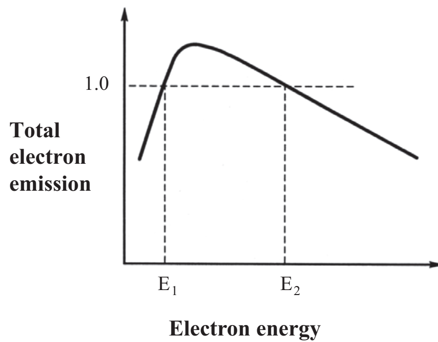

Electron yield exceeds 1 between crossover points E_1 and E_2

Figure 8.8. Electron yield versus primary electron energy.

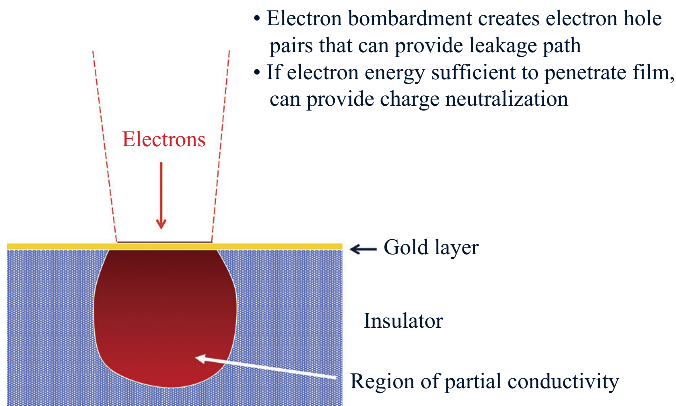

Figure 8.9. Electron beam induced conductivity (EBIC).

path from the surface to the substrate [12]. The electron penetration or range can be estimated from the Kanaya-Okayama equation [13].

$$R_{KO} = \frac{0.0276 W E_0^{1.67}}{Z^{0.89} \rho}$$

Where R_{KO} is the range in µm, E_0 is the incident beam energy in keV, W is the average atomic weight in g/mol, Z is the average atomic number, and ρ is the average density in g/cm^3. The electron beam is at normal incidence to the sample.

Only a few electron volts are required to create an electron hole pair, so a few kV electron beam will create a significant number of these pairs. Figure 8.10 shows an example of good neutralization for positive secondary ions achieved when the energy of the electron beam is adjusted to match the penetration required for the thickness of an insulator layer [12]. Repeat analyses in adjacent areas could be made without significant change in the alkali element profile. Creation of a surface EBIC region with the use of a high electron flux on a coated sample has been demonstrated [14]. Another approach is to match the penetration depth of the electron beam to the penetration depth of the primary ion beam. This has been successful for a glass substrate where positive secondary ions were analyzed [15].

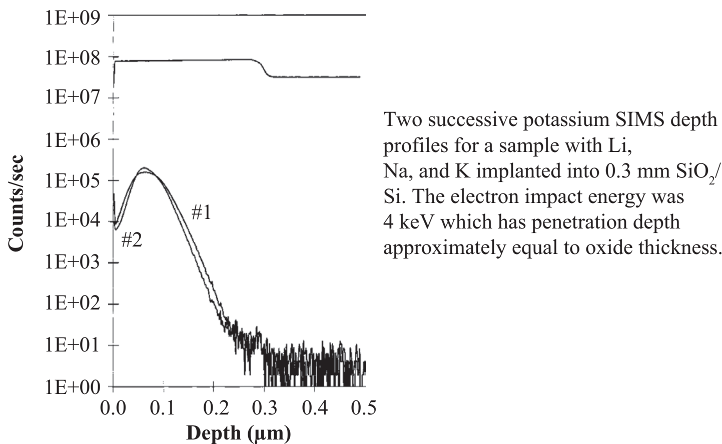

Figure 8.10. Example of EBIC analysis.
Source: McKinley et al. [12], reproduced with permission from American Institute of Physics, copyright 2000, American Vacuum Society.

8.3.1 QUADRUPOLE

The electron beam approach to charge neutralization varies for the different SIMS analyzers. The quadruple mass analyzer has a relatively open geometry in which the specimen can be at ground and the extractor at only a few hundred volts. Therefore it is relatively easy to deploy an electron beam at almost any angle of incidence relative to the specimen, and to accurately aim the electron beam. Figure 8.11 shows a schematic drawing of quadrupole analyzer geometry. The grounded sample allows low energy electrons to be used without acceleration or retardation by a sample potential. Typically the electron beam is coincident with the ion beam sputtered area.

Low energy electron beam neutralization has been employed at an early point in SIMS development using an electron beam coincident with the ion beam and the electron current density on the order of the ion current density [16–18]. Figure 8.12 shows the ion intensity of GdO^+ as a function of electron current and indicates that a minimum electron current was required for neutralization and that excess electron current had little effect on the ion intensity [18]. Note that even low energy electrons have a short interaction time with a molecule. For a molecule 0.5 nm in diameter and with a range of interaction of 1 nm, a 70 eV electron travels at 6×10^6 m/s, and the range of interaction would be traversed in 2×10^{-16} s.

Higher energy electron neutralization has also been successful. Figure 8.13 shows a schematic example of quadrupole analysis using 2 keV electrons. This example is for a PHI-6300 quadrupole analyzer with 1,000 μm diameter electron impact area and 400 μm × 400 μm ion

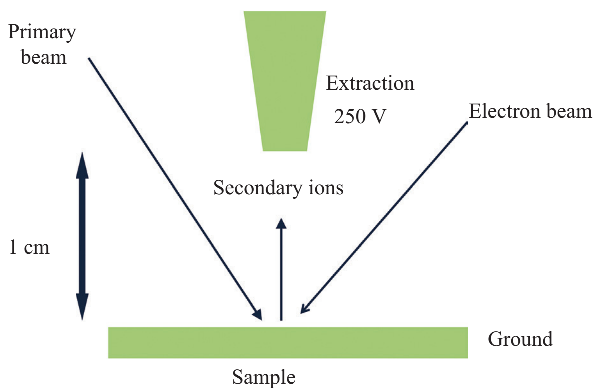

Figure 8.11. Quadrupole geometry.

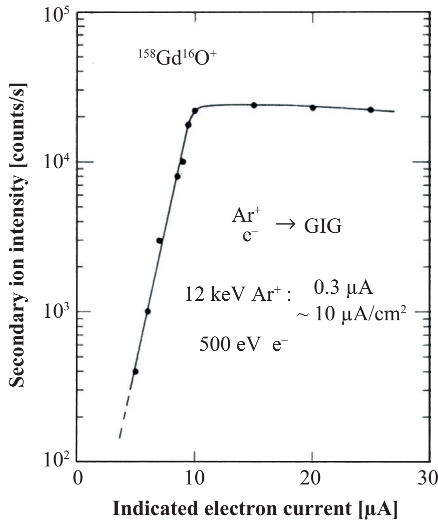

Figure 8.12. GdO^+ intensity versus electron beam current.
Source: Wittmaack [18], reprinted with permission from Journal of Applied Physics, copyright 1979, AIP Publishing LLC.

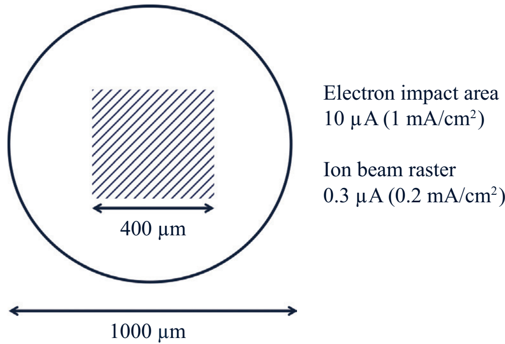

Figure 8.13. Quadrupole 2 kV electron beam neutralization.

beam raster. A typical quadrupole electron beam energy was 2 kV and 60° from normal. The electron beam was unrastered and centered on the ion beam raster, with the beam defocused to exceed the ion beam raster. Ions were O_2^+ at 6 keV and 60° from normal, with the electron to ion current density ratio greater than a factor of five for SiO_2 [3, 19]. The ratio

varied for different materials and was higher for Si_3N_4 than for SiO_2. This approach was viable for a wide range of insulators. Examples are provided for the glass industry where oxides may be added to SiO_2 to obtain desired properties. Figure 8.14 shows mass spectra for quartz watch glass and Pyrex [20]. The mass spectra show the presence of many elements but B is absent in the watch glass and is an important additive in Pyrex. It is

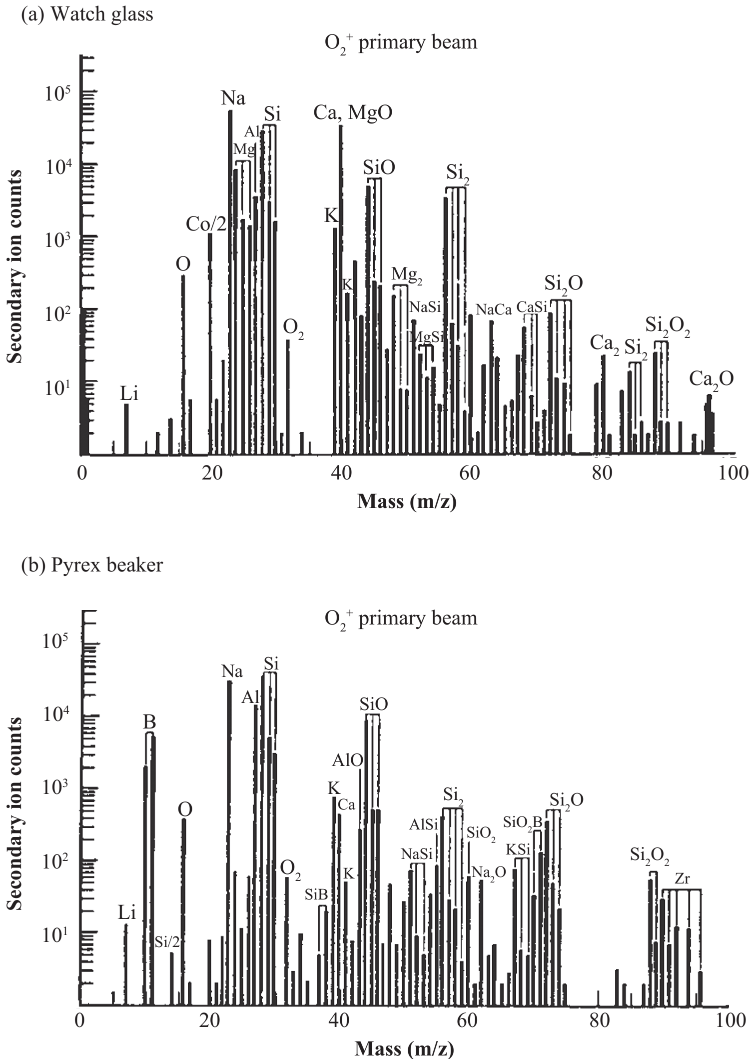

Figure 8.14. Quadrupole bulk insulator mass spectral analysis. (a) Watch glass and (b) Pyrex.
Source: Stevie [20], reprinted with permission from John Wiley and Sons.

important to characterize the glass surface and the near-surface region. Figure 8.15 shows depth profiles in red actinic glass, which is used to protect the contents from certain light wavelengths [20]. Copper in particular is significantly lower in the near-surface region but has a high and gradually decreasing level in the bulk. Note that because of the high concentration of oxygen in the oxide, the secondary ion yield is not affected by the pre-equilibrium region that would be present if silicon were analyzed.

Analyses can be made at high sputtering rate if the electron current density is sufficient. Figure 8.16 shows the analysis of titanium diffused

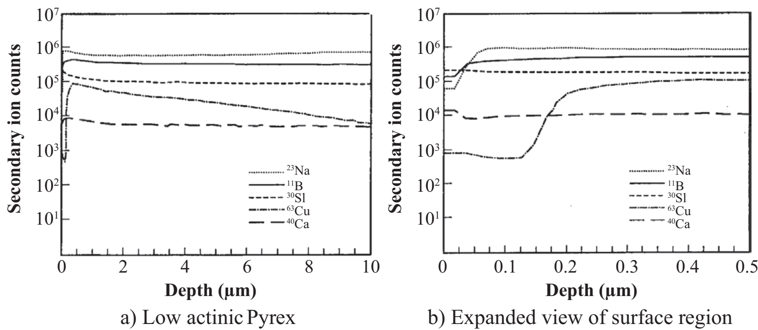

Figure 8.15. Quadrupole actinic Pyrex analysis. (a) Low actinic Pyrex and (b) expanded view of the surface region.
Source: Stevie [20], reprinted with permission from John Wiley and Sons.

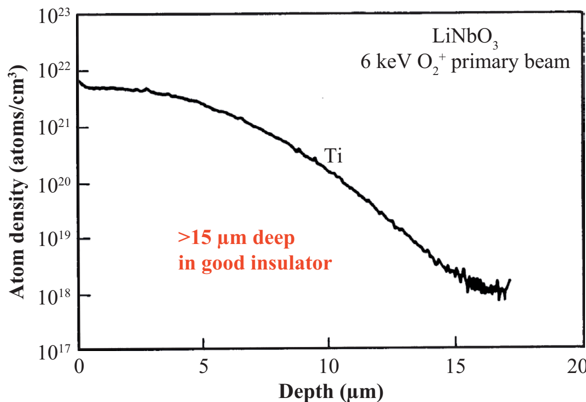

Figure 8.16. $LiNbO_3$ bulk insulator analyzed with PHI-6300 quadrupole.
Source: Stevie et al. [19], reproduced with permission from American Institute of Physics, copyright 1988, American Vacuum Society.

into $LiNbO_3$ to a depth beyond 15 μm. Titanium doping of this material affects the ability to switch at high speeds but the titanium diffusion depth can be relatively deep for SIMS analysis.

8.3.2 MAGNETIC SECTOR

Charge neutralization using a magnetic sector analyzer is complicated by the dimensions of the region where the ion beam interacts with the sample. This region is small and makes deployment of an electron gun difficult. Secondary ion extraction is through a grounded cover plate only 4.5 mm from the sample surface. The initial design for electron gun neutralization for positive secondary ions was achieved by a 30° from normal electron source with voltage adjustable from −300 V to −2500 V. The sample at 4,500 V results in an electron impact energy from 4800 to 7000 V and a penetration range in SiO_2 of approximately 500 nm. This was a limitation to electron penetration of a layer, and bulk insulators were very difficult to analyze. However, good results were obtained for certain materials such as Al_2O_3 [21].

A normal incidence electron gun (NEG) was developed (Figure 8.17) that provides electrons to the sample along the optical path of the secondary ions, but in the opposite direction [22]. For positive secondary ions, the electron impact energy will be the energy of the electron plus the accelerating potential of the sample holder. For negative secondary ions, the electron energy of this normal incidence electron source can be set to just below the value for the sample potential so that the electrons approach but do not actually impact the sample. Once the sample starts to charge,

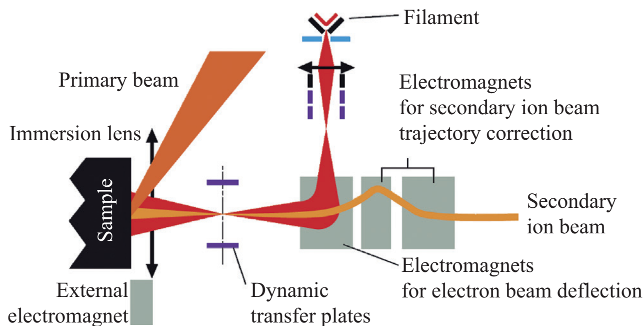

Figure 8.17. CAMECA NEG.
Source: CAMECA instruments, reproduced with permission from CAMECA.

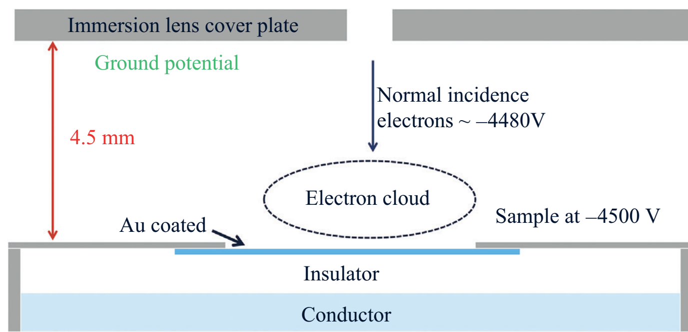

Figure 8.18. Magnetic sector negative secondary ion neutralization.

electrons in the cloud just above the surface will be used to compensate the sample as shown in Figure 8.18 [23]. Alignment of the NEG can be difficult but the use of a sample that exhibits cathodoluminescence can assist in this procedure [24].

For positive primary beams, the electrons typically strike at high impact energy because the electron gun high voltage is added to the sample potential. If the insulating layer is not too thick and the substrate is conductive, then the electron energy may be sufficient to penetrate the layer into the substrate. As described previously, the generation of electron hole pairs due to the interaction of the electron beam with the insulator causes the insulator to be conductive in this region. This EBIC has made possible the analysis of alkali elements in thin insulating films [12]. This type of SIMS analysis is difficult because of the motion of alkali elements in the film if any net charge is applied [25]. More details on this analysis are provided later in this chapter.

Typical NEG analysis conditions for secondary positives on a CAMECA IMS-6F would be 9 keV electrons at 40 µA into a 1400 µm diameter circle. This represents an electron current density of 0.0025 A/cm^2 and 0.36 watts of power applied to the sample.

For layers too thick to use the electron penetration method and for bulk insulators, analysis using positive primary ions on a magnetic sector has been problematic. One method is to reduce the sample and electron voltages to about 1 to 2 keV each. Analyses of bulk insulators without a conductive coating have been made using this method [15]. An adjacent electron method was developed that has simplified this analysis [26–28]. In this method the electron beam is aligned to impact a coated region that is adjacent to the ion beam analysis area. Some combination of secondary electrons, backscattered electrons, or EBIC provides a neutralization

capability that is self-regulated. The charging region will only use the electron compensation that is required. For certain samples, such as GaN, cathodoluminescence can indicate the electron impact area. Figure 8.19 shows the size and location of the electron beam for two different electron beam energies and a sample potential of 4.5 kV for detection of positive secondary ions. For the CAMECA NEG, the electron beam size and current density vary with electron energy because of immersion lens focusing. Figure 8.20 shows the relationship of the adjacent electron region

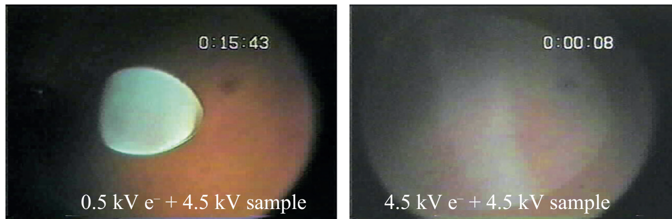

CAMECA IMS-6F
^{63}Cu implanted in 0.3 μm SiO_2/Si to a
dose of 1×10^{14} atoms/cm^2

Figure 8.19. Cathodoluminescence indication of electron beam irradiation.
Source: F. Stevie and J. McKinley, Lucent Technologies.

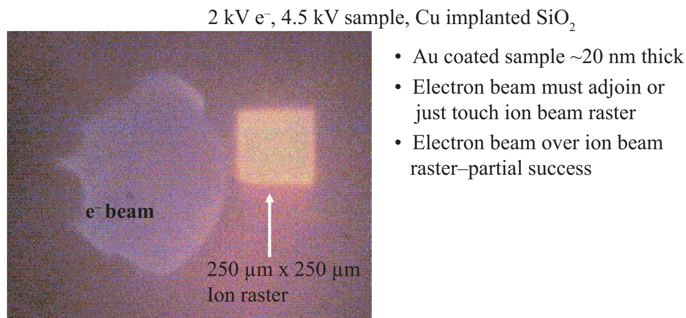

Neutralization self-regulating over large range:
- Electron sample current from 2.5 to 70 μA
- 10 kV O_2^+ 100 to 400 nA, 230 μm × 230 μm raster (5.5 keV impact energy)

Figure 8.20. Magnetic sector neutralization for positive secondary ions.
Source: Pivovarov, Stevie, and Griffis [26], reprinted from Applied Surface Science, copyright 2004, with permission from Elsevier.

with the ion beam raster. Figure 8.21 shows the analysis of an implant of ^{9}Be into crystalline Al_2O_3 analyzed with the adjacent electron method. The mass resolution required to separate ^{9}Be from $^{27}Al^{3+}$ is 750 and is beyond the capability of the generally available quadrupole SIMS analyzers. The detection limit with a quadrupole analyzer was 5×10^{16} atoms/cm^3 and has been improved to 1×10^{15} atoms/cm^3 with high mass resolution analysis on a magnetic sector instrument. The adjacent electron method can be used to provide sufficient electron current for high sputtering rate analysis of insulators. Figure 8.22 shows 2.2 nm/s sputtering rate analysis of B implanted

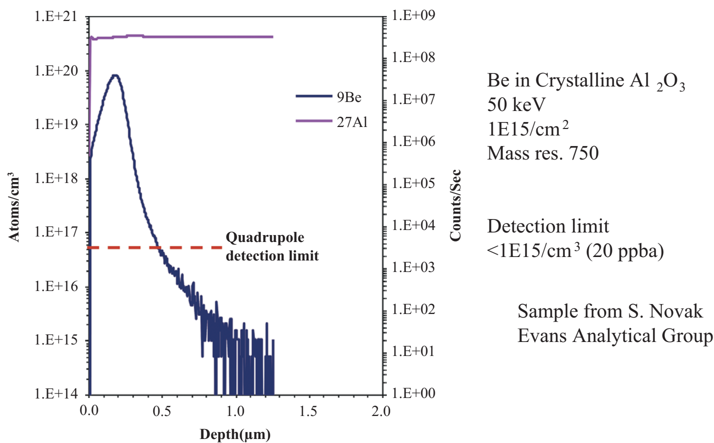

Figure 8.21. Magnetic sector analysis of Be in crystalline Al_2O_3. *Source*: F. Stevie, Analytical Instrumentation Facility, North Carolina State University.

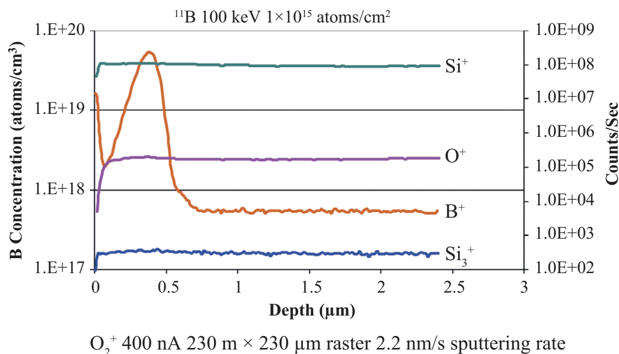

Figure 8.22. High sputtering rate analysis of B implanted bulk SiO_2 using adjacent electron beam method with Au coating. *Source*: Pivovarov, Stevie, and Griffis [26], reprinted from Applied Surface Science, copyright 2004, with permission from Elsevier.

into bulk SiO_2. With a high current electron beam, the wattage applied to the sample holder can be significant and if the holder is removed directly after analysis it can be too hot to hold in your hand. This means that if a sample can be affected by low level heating, the analysis may have to be at low sputtering rate and low electron beam current.

8.3.3 TIME OF FLIGHT

The time of flight (TOF) analyzer uses pulses of electrons between the pulses of extracted ions. The time in which the analysis beam is turned on is normally a small fraction of the total time, so it is possible to employ the electron beam during the time the analysis beam is off. Figure 8.23 shows a timing diagram for charge neutralization on a TOF-SIMS. For TOF-SIMS analysis of a surface, the total sputtering rate is much lower than that for depth profiling applications, and some of the charge at the surface can leak off between sputtering pulses, therefore less electron neutralization is required. This is usually accomplished with low energy electrons, on the order of 20 eV. Many charge neutralization effects are not dramatic and may need to be confirmed by analyzing with and without charge neutralization. In general, neutralization for TOF-SIMS has been very successful.

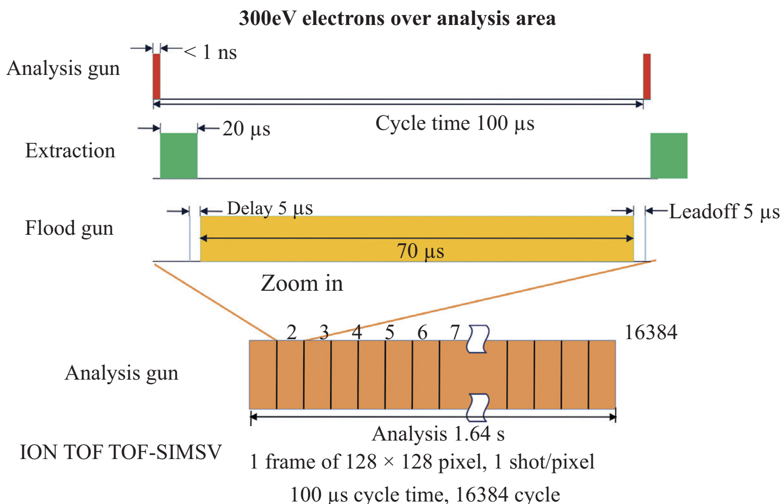

Figure 8.23. TOF analysis for insulator.
Source: C. Zhou, Analytical Instrumentation Facility, North Carolina State University.

8.3.4 ELECTRON BEAM DEGRADATION OF SAMPLE

Some materials degrade with electron impact. For organic materials, such as low-k dielectrics used in semiconductor technology, use of electron beams for charge neutralization can affect the analysis because the electron beam can degrade the specimen [29, 30]. The specimen will show a decrease in thickness where the electron beam has impacted the sample. The low energy electrons used by TOF-SIMS will have less impact on the sample than the keV electron sources. If the magnetic sector electron cloud method is used for neutralization, the electron impact on the sample should be minimal.

8.4 SPECIES MOBILE UNDER ION BOMBARDMENT

Certain species, particularly lithium, sodium, and potassium, but also hydrogen in some cases, can be mobile in an insulator when an electric field is applied [25]. Analysis of these elements is important because the application of electric fields causes these elements to move and therefore reduces the effective insulating capability of the layer. It can be difficult to analyze these species using SIMS and provide an accurate depth profile because the SIMS analysis provides a voltage to the sample if sample charging causes a net voltage to be present. Figure 8.24 shows a schematic drawing of analysis of sodium implanted into SiO_2 on a silicon substrate.

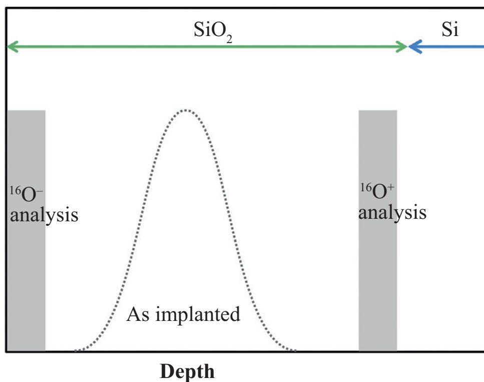

Figure 8.24. Schematic of Na profiles in SiO_2/Si for Na implanted and analyzed using $^{16}O^-$ and $^{16}O^+$ primary beams.

When analyzed with an $^{16}O^+$ primary beam, the sodium does not have the expected Gaussian shape but has been pushed to the SiO_2/Si interface. When analyzed with an $^{16}O^-$ primary beam, the sodium has been moved to the surface. This figure demonstrates why SIMS depth profiles of mobile insulator species must be performed under very well balanced charge compensation conditions, as shown in Figure 8.25 [31]. A sample with lithium, sodium, and potassium implanted into 1 μm SiO_2/Si provided quantification for all three alkali elements in one profile but proved to be a very difficult sample to analyze. Examples are shown for the analysis of an uncoated sample with a quadrupole analyzer (Figure 8.26) and for a gold-coated sample with a magnetic sector analyzer (Figure 8.27). Analysis of the same sample was also achieved using TOF-SIMS. Figure 8.28 shows the analysis with dual beam interleaved mode.

There is another approach to this analysis. By the use of a magnetic sector analyzer with a Cs^+ bombardment and NEG, detection of negative secondary ions was successful [32]. The species monitored was $^{23}Na^-$ for sodium. The negative secondary ion yield was sufficient for a detection limit in the 10^{16} atoms/cm^3 range. More recent work shows similar results on a gold coated sample [33].

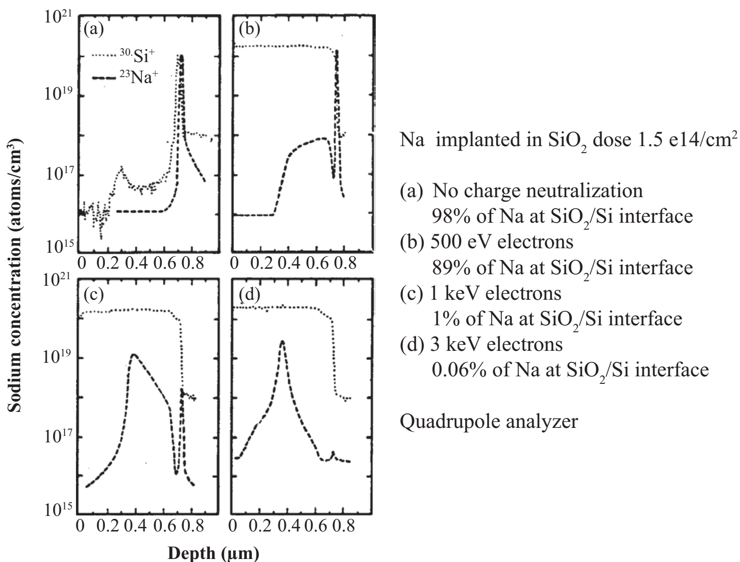

Figure 8.25. Quadrupole insulator analysis of mobile ion species.
Source: Magee and Harrington [31], reprinted with permission from Applied Physics Letters, copyright 1978, AIP Publishing LLC.

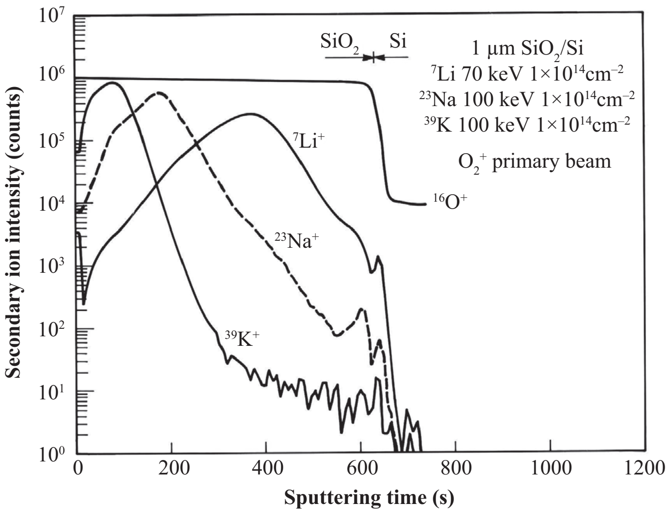

Figure 8.26. Quadrupole analysis of Li, Na, K implanted SiO_2/Si.
Source: F. Stevie, AT&T Bell Laboratories.

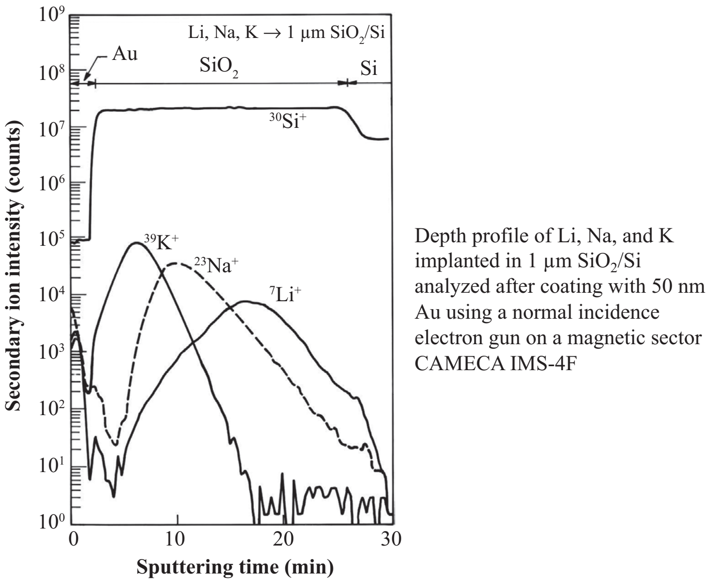

Figure 8.27. Magnetic sector analysis of Li, Na, K implanted 1 μm SiO_2/Si coated with 50 nm Au.
Source: Wilson, Stevie, and Magee [3].

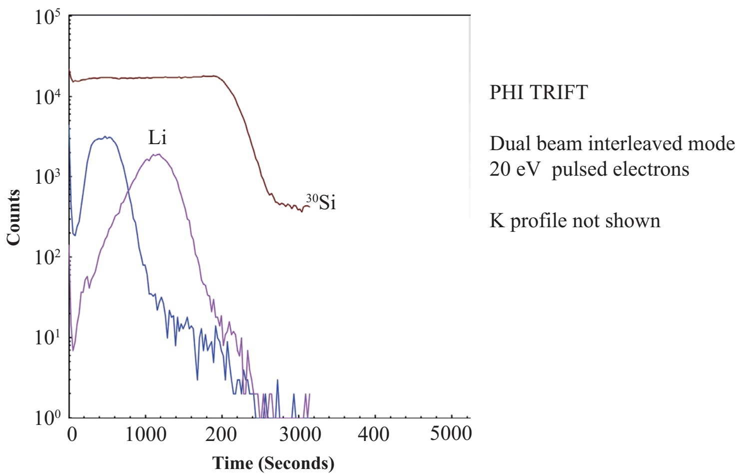

Figure 8.28. 1 µm SiO_2/Si implanted with Li, Na, K.
Source: Physical Electronics, reproduced with permission.

8.5 BURIED INSULATORS

Buried insulator layers present a special problem for analysis. The surface layer and substrate are typically conductive but the insulating layer is located below the surface layer. A successful analysis approach is to sputter into the insulating layer, establish charge balance conditions, and then perform the analysis. One example of this type of structure is used in semiconductor technology and is referred to as silicon on insulator. This layer can be created by implanting a high dose of oxygen (critical dose to form SiO_2 is 1.2×10^{18} atoms/cm^2) and then annealing (1350°C for 2.5 h) to form the oxide. This method is referred to as separation by implantation of oxygen (SIMOX). Typically impurities will move from the layer as it is formed and any nitrogen that is present will move to the interfaces. Figure 8.29 shows an example of SIMOX analysis [34]. Note that certain impurities are concentrated at or adjacent to the Si/SiO_2 interfaces.

8.6 ELECTRON STIMULATED DESORPTION

The use of an electron beam for charge neutralization can affect analysis of certain species, particularly halides in conductors [5]. The profile in the insulating region will be correct but the profile in the conductor will

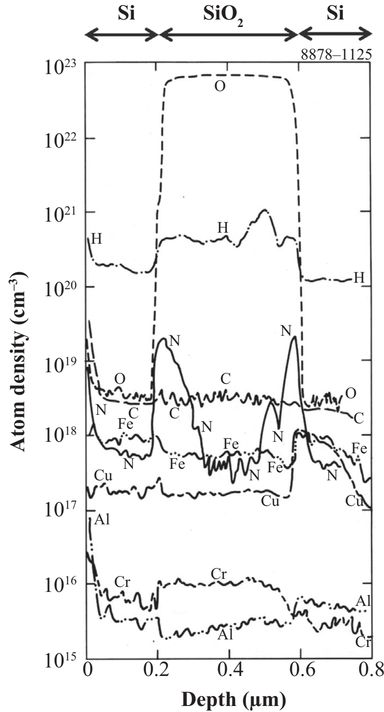

Figure 8.29. SIMOX analysis.
Source: Wilson and Hitzman [34], reprinted with permission from John Wiley and Sons.

be distorted. Electron stimulated desorption (ESD) is the cause and can produce high background levels in conductors for halide positive ions, but also for H^+, O^+, and OH^+ [35]. Profiles with and without an electron beam are recommended to check for this effect, and analysis with detection of negative ions such as F^- should avoid the problem. ESD ions typically have a very narrow energy distribution and can be removed with an energy offset. Figure 8.30 shows an example of analysis with and without charge neutralization for fluorine implanted in silicon and analyzed using O_2^+ with detection of positive secondary ions.

8.7 SUMMARY

For most analyses, charge neutralization is accomplished with the use of an electron beam. The type of analysis to be performed dictates the optimum choice of SIMS analyzer. If analysis of the surface is desired, the TOF

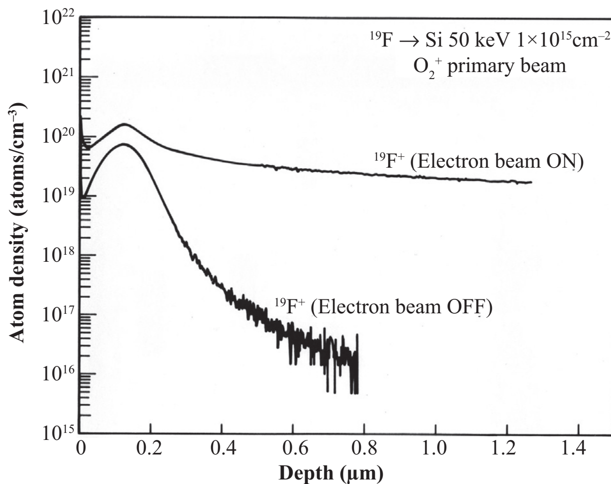

Figure 8.30. Electron stimulated desorption.
Source: Wilson, Stevie, and Magee [3].

analyzer is the preferred choice. If a layer or bulk sample requires analysis and low mass resolution is sufficient, then the quadrupole analyzer will provide a good result. For best sensitivity and high mass resolution, the magnetic sector analyzer is preferred. The electron beam arrangement varies with each analyzer. A summary of electron bombardment neutralization methods is provided:

Electrons applied to analysis crater—quadrupole
Electron penetration of thin film—magnetic sector positives
Electrons adjacent to crater—magnetic sector positives
Electron cloud—magnetic sector negatives
Electron pulses—TOF

REFERENCES

[1] Werner, H.W., and N. Warmoltz. 1984. "Beam Techniques for the Analysis of Poorly Conducting Materials." *Journal of Vacuum Science & Technology A* 2, no. 2, p. 726. doi: http://dx.doi.org/10.1116/1.572559

[2] Baragiola, R.A. 1993. "Principles and Mechanisms of Ion Induced Electron Emission." *Nuclear Instruments and Methods in Physics Research B* 78, no. 1–4, pp. 223–38. doi: http://dx.doi.org/10.1016/0168-583x(93)95803-d

[3] Wilson, R.G., F.A. Stevie, and C.W. Magee. 1989. Section 4.3. In *Secondary Ion Mass Spectrometry*, 4.3–1. New York: John Wiley & Sons.

[4] Dowsett, M.G., R. Morris, Pei-Fen Chou, S.F. Corcoran, H. Kheyrandish, G.A. Cooke, J.L. Maul, and S.B. Patel. 2003. "Charge Compensation Using Optical Conductivity Enhancement and Simple Analytical Protocols for SIMS of Resistive $Si_{1-x}Ge_x$ Alloy Layers." *Applied Surface Science* 203–204, pp. 500–03. doi: http://dx.doi.org/10.1016/s0169-4332(02)00765-1

[5] McPhail, D.S., M.G. Dowsett, and E.H.C. Parker. 1986. "Profile Distortions During Secondary Ion Mass Spectrometry Analyses of Resistive Layers Due to Electron Stimulated Desorption and Charging." *Journal of Applied Physics* 60, no. 7, p. 2573. doi: http://dx.doi.org/10.1063/1.337123

[6] Werner, H.W., and A.E. Morgan. 1976. "Charging of Insulators by Ion Bombardment and Its Minimization for Secondary Ion Mass Spectrometry (SIMS) Measurements." *Journal of Applied Physics* 47, no. 4, pp. 1232–42. doi: http://dx.doi.org/10.1063/1.322845

[7] Andersen, C.A., H.J. Roden, and C.F. Robinson. 1969. "Negative Ion Bombardment of Insulators to Alleviate Surface Charge-up." *Journal of Applied Physics* 40, no. 8, p. 3419. doi: http://dx.doi.org/10.1063/1.1658212

[8] Bojan, V.J., T.H. Buyuklimanli, and C.G. Pantano. 1994. "Quantification of SIMS Data for Multicomponent Glasses." *Surface and Interface Analysis* 21, no. 2, pp. 87–94. doi: http://dx.doi.org/10.1002/sia.740210205

[9] Inoue, K., and A. Isogai. 1986. "Primary-Ion Charge Compensation in Secondary Ion Mass Spectrometry Analysis of Insulators." *Journal of Applied Physics* 59, no. 5, p. 1764. doi: http://dx.doi.org/10.1063/1.336444

[10] Salem, A.A., G. Stingeder, M. Grasserbauer, M. Shreiner, K.H. Giessler, and F. Rauch. 1996. "SIMS and RBS Analysis of Leached Glass: Reliability of RSF Method for SIMS Quantification." *Journal of Materials Science: Materials in Electronics* 7, no. 6, pp. 373–79. doi: http://dx.doi.org/10.1007/bf00180772

[11] Goldstein, J.I., A.D. Romig, Jr., D.E. Newbury, C.E. Lyman, P. Echlin, C. Fiori, D.C. Joy, and E. Lifshin. 1992. *Scanning Electron Microscopy and X-Ray Microanalysis*, 111. New York: Plenum Press.

[12] McKinley, J.M., F.A. Stevie, C.N. Granger, and D. Renard. 2000. "Analysis of Alkali Elements in Insulators Using a CAMECA IMS-6f." *Journal of Vacuum Science & Technology A* 18, no. 1, p. 273. doi: http://dx.doi.org/10.1116/1.582146

[13] J. I. Goldstein and D. E. Newbury (1992) *Scanning Electron Microscopy and X-ray* Mocroanalysis, 2nd ed., 89. New York and London: Plenum Press.

[14] Ikebe, Y., H. Iwamoto, H. Toita, and H. Tamura. 1990. "SIMS Analysis of Insulating Materials Using EBIC." In *Secondary Ion Mass Spectrometry, SIMS VII*, eds. A. Benninghoven, C.A. Evans, K.D. McKeegan, H.A. Storms, and H.W. Werner, 891. Chichester, United Kingdom: Wiley.

[15] Nakatsu, K., S. Hatekeyama, and S. Saito. 1998. "Charge Compensation in High-Resistivity Insulator Analysis with Electron Bombardment by CAMECA ims-4f." In *Secondary Ion Mass Spectrometry, SIMS XI*, eds. by G. Gillen, R. Lareau, J. Bennett, F.Stevie, 627. Chichester, United Kingdom: Wiley.

[16] Wittmaack, K. 1977. "Raster Scanning Depth Profiling of Layer Structures." *Applied Physics* 12, no. 2, pp. 149–56. doi: http://dx.doi.org/10.1007/bf00896140

[17] Wittmaack, K. 1977. "The Use of Secondary Ion Mass Spectrometry for Studies of Oxygen Adsorption and Oxidation." *Surface Science* 68, pp. 118–29. doi: http://dx.doi.org/10.1016/0039-6028(77)90196-0

[18] Wittmaack, K. 1979. "Primary-Ion Charge Compensation in SIMS Analysis of Insulators." *Journal of Applied Physics* 50, no. 1, p. 493. doi: http://dx.doi.org/10.1063/1.325640

[19] Stevie, F.A., V.V.S. Rana, A.S. Harrus, T.H. Briggs, and P. Skeath. 1988. "High Sputter Rate Secondary Ion Mass Spectrometry Analysis of Insulators Used in Microelectronics and Lightwave Applications." *Journal of Vacuum Science & Technology A* 6, no. 3, p. 2082. doi: http://dx.doi.org/10.1116/1.575189

[20] Stevie, F.A. 1992. "Secondary Ion Mass Spectrometry—First Microelectronics, Now the Rest of the World." *Surface and Interface Analysis* 18, no. 2, pp. 81–86. doi: http://dx.doi.org/10.1002/sia.740180203

[21] Smith, S.P., and R.G. Wilson. 1988. "SIMS Depth Profiling and Implantation Profiles in Crystalline Al_2O_3." In *Secondary Ion Mass Spectrometry, SIMS VI*, eds. A. Benninghoven, A.M. Huber, and H.W. Werner, 525. Chichester, United Kingdom: Wiley.

[22] Slodzian, G., M. Chaintreau, and R. Dennebouy. 1986. "The Emission Objective Lens Working as an Electron Mirror: Self Regulated Potential at the Surface of an Insulating Sample." *Secondary Ion Mass Spectrometry, SIMS V*, eds. A. Benninghoven, R.J. Colton, D.S. Simons, and H.W. Werner, 158. Berlin, Germany: Springer.

[23] Migeon, H.N., M. Schuhmacher, and G. Slodzian. 1990. "Analysis of Insulating Specimens with the Cameca IMS4f." *Surface and Interface Analysis* 16, no. 1–12, pp. 9–13. doi: http://dx.doi.org/10.1002/sia.740160105

[24] Chen, J., S. Schauer, and R. Hervig. 2013. "Normal-Incidence Electron Gun Alignment Method for Negative Ion Analysis by Magnetic Sector SIMS." *Nuclear Instruments and Methods in Physics Research Section B* 295, pp. 50–54. doi: http://dx.doi.org/10.1016/j.nimb.2012.11.001

[25] Hughes, H.L., R. D. Baxter, and B. Phillips. 1972. "Dependence of MOS Device Radiation Sensitivity on Oxide Impurities." *IEEE Transactions on Nuclear Science* 19, no. 6, pp. 256–63. doi: http://dx.doi.org/10.1109/tns.1972.4326842

[26] Pivovarov, A.L., F.A. Stevie, and D.P. Griffis. 2004. "Improved Charge Neutralization Method for Depth Profiling of Bulk Insulators Using O_2^+ Primary Beam on a Magnetic Sector SIMS Instrument." *Applied Surface Science* 231–232, pp. 786–90. doi: http://dx.doi.org/10.1016/j.apsusc.2004.03.070

[27] Zhu, Z., C. Gu, F.A. Stevie, and D.P. Griffis. 2007. "Improved Understanding of an Electron Beam Charge Compensation Method for Magnetic Sector Secondary Ion Mass Spectrometer Analysis of Insulators." *Journal of Vacuum Science & Technology A* 25, no. 4, p. 769. doi: http://dx.doi.org/10.1116/1.2746044

[28] Zhu, Z., F.A. Stevie, and D.P. Griffis. 2008. "Model Study of Electron Beam Charge Compensation for Positive Secondary Ion Mass Spectrometry Using a Positive Primary Ion Beam." *Applied Surface Science* 254, no. 9, pp. 2708–11. doi: http://dx.doi.org/10.1016/j.apsusc.2007.10.008

[29] Yamada, K., N. Fujiyama, J. Sameshima, R. Kamoto, and A. Karen. 2003 "SIMS Depth Profile of Copper in Low-k Dielectrics Under Electron Irradiation for Charge Compensation." *Applied Surface Science* 203–204, pp. 512–15. doi: http://dx.doi.org/10.1016/s0169-4332(02)00767-5

[30] McKinley, J.M., F.A. Stevie, and C.N. Granger. 2000. "Analysis of Low-k Dielectrics Using a Magnetic Sector Instrument." In *Secondary Ion Mass Spectrometry, SIMS XII*, eds. A. Benninghoven, P. Bertrand, H-N. Migeon, and H.W. Werner, 607. Amsterdam, Netherlands: Elsevier.

[31] Magee, C.W., and W.L. Harrington. 1978. "Depth Profiling of Sodium in SiO_2 Films by Secondary Ion Mass Spectrometry." *Applied Physics Letters* 33, no. 2, p. 193. doi: http://dx.doi.org/10.1063/1.90271

[32] Nagayama, S., S. Makinouchi, A. Takano, M. Tezuka, K. Takahashi, and M. Kudo. 1990. "Self Charge Compensation During Depth Profiling of Electromigrating Impurities in Insulating Films." In *Secondary Ion Mass Spectrometry, SIMS VII*, eds. A. Benninghoven, C.A. Evans, K.D. McKeegan, H.A. Storms, and H.W. Werner, 655. Chichester, United Kingdom: Wiley.

[33] Pivovarov, A.L., and G.M. Guryanov. 2012. "Optimizing Charge Neutralization for a Magnetic Sector SIMS Instrument in Negative Mode." *Journal of Vacuum Science & Technology A* 30, no. 4, p. 040601. doi: http://dx.doi.org/10.1116/1.4719960

[34] Wilson, R.G., and C.J. Hitzman. 1990. "Charge Compensated Cs SIMS Applied to Semiconductor/Dielectric Hetereostructures." In *Secondary Ion Mass Spectrometry, SIMS VII*, eds. A. Benninghoven, C.A. Evans, K.D. McKeegan, H.A. Storms, and H.W. Werner, 683. Chichester, United Kingdom: Wiley.

[35] Lanzillotto, A-M., and C.W. Magee. 1990. "Electron Stimulated Desorption Effects in Secondary Ion Emission from BF_2^+ Implanted SiO_2." *Journal of Vacuum Science & Technology A* 8, no. 2, p. 983. doi: http://dx.doi.org/10.1116/1.576908

CHAPTER 9

Residual and Rare Gas Elements

9.1 RESIDUAL GAS ELEMENTS, RASTER REDUCTION

The elements hydrogen, carbon, nitrogen, and oxygen are commonly referred to as residual gas elements because they are present as gas species in the vacuum system even after pump down. These elements are of particular interest because they are present in almost every material, and hydrogen is not detected by most common analytical techniques. Analysis of these species requires special attention because their presence in the vacuum system results in redeposition on the region of interest during analysis. Analysis is additionally complicated by the presence of native oxide or surface contamination of these elements.

There are several methods to improve residual gas detection limits. Increased sputtering rate reduces the impact of redeposition. Improvement of vacuum also reduces redeposition. Use of a minor isotope or a molecular species may provide an improvement. Another method that has been successful is raster reduction (raster collapse) [1–3]. Material is first removed with a larger raster, then the raster is reduced but the primary current is kept constant. As diagrammed in Figure 9.1, a 150 µm × 150 µm surface raster is applied at the start of the profile followed by raster collapse to 75 µm × 75 µm at depth A. For a constant current this would result in an increase in the sputtering rate by approximately a factor of four. The matrix species should be monitored and as seen in the figure would show an increase in count rate. If the impurity species shows a similar increase, then the impurity is present at a constant level in the specimen. If the impurity level increases at raster collapse but not by a factor of four, then there is some impurity present but it is near the detection limit. If the

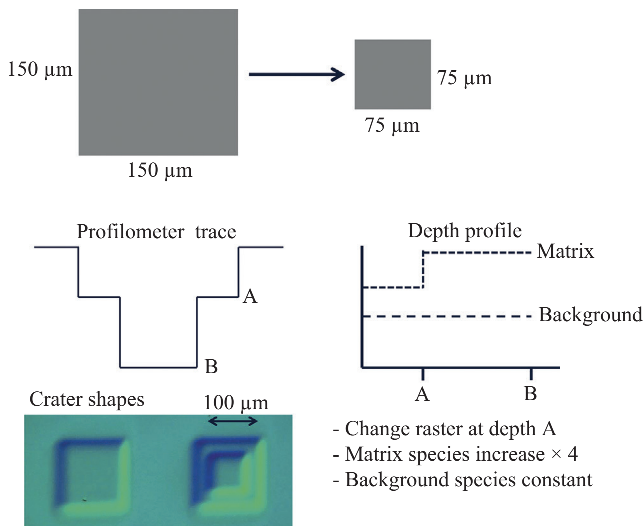

Figure 9.1. Raster reduction to improve detection limit.

impurity level remains constant at raster collapse, then the impurity has not been detected and the detection limit will be a factor of four better than that before raster collapse was employed. The impurity secondary ion intensity from a sample should have a linear relationship with the primary current density. Images of craters after analysis with and without raster reduction are also shown in Figure 9.1. In general, removal of a surface region with high concentration of the species of interest followed by higher sputtering rate in a reduced area should improve the detection limit. This technique can also be used to reduce memory effect on a magnetic sector instrument [4].

9.1.1 HYDROGEN

An early study showed that the detection limit for hydrogen was directly related to the vacuum level in the analysis chamber [5]. The hydrogen detection limit in silicon improved with improved vacuum. Figure 9.2 shows a hydrogen implant in silicon analyzed at different analysis chamber pressures. Lower vacuum leads to reduced redeposition on the sample. The detection limit can be additionally improved with faster sputtering rate. In Figure 9.2, the gradual leading edge and sharp trailing edge are, for a light element such as hydrogen, indicative of backscattering of hydrogen from the silicon sample atoms during implantation. Any difference

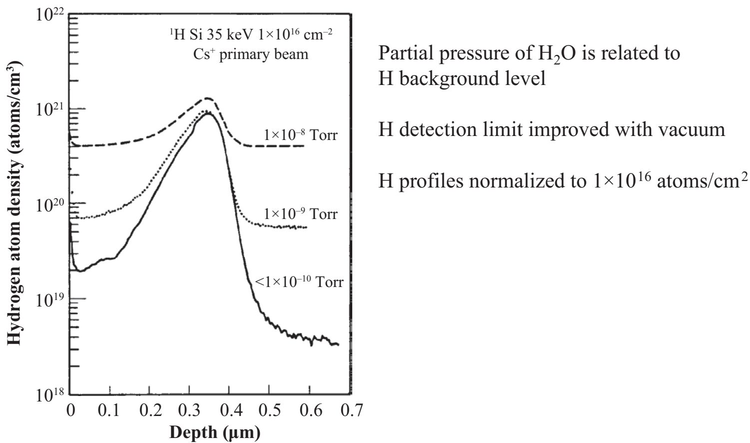

Figure 9.2. H detection limit versus instrument vacuum.
Source: Magee [5], reproduced with permission from American Institute of Physics, copyright 1983, American Vacuum Society.

in response of the mass spectrometer to hydrogen and deuterium (isotope fractionation) can be determined by analysis of a sample implanted with HD^+ [6].

For the analysis of deuterium, a mass resolution of 1220 is required to separate H_2 from ^2H. Analysis with Cs^+ and detection of negative secondary ions has two advantages. The negative secondary ion yield for deuterium is higher than the positive secondary ion yield, and the mass interference from H_2^- is at a low level, which means analysis can be conducted at low mass resolution. For one study with samples that contained a high level of hydrogen, the background due to H_2^- was less than 0.5 percent of the $^2H^-$ signal [7]. Materials can be ion implanted or plasma treated with deuterium to study effects that may be difficult to discern when the high background for hydrogen can be a limiting factor [6, 8].

Hydrogen is known to have a high mobility in metals, and hydrogen embrittlement of steel can cause structural failures. However, the mobility of hydrogen complicates secondary ion mass spectrometry (SIMS) analysis. Hydrogen measurements in metals are often made using bulk analysis or nuclear methods.

It can be important to monitor hydrogen content in an insulator. Hydrogen in a semiconductor SiO_2 layer that is 0.8 μm thick was measured for three different conditions as shown in Figure 9.3. The hydrogen concentration was quantified with the analysis of hydrogen ion implanted in SiO_2. The profiles in Figure 9.3 show a significant decrease for two

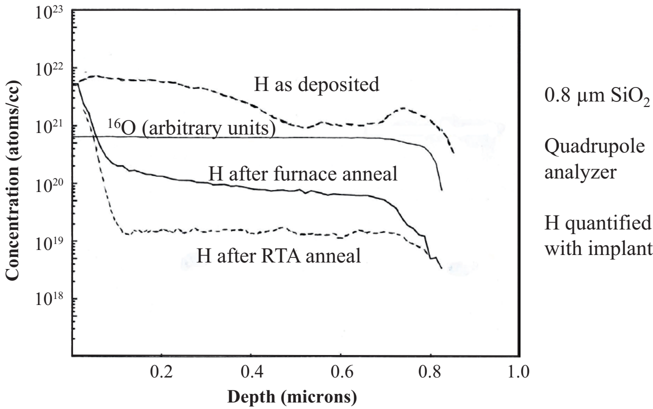

Figure 9.3. Effect of heat treatments on H in SiO_2.
Source: F. Stevie, AT&T Bell Laboratories.

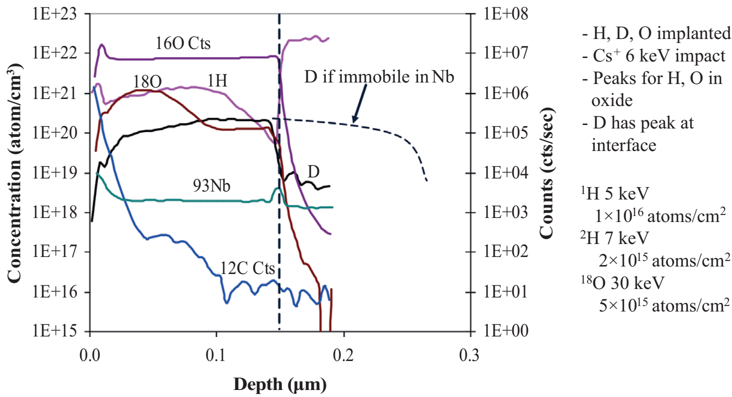

Figure 9.4. H mobility in Nb versus Nb_2O_5.
Source: Maheshwari et al. [9].

types of anneals. Hydrogen mobility in an oxide can be quite different from the mobility in a metal. Niobium is used in high energy accelerator modules since it is the highest temperature superconducting metal and has other properties useful for this application [9]. Significant amounts of hydrogen were observed in the accelerator modules but accurate depth profiles of hydrogen in niobium are compromised by the very high mobility of this element [9]. However, hydrogen and deuterium are not mobile in niobium oxide, Nb_2O_5. Figure 9.4 shows a layer of Nb_2O_5 on a niobium substrate implanted with hydrogen, deuterium, and ^{18}O. The hydrogen and

oxygen implant energies were chosen to place the implant peak in the oxide, and expected implant peaks for both are observed. The implant dose of ^{18}O was sufficient to show a peak above the constant level of ^{18}O in the oxide. The energy of the deuterium implant was chosen to place the peak at the interface between the oxide and the substrate. The deuterium profile shows half of the implant shape in the oxide and then a sharp decrease at the interface. The matrix signal $^{93}Nb^-$ does not show a significant change from oxide to substrate so the decrease is not a secondary ion yield effect. The absence of a profile shape for deuterium in the substrate is due to the high mobility. The implanted deuterium atoms have moved from the original implant location.

9.1.2 CARBON

Carbon is another element of high interest. Many materials are carbon based and carbon contamination can affect material properties, especially at interfaces. A complicating factor is that carbon is almost universally found on the surface of a sample. Analysis of background contributions shows that memory effect and the type of residual gas species present are significant contributors to background [10].

A combination of two methods, molecular species and minor isotope, can provide significant improvement in detection limit. Figure 9.5 shows a very low detection limit of 2×10^{14} atoms/cm^3 for carbon in GaAs [11]. In this case a minor isotope, ^{13}C, is analyzed as part of a molecular ion,

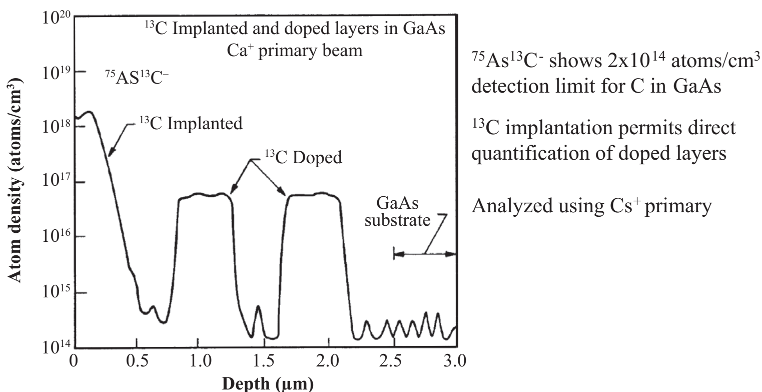

Figure 9.5. C in GaAs.
Source: Lum et al. [11], reprinted from J. Crystal Growth, copyright 1988, with permission from Elsevier.

$^{13}C^{75}As^-$ [11, 12]. Use of a molecular species shows a different profile near the surface than ^{12}C and is less dependent on surface contamination. Use of the ^{13}C ion implant in the top layer allows direct quantification of carbon in the layers below.

9.1.3 NITROGEN

Analysis of nitrogen presents a special problem as the secondary ion yield for N^+ is low and the secondary ion yield for N^- is essentially zero. As a result nitrogen is usually analyzed by means of a molecular species. For silicon samples, the species SiN^- and Si_2N^- have high secondary ion yields. For a substrate that contains carbon, the molecular ion CN^- can have a very high intensity. For ZnSe and ZnTe, good detection limits can be obtained by monitoring SeN^- and TeN^-, respectively, with a Cs^+ primary beam [13].

The raster reduction method has been applied to obtain detection limits below 1×10^{16} atoms/cm^3 for N in epitaxial SiC [3]. In Figure 9.6 the dependence of the secondary ion intensity of $(^{12}C^{15}N + {}^{13}C^{14}N)^-$, $^{12}C^{11}B^-$, and $^{12}C^{13}C^-$ as a function of the sputtering time is presented. Raster reduction with fixed primary current results in equal increase of the molecular species used to monitor the matrix (C_2^-) and boron concentration (CB^-) but no increase in the species used to monitor N (CN^-). This indicates that the boron signal must result from boron in the bulk of the sample and the nitrogen is due to redeposition from the vacuum system. The result is an improvement in the nitrogen detection limit.

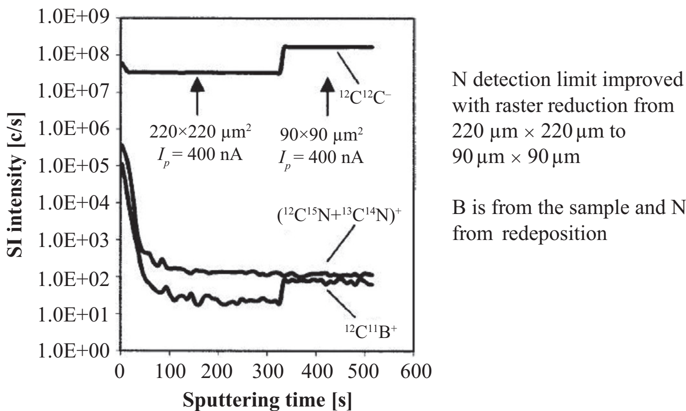

Figure 9.6. Raster reduction to improve detection limit for N in SiC. *Source*: Pivovarov et al. [3], reproduced with permission from American Institute of Physics, copyright 2003, American Vacuum Society.

Measurement of nitrogen in semiconductor SiON gate oxides has been of significant interest. Analyses have been achieved with oxygen [14] and cesium beams [15]. Nitrogen in oxide layers has also shown anomalous diffusion during analysis [16]. This effect is important for studies of nitride gate oxides used in semiconductor technology. Analysis using a Cs^+ primary beam with detection of molecular positive secondary ions and back side analysis (see Chapter 7) have been helpful to show the diffusion and resolve the uncertainty in the analysis.

9.1.4 OXYGEN

This is an important element to analyze yet a good detection limit can be difficult to achieve. Memory effect due to redeposition and adsorption of oxygen from the residual vacuum are significant contributors to the oxygen background. Many analyses are made at a very high sputtering rate with small detected area to achieve the detection limit desired. Heating the sample holder can also be beneficial [17]. Since $^{16}O_2^+$ is often used as the primary beam, the background for this isotope may be high. Implantation of a minor isotope, ^{18}O, can be of use. Figure 9.7 shows profiles of ^{16}O and ^{18}O and a much improved detection limit with ^{18}O [18]. However,

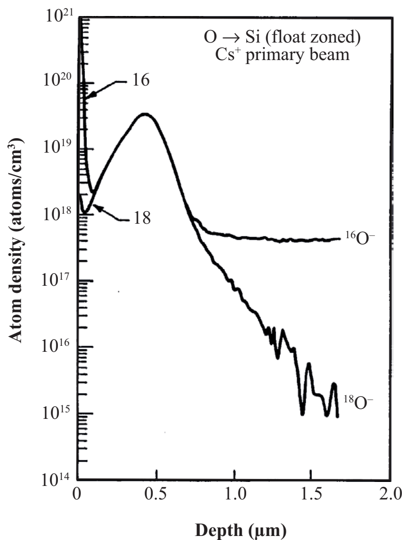

Improved detection limit for O in float zoned Si using ^{18}O as the implanted species

Figure 9.7. Use of rare isotope.
Source: Wilson, Stevie, and Magee [18].

the abundance is 99.762 percent for ^{16}O and 0.200 percent for ^{18}O, which is a difference of a factor of approximately 500. This means a detection limit improvement greater than 500 for ^{18}O is needed to improve the actual elemental oxygen detection limit.

It is not uncommon to desire a low detection limit for oxygen in a layer under an oxide. In this case it can be very useful to chemically etch away the oxide, presputter the surface, or use raster reduction to remove the oxide.

9.1.5 MULTIPLE ELEMENT PROFILES

Since the residual gas species are typically best analyzed using a Cs^+ primary beam, multiple elements are commonly analyzed in one profile. Multiple element standards are also very useful and it is possible to combine hydrogen, carbon, nitrogen, and oxygen in one standard. Since residual gas elements often have to be detected above significant contaminant levels, the implanted doses often exceed 1×10^{15} atoms/cm^2 for each element. As a result it is necessary to be aware that if the total dose is too high the dilute limit of a few percent atomic may be exceeded. Figure 9.8 shows a profile of hydrogen, carbon, and oxygen in GaN where the total implanted dose is less than 1 percent atomic.

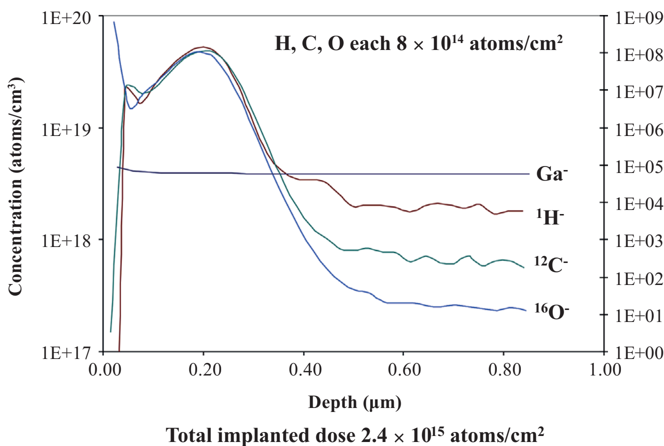

Figure 9.8. Multiple residual gas element implants into GaN. *Source*: F. Stevie, Analytical Instrumentation Facility, North Carolina State University.

9.1.6 SURFACE CONTAMINATION

Samples typically have residual gas elements on the surface, which can be pushed in (knock-on effect) by energetic bombardment. Reducing the bombardment energy provides better depth resolution and reduces the effect of contamination at the surface. Figure 9.9 shows carbon, nitrogen, and oxygen implanted in niobium to permit quantification of all three elements. Because of contamination at the surface, analysis with high energy, 14.5 keV, Cs^+ shows that some of the carbon, nitrogen, and oxygen at the surface have been pushed deeper into the material during analysis and the near-surface region is not well characterized. Reduction of the Cs^+ impact energy to 6 keV shows a more rapid decrease of the surface contamination and better resolution of these elements in the near-surface region. However, note that the secondary ion count levels were not as high with the lower energy bombardment.

Figure 9.10 shows more significant surface contamination in the analysis of carbon and oxygen in a polysilicon layer on a silicon substrate structure [19]. The interface between the layer and the substrate is of interest. In the depth profile on the contaminated surface, some significant

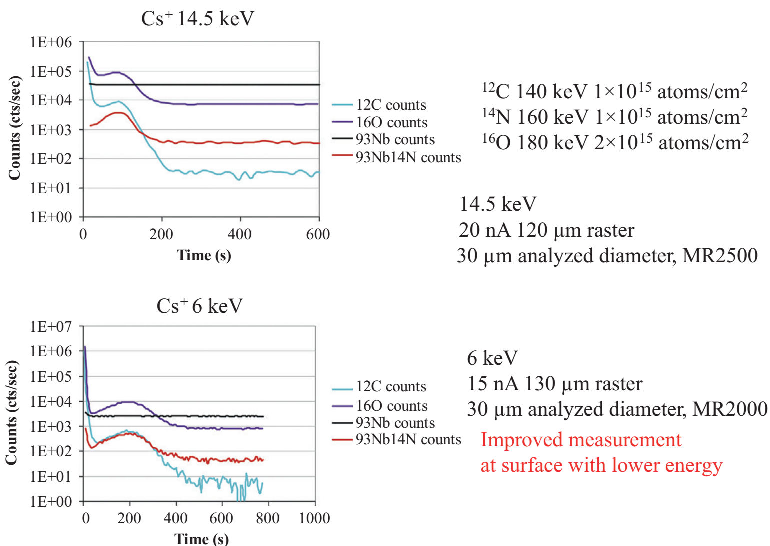

Figure 9.9. Depth resolution. Cs^+ bombardment of Nb.
Source: P. Maheshwari, Analytical Instrumentation Facility, North Carolina State University.

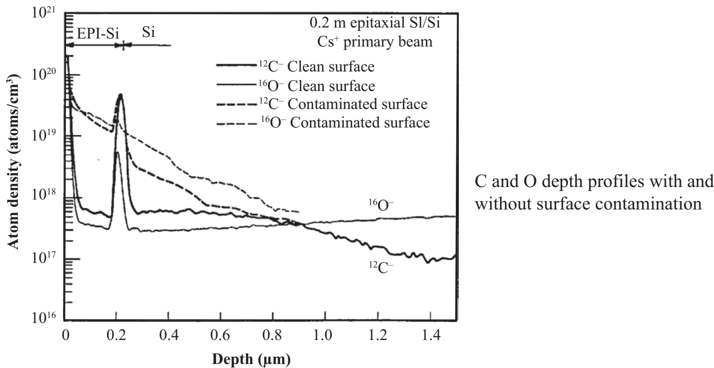

Figure 9.10. Effect of contamination at the surface.
Source: Wilson, Stevie, and Magee [19].

sputtering is needed to remove the contamination, and the carbon and oxygen profiles show tails through the polysilicon layer. The result is poor depth resolution and a lack of clarity at the interface. When the sample is analyzed in a relatively clean region, the carbon and oxygen drop off rapidly at the surface and the interface can be properly analyzed.

9.2 RARE GAS ELEMENTS

Rare gas elements helium, neon, argon, krypton, and xenon are a special case for SIMS as detection sensitivity using O_2^+ is very low. High dose ion implant standards and high sputtering rate analysis have made it possible to obtain depth profiles of elements such as helium in silicon shown in Figure 9.11 [20]. Discovery of improved yields with Cs^+ bombardment and detection of cesium molecular positive ions provides a different approach [21, 22]. Analysis of helium using $CsHe^+$ molecular ions is able to overcome the very high first ionization potential of helium, and a detection limit of 5×10^{18} atoms/cm^3 or 60 ppma could be achieved [22]. This level is sufficient to monitor helium diffusion in materials such as that used in nuclear technology.

Argon is important because it is an element with a significant concentration in air (0.9 percent by volume) and is used in many processing applications, such as for sputtering. If present at an interface, it can cause delamination. Argon entrapped in the near surface during sputtering can move to the surface after anneal and cause separation of an overlayer. This element is difficult to analyze because it has the same nominal mass as calcium, and high mass resolution will not resolve the two elements

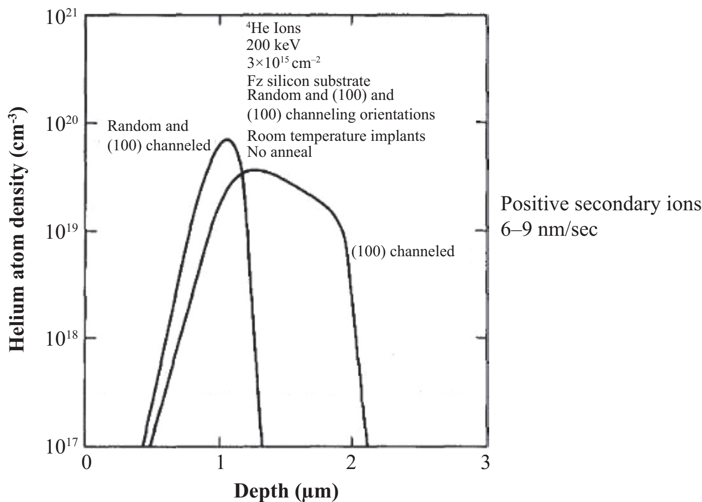

Figure 9.11. He in Si using O_2^+ primary beam.
Source: Wilson [20], reprinted with permission from Journal of Applied Physics, copyright 1987, AIP Publishing LLC.

because the mass resolution needed is 193,000. It may be helpful to first analyze for mass 40 with an O_2^+ primary beam and detection of secondary positive ions. If a high count rate is detected then the species is probably calcium. Use of other techniques such as x-ray photoelectron spectroscopy and Rutherford backscattering spectrometry can be very useful.

Xenon is only found in trace amounts in air, but even though much more expensive than argon, it is also used for sputtering.

REFERENCES

[1] Okuno, K., A. Karen, S. Karen, F. Soeda, and A. Ishitani. 1990. "Improvement of Detection Limits of C, O, N in GaP by the Background Subtraction Method." In *Secondary Ion Mass Spectrometry, SIMS VII*, eds. A. Benninghoven, C.A. Evans, H.A. Storms, and H.W. Werner, 515. Chichester, United Kingdom: Wiley.

[2] Wilson, R.G., F.A. Stevie, and C.W. Magee. 1989. *Secondary Ion Mass Spectrometry*, 2.8–1. New York: Wiley.

[3] Pivovarov, A.L., F.A. Stevie, D.P. Griffis, and G.M. Guryanov. 2003. "Optimization of Secondary Ion Mass Spectrometry Detection Limit for N in SiC." *Journal of Vacuum Science & Technology A* 21, no. 5, p. 1649. doi: http://dx.doi.org/10.1116/1.1595108

[4] Le Goux, J.J., and H.N. Migeon. 1982. "Principles and Applications of a Dual Beam Primary Ion Source and Mass Filter for an Ion Microanalyzer." In *Secondary Ion Mass Spectrometry: SIMS III, Springer Series in Chemical Physics 19*, eds. A. Benninghoven, J. Lazlo, M. Riedel, and H.W. Werner, 52. Berlin, Germany: Springer.

[5] Magee, C.W. 1983. "Analysis of Hydrogen and Deuterium by Secondary Ion Mass Spectrometry as Applied to Fusion Technology." *Journal of Vacuum Science &* Technology *A* 1, no. 2, p. 901. doi: http://dx.doi.org/10.1116/1.572147

[6] Zinner, E., K.D. McKeegan, and R.M. Walker. 1983. "Laboratory Measurements of D/H Ratios in Interplanetary Dust." *Nature* 305, no. 5930, pp. 119–21. doi: http://dx.doi.org/10.1038/305119a0

[7] Williams, P., K.M. Stika, J.A. Davies, and T.E. Jackman. 1983. "Quantitative SIMS Analysis of Hydrogenated Amorphous Silicon Using Superimposed Deuterium Implant Standards." *Nuclear Instruments and Methods in Physics Research* 218, no. 1, pp. 299–302. doi: http://dx.doi.org/10.1016/0167-5087(83)90994-8

[8] Wilson, R.G., S.J. Pearton, C.R. Abernathy, and J.M. Zavada. 1995. "Diffusion of Deuterium from GaN, AlN, InN." *Journal of Vacuum Science & Technology A* 13, no. 3, p. 719. doi: http://dx.doi.org/10.1116/1.579814

[9] Maheshwari, P., F.A. Stevie, G. Myneni, G. Ciovati, J.M. Rigsbee, and D.P. Griffis. 2011. "Analysis of Interstitial Elements in Niobium with Secondary Ion Mass Spectrometry (SIMS)." In *Symposium on the Superconducting Science and Technology of Ingot Niobium, AIF Conference Proceedings*, eds. G.R. Mynenei, G. Ciovati, and M. Stuart, 1352, 151.

[10] Kobayashi, J., M. Nakajima, and K. Ishida. 1989. "Study of the Background Sources in the Trace Analysis of Carbon Using Secondary Ion Mass Spectrometry." *Journal of Vacuum Science & Technology A* 7, no. 4, p. 2542. doi: http://dx.doi.org/10.1116/1.575794

[11] Lum, R.M., J.K. Klingert, D.W. Kisker, S.M. Abys, and F.A. Stevie. 1988. "^{13}C Isotopic Labeling Studies of Growth Mechanisms in the Metalorganic Vapor Phase Epitaxy of GaAs." *Journal of Crystal Growth* 93, no. 1–4, pp. 120–26. doi: http://dx.doi.org/10.1016/0022-0248(88)90516-7

[12] Scilla, G.J., T. Kuech, and F. Cardone. 1988. "Improved Detection Limit of Carbon in GaAs by Secondary Ion Mass Spectroscopy: The Influence of Hydrocarbons in Metalorganic Vapor Phase Epitaxy." *Applied Physics Letters* 52, no. 20, p. 1704. doi: http://dx.doi.org/10.1063/1.99023

[13] Miwa, S., K. Kimura, T. Yasuda, I. Nomachi, H. Kobayashi, and T. Yao. 1997. "Nitrogen Detection in ZnSe and ZnTe." In *Secondary Ion Mass Spectrometry, SIMS X*, eds. A. Benninghoven, B. Hagenhoff, and H.W. Werner, 533. Chichester, United Kingdom: Wiley.

[14] Jiang, Z.X., K. Kim, D.D. Sieloff, T.Y. Luo, A. Varghese, D.H. Triyoso, T. Guenther, B. Robichaud, and J. Benavides. 2008. "Toward Accurate Characterization of Nitrogen Depth Profiles in Ultrathin Oxynitride Films." *Surface and Interface Analysis* 40, no. 10, pp. 1397–401. doi: http://dx.doi.org/10.1002/sia.2914

[15] Reich, D.F., B.W. Schueler, and J. Bennett. 2000. "Characterization of Ultra-thin Oxide and Oxynitride Films." In *Secondary Ion Mass Spectrometry, SIMS XII*, eds. by A. Benninghoven, P. Bertrand, H.–N. Migeon, and H.W. Werner, 557. Amsterdam, Netherlands: Elsevier.

[16] Bannerjee, I., and D. Kuzminov. 1993. "Anomalous Diffusion of Nitrogen in SiO_2 Under Ion Bombardment." *Applied Physics Letters* 62, no. 13, p. 1541. doi: http://dx.doi.org/10.1063/1.108634

[17] Meuris, M., W. Vandervorst, and G. Borghs. 1989. "Improved Quantification and Detection Limits for Oxygen Analysis in $Al_xGa_{1-x}As$/GaAs Multilayers with Secondary Ion Mass Spectroscopy." *Journal of Vacuum Science & Technology A* 7, no. 3, p. 1663. doi: http://dx.doi.org/10.1116/1.576067

[18] Wilson, R.G., F.A. Stevie, and C.W. Magee. 1989. *Secondary Ion Mass Spectrometry*, 1.6–11. New York: Wiley.

[19] Wilson, R.G., F.A. Stevie, and C.W. Magee. 1989. *Secondary Ion Mass Spectrometry*, 4.4–7. New York: Wiley.

[20] Wilson, R.G. 1987. "Range and Depth Distribution of 200-keV He Ions Channeled in Si, Ge, and GaAs Crystals." *Journal of Applied Physics* 61, no. 7, p. 2489. doi: http://dx.doi.org/10.1063/1.337921

[21] Ray, M.A., J.E. Baker, C.M. Loxton, and J.E. Greene. 1988. "Quantitative Analysis and Depth Profiling of Rare Gases in Solids by Secondary Ion Mass Spectrometry: Detection of $(CsR)^+$ Molecular Ions (R = rare gas)." *Journal of Vacuum Science & Technology A* 6, no. 1, p. 44. doi: http://dx.doi.org/10.1116/1.574966

[22] Lefaix-Jeuland, H., S. Moll, F. Legendre, and F. Jomard. 2013. "SIMS Depth Profiling of Implanted Helium in Pure Iron Using $CsHe^+$ Detection Mode." *Nuclear Instruments and Methods in Physics Research B* 295, pp. 69–71. doi: http://dx.doi.org/10.1016/j.nimb.2012.11.003

CHAPTER 10

APPLICATIONS

Secondary ion mass spectrometry (SIMS) has been utilized to characterize a very wide range of materials. Many examples have already been shown in the preceding chapters to demonstrate specific aspects of the technique. The purpose of this section is to provide some indication of the range of applications for this technique.

10.1 SEMICONDUCTORS

10.1.1 SILICON

The semiconductor industry has been a major driver for the development of SIMS instrumentation and analysis. Depth profiling in particular has been extensively used. SIMS has provided support to research, development, and production for almost every part of the semiconductor manufacturing process. Table 10.1 contains a listing of typical silicon semiconductor process steps and the use of SIMS to characterize them. Examples will be presented for a number of these steps to show the versatility of the SIMS technique.

Some useful parameters for characterization of Si:

Si density = 5×10^{22} atoms/cm^3
Areal density for 1 monolayer = 1×10^{15}atoms/cm^2
Atoms in 1 μm^3 = 4.9×10^{10}

Figure 10.1 shows a complementary metal oxide semiconductor (CMOS) structure for 0.35 μm technology. This technology is dated but the figure demonstrates the basics of semiconductor fabrication. Metal

Table 10.1. Si semiconductor processing steps and related SIMS analyses

Crystal growth—O, C contaminants
Epitaxy—B, P, As dopants, O, C contaminants, layer thickness
Surface cleans—contaminants
Oxidation—Li, Na, K, Cl, N
Inter Level Dielectric deposition—e.g.,Tetraethylorthosilicate (TEOS) H, Li, Na, K, C
Polycrystalline silicon deposition—O, C contaminants, dopant concentration
Ion implantation—B, P, As, In dopants F, Al, Cr, Fe, Cu contaminants
Diffusion—B, P, As
Lithography—B, P, As penetration, Na contaminant
Dry etch—O, C, F, Cl, Al, Cr, Fe, Cu
Metallization—Al, Si, Cu, Ti, W, N, O, C
Process simulation—B, P, As
Process integration and failure analysis—analysis using SIMS patterns
Packaging—Au, Ni, Cu, Tl

oxide semiconductor (MOS) transistors operate by applying a voltage to the source and drain regions, which are doped either n or p type, and then controlling the conduction between the source and the drain by applying a voltage to the gate. The gate is insulated from the substrate with a thin oxide. TiN is used as a barrier layer for the aluminum metallization. To match the increased complexity of current technology, change the metal to copper, add several more layers of metal, and reduce feature size to less than 50 nm.

10.1.1.1 Contaminants in Substrate

The purity of the substrate is very important, and elements such as iron, nickel, copper, sodium, lithium, and potassium should be at very low levels. SIMS detection limits for these elements can be in the parts per billion atomic (ppba) range [1]. Oxygen is also intentionally added to silicon at approximately 1×10^{18} atoms/cm^3. SIMS can measure the oxygen concentration and determine any oxygen out-diffusion from the surface of the wafer.

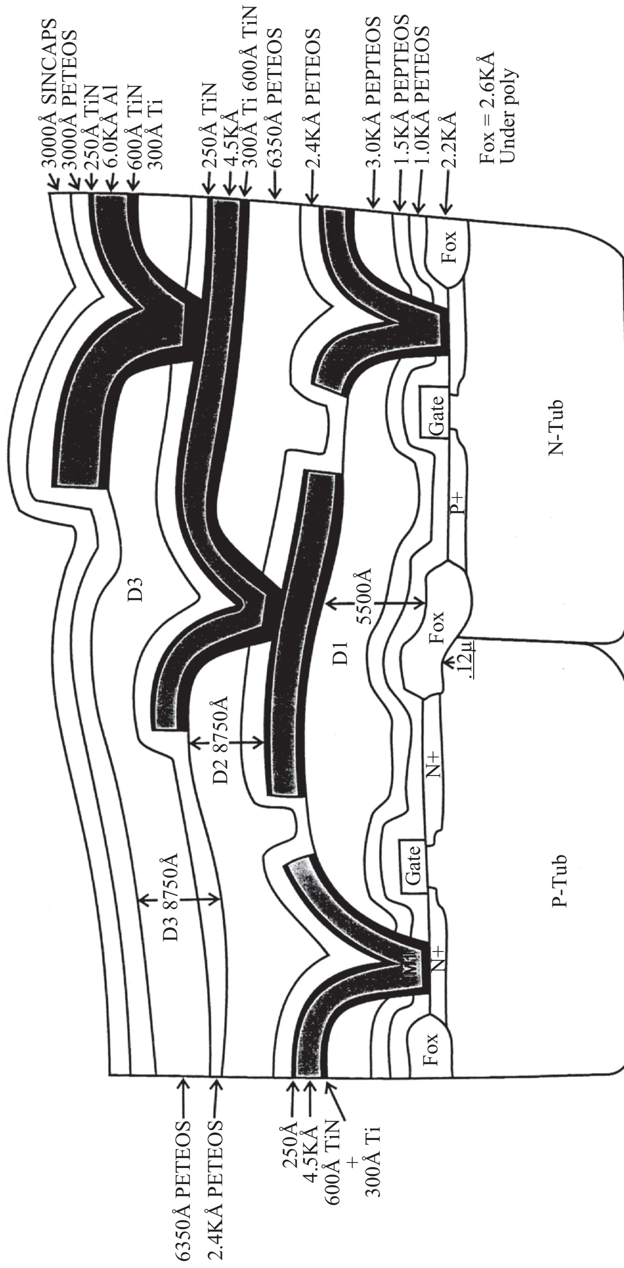

Figure 10.1. 0.35 µm technology CMOS.
Source: AT&T Bell Laboratories.

10.1.1.2 Epitaxial Layer

The deposition of an epitaxial layer can be very difficult to characterize. The interface between the layer and the substrate can be undetectable even using transmission electron microscopy (TEM). Figure 10.2 shows a SIMS depth profile of an undoped epitaxial layer of silicon on a boron doped silicon substrate. Not only can the thickness of the layer be clearly determined, but the dopant concentration can also be measured. The 7×10^{18} atoms/cm^3 (140 ppm atomic) boron concentration is below the detection limit for energy dispersive spectroscopy, Auger electron spectroscopy, and x-ray photoelectron spectroscopy techniques. It should be noted that this analysis was made with a CAMECA magnetic sector instrument using a Cs^+ primary beam because of surface roughening that occurs about 2 to 3 μm deep in silicon when O_2^+ is used [2].

10.1.1.3 Ion Implantation

SIMS and ion implantation are very closely related. The SIMS instrument is an ion implanter with a secondary ion analyzer. SIMS has been used extensively to monitor the amount and distribution of dopant present after ion implantation and subsequent heat treatments [3]. Figure 10.3 shows an example of dopant profiles for arsenic and boron in a bipolar transistor [3]. With careful work, the areal density of a dopant can be obtained within less than 1 percent atomic concentration based on National Institute for

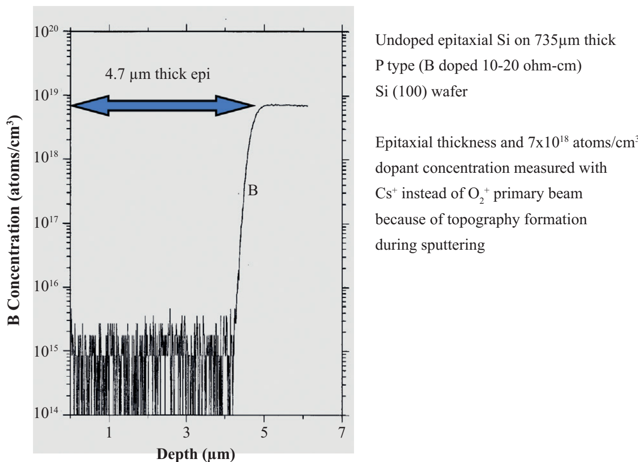

Figure 10.2. SIMS depth profile analysis of epitaxial Si layer.
Source: F. Stevie, AT&T Bell Laboratories.

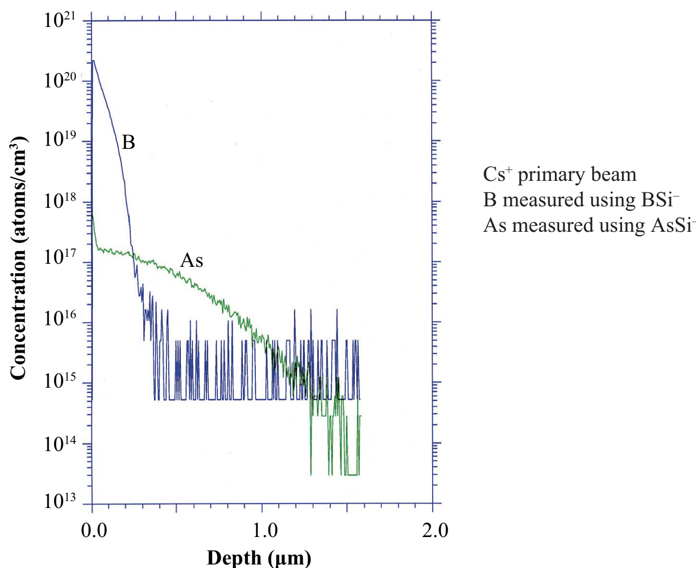

Figure 10.3. Dopant profiles.
Source: F. Stevie, AT&T Bell Laboratories.

Standards and Technology standards [4]. This accuracy has been achieved using quadrupole, magnetic sector, and time of flight instruments.

It is also important to detect cross-contamination [5]. Ion implanters are very expensive and are often used to implant both n and p type dopants. If an implanter has just been used to implant boron and is then used to implant arsenic, it is possible to have some boron implanted with the arsenic implant. This is a concern because boron is a faster diffuser than arsenic. Phosphorus will also diffuse faster than arsenic. The presence of phosphorus, arsenic, or antimony at 1 percent of the boron dose can cause as much as a 5 percent shift in sheet resistance. Another issue is implantation of metallic contamination. Iron, copper, sodium, aluminum, molybdenum, and tungsten are among the elements checked frequently. Fast diffusers such as iron and copper are always a concern because they can collect in active transistor sites and affect performance.

10.1.1.4 Gate Oxide

The gate oxide between the gate conductor and the silicon substrate is an especially sensitive area of a CMOS transistor. The drive to smaller technologies has resulted in the development of oxides that are not just

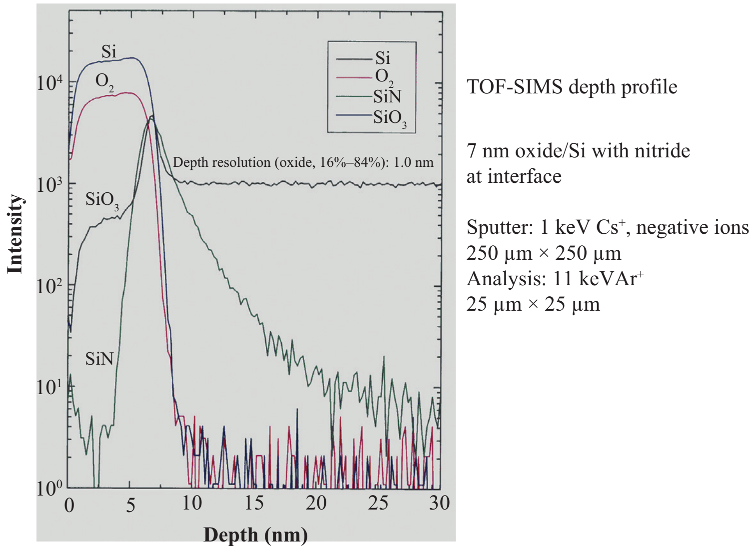

Figure 10.4. Nitrided gate oxide.
Source: ION-TOF TOF-SIMS IV reproduced with permission.

SiO_2. Figure 10.4 shows a SIMS depth profile of a nitrided gate oxide. The addition of nitrogen changes the dielectric constant, k, so that the insulator can be physically thicker and simpler to manufacture but will have the dielectric equivalent of a thinner oxide. High k dielectric materials have been extensively studied for this purpose. The gate oxide is also very susceptible to alkali element contamination since a small amount can affect the insulating property of the layer. Figure 10.5 shows a depth profile of K in SiO_2 and a detection limit of 7×10^{13} atoms/cm^3 or 1.4 ppb atomic concentration.

10.1.1.5 Barrier Layers

The use of barrier materials to prevent a high diffuser from moving to other areas of the device is especially important because copper is now used as a metallization material for conductors. One approach to check the viability of a barrier layer is to ion implant the diffuser into a layer of the barrier material and to monitor the diffusion after a series of heat treatments. Figure 10.6 shows the SIMS depth profiles of copper ion implanted into a 0.5 µm thick layer of low pressure chemical vapor deposition

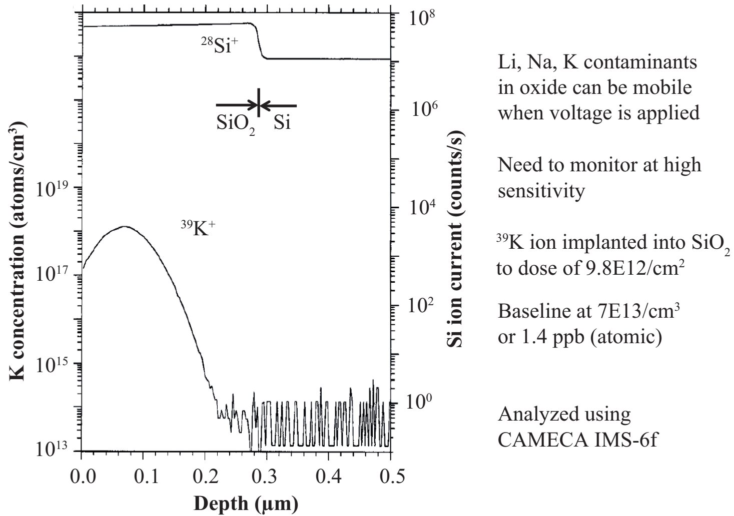

Figure 10.5. K in gate oxide.
Source: F.A. Stevie and J.M. McKinley, Agere Systems.

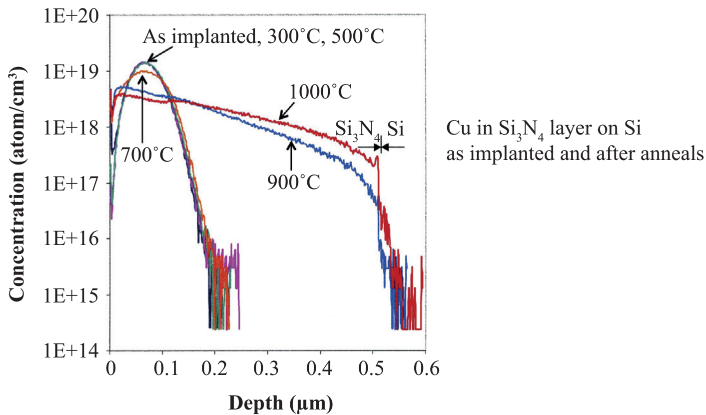

Figure 10.6. Diffusion in barrier layers.
Source: Harris et al. [6], reprinted with permission from Cambridge University Press.

(LPCVD) Si_3N_4 [6]. No significant copper diffusion was noted after 300°C and 500°C anneals. Some diffusion was observed after a 700°C anneal, and diffusion through the entire layer was noted after 900°C and 1000°C heat treatments.

10.1.1.6 Photoresist

Even though the photoresist is removed from the structure, it is important to know the penetration of the implanted dopants into the photoresist and whether the dopants show movement during processing before photoresist removal. The goal is to minimize photoresist thickness but avoid penetration by ion implantation. This has been investigated using SIMS [7, 8]. Analyses were made with gold (100 nm) or carbon (35 nm) coating to minimize sample charging. The carbon coated samples showed less surface roughening and carbon coating was primarily used.

10.1.1.7 Insulators for Metal Layers

The multiple levels of metal are separated with insulating layers. The addition of certain elements, such as boron and phosphorus, was found to change the properties of silicon oxide so as to promote flow at a lower anneal temperature. The flow process would make the surface of the structure more uniform. This borophosphosilicate glass (BPSG) could be characterized using SIMS. Depth profiles of a BPSG layer with three composite layers that have different concentrations of boron and phosphorus were verified with the use of Rutherford backscattering spectrometry [9]. Figure 10.7 shows that SIMS could determine the penetration depth of additional phosphorus obtained from PBr_3 treatment so that the top portion of the layer would flow faster than the remainder of the film [10].

10.1.1.8 Small Areas

The actual semiconductor device structures are too small to analyze directly using SIMS and obtain ppm sensitivity (see Chapter 5). Current development is for 14 nm technology. However, the ability to obtain analyses from as small a region as possible is desired. Focused ion beam columns have lateral resolution of less than 10 nm and can be attached to SIMS instruments but the liquid metal ion sources used are typically gallium. The secondary ion yields for Ga^+ bombardment are low compared with those of O_2^+ and Cs^+ bombardment but can be enhanced with the use of an oxygen flood or a low energy oxygen ion beam [11]. The introduction of plasma ion sources offers new possibilities for reduction of the analysis area. Secondary ion profiles for implanted alkali elements with a xenon plasma source are shown in Figure 10.8 [12].

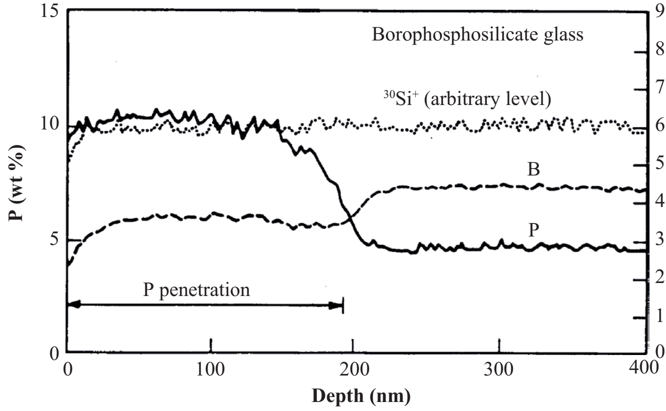

Figure 10.7. Borophosphosilicate glass.
Source: Rana et al. [10], reproduced with permission from the Electrochemical Society.

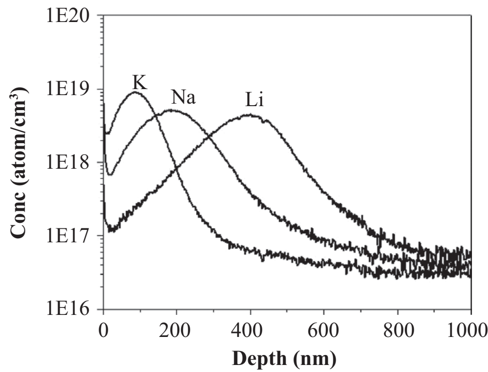

Figure 10.8. Focused ion beam SIMS of Na Li K using Xe plasma source.
Source: Stevie et al. [12], reprinted with permission from John Wiley and Sons.

10.1.1.9 Entire Structure

Despite the complications of analysis of a multilayer structure comprised of semiconductors, metals, and insulators, it is possible to simultaneously employ the methods of sample rotation and charge neutralization in a

depth profile. The sample rotation reduces the topography formation due to the sputtering of a polycrystalline material and the charge neutralization is necessary to prevent sample charging for analysis of SiO_2 and Si_3N_4. Figure 10.9 shows a depth profile through a three-level metal structure from surface passivation Si_3N_4 layer to gate oxide [13]. It was possible to locate etch back points for the oxide layers by monitoring boron contamination as shown by the locations marked E. The data were obtained using a PHI-6300 quadrupole instrument, which has limited mass resolution. There is a mass interference with ^{30}Si due to $^{46}Ti^{14}N^{++}$, which affects the ^{30}Si profile where noted.

10.1.1.10 Packaging

Once the semiconductor chip has been manufactured and tested, it is devastating to then lose the chip due to packaging issues. The device may be covered with a polymer [14]. However, the presence of halide elements such as F at a polymer interface can cause delamination of the polyimide. Figure 10.10 shows a SIMS depth profile obtained with a CAMECA magnetic sector (both IMS-3F and 5F were used in the study). The primary beam was O_2^+ at a mass resolution of 2500 on a gold coated sample with sputtering rates of 2 to 5 nm/s. Layers up to 40 μm thick were analyzed and it was shown that the delamination observed at 13 μm depth was due to the presence of fluorine contamination.

The hardness of gold plating used in the package can be affected by impurities. Figure 10.11 shows depth profiles for gold plating, which was deposited over a nickel layer and the diffusion of nickel into the gold layer resulted in poor bonding [15]. The good bonding sample showed a much lower concentration of nickel in the gold. Certain elements, such as thallium, can affect gold hardness at ppm levels and may be intentionally added to the gold to obtain the hardness desired. Figure 10.12 shows the SIMS analysis of gold implanted with thallium, which permitted thallium quantification [15].

10.1.1.11 Soft Memory Errors

Soft or random errors in dynamic random access memory can occur because the amount of stored charge for one bit of memory has decreased with feature size to the point where external radiation can change the

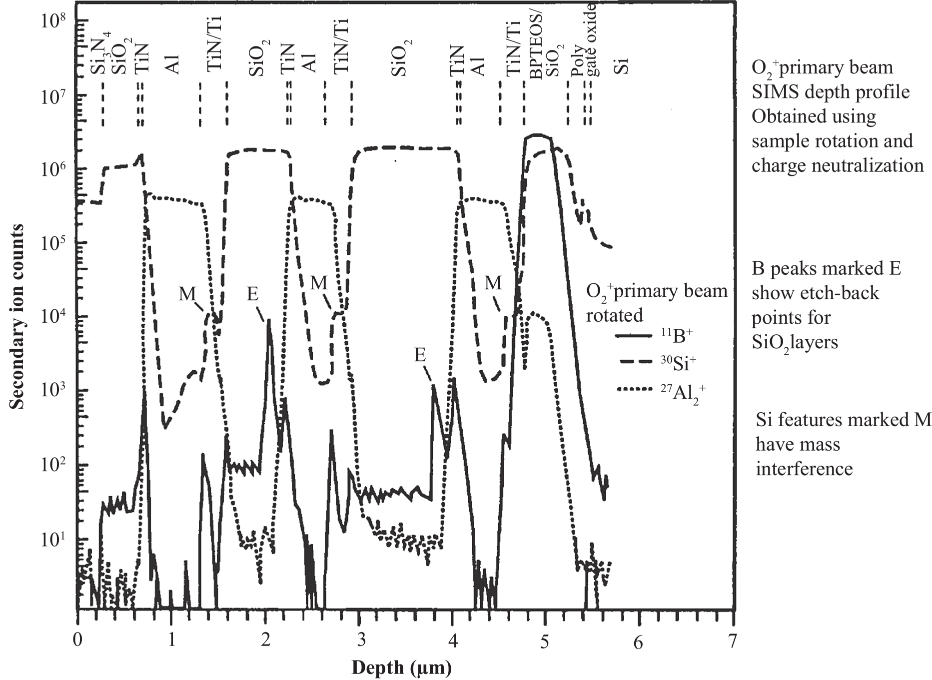

Figure 10.9. SIMS analysis of three-level metal structure.
Source: Stevie et al. [13], reproduced with permission from American Institute of Physics, copyright 1994, American Vacuum Society.

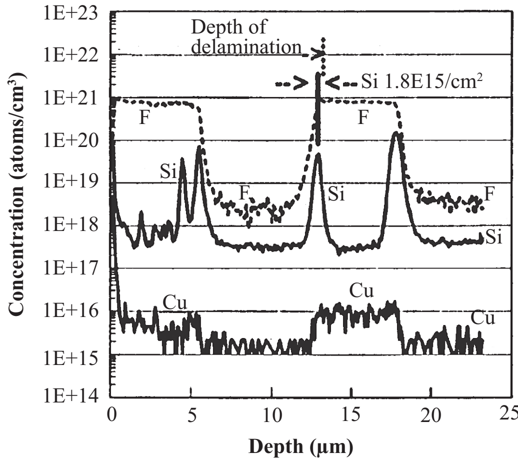

SIMS depth profile of polymer stack of alternating F containing and standard polyimide. Adjacent to analysis area was region where top 13μm of polyimide had delaminated.

Figure 10.10. Fluorine contamination in polymer layers.
Source: Parks [14], reproduced with permission from American Institute of Physics, copyright 1997, American Vacuum Society.

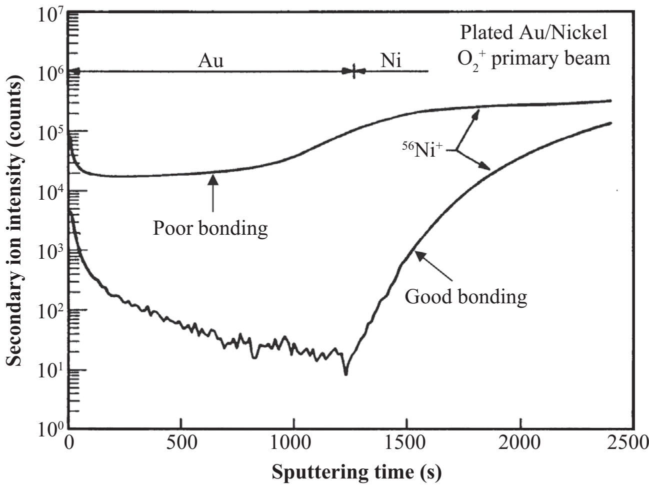

Poor bonding shows Ni diffusion through Au layer

Figure 10.11. Au plating: Ni diffusion.
Source: Wilson, Stevie, and Magee [15].

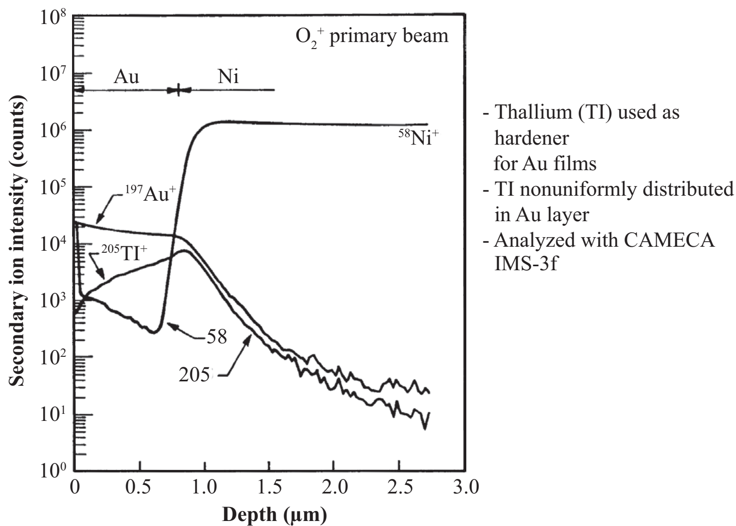

Figure 10.12. Au plating: Thallium concentration.
Source: Wilson, Stevie, and Magee [15].

memory state. External radiation can be from packaging material or from some of the materials, such as silicides, used in semiconductor manufacturing. Alpha particles typically have about 5 MeV energy and can penetrate about 30 µm. Packaging material can be screened to remove the uranium and thorium radiation sources or a coating of 70 µm of polyimide can be added to the die as a protective cover. However, some materials used in semiconductor fabrication were found to have trace amounts of uranium or thorium. SIMS has been used to check for this contamination, and uranium and thorium ion implants at low dose levels have been obtained to quantify the results. From the secondary ion yield plots shown in Chapter 3 the bombardment choice should be O_2^+ and detection of positive secondary ions. Figure 10.13 shows the analysis of thorium implanted in silicon with a detection limit of 1×10^{15} atoms/cm^3 and also shows the effect of a high temperature anneal on the thorium distribution. Thorium shows movement to the surface and a peak at the interface between amorphous and damaged silicon (about 0.18 µm deep). Results for uranium were similar and a detection limit of approximately 5×10^{14} atoms/cm^3 was obtained. The uranium and thorium results show the utility of the high sensitivity of the SIMS technique.

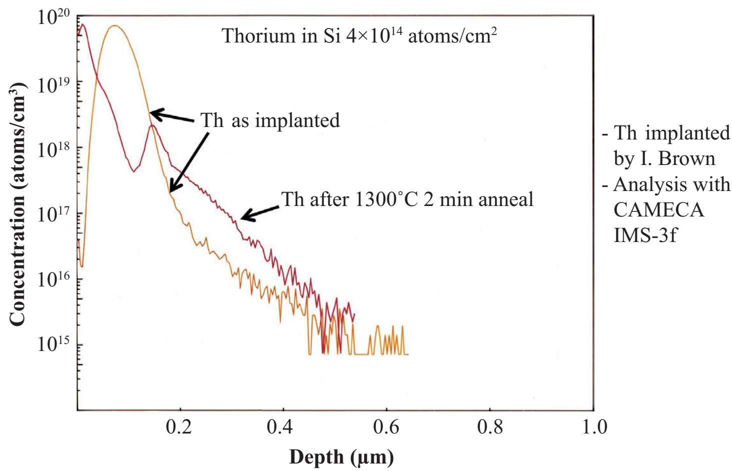

Figure 10.13. Diffusion of Th in Si.
Source: F. Stevie, AT&T Bell Laboratories.

10.1.1.12 Current Technologies

The latest silicon technology, FinFet, uses structures where the features can be described as fins protruding from a central feature. For some time, semiconductor structures have been too small to analyze directly using SIMS because there was not enough surface area to obtain depth profiles with the desired sensitivity. FinFet characterization is additionally difficult because of the shape and even smaller size of the features but SIMS has been used to probe the dopant concentration on FinFeT top and sidewall regions [16]. Characterization can be improved by the use of additional techniques such as atom probe technology [17] and TEM. Traditional SIMS depth profiling can be of use through dedicated patterns on the wafers (Chapter 5).

10.1.2 InP AND GaAs

InP and GaAs are technologies that have been extensively characterized using SIMS. Combinations of varying amounts of indium, gallium, arsenic, and phosphorus complicate quantification and require many standards to account for matrix effects. Figure 10.14 shows a SIMS depth profile of an InP laser structure where the active region consists of $In_{0.52}Ga_{0.48}P$ [18]. The complexity of the analyses often encountered in GaAs technology is shown in Figure 10.15. Region 1 contains a GaAs/AlGaAs silicon doped

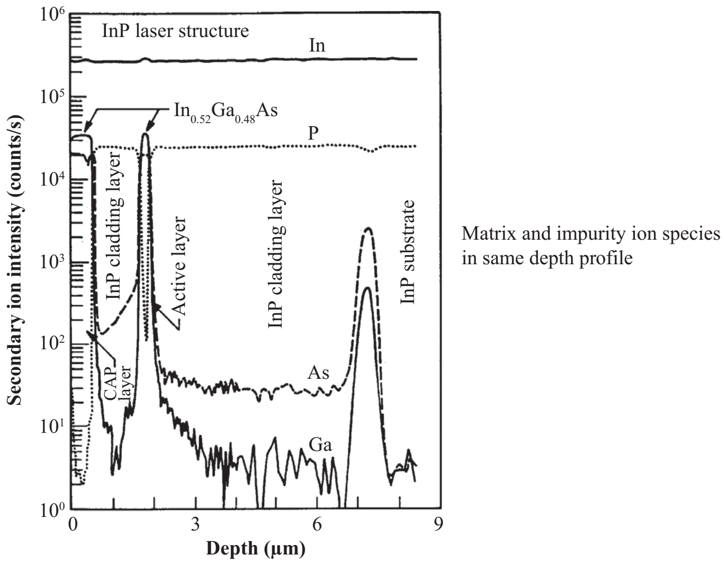

Figure 10.14. InP laser structure.
Source: Wilson, Stevie, and Magee [18].

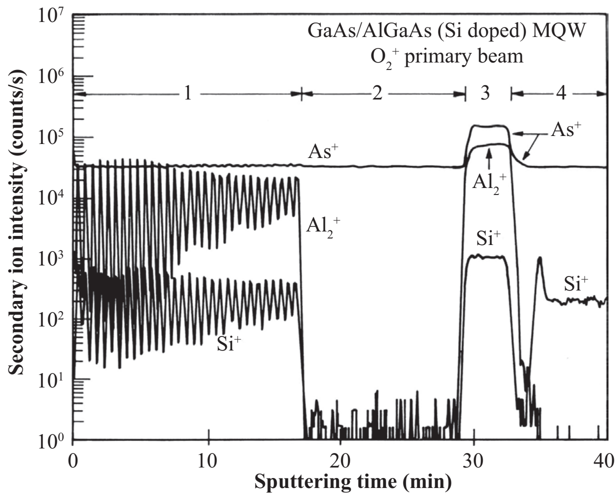

Figure 10.15. GaAs MQW structure.
Source: Wilson, Stevie, and Magee [19].

multiquantum well (MQW) structure, which consists of 30 repetitions of 14.2 nm GaAs/1.3 nm $Al_{0.3}Ga_{0.7}As$/3.8 nm AlGaAs doped with 2×10^{18} atoms/cm^3 Si /1.3 nm AlGaAs. Region 2 is 442 nm GaAs, region 3 has

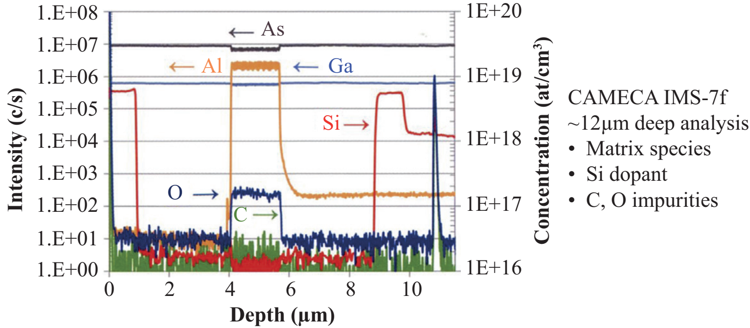

Figure 10.16. GaAs based LED structure.
Source: CAMECA instruments, reproduced with permission from CAMECA.

10 repetitions of 4 nm GaAs/ 4 nm $Al_{0.5}Ga_{0.5}As$, and region 4 is the GaAs substrate [19]. The depth resolution and sensitivity attributes of SIMS are fully utilized in these analyses. Figure 10.16 displays a GaAs laser structure with Si as a dopant species. C, O, and Si are quantified.

10.1.3 GaN AND AlN

Gallium nitride (GaN) has been used as a matrix for the development of light-emitting diodes. The dopants are typically magnesium for p type and silicon for n type. Indium and aluminum are used with the gallium to provide the laser-producing structure, which may contain alternating layers of AlGaN or AlGaInN with GaN. Aluminum nitride (AlN) can be used as an intermediate layer to reduce the lattice mismatch between GaN and a substrate that is SiC, Al_2O_3, or silicon. Figure 10.17 shows a GaN laser structure and indicates that many layers are present but can be resolved by monitoring profiles of aluminum and indium with a Cs^+ primary beam.

AlN is another optical technology material, and SIMS has been instrumental in characterizing impurity and dopant profiles. Analysis is complicated by the insulating nature of this material. Figure 10.18 shows the difference in C, O, and Si between the top homoepitaxial layer grown at 1100°C and the AlN substrate [20]. Figure 10.19 shows AlN successfully doped with magnesium at different concentrations.

10.1.4 LITHIUM NIOBATE ($LiNbO_3$)

$LiNbO_3$ is used as a high speed switch for lightwave applications. Titanium is of particular interest as it is used to provide conductive regions in the

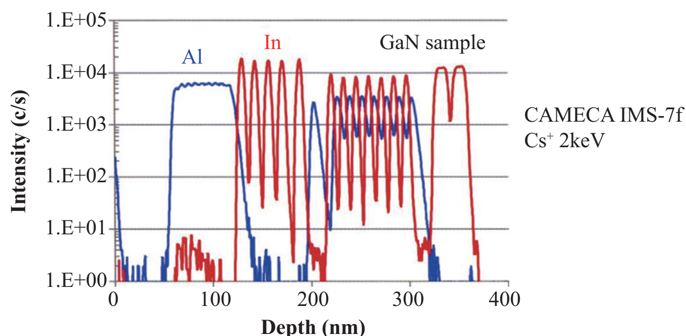

Depth profile of matrix species using MCs+ mode

Figure 10.17. AlGaN/InGaN LED structure.
Source: CAMECA instruments, reproduced with permission from CAMECA.

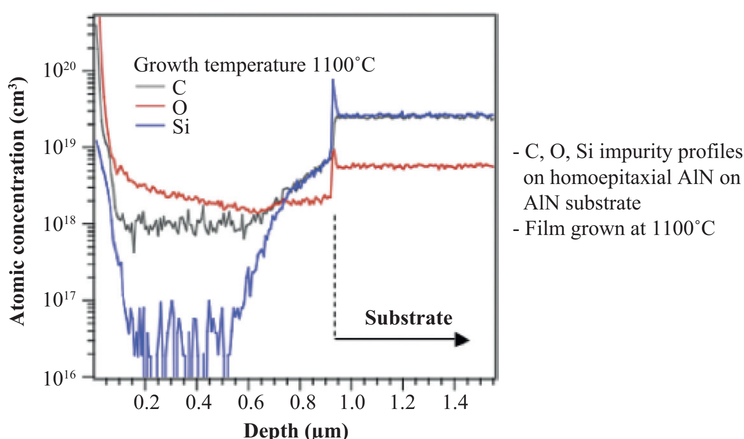

Figure 10.18. AlN impurity depth profile.
Source: Dalmau et al. [20], reproduced with permission from the Electrochemical Society.

niobate. Figure 10.20 shows implanted titanium and indium in $LiNbO_3$ analyzed using a quadrupole with an O_2^+ primary beam. The detection limit for indium is limited by a mass interference for ^{115}In due to $^{93}Nb^{16}O^{6}Li$ with a mass difference (ΔM) of 0.0226 which requires $M/\Delta M$ 5088 mass resolution, which is not possible to achieve with a quadrupole analyzer. A better detection limit might be achieved with the weaker isotope ^{113}In.

There are other semiconductor technologies, such as HgCdTe based structures, that have multiple layers and have been characterized using SIMS. The ability to obtain a depth profile with high sensitivity and depth

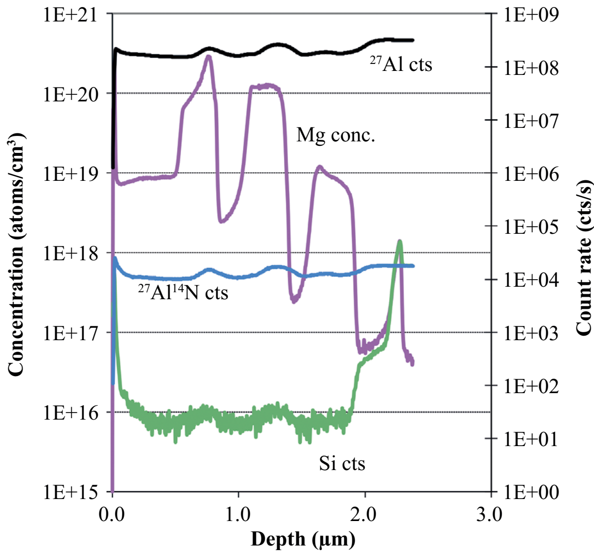

Figure 10.19. AlN structure.
Source: R. Collazo, Materials Science, North Carolina State University.

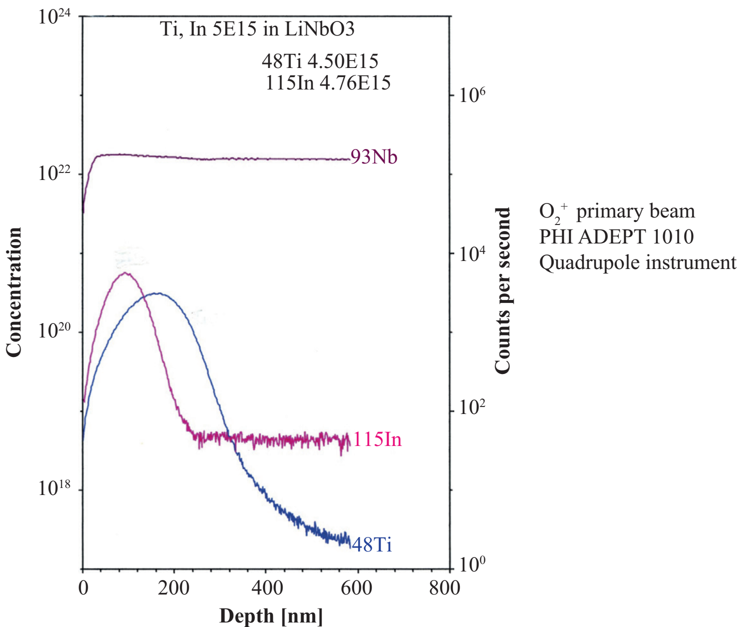

Figure 10.20. $LiNbO_3$ doped with Ti.

resolution has made SIMS a major technique for characterization of semiconductors.

10.2 ORGANIC MATERIALS

Organic materials can be depth profiled, but analysis has been complicated due to sample charging and the degradation of the material when exposed to an electron beam for charge neutralization. Some materials could be analyzed without neutralization. Figure 10.21 shows depth profiles of ^{13}C in polystyrene, which was used as an alternative to deuterium labeling [21].

Sputtering with typical sources such as O_2^+, Cs^+, and Ga^+ causes damage to the molecular structure and results in poor molecular depth profiles [22]. Organic depth profiling developed rapidly with the introduction of cluster beam sources that can remove material without normal molecular damage due to sputtering [23]. In particular, C_{60}^+ and argon cluster beams have the capability to avoid changes in chemical state during profiling. Figure 10.22 shows the increase in secondary ion yield

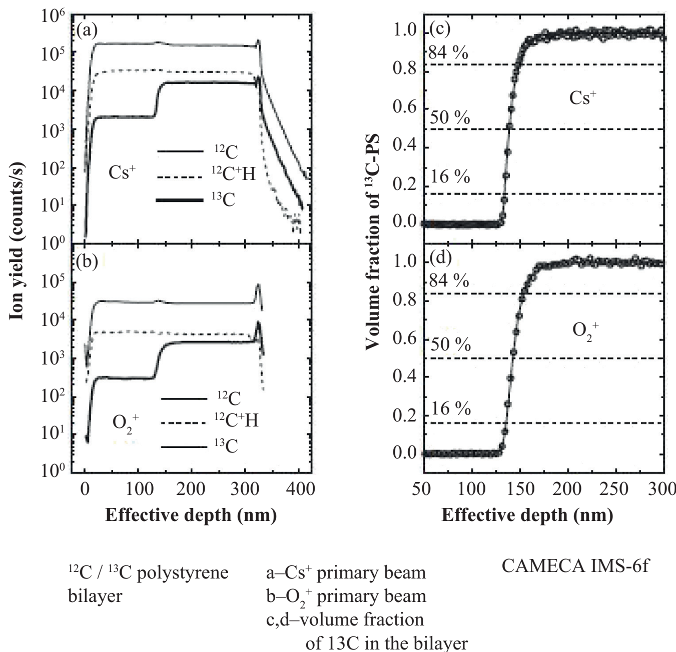

Figure 10.21. ^{13}C labeling in polystyrene analyzed with O_2^+ and Cs^+ beams. *Source*: Harton, Stevie, and Ade [21], with kind permission from Springer Science + Business Media.

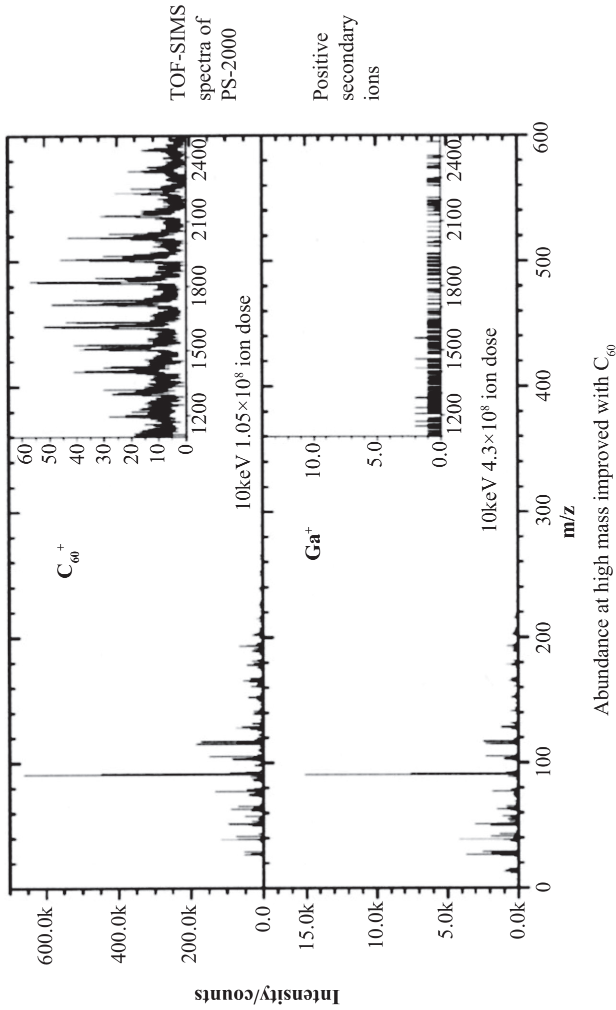

Figure 10.22. Improved high mass abundance with C_{60} cluster source.
Source: Weibel et al. [24], reprinted with permission from Analytical Chemistry, copyright 2003 American Chemical Society.

at high mass using C_{60}^{+} versus Ga^{+} [24]. Trehalose is just one example of an organic material that has been successfully depth profiled using a C_{60}^{+} primary beam [25]. Many of the lessons learned from the analysis of semiconductors, such as sample roughening during bombardment, have shown applicability to organic depth profiling. Figures 10.23 and 10.24 show how sample rotation and sample cooling may improve depth

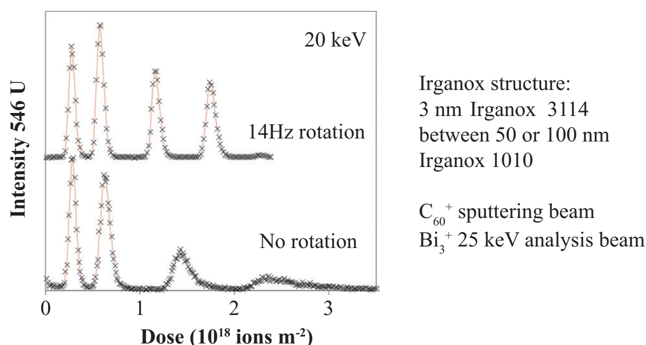

Figure 10.23. Depth resolution improved with sample rotation.
Source: Sjovall et al. [26], reprinted with permission from Journal of Physical Chemistry, copyright 2010 American Chemical Society.

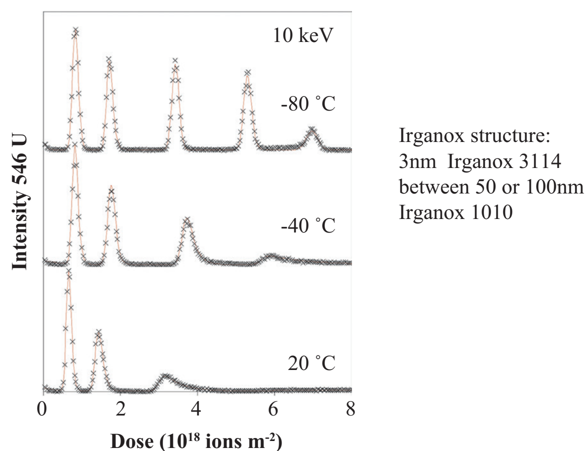

Figure 10.24. Depth resolution improved with sample cooling.
Source: Sjovall et al. [26], reprinted with permission from Journal of Physical Chemistry, copyright 2010 American Chemical Society.

resolution [26]. The introduction of gas cluster beams such as Ar_{2500}^+ has further enhanced the ability to obtain depth profiles in organic materials. Figure 10.25 shows the argon cluster beam analysis of two 100 nm organic layers [27]. Figure 10.26 shows the argon cluster beam analysis of an entire optical light-emitting diode structure.

Note that nondepth profiling applications of SIMS, such as imaging analyses of organic materials, have been made for some time. Examples of analyses include freeze fracture of cells [28, 29], mapping of chromosomes [30], and analysis of fluorine in teeth [31]. The improved lateral

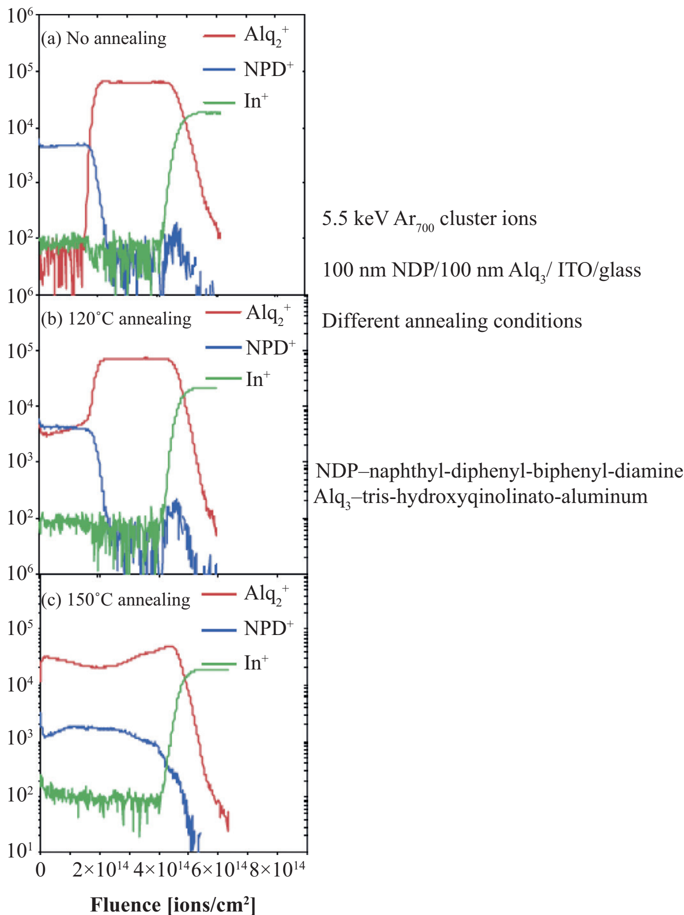

Figure 10.25. Ar cluster depth profiling.
Source: Matsuo et al. [27], reprinted with permission from John Wiley and Sons.

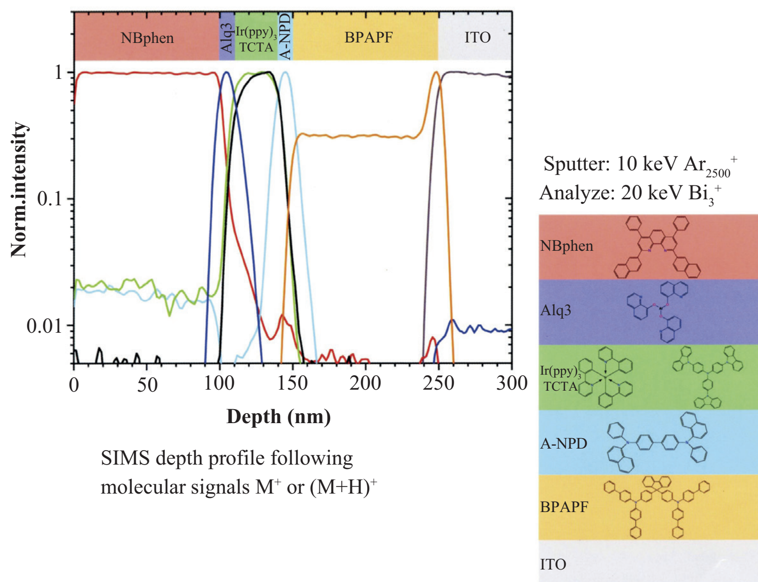

Figure 10.26. Organic light emitting diode.
Source: ION TOF, reproduced with permission.

resolution on instruments such as the CAMECA NanoSIMS50 makes possible high resolution elemental analysis [32].

10.3 MINERALS, CERAMICS, CATALYSTS

The mineral specimens found in nature are typically not homogeneous, and contain many regions of different composition. In order to resolve species in these regions, it is almost essential to have the advantage of high mass resolution because there are commonly a very large number of mass interferences [33–35]. Minerals are also usually nonconductive and require charge neutralization for analysis. Take for example the mineral labradorite in the mass region 54 to 57, which contains iron isotopes and manganese. Each iron isotope has significant mass interferences as shown in Table 10.2. A mass resolution of 3000 would be sufficient to resolve the mass interferences in this example.

Ion implantation of an element into the actual sample to be measured makes possible a direct measurement of the concentration of the element of interest. Figure 10.27 shows calibration of gold in arsenopyrite with an ion implant [36]. This analysis is made using a Cs^+ primary beam

Table 10.2. Mass interferences in Fe region of labradorite

Species of interest	Mass interference	Mass resolution required
^{54}Fe	$^{12}C_4{}^1H_6$	500
^{54}Fe	$^{27}Al_2$	2250
^{55}Mn	$^{12}C_4{}^1H_7$	466
^{55}Mn	$^{27}Al^{28}Si$	2619
^{55}Mn	$^{39}K^{16}O$	2619
^{56}Fe	$^{12}C_4{}^1H_8$	434
^{56}Fe	$^{40}Ca^{16}O$	2735
^{57}Fe	$^{12}C_4{}^1H_9$	416
^{57}Fe	$^{40}Ca^{16}O^1H$	1834

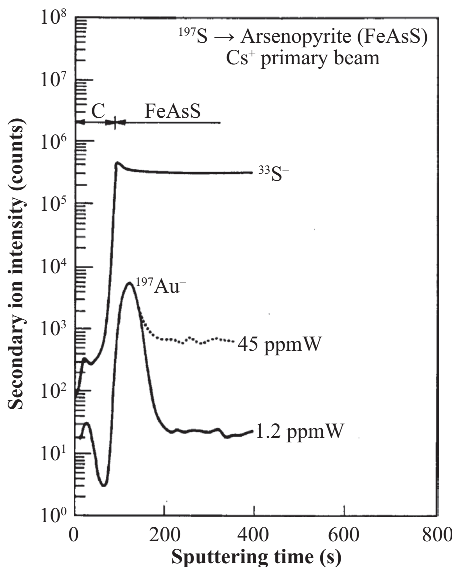

Calibration of Au in minerals using ion implantation. Samples were carbon coated and then analyzed using Cs^+ at a sputtering rate of about 2 nm/s. The baseline Au level in the two samples of Arsenopyrite is different by almost a factor of 40.

Figure 10.27. Minerals quantification.
Source: Wilson, Stevie, and Magee [36].

and it is important to be aware of the mass interference of $^{133}Cs^{32}S_2^-$ with $^{197}Au^-$, which requires a mass resolution of approximately 1700 for separation [37, 38]. Implantation of many elements of interest for mining has been made for quantification [39]. High energy implantation is required to place the peak of ion implanted heavy elements far enough

into the specimen to exceed the equilibration depth. Isotope measurements and geochronology of materials such as U–Pb in zircon have been made extensively using the sensitive high resolution ion microprobe magnetic sector instrument [40] and the CAMECA IMS 1270 and IMS 1280 instruments.

Extraterrestrial materials have been a fruitful area of analysis for SIMS. This type of analysis often consists of isotope ratio measurements made at high precision [41]. TOF-SIMS instruments have also been employed for this work [42].

Catalysts are an important class of material. A major use of catalysts is in the petroleum industry. The determination of good versus bad catalysts can be made using SIMS. Zeolite catalysts have been characterized with this technique [43]. Figure 10.28 shows an example of high spatial resolution analysis of silicon in zeolite [44].

10.4 METALS

The use of SIMS to study metals is complicated by the uneven sputtering of polycrystalline materials. Rotation of the sample during analysis can reduce or remove this effect. The earliest instrument designed for sample rotation was developed for analysis of coatings on steel [45]. Sensitivity factors for quantification have been obtained for over 50 elements [46]. High resolution imaging of materials such as Al–Si–Mg–Cu has been demonstrated [47].

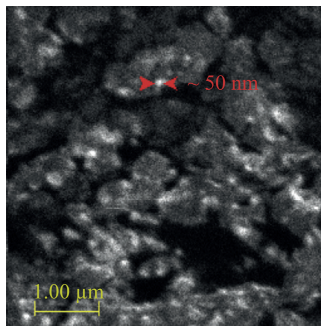

- Si^+ ion image of FCC zeolite crystals
- Si rich islands are resolved within individual zeolites

Figure 10.28. Silicon regions in zeolite. *Source*: Lamberti, Horn, and Keenan [44], reprinted with permission, Cambridge University Press.

REFERENCES

[1] Wilson, R.G., F.A. Stevie, and C.W. Magee. 1989. *Secondary Ion Mass Spectrometry*, Appendix F. New York: Wiley.

[2] Stevie, F.A., P.M. Kahora, D.S. Simons, and P. Chi. 1988. "Secondary Ion Yield Changes in Si and GaAs Due to Topography Changes During O_2^+ or Cs^+ Ion Bombardment." *Journal of Vacuum Science & Technology A* 6, p. 76. doi: http://dx.doi.org/10.1116/1.574972

[3] Magee, C.W., and M.R. Frost. 1995. "Recent Successes in the Use of Secondary Ion Mass Spectrometry in Microelectronics Materials and Processing." *International Journal of Mass Spectrometry and Ion Processes* 143, p. 29. doi: http://dx.doi.org/10.1016/0168-1176(94)04115-n

[4] Simons, D.S., R.G. Downing, G.P. Lamaze, R.M. Lindstrom, R.R. Greenberg, R.L. Paul, S.B. Schiller, and W.F. Guthrie. 2007. "Development of Certified Reference Materials of Ion-Implanted Dopants in Silicon for Calibration of Secondary Ion Mass Spectrometers." *Journal of Vacuum Science & Technology B* 25, p. 1365. doi: http://dx.doi.org/10.1116/1.2759937

[5] Stevie, F.A., R.G. Wilson, D.S. Simons, M.I. Current, and P.C. Zalm. 1994. "A Review of SIMS Characterization of Contamination Associated with Ion Implantation." *Journal of Vacuum Science & Technology B* 12, p. 2263. doi: http://dx.doi.org/10.1116/1.587753

[6] Harris, K.K., F.A. Stevie, J.M. McKinley, S.M. Merchant, and M. Oh. 2000. "SIMS Study of Copper Quantification and Diffusion in Silicon, Silicon Dioxide, and Silicon Nitride." *Proceedings of Advanced Metallization Conference*, September 28–30, 1999, p. 307, Warrendale, PA: Materials Research Society.

[7] Glawischnig, H., and C.C. Parks. 1996. "SIMS and Modeling of Ion Implants into Photoresist." *Proceedings of the XIth International Ion Implantation Technology Conference*, 1, Austin, TX.

[8] Parks, C.C., H. Glawischnig, and R. Murphy. 1998. "SIMS Study of Post Implant Migration of Boron in Photoresist." *Secondary Ion Mass Spectrometry, SIMS XI*, eds. G. Gillen, R. Lareau, J. Bennett, and F. Stevie, 209. Chichester, United Kingdom: Wiley.

[9] Chu, P.K., and S.L. Grube. 1985. "Quantitative Determination of Boron and Phosphorus in Borophosphosilicate Glass by Secondary Ion Mass Spectrometry." *Analytical Chemistry* 57, p. 1071. doi: http://dx.doi.org/10.1021/ac00283a024

[10] Rana, V.V.S., A.S. Harrus, F.A. Stevie, A.S. Manocha, and A.K. Sinha. 1987. "The Flow of Borophosphosilicate Glass in PBr_3 Ambient." *Electrochemical Society Extended Abstracts* 87–2, p. 1530.

[11] Stevie, F.A., and D.P. Griffis. 2008. "Quantification in Dynamic SIMS; Current Status and Future Needs." *Applied Surface Science* 255, p. 1364. doi: http://dx.doi.org/10.1016/j.apsusc.2008.05.041

[12] Stevie, F.A., L. Sedlacek, P. Babor, J. Jiruse, E. Principe, and K. Klosova. 2014. "FIB-SIMS Quantification Using TOF-SIMS with Ar and Xe Plasma Sources." *Surface and Interface Analysis* 46, p. 285. doi: http://dx.doi.org/10.1002/sia.5483

[13] Stevie, F.A., J.L. Moore, S.M. Merchant, C.A. Bollinger, and E.A. Dein. 1994. "Secondary Ion Mass Spectrometry Analysis of Three Level Metal Structure Using Sample Rotation." *Journal of Vacuum Science & Technology A* 12, p. 2363. doi: http://dx.doi.org/10.1116/1.579215

[14] Parks, C.C. 1997. "Secondary Ion Mass Spectrometry of a Copper Polyimide Thin Film Packaging Technology." *Journal of Vacuum Science & Technology A* 15, p. 1328. doi: http://dx.doi.org/10.1116/1.580584

[15] Wilson, R.G., F.A. Stevie, and C.W. Magee. 1989. *Secondary Ion Mass Spectrometry*, 4.2–4. New York: Wiley.

[16] Mody, J., R. Duffy, P. Eyben, J. Goossens, A. Moussa, W. Polspoel, B. Berghmans, M.J.H. van Dal, B.J. Pawlak, M. Kaiser, R.G.R. Weemaes, and W. Vandervorst. 2010. "Experimental Studies of Dose Retention and Activation in Fin Field-Effect-Transistor-Based Structures." *Journal of Vacuum Science & Technology B* 28, p. C1H5. doi: http://dx.doi.org/10.1116/1.3269755

[17] Gnaser, H. 2014. "Atom Probe Tomography of Nanostructures." *Surface and Interface Analysis* 46, p. 383. doi: http://dx.doi.org/10.1002/sia.5507

[18] Wilson, G., F.A. Stevie, and C.W. Magee. 1989. *Secondary Ion Mass Spectrometry*, 1.6–13. New York: Wiley.

[19] Wilson, R.G., F.A. Stevie, C.W. Magee. 1989. *Secondary Ion Mass Spectrometry*, 4.5–4, New York: Wiley.

[20] Dalmau, R., B. Moody, R. Schlesser, S. Mita, J. Xie, M. Feneberg, B. Neuschl, K. Thonke, R. Collazo, A. Rice, J. Tweedie, and Z. Sitar. 2011. "Growth and Characterization of AlN and AlGaN Epitaxial Films on AlN Single Crystal Substrates." *Journal of the Electrochemical Society* 158, p. H530. doi: http://dx.doi.org/10.1149/1.3560527

[21] Harton, S.E., F.A. Stevie, and H. Ade. 2006. "Carbon-13 Labeling for Improved Tracer Depth Profiling of Organic Films Using Secondary Ion Mass Spectrometry." *Journal of the American Society for Mass Spectrometry* 17, p. 1142. doi: http://dx.doi.org/10.1016/j.jasms.2006.03.018

[22] Mahoney, C.M., A.J. Fahey, A.M. Belu, J.A. Gardella Jr. 2011. "Challenges of 3-D Characterization of Polymer-Based Drug Delivery Devices with Cluster Secondary Ion Mass Spectrometry." *Journal of Surface Analysis* 17, no. 3, p. 299.

[23] Mahoney, C.M., ed. 2013. *Cluster Secondary Ion Mass Spectrometry: Principles and Applications*. New York: Wiley.

[24] Weibel, D., S. Wong, N. Lockyer, P. Blankinsopp, R. Hill, and J.C. Vickerman. 2003. "A C_{60} Primary Ion Beam System for Time of Flight Secondary Ion Mass Spectrometry: Its Development and Secondary Ion

Yield Characteristics." *Analytical Chemistry* 75, p. 1754. doi: http://dx.doi.org/10.1021/ac026338o

[25] Wucher, A., and N. Winograd. 2010. "Molecular Sputter Depth Profiling Using Carbon Cluster Beams." *Analytical and Bioanalytical Chemistry* 396, p. 105. doi: http://dx.doi.org/10.1007/s00216-009-2971-x

[26] Sjövall, P., D. Rading, S. Ray, L. Yang, and A.G. Shard. 2010. "Sample Cooling or Rotation Improves C_{60} Organic Depth Profiles of Multilayered Reference Samples: Results from a VAMAS Interlaboratory Study." *Journal of Physical Chemistry B* 114, p. 769. doi: http://dx.doi.org/10.1021/jp9095216

[27] Matsuo, J., S. Ninomiya, H. Yamada, K. Ichiki, Y. Wakamatsu, M. Hada, T. Seki, and T. Aoki. 2010. "SIMS with Highly Excited Primary Beams for Molecular Depth Profiling and Imaging of Organic and Biological Materials." *Surface and Interface Analysis* 42, p. 1612. doi: http://dx.doi.org/10.1002/sia.3585

[28] Chandra, S., and G.H. Morrison. 1985. "Imaging Elemental Distribution and Ion Transport in Cultured Cells with Ion Microscopy." *Science* 228, p. 1543. doi: http://dx.doi.org/10.1126/science.2990033

[29] Chandra, S., and G.H. Morrison. 1997. "Evaluation of Fracture Planes and Cell Morphology in Complementary Fractures of Cultured Cells in the Frozen-Hydrated State by Field-Emission Secondary Electron Microscopy: Feasibility for Ion Localization and Fluorescence Imaging Studies." *Journal of Microscopy* 186, p. 232. doi: http://dx.doi.org/10.1046/j.1365-2818.1997.2030763.x

[30] Levi-Setti, R., J.M. Chabala, K. Gavrilov, R. Strick, and P.L. Strissel. 1998. "High Resolution SIMS Mapping of Divalent Cations in Active Chromosomes." *Secondary Ion Mass Spectrometry, SIMS XI*, eds. G. Gillen, R. Lareau, J. Bennett, and F. Stevie, 105. Chichester, United Kingdom: Wiley.

[31] Griffis, D.P., J.W. Bawden, D.A. Ricks, R.G. Rozier, B.P. Crawford, and T.G. Deaton. 1998. "SIMS Assay of Fluorine Across the Dentin of Exfoliated Primary Teeth." *Secondary Ion Mass Spectrometry, SIMS XI*, eds. G. Gillen, R. Lareau, J. Bennett, and F. Stevie, 131. Chichester, United Kingdom: Wiley.

[32] Brismar, H., A. Aperia, L. Westin, J. Moy, M. Wang, C. Guillermier, J.C. Poczatek, and C. Lechene. 2014. "Study of Protein and RNA in Dendritic Spines Using Multi-Isotope Imaging Mass Spectrometry." *Surface and Interface Analysis* 46, p. 158. doi: http://dx.doi.org/10.1002/sia.5617

[33] Williams, P., and C.A. Evans Jr. 1975. "High Mass Resolution Secondary Ion Mass Spectrometry." In *Secondary Ion Mass Spectrometry*, eds. K.F.J. Heinrich and D.E. Newbury, 63. Washington, DC.: NBS Special Publication 427.

[34] Loverling, J.F. 1975. “Application of SIMS Microanalysis Techniques to Trace Element and Isotopic Studies in Geochemistry and Cosmochemistry.” In *Secondary Ion Mass Spectrometry*, eds. K.F. Heinrich and D.E. Newbury, 135. Washington, DC.: NBS Special Publication 427.

[35] Metson, J.B. 1990. “Secondary Ion Mass Spectrometry.” In *Instrumental Surface Analysis of Geologic Materials*, ed. D.L. Perry, 311. New York: VCH Publishers.

[36] Wilson, R.G., F.A. Stevie, and C.W. Magee. 1989. *Secondary Ion Mass Spectrometry*, 3.2–12. New York: Wiley.

[37] Cabri, L.J., and G. McMahon. 1995. “SIMS Analysis of Sulfide Materials for Pt and Au: Methodology and Relative Sensitivity Factors (RSF).” *The Canadian Mineralogist* 33, p. 349.

[38] Agha, U., S.L. Chryssoulis, A. Margaritis, and R. Dunne. 1998. “An Intergrated Mineralogical Approach to the Biooxidation of Sulphide-Bearing Refractory Gold Ores.” *Mineral Processing and Extractive Metallurgy Review* 19, p. 199. doi: http://dx.doi.org/10.1080/08827509608962440

[39] Wilson, R.G., F.A. Stevie, S.L. Chryssoulis, and R.B. Irwin. 1994. “Secondary Ion Mass Spectrometry Relative Sensitivity Factors for Ru, Rh, Pr, Eu, Tm, Lu, Re, Os, and Ir.” *Journal of Vacuum Science Technology A* 12, p. 2415. doi: http://dx.doi.org/10.1116/1.579224

[40] Magee, C., Jr., J. Ferris, and C. Magee Sr. 2014. “Effect of Impact Energy on SIMS U-Pb Zircon Geochronology.” *Surface and Interface Analysis* 46, p. 322. doi: http://dx.doi.org/10.1002/sia.5629

[41] Slodzian, G., M. Chaintreau, R. Dennebouy, and B. Rasser. 1998. “Isotope Ratio Measurements Over Micro-Areas, the Challenge of High Precision Repeatability.” *Secondary Ion Mass Spectrometry, SIMS XI*, eds. G. Gillen, R. Lareau, J. Bennett, and F. Stevie, 29. Chichester, United Kingdom: Wiley.

[42] Stephan, T. 2001. “TOF-SIMS in Cosmochemistry.” *Planetary and Space Science* 49, p. 859. doi: http://dx.doi.org/10.1016/s0032-0633(01)00037-x

[43] Hofmann, J.P., M. Rohnke, and B.M. Weckhuysen. 2014. “Recent Advances in Secondary Ion Mass Spectrometry of Solid Acid Catalysts: Large Zeolite Crystals Under Bombardment.” *Physical Chemistry Chemical Physics* 16, p. 5465. doi: http://dx.doi.org/10.1039/c3cp54337d

[44] Lamberti, W.A., W.C. Horn, and J.A. Keenan IV. 2007. “Nano-Particle Analysis in the Petrochemical Industry: Probing Catalysts and Materials with Electron and Ion Beams.” *Microscopy and Microanalysis* 13, no. S02, p. 564. doi: http://dx.doi.org/10.1017/s1431927607079226

[45] Dittmann, J. 1982. “Development and Operation of Special SIMS-Equipment for Use in Iron and Steel Analysis.” *Secondary Ion Mass Spectrometry, SIMS III*, eds. A. Benninghoven, J. Giber, J. Laszlo, M. Riedel, and H.W. Werner, 61. Berlin, Germany: Springer.

[46] Wilson, R.G., F.A. Stevie, G.E. Lux, C.L. Kirschbaum, S. Frank, and J. Pallix. 1992. “Depth Profiles, Projected Ranges, and Secondary Ion Mass

Spectrometry Relative Sensitivity Factors for More Than 50 Elements from Hydrogen to Uranium Implanted into Metals." *8th International Conference on Surface Modification of Metals by Ion Beams, Surface Coatings Technology* 51, p. 358. doi: http://dx.doi.org/10.1016/0257-8972(92)90264-b

[47] Levi-Setti, R., J.M. Chabala, J. Gavrilov, K.I. Li, R. Mogilevsky, and K.K. Soni. 1993. "Imaging-SIMS (Secondary Ion Mass Spectrometry) Studies of Advanced Materials." *Scanning Microscopy* 7, p. 1161.

CHAPTER 11

Analysis Approach

11.1 INITIAL CONSIDERATIONS

When you have analyzed a series of samples and now have one more to analyze, the conditions for analysis have been determined and the required data can be obtained very quickly. However, if you have a sample type you have never analyzed previously and some of the information about the sample, such as layer thickness, cannot be guaranteed, then is there a procedure that would be helpful?

You should have some information about the sample such as substrate, layers, and elements of interest. Secondary ion mass spectrometry (SIMS) is more effective if some initial information is available. If the sample is totally unknown, it may be best to perform scanning electron microscopy (SEM) with energy dispersive spectroscopy (SEM-EDS) elemental analysis first. This would provide information regarding the major species present.

Based on the elements of interest, select a primary beam species for best detection limit for the most important elements. This choice will also include secondary ion polarity and the initial secondary ions to be profiled. Sometimes all the elements of interest cannot be properly analyzed with one primary beam and two analyses will be required.

The next decision level regards the primary beam parameters: voltage, angle of incidence, current, and the analysis choices of raster and gating. If depth resolution is important, then the primary voltage will be low and you may consider bombardment at high angle of incidence from normal. Note that for some materials, topography formation can occur at certain incidence angles (see Chapter 5). The current and raster size are the two most important parameters to determine sputtering rate, and if you have information on the depth to be analyzed, then you should arrange a sputtering rate that can complete the profile in a reasonable time, such as 15 to 30 min.

If there is an overlayer that can be removed before analysis, then this will improve depth resolution. If the sample or one of the layers is an insulator, then one needs to have a plan for charge neutralization. Chapter 8 provides information on insulator analysis. A nonconductive sample would often be coated with a conductor, such as gold, before analysis.

If quantification is required, determine whether the standards, typically ion implanted samples of the same matrix, are available and if not, use Transport of Ions in Matter (TRIM) to calculate the implantation energy needed and assess what standards could be fabricated. Quantification methods are described in Chapter 6.

11.2 ANALYSIS SEQUENCE

A depth profile should be made through the region of interest. This will show if the depth resolution is adequate and how long it takes to sputter through individual layers. One can now profile into each layer, one at a time and take mass spectra. This is very important because the mass spectrum will show the presence of any significant unexpected species, which may cause mass interferences. The spectrum will also show if another species would be a better choice for the depth profile. If the depth axis needs to be accurately determined, then profiles can be made in a sequence where the profile is stopped at the interface between layers. If this is done separately for each layer, then the sputtering rate can be calculated for each one.

With this information, one can perform the analysis as intended for the sample and the species of interest. Because the analysis area is quite small, two profiles should be obtained and checked to see if they match. If they do not match and a third profile shows yet another variation, then it is likely that the species of interest is nonuniform on the sample.

To summarize:

Choose primary beam species, polarity
Choose secondary beam species, polarity
Choose primary beam parameters (angle of incidence, voltage, raster, current)
Sample preparation if necessary (remove overlayers)
For insulators, prevent sample charging (coat sample, use electron beam)
Decide if quantification needed, determine if standards can be made
Depth profile to determine sputtering rates, identify layers
Mass spectra to check for unexpected elements, mass interferences, and interfacial contaminants
Depth profiles to obtain at least two matching analyses
If profiles do not match, check for nonuniform distribution

As an example, Figure 11.1 shows a drawing of a structure with two layers. It is important to determine the information that is desired. Since SIMS has excellent sensitivity, it is very common to detect a trace amount of an element that may not be of importance. For this theoretical two-layer structure, it would be very helpful to know the past history, such as whether there were issues at an interface. One should also remember that one technique may not provide all the answers. Much value has been obtained from analysis with two techniques, such as SIMS and TEM, SIMS and SEM-EDS, or SIMS and AES.

Figures 11.2, 11.3, and 11.4 illustrate the importance of the details in SIMS. In Figure 11.2, we note two boron profiles on the same sample. The overall shape for each is similar and is reasonable since this is a sample with both shallow and deep boron implants. However, the depth scales are significantly different. The answer is in the raw data for the two samples shown in figures 11.3 and 11.4. The matrix species was monitored for both

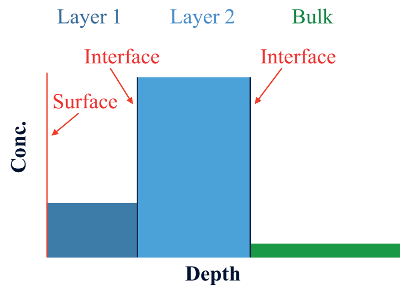

Figure 11.1. Quantification regions.

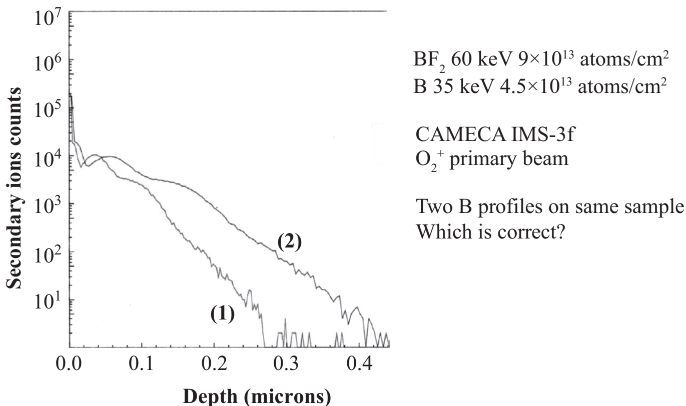

Figure 11.2. Matrix measurement.
Source: F. Stevie, AT&T Bell Laboratories.

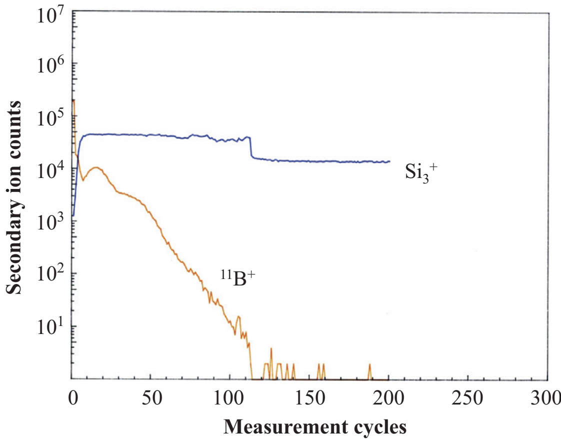

Problem with primary beam mass filter, beam current decreased at ~110 cycles
Overall sputter rate 0.27 nm/s

Figure 11.3. Matrix measurement (profile 1).
Source: F. Stevie, AT&T Bell Laboratories.

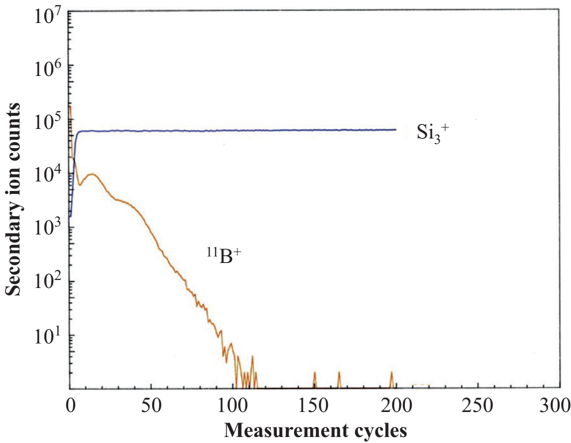

Stable primary current, sputter rate constant at 0.45 nm/s

Figure 11.4. Matrix measurement (profile 2).
Source: F. Stevie, AT&T Bell Laboratories.

profiles but the matrix in profile 1 was not constant. The problem was a fluctuation in power supply for the primary beam mass filter used on the CAMECA IMS-3f. Profile 2 shows a constant matrix signal and the correct sputtering rate.

APPENDIX

A.1 ISOTOPIC ABUNDANCES, IONIZATION POTENTIALS, ELECTRON AFFINITIES FOR ELEMENTS

Table A.1. Mass, abundance, ionization potential, electron affinity

Atomic number	Element	Integer mass	Exact mass	Abundance (%)	IP [eV]	EA [eV]
1	H	1	1.007825032	99.9885%	13.6	0.75
		2	2.014101778	0.0115%		
2	He	3	3.016029319	0.0001%	24.59	
		4	4.002603254	99.9999%		
3	Li	6	6.015122795	7.5900%	5.39	0.62
		7	7.01600455	92.4100%		
4	Be	9	9.0121822	100.0000%	9.32	
5	B	10	10.012937	19.9000%	8.3	0.28
		11	11.0093054	80.1000%		
6	C	12	12	98.9300%	11.26	1.26
		13	13.00335484	1.0700%		
7	N	14	14.003074	99.6360%	14.53	0
		15	15.0001089	0.3640%		
8	O	16	15.99491462	99.7570%	13.62	1.46
		17	16.9991317	0.0380%		
		18	17.999161	0.2050%		
9	F	19	18.99840322	100.0000%	17.42	3.4
10	Ne	20	19.99244018	90.4800%	21.56	0
		21	20.99384668	0.2700%		
		22	21.99138511	9.2500%		
11	Na	23	22.98976928	100.0000%	5.14	0.55

(*Continued*)

Atomic number	Element	Integer mass	Exact mass	Abundance (%)	IP [eV]	EA [eV]
12	Mg	24	23.9850417	78.9900%	7.65	0
		25	24.98583692	10.0000%		
		26	25.98259293	11.0100%		
13	Al	27	26.98153863	100.0000%	5.99	0.44
14	Si	28	27.97692653	92.2230%	8.15	1.39
		29	28.9764947	4.6850%		
		30	29.97377017	3.0920%		
15	P	31	30.97376163	100.0000%	10.49	0.75
16	S	32	31.972071	94.9900%	10.36	2.08
		33	32.97145876	0.7500%		
		34	33.9678669	4.2500%		
		36	35.96708076	0.0100%		
17	Cl	35	34.96885268	75.7600%	12.97	3.62
		37	36.96590259	24.2400%		
18	Ar	36	35.96754511	0.3365%	15.76	0
		38	37.9627324	0.0632%		
		40	39.96238312	99.6003%		
19	K	39	38.96370668	93.2581%	4.34	0.5
		40	39.96399848	0.0117%		
		41	40.96182576	6.7302%		
20	Ca	40	39.96259098	96.9410%	6.11	
		42	41.95861801	0.6470%		
		43	42.9587666	0.1350%		
		44	43.9554818	2.0860%		
		46	45.9536926	0.0040%		
		48	47.952534	0.1870%		
21	Sc	45	44.9559119	100.0000%	6.54	0.19
22	Ti	46	45.9526316	8.2500%	6.82	0.08
		47	46.9517631	7.4400%		
		48	47.9479463	73.7200%		
		49	48.94787	5.4100%		
		50	49.9447912	5.1800%		
23	V	50	49.9471585	0.2500%	6.74	0.53
		51	50.9439595	99.7500%		
24	Cr	50	49.9460442	4.3450%	6.77	0.67

		52	51.9405075	83.7890%		
		53	52.9406494	9.5010%		
		54	53.9388804	2.3650%		
25	Mn	55	54.9380451	100.0000%	7.44	0
26	Fe	54	53.9396105	5.8450%	7.87	0.16
		56	55.9349375	91.7540%		
		57	56.935394	2.1190%		
		58	57.9332756	0.2820%		
27	Co	59	58.933195	100.0000%	7.86	0.66
28	Ni	58	57.9353429	68.0769%	7.64	1.16
		60	59.9307864	26.2231%		
		61	60.931056	1.1399%		
		62	61.9283451	3.6345%		
		64	63.927966	0.9256%		
29	Cu	63	62.9295975	69.1500%	7.73	1.23
		65	64.9277895	30.8500%		
30	Zn	64	63.9291422	48.2680%	9.39	0
		66	65.9260334	27.9750%		
		67	66.9271273	4.1020%		
		68	67.9248442	19.0240%		
		70	69.9253193	0.6310%		
31	Ga	69	68.9255736	60.1080%	6	0.3
		71	70.9247013	39.8920%		
32	Ge	70	69.9242474	20.3800%	7.9	1.2
		72	71.9220758	27.3100%		
		73	72.9234589	7.7600%		
		74	73.9211778	36.7200%		
		76	75.9214026	7.8300%		
33	As	75	74.9215965	100.0000%	9.81	0.81
34	Se	74	73.9224764	0.8900%	9.75	2.02
		76	75.9192136	9.3700%		
		77	76.919914	7.6300%		
		78	77.9173091	23.7700%		
		80	79.9165213	49.6100%		
		82	81.9166994	8.7300%		
35	Br	79	78.9183371	50.6900%	11.81	3.36
		81	80.9162906	49.3100%		

(*Continued*)

Atomic number	Element	Integer mass	Exact mass	Abundance (%)	IP [eV]	EA [eV]
36	Kr	78	77.9203648	0.3550%	14	0
		80	79.916379	2.2860%		
		82	81.9134836	11.5930%		
		83	82.914136	11.5000%		
		84	83.911507	56.9870%		
		86	85.91061073	17.2790%		
37	Rb	85	84.91178974	72.1700%	4.18	0.49
		87	86.90918053	27.8300%		
38	Sr	84	83.913425	0.5600%	5.7	
		86	85.9092602	9.8600%		
		87	86.9088771	7.0000%		
		88	87.9056121	82.5800%		
39	Y	89	88.9058483	100.0000%	6.38	0.31
40	Zr	90	89.9047044	51.4500%	6.84	0.43
		91	90.9056458	11.2200%		
		92	91.9050408	17.1500%		
		94	93.9063152	17.3800%		
		96	95.9082734	2.8000%		
41	Nb	93	92.9063781	100.0000%	6.88	0.89
42	Mo	92	91.906811	14.7700%	7.1	0.75
		94	93.9050883	9.2300%		
		95	94.9058421	15.9000%		
		96	95.9046795	16.6800%		
		97	96.9060215	9.5600%		
		98	97.9054082	24.1900%		
		100	99.907477	9.6700%		
43	Tc	97	no naturally occurring isotopes		7.28	0.55
44	Ru	96	95.907598	5.5400%	7.37	1.05
		98	97.905287	1.8700%		
		99	98.9059393	12.7600%		
		100	99.9042195	12.6000%		
		101	100.9055821	17.0600%		
		102	101.9043493	31.5500%		
		104	103.905433	18.6200%		
45	Rh	103	102.905504	100.0000%	7.46	1.14

46	Pd	102	101.905609	1.0200%	8.34	0.56
		104	103.904036	11.1400%		
		105	104.905085	22.3300%		
		106	105.903486	27.3300%		
		108	107.903892	26.4600%		
		110	109.905153	11.7200%		
47	Ag	107	106.905097	51.8390%	7.58	1.3
		109	108.904752	48.1610%		
48	Cd	106	105.906459	1.2500%	8.99	0
		108	107.904184	0.8900%		
		110	109.9030021	12.4900%		
		111	110.9041781	12.8000%		
		112	111.9027578	24.1300%		
		113	112.9044017	12.2200%		
		114	113.9033585	28.7300%		
		116	115.904756	7.4900%		
49	In	113	112.904058	4.2900%	5.79	0.3
		115	114.903878	95.7100%		
50	Sn	112	111.904818	0.9700%	7.34	1.15
		114	113.902779	0.6600%		
		115	114.903342	0.3400%		
		116	115.901741	14.5400%		
		117	116.902952	7.6800%		
		118	117.901603	24.2200%		
		119	118.903308	8.5900%		
		120	119.9021947	32.5800%		
		122	121.903439	4.6300%		
		124	123.9052739	5.7900%		
51	Sb	121	120.9038157	57.2100%	8.64	1.07
		123	122.904214	42.7900%		
52	Te	120	119.90402	0.0900%	9.01	1.97
		122	121.9030439	2.5500%		
		123	122.90427	0.8900%		
		124	123.9028179	4.7400%		
		125	124.9044307	7.0700%		
		126	125.9033117	18.8400%		

(*Continued*)

Atomic number	Element	Integer mass	Exact mass	Abundance (%)	IP [eV]	EA [eV]
		128	127.9044631	31.7400%		
		130	129.9062244	34.0800%		
53	I	127	126.904473	100.0000%	10.45	3.06
54	Xe	124	123.905893	0.0952%	12.13	0
		126	125.904274	0.0890%		
		128	127.9035313	1.9102%		
		129	128.9047794	26.4006%		
		130	129.903508	4.0710%		
		131	130.9050824	21.2324%		
		132	131.9041535	26.9086%		
		134	133.9053945	10.4357%		
		136	135.907219	8.8573%		
55	Cs	133	132.9054519	100.0000%	3.89	0.47
56	Ba	130	129.9063208	0.1060%	5.21	
		132	131.9050613	0.1010%		
		134	133.9045084	2.4170%		
		135	134.9056886	6.5920%		
		136	135.9045759	7.8540%		
		137	136.9058274	11.2320%		
		138	137.9052472	71.6980%		
57	La	138	137.907112	0.0900%	5.58	0.5
		139	138.9063533	99.9100%		
58	Ce	136	135.907172	0.1850%	5.47	
		138	137.905991	0.2510%		
		140	139.9054387	88.4500%		
		142	141.909244	11.1140%		
59	Pr	141	140.9076528	100.0000%	5.42	
60	Nd	142	141.9077233	27.2000%	5.49	
		143	142.9098143	12.2000%		
		144	143.9100873	23.8000%		
		145	144.9125736	8.3000%		
		146	145.9131169	17.2000%		
		148	147.916893	5.7000%		
		150	149.920891	5.6000%		
61	Pm	145	no naturally occurring isotopes		5.55	

62	Sm	144	143.911999	3.0700%	5.63
		147	146.9148979	14.9900%	
		148	147.9148227	11.2400%	
		149	148.9171847	13.8200%	
		150	149.9172755	7.3800%	
		152	151.9197324	26.7500%	
		154	153.9222093	22.7500%	
63	Eu	151	150.9198502	47.8100%	5.67
		153	152.9212303	52.1900%	
64	Gd	152	151.919791	0.2000%	6.14
		154	153.9208656	2.1800%	
		155	154.922622	14.8000%	
		156	155.9221227	20.4700%	
		157	156.9239601	15.6500%	
		158	157.9241039	24.8400%	
		160	159.9270541	21.8600%	
65	Tb	159	158.9253468	100.0000%	5.85
66	Dy	156	155.924283	0.0560%	5.93
		158	157.924409	0.0950%	
		160	159.9251975	2.3290%	
		161	160.9269334	18.8890%	
		162	161.9267984	25.4750%	
		163	162.9287312	24.8960%	
		164	163.9291748	28.2600%	
67	Ho	165	164.9303221	100.0000%	6.02
68	Er	162	161.928778	0.1390%	6.1
		164	163.9292	1.6010%	
		166	165.9302931	33.5030%	
		167	166.9320482	22.8690%	
		168	167.9323702	26.9780%	
		170	169.9354643	14.9100%	
69	Tm	169	168.9342133	100.0000%	6.18
70	Yb	168	167.933897	0.1300%	6.25
		170	169.9347618	3.0400%	
		171	170.9363258	14.2800%	
		172	171.9363815	21.8300%	

(*Continued*)

Atomic number	Element	Integer mass	Exact mass	Abundance (%)	IP [eV]	EA [eV]
		173	172.9382108	16.1300%		
		174	173.9388621	31.8300%		
		176	175.9425717	12.7600%		
71	Lu	175	174.9407718	97.4100%	5.43	
		176	175.9426863	2.5900%		
72	Hf	174	173.940046	0.1600%	7.0	
		176	175.9414086	5.2600%		
		177	176.9432207	18.6000%		
		178	177.9436988	27.2800%		
		179	178.9458161	13.6200%		
		180	179.94655	35.0800%		
73	Ta	180	179.9474648	0.0120%	7.89	0.32
		181	180.9479958	99.9880%		
74	W	180	179.946704	0.1200%	7.98	0.82
		182	181.9482042	26.5000%		
		183	182.950223	14.3100%		
		184	183.9509312	30.6400%		
		186	185.9543641	28.4300%		
75	Re	185	184.952955	37.4000%	7.88	0.12
		187	186.9557531	62.6000%		
76	Os	184	183.9524891	0.0200%	8.7	1.12
		186	185.9538382	1.5900%		
		187	186.9557505	1.9600%		
		188	187.9558382	13.2400%		
		189	188.9581475	16.1500%		
		190	189.958447	26.2600%		
		192	191.9614807	40.7800%		
77	Ir	191	190.960594	37.3000%	9.1	1.57
		193	192.9629264	62.7000%		
78	Pt	190	189.959932	0.0140%	9.0	2.13
		192	191.961038	0.7820%		
		194	193.9626803	32.9670%		
		195	194.9647911	33.8320%		

		196	195.9649515	25.2420%		
		198	197.967893	7.1630%		
79	Au	197	196.9665687	100.0000%	9.23	2.31
80	Hg	196	195.965833	0.1500%	10.44	0
		198	197.966769	9.9700%		
		199	198.9682799	16.8700%		
		200	199.968326	23.1000%		
		201	200.9703023	13.1800%		
		202	201.970643	29.8600%		
		204	203.9734939	6.8700%		
81	Tl	203	202.9723442	29.5200%	6.11	0.3
		205	204.9744275	70.4800%		
82	Pb	204	203.9730436	1.4000%	7.42	0.37
		206	205.9744653	24.1000%		
		207	206.9758969	22.1000%		
		208	207.9766521	52.4000%		
83	Bi	209	208.9803987	100.0000%	7.29	0.95
84	Po		no naturally occurring isotopes		8.42	1.9
85	At		no naturally occurring isotopes		9.5	2.8
86	Rn		no naturally occurring isotopes		10.75	0
87	Fr		no naturally occurring isotopes			
88	Ra		no naturally occurring isotopes		5.28	
89	Ac		no naturally occurring isotopes		6.9	
90	Th	232	232.0380553	100%	7.0	
91	Pa		no naturally occurring isotopes			
92	U	234	234.0409521	0.0054%	6.1	
		235	235.0439299	0.7204%		
		238	238.0507882	99.2742%		

Source: National Institute of Standards and Technology (NIST) database, www.nist.gov

A.2 SPUTTERING RATES RELATIVE TO SILICON

Table A.2. Relative sputtering rates

Matrix	O_2^+	Cs^+
Al	0.51	1.07
Al2O3	0.34	
Au	1.38	4.42
Be	0.35	0.95
Cr	0.69	1.26
GaAs	1.99	3.2
GaP	1.74	3.2
GaSb	2.8	2.9
Ge	1.71	2.3
HgCdTe	5.6	16
InP	3.04	6.6
InSb	3.36	6.5
LiNbO3	0.36	
Si	1	1
αSi	0.94	0.92
Si3N4	0.82	0.98
SiO2	0.95	0.94
SnPb		4.3
Ti	0.54	1.03

O_2^+ 8keV 38º incidence
Cs^+ 14.5keV 26º incidence

CAMECA IMS series magnetic sector instruments

Source: Wilson et al. [1], data obtained using CAMECA IMS series magnetic sector instruments with O_2^+ 8 keV 38° incidence and Cs^+ 14.5 keV 26° incidence.

A.3 SILICON RSFS

Table A.3. Si RSFs

Element	E+	EO+	ESi+	ECs+	E-	ESi-
H	6.0E+24	4.E+26	1.4E+25		4.8E+23	
He	3.6E+27					
Li	6.0E+20	1.5E+24	2.4E+23	1.4E+21	5.9E+24	
Be	3.2E+22	5.E+23	1.6E+24	8.E+21		5.1E+23
B	7.E+22	3.2E+25	4.E+24	5.E+22	2.4E+24	
C	7.E+24	1.3E+25	6.E+24	6.E+23	4.8E+22	
N	2.9E+25		3.7E+24	4.E+23		2.0E+22
O	8.E+25	1.8E+26	9.E+25	1.4E+24	2.4E+22	
F	4.E+23	2.6E+26	8.E+22		7.6E+21	
Ne	1.5E+27			4.7E+24		
Na	4.E+20	1.0E+24	1.1E+23	1.4E+22	6.E+25	
Mg	2.8E+21	2.6E+23	2.1E+23	4.E+21		5.3E+23
Al	1.4E+21	6.E+23	4.0E+23	1.6E+21	1.2E+25	
Si	[5.0E22]	2.2E+23	2.7E+23		[5.0E22]	
P	1.1E+24	1.8E+24	4.E+24	1.1E+23	1.2E+23	
S	6.E+24	2.9E+25	1.4E+24		8.0E+21	
Cl	6.E+24	1.1E+26	4.E+23		6.9E+21	
Ar	2.E+26		4.E+25	3.5E+23		
K	4.E+20	2.1E+24	1.8E+23	1.6E+21	1.1E+25	
Ca	1.3E+21		1.9E+23	1.1E+21		1.1E+24
Sc	1.3E+21	9.0E+21		4.E+21		9.E+23
Ti	4.E+21	2.9E+22	2.4E+23	7.E+21	9.E+25	
V	4.E+21	2.2E+23	2.7E+23	8.E+21	1.4E+25	
Cr	7.E+21	8.E+23	2.5E+23	2.8E+22	3.8E+24	
Mn	1.3E+22	1.6E+24	5.E+23	2.0E+23		1.3E+24
Fe	2.7E+22	4.E+24	2.8E+23	6.E+21	5.3E+25	
Co	5.E+22		5.E+23	1.3E+22	2.0E+24	
Ni	4.E+22	1.5E+25	4.E+23	3.4E+22	5.3E+23	
Cu	3.1E+22	5.0E+25	6.E+23	6.E+22	4.2E+23	
Zn	1.1E+24	1.0E+26	7.E+24	4.E+21		8.2E+24

(*Continued*)

Element	E+	EO+	ESi+	ECs+	E-	ESi-
Ga	1.4E+21		2.9E+23	3.1E+22	1.6E+26	
Ge	1.5E+23	1.7E+25	1.4E+24	3.1E+22	1.5E+23	
As	2.2E+24	8.E+24	5.E+24	5.E+22	4.6E+23	1.2E+22
Se	6.E+24	6.E+25	3.4E+24	2.4E+23	7.2E+21	
Br	1.6E+25	1.1E+26	7.E+23		7.0E+21	
Kr	1.6E+26		6.E+26			
Rb	8.E+20	5.E+24	7.E+23			
Sr	8.E+20	2.4E+22	1.2E+23			
Y	1.7E+21	1.1E+22	2.2E+23			1.4E+24
Zr	2.4E+21	4.E+21	8.E+22		1.0E+25	
Nb	1.0E+22	6.E+22	1.3E+23		4.6E+24	
Mo	2.3E+22	3.2E+23	2.2E+23	2.1E+22	2.0E+25	
Ru	3.5E+22		3.0E+23		5.E+24	5.E+23
Rh	2.7E+22	6.E+25	9.E+22		1.2E+24	2.7E+23
Pd	1.4E+23		6.E+23		4.9E+24	
Ag	7.E+22	1.1E+26	1.4E+24	1.4E+22	1.1E+23	
Cd	8.E+23	2.2E+26	6.E+24	1.6E+22		1.3E+25
In	1.5E+21	1.6E+25	4.E+23	2.4E+21	1.8E+26	
Sn	3.0E+22	4.0E+24	9.E+23	1.9E+22	1.8E+23	
Sb	6.E+23	5.0E+24	4.E+24	9.0E+21	2.7E+23	3.0E+22
Te	1.5E+24	4.0E+25	2.2E+24	1.5E+23	8.4E+21	
I	3.1E+24		7.E+23		7.2E+21	
Xe	1.6E+26		1.9E+26			
Cs	3.4E+20	3.1E+24	7.E+23			
Ba	1.5E+21	4.0E+22	1.8E+23		1.6E+26	4.4E+24
La	2.8E+21	4.5E+21	3.E+23			8.6E+24
Ce	3.3E+21	3.5E+21	8.E+22			
Pr	1.7E+21	3.7E+21				
Nd	1.2E+21	6.E+21	2.8E+23			4.E+24
Sm	2.4E+21	1.2E+22	1.9E+23			2.9E+24
Eu	1.6E+22	2.5E+23	2.0E+23		3.8E+25	6.5E+25
Tb	2.1E+21	9.E+21	2.7E+23			1.4E+24
Dy	2.0E+21	1.4E+22	2.7E+23			2.8E+24

Ho	2.2E+21	1.2E+22	4.E+23		1.5E+27	5.E+24
Er	2.5E+21	1.8E+22	9.E+23		4.E+26	1.8E+24
Tm	2.8E+21	2.4E+22	1.9E+23			1.9E+24
Yb	2.2E+21	3.E+22	2.0E+23		5.E+26	3.5E+24
Lu	3.E+21	2.5E+22			2.7E+26	3.1E+24
Hf	1.5E+22	6.E+22	2.0E+24		7.E+26	6.7E+22
Ta	6.E+22	1.2E+23	3.3E+23		1.E+26	3.E+23
W	6.E+22	6.E+23	8.E+23		6.5E+24	3.6E+23
Re	4.6E+24	8.E+21	3.E+25		2.7E+27	4.E+24
Os	2.5E+23	6.E+24	2.8E+23		2.2E+24	3.6E+22
Ir	8.E+23	5.E+25	2.2E+23		8.E+22	1.0E+23
Pt	1.0E+24	9.E+25	1.5E+23		1.6E+23	
Au	2.5E+24	1.0E+26	7.E+23		1.0E+22	
Hg	2.9E+24		6.E+25			5.6E+25
Tl	4.E+21	6.E+25	2.E+24		3.4E+26	
Pb	7.E+22	4.E+25	5.E+24		3.2E+25	
Bi	1.4E+23	3.0E+25	6.E+24		5.1E+23	1.0E+23
Th	1.4E+22	9.E+21	1.4E+24		4.9E+25	3.3E+23
U	4.E+22	5.E+22	6.E+23		6.3E+25	3.4E+24

Source: Wilson, Stevie, and Magee [2]; Stevie, and Wilson [3]; and Wilson et al. [4], data obtained from bombardment of silicon substrate with O_2^+ for E^+, EO^+, ESi^+, and ECs^+, and with Cs^+ for E and ESi, where E is the element. ^{28}Si was used for matrix species.

REFERENCES

[1] Wilson, R.G., S.W. Novak, S.P. Smith, S.D. Wilson, and J.C. Norberg. 1988. "Relative Sputtering Rates and Ion Yields of Semiconductors, Metals, and Insulators Under Oxygen and Cesium Bombardment." *Secondary Ion Mass Spectrometry, SIMS VI*, eds. by A. Benninghoven, A.M. Huber, and H.W. Werner, 133. Chichester, United Kingdom: Wiley.

[2] Wilson, R.G., F.A. Stevie, and C.W. Magee. 1989. *Secondary Ion Mass Spectrometry*, Appendix E. New York: Wiley.

[3] Stevie, F.A., and R.G. Wilson. 1991. "Relative Sensitivity Factors for Positive Atomic and Molecular Ions Sputtered from Si and GaAs." *Journal of Vacuum Science & Technology A* 9, no.6, p. 3064. doi: http://dx.doi.org/10.1116/1.577174

[4] Wilson, R.G., F.A. Stevie, S.L. Chryssoulis, and R.B. Irwin. 1994. "Secondary Ion Mass Spectrometry Relative Sensitivity Factors for Ru, Rh, Pr, Eu, Tm, Lu, Re, Os, and Ir." *Journal of Vacuum Science & Technology A* 12, no. 4, p. 2415. doi: http://dx.doi.org/10.1116/1.579224

INDEX

A

Absolute positive secondary ion yields in SIMS, 40
Accuracy, 135–137
AES. *See* Auger electron spectroscopy
AFM. *See* Atomic force microscope
AlGaN/InGaN LED structure, 221*f*
AlN. *See* Aluminum nitride
Aluminum nitride (AIN), 220–222, 221*f*
Analysis parameters of SIMS
  absolute positive secondary ion yields, 40*t*
  analysis using an oxygen beam, 39–41
  for Ar^+ bombardment of Al, 43, 45*t*
  best detection limit, 46
  for Cs^+ bombardment of germanium in InP, 46, 47*f*
  for depth profiling, 39
  mass interferences, mass resolution, 52–58
  for O_2+ bombardment of Si, 45*t,* 46
  optimum choice of primary beam of an element, 42, 44*f*
  primary beam angle of incidence, 48–49
  primary beam current and raster size, 49
  primary beam energy, 47–48
  relative sensitivity factors (RSFs), 41–43
  secondary beam energy distribution–voltage offset, 49–52
  secondary ion polarity and species, 43–47
  secondary ion yields for O_2+ or Cs^+ bombardment, 41*f*–43*f*
Analysis sequence in mass spectrometry, 236–238
Analytical instrumentation
  comparison of mass analyzers, 76*t*
  computers and data manipulation, 77
  focused ion beam SIMS (FIB-SIMS), 76–77
  ion detectors, 75–76
  ion sources, 63–66
  magnetic sector, 69–72
  postionization instruments, 77–78
  primary ion column, 66, 67*f*
  quadrupole analyzer, 67–68, 68*f*
  radio frequency (RF) plasma sources, 64
  sample chamber and sample, 66–67
  secondary ion column and mass analyzers, 67–75
  thermal ionization cesium sources, 64
  time of flight (TOF), 73–75, 73*f*

vacuum systems, 61–62
Applications of SIMS. *See also* Secondary ion mass spectrometry (SIMS)
analysis of thorium implanted in silicon, 218*f*
deposition of an epitaxial layer, analysis of, 208
depth profile of gate oxides, determining, 209–210, 210*f*–211*f*
determining penetration depth, 212–213
FinFet characterization, 218
gold implanted with thallium, analysis of, 214
InP and GaAs technologies, 218–220, 219*f*–220*f*
ion implantation measurements, 208–209
mass interferences, analysis of, 227–228, 228*t*
measurement of minerals, ceramics, catalysts, 227–229
in minimizing photoresist thickness, 212
nondepth profiling applications, 226
in organic depth profiling, 223–227
packaging of semiconductor chips, 214
in semiconductor industry, 205–223
small areas, analysis of, 212–213
soft memory errors, 214–217, 216*f*
study of entire stucture, 213–214
study of metals, 229
thorium implanted in silicon, analysis of, 217
three-level metal structure, analysis of, 215*f*
viability of a barrier layer, analysis of, 210–211, 211*f*
Applied Research Laboratories (ARL) IMMA, 6
Atomic force microscope (AFM), 97
Atomika 3000, 6
Auger electron spectroscopy (AES), 1, 2*t,* 7, 208
depth profile, 8, 9*f*

B

Back side analysis, 157–160, 157*f*–158*f,* 160*f*
Bond-breaking model for secondary ion emission, 29
Boron implant standard, 125
Borophosphosilicate glass (BPSG), 212, 213*f*
depth profile of, 11, 12*f*
BPSG. *See* Borophosphosilicate glass
Bulk analysis measurements, 160–161
of concentration or atom density, 161*t*
of HgCdTe, 161*f*
Bulk standards, 131–132
Buried insulators, 185

C

CAMECA IMS-f series instruments, 135, 179*f,* 238
atom densities in HgCdTe, 161
gating method in, 82
penetration in GaN for, 91*f*
CAMECA NanoSIMS50, 227
CAMECA normal incidence electron gun (NEG), 177–179, 177*f*
Capping method, 92, 153*f*
Carbon detection limit, 195–196
in GaAs, 195–196, 195*f*
Carbon segregation in niobium bicrystals, 11, 12*f*
Catalysts, 229
Ceramics, 137

Cesium attachment, 137
Cesium cluster ions, 137–138
Cesium microbeam source, 64*f*
  matrix concentration, 137–138
Charge compensation methods, 168–169
Cherepin instrumentation, 6
Chlorine, isotope abundance for, 3*f*
CMOS technology. *See* Complementary metal oxide semiconductor (CMOS) technology
Complementary metal oxide semiconductor (CMOS) technology, 108*f,* 205, 207*f*
Computers, and data manipulation, 77. *See also* Analytical instrumentation
Contamination, effect on sputtering, 199–200
Count rate saturation, 104–105

D

Da. *See* Dalton
Dalton (Da), 5, 151
Depth profiles
  AlN impurity, 221*f*
  of an ion implant of molybdenum in silicon, 130*f*
  Ar cluster, 226*f*
  characteristics, 84*f*
  of ^{13}C in polystyrene, 223*f*
  of copper ion implanted (LPCVD) Si_3N_4, 210–211
  count rate saturation-detector dead time, 104–105, 105*f*–106*f*
  crater perspective, 84, 86*f*
  depth resolution range, 83–96
  detection limit, 100–104, 101*f*
  dynamic range, 100–104
  of epitaxial Si layer, 208, 208*f*
  of Fe in TiW, TiN, and $TiSi_2$, 129*f*
  of F implanted into 500 nm SiO_2/Si, 166*f*
  for gold plating, 214
  image, 111, 112*f*
  lateral resolution limits, 111
  memory effect, 100–104
  of movement of species due to chemical effect, 111–112
  nonuniformities, 109–111, 110*f*–111*f*
  nonuniformity and sample rotation, 96–100, 97*f*–100*f*
  pre-equilibrium zone, 87–92
  quantification of, 125
  of rare gas elements, 200–202
  raster and gate values, 81–83, 82*f*–83*f*
  RMS roughness *vs* incidence angle, 98*f*
  of SiO_2/BPSG, 91*f*
  small area analysis, 105–109, 106*f,* 109*f*
  of sphalerite bulk insulator using O^-, 170*f*
  sputtering rate and, 96
  ultra-shallow analysis, 92–96, 95*f*–96*f*
Depth resolution, 83–96. *See also* Depth profiles
  Cs^+ bombardment of Nb, 199*f*
  for delta layer, 88*f*
  detected area *vs* raster size, 85*f*
  interface location, 87*f*
  knock-on and nonuniform removal, 85*f*
  knock-on variation with primary energy, 90*f*
  parameters for interface, 86*f*
  sample cooling and, 225*f*
  sample rotation and, 225*f*
  surface equilibration region, 89*f*
  TOF-SIMS, 88*f*
Detection limit, 100–104
Detectors, 75–76
Duoplasmatron, 63, 63*f*
Dynamic range, 100–104

E

EBIC. *See* Electron beam induced conductivity
EDS. *See* Energy dispersive spectroscopy
EI-MS. *See* Electron impact mass spectrometry
Electron affinity, 29
  RSF relationship with, 140–142
Electron beam induced conductivity (EBIC), 171–172, 172*f*
Electron beam neutralization, 169–182
  electron beam degradation of sample, 182
  electron emission *vs* electron energy, 171*f*
  ion intensity of GdO^+, 173–174
  magnetic sector analysis for, 177–181
  in quadrupole analyzer, 173–177
  TOF analysis for, 181
Electron impact (EI-MS) mass spectrometry, 7–8
Electron multiplier, 76, 76*f*
Electron stimulated desorption (ESD), 185–187, 187*f*
Electron-tunneling model for secondary ion emission, 29
Elemental surface analysis techniques, 1–2
Energy dispersive spectroscopy (EDS), 1
Energy distribution, 20, 50
ESD. *See* Electron stimulated desorption

F

Faraday cup detector, 76, 76*f*
FIB-SIMS. *See* Focused ion beam SIMS
Focused Ion Beam SIMS (FIB-SIMS), 76–77

G

GaAs technology, 218–220, 219*f*–220*f*
Gallium nitride (GaN), 220
GaN. *See* Gallium nitride
Gas chromatograph mass spectrometer, 7
Gas chromatograph mass spectrometry (GC-MS), 5
Gas chromatography (GC-MS) mass spectrometry, 7
Gate oxide, 209–210
Gating method, 81–83
GCA Corporation IMS101 magnetic sector, 6
GC-MS. *See* Gas chromatograph mass spectrometry
GDMS. *See* Glow discharge mass spectrometry
Glow discharge (GDMS) mass spectrometry, 7

H

Higher energy electron neutralization, 173
Hydrogen detection limit, 192–195, 193*f*–194*f*
  deuterium, 193
  vs instrument vacuum, 192–193
  mobility in an oxide, 194
  in Nb *vs* Nb_2O_5, 194
  in SiO_2, 194

I

ICP-MS. *See* Inductively coupled plasma mass spectrometry
Image depth profile, 111
Inductively coupled plasma (ICP-MS) mass spectrometry, 7
InP technology, 218–220, 219*f*
Insulators
  buried, 185
  charge compensation methods, 168–169

electron beam neutralization, 169–182
electron stimulated desorption (ESD), 185–187
for metal layers, 212
sample charging of, 165–168, 166*f*–168*f*
species mobile under ion bombardment, 182–185
Interfaces, 151–156, 153*f*–155*f*
fluorine profile through a SiO_2 layer on silicon, 154–155
quantification of contaminant at, 153, 155
between a Si_3N_4 layer and a silicon substrate, 154
Ion detectors, 75–76
Ion implantation, 100–101, 124–126
Ion implanted standards, 124–126, 127*f,* 208–209
boron implant standard, 125
dopant profiles for arsenic and boron in a bipolar transistor, 208, 209*f*
of ^{24}Mg in GaN, 125, 125*f*
of ^{58}Ni in silicon, 122, 123*f*
preparation of, 126–131
Ionization potentials
RSF relationship with, 140–142
Ion sources, 63–66
argon cluster source, 65
cesium microbeam source, 64*f*
in common use, 66*t*
liquid metal ion source (LMIS), 64–65, 65*f*
radio frequency (RF) plasma sources, 64
Isotope-specific analysis, 2
Isotopic abundances, 3

K

Kanaya–Okayama equation, 172

L

Lateral resolution, 111
LC-MS. *See* Liquid chromatography mass spectrometry
$LiNbO_3$. *See* Lithium niobate
Liquid chromatography (LC-MS) mass spectrometry, 7
Liquid metal ion source (LMIS), 2, 6, 64–65, 65*f,* 77
Lithium niobate ($LiNbO_3$), 220–223, 222*f*
LMIS. *See* Liquid metal ion source
Local thermal equilibrium (LTE) model, 30
Low energy electron beam neutralization, 173, 181–182

M

Magnetic sector analyzer, 69–72. *See also* Analytical instrumentation
Be in crystalline Al_2O_3, analysis of, 180*f*
CAMECA IMS-7F and NanoSIMS50L, 71*f,* 72
double focusing, 69*f*
electron beam neutralization in, 177–181
geometry, 104*f*
imaging strategies, 70
ion trajectories for, 69*f*
Li, Na, K implanted SiO_2/Si, analysis of, 184
mass resolution of, 70
parameters for primary and secondary beams using, 72
potential energy of an ion, calculation of, 69–70
Mass interferences in SIMS, 52–58, 53*t,* 57*f*
of copper in a SiO_2 layer on silicon, 55, 57

in Fe region of labradorite, 227–228, 228*t*
in Si, 56
Mass resolution in SIMS, 52–58, 54*f,* 56*f*
for Cs^+ and for O_2+ bombardment, 56
of P in amorphous Si, 55–56
Mass spectrometry. *See also* Secondary ion mass spectrometry (SIMS)
analyzers, 3–4
application, 5
block diagram, 4*f*
brief history, 5
of chlorine dimer ion, 3
defined, 3
of European crude oil, 4
instrument operation and data acquisition, 3–5
mass analyzers, types of, 3–4
types of, 7*t,* 8
Matrix effects, 32–34
measurements, 237*f*–238*f*
P in Si *vs* SiO_2, 32, 32*f*–33*f*
for Pt analysis, 32, 33*f*
Matrix quantification, 132–134, 137–138
Mean free path for air at room temperature, 61
Measurement of minerals, ceramics, catalysts using SIMS, 227–229
Memory effect, 227–228
Metals, study using SIMS, 229
Minerals, 103, 197
Multilayers, 156–157, 156*f*
of AlGaAs/GaAs, 156
Multiple element profiles of residual gas species, 198, 198*f*

N

Nitrogen detection limit, 196–197
in SiC, 196, 196*f*
SiON gate, 197
Nondepth profiling applications of SIMS, 226
Non-uniform distribution, 109–111
Non-uniform sputtering, 96–100

O

Organic depth profiling, 223–227
Organic light emitting diode, 227*f*
Organic materials, 223–227
Oxygen detection limit, 197–198, 197*f,* 206
Oxygen flood (oxygen leak, oxygen backfill), 30–31, 31*f,* 62, 66

P

PDMS. *See* Polydimethylsiloxane (PDMS)
PHI-6300 quadrupole analyzer, 173
Photoresist, 212
Physical Electronics PHI-6300, 6
Polishing sequence for silicon, 158
Polydimethylsiloxane (PDMS), 151, 152*f*
Postionization instruments, 77–78
Precision, 135–136
Pre-equilibrium zone, 87–92
Preferential sputtering, 28
Primary beam angle of incidence in SIMS, 48–49, 48*f*–49*f*
Primary beam current and raster size in SIMS, 49
Primary beam energy in SIMS, 47–48
Primary beam polarity, 39
Primary column, 40, 64, 128

Q

Quadrupole analyzer, 67–68, 151. *See also* Analytical instrumentation
analysis of titanium diffused into

LiNbO$_3$, 176–177, 176*f*
charge neutralization in, 173–177
geometry, 104*f*, 173*f*
ion intensity of GdO$^+$, 173–174, 174*f*
Li, Na, K implanted SiO$_2$/Si, analysis of, 184*f*
mass spectra for quartz watch glass and Pyrex, 175*f*–176*f*
mobile ion species, analysis of, 183*f*

Quantification
analysis of high-k dielectric layers, 159
analysis of SiGe elements, 132–134
back side analysis, 157–160, 157*f*–158*f*, 160*f*
bulk analysis measurements, 160–161
bulk standard, 131–132, 132*f*
of depth profiles, 125
dose precision, 136
front side analysis of hafnium silicate, 159–160, 159*f*
implant energy, 125, 128*f*
interfaces, 151–156, 153*f*–155*f*
ion implantation, 124–131, 125*f*–129*f*
isotopic distribution, 129–130
of matrix and trace elements, 132–134
of minerals, ceramics, catalysts using SIMS, 227–229, 227*f*
multilayer analysis, 156–157, 156*f*
need for secondary standards, 121
nonlinear region, 132–133, 133*f*
peak concentration, 131
of an ion implant, 138–139
precision and accuracy, 135–137, 136*f*
preparation of ion implanted standards, 126–131
regions, 237*f*
relative sensitivity factors (RSFs), 121–124, 123*f*–124*f*, 140–142
sample considerations, 149
sequence for the element of interest, 124
site-specific back side analyses, 159
species mobile under ion bombardment, 182–185
static, 138–140
total concentration of the element, 126
useful yield, 134–135
using cesium cluster ions, 137–138, 138*f*
using multiple matrixes, 137–138

R

Radio frequency (RF) plasma sources, 64
Rare gas elements, depth profiles of, 200–202
argon, 201–202
helium, 201, 201*f*
xenon, 202
Raster, and gate, 81–83
Raster reduction method, 191, 192*f*, 196, 198
Raster size, 49, 84–85, 96
RBS. *See* Rutherford backscattering spectrometry (RBS)
Relative sensitivity factors (RSFs), 41–43, 121–124, 126, 140–142
for a bulk doped sample, 131
for a depth profile of an ion implanted standard, 121–124
of HgCdTe, 161*t*
patterns for secondary negative ions, 142*f*
for positive secondary ion, 141

relationship with ionization potential and electron affinity, 140–142
for secondary positive ions, 142
Residual gas detection limits
for carbon, 195–196
effect of contamination and, 199–200, 200*f*
for hydrogen, 192–195
for multiple elements, 198
for nitrogen, 196–197
for oxygen, 197–198
Residual gas elements, 191, 198
RF plasma sources. *See* Radio frequency plasma sources
Riber MIQ 256, 6
RSF. *See* Relative sensitivity factors
Rutherford backscattering spectrometry (RBS), 8, 130, 212

S

Sample chamber, 66
Sample requirements, 66–67
Sample rotation, 97–100
Scanning electron microscopy (SEM), 1, 97
analysis sequence, 236–238
Secondary beam energy distribution–voltage offset in SIMS, 49–52, 50*f*–52*f*
Secondary beam polarity [not found]
Secondary ion column, 67
Secondary ion mass spectrometry (SIMS), 1, 2*t*, 7. *See also* Analytical instrumentation; Applications of SIMS; Mass spectrometry; Quantification
advantages of, 8, 10*t*
analysis sequence, 236–238
block diagram of instrument, 62*f*
brief history of, 6–7
depth profile
vs AES depth profile, 8, 9*f*
of BPSG layers, 11–12
detection limits, 8
differences between static and dynamic, 150*t*
disadvantages of, 10*t*
dynamic range for, 2
interaction of ions with matter, 19
literature on, 6–7
mass spectrum y-axis display, 10*f*
matrix effects, 32–34
oxygen flood (oxygen leak, oxygen backfill), 30–31
parameters (*see* Analysis parameters of SIMS)
preferential sputtering, 28
sample requirements for analysis, 66–67
secondary ion yields, 28–30
sensitivity of, 8
sources of information for, 7
sputtering process, 19–22
sputtering yield, 23–28
static, 6
types of data, 11–12
utility of, 6, 8
vacuum system of, 62
Secondary ion yields in SIMS, 28–30
for Ar^+ bombardment of silicon at normal incidence, 31
with C_{60} cluster source, 223–225, 224*f*
due to oxygen or cesium, 28–29
due to primary beam energy and angle of incidence, 29*f*–30*f*
models for, 29–30
SEM. *See* Scanning electron microscopy
Sensitive High Resolution Ion Microprobe magnetic sector, 6

Separation by implantation of oxygen (SIMOX) method, 185–186, 186*f*
Si. *See* Silicon
Silicon (Si)
  barrier layers, 210–211, 211*f*
  contaminants in, 206
  detection of boron, 93*f*
  effect of primary beam energy and incidence angle on Sb depth profile in, 90*f*
  epitaxial layer, deposition of, 208, 208*f*
  GaAs/AlGaAs doped, 218–220
  gate oxide of, 209–210, 210*f*–211*f*
  as insulator for metal layers, 212
  ion implantation in, 208–209
  mass interferences, 56
  parameters for characterization of, 205
  photoresist of, 212
  processing steps and related SIMS analyses, 206*t*
  regions in zeolite, 229*f*
  secondary ion yields, 29*f*–30*f*, 41*f*–43*f*, 45*t*, 46, 141*f*
  SIMS patterns on, 108*f*
SIMOX method. *See* Separation by implantation of oxygen method
SIMS. *See* Secondary ion mass spectrometry
Small area analysis, 105–109
Small areas, 105
Soft memory errors, 214–218
Species mobile under ion bombardment, 182–185
  analysis of sodium implanted into SiO_2 on a silicon substrate, 182–183, 182*f*
Spectrometry, defined, 7
Spectroscopy, defined, 7
Sputtered neutral mass spectrometry, 77
Sputtering process, 19–22
  energy distribution of sputtered particles, 20*f*
  interaction of ions with matter, 20*f*
  method, 19–21
  simulation methods used, 21
  simulation of Ar^+ into rhodium, 22*f*
  sputtering rate for silicon, 22
  sputtering simulation of C_{60}+ *versus* Ga^+ on Ag, 23*f*
  sputtering simulations for SF_5+, 22*f*
  three-dimensional sputtering simulations, 21–22
Sputtering rate, 96
Sputtering yield, 23–28
  angular distribution of sputtered material, 26*f*
  impact of oxygen flood, 31
  peak calculation, 24
  penetration *vs* incidence angle, 24*f*, 25–26, 26*f*
  vs primary ion atomic number, 27
  vs primary ion energy, 23*f*–24*f*
  relationship with bombarding ion, 27
  vs target atomic number, 27*f*
Static SIMS, 138–140
Sticking coefficient, 62
Surface-excitation model, 30
Surface-polarization model, 30
Surface–static SIMS, 149–151

T

Tantalum silicide ($TaSi_2$) with O_2+ bombardment, analysis of, 28
TEM. *See* Transmission electron microscopy

TEM-EDS. *See* Transmission electron microscopy EDS
TG-MS. *See* Thermogravimetric mass spectrometry
Thermal ionization (TIMS) mass spectrometry, 7
Thermogravimetric (TG-MS) mass spectrometry, 7
Time-Of-Flight (TOF) mass analyzer, 4, 43, 73–75, 73*f,* 151, 181*f,* 183. *See also* Analytical instrumentation
  depth profile of thin $MoSi_2$ film on silicon, 153
  depth resolution, 88*f*
  electron beam neutralization in, 181
  electrostatic analyzer, 75*f*
  expression of flight time, 73
  of implants through SiO_2, 139*t*
  pulsing of primary beam and cycle time, 73–74
  reflectron analyzer, 74*f*
  reflectron based, 74
  timing diagram, 74*f*
TIMS. *See* Thermal ionization mass spectrometry
TOF–SIMS. *See* Time-of-flight (TOF) mass analyzer
Transmission electron microscopy EDS (TEM-EDS), 1
Transmission electron microscopy (TEM), 208
Transport of Ions in Matter (TRIM), 128, 236
Transport of Ions in Matter (TRIM) Monte Carlo simulation, 21
  for boron implanted into silicon, 21*f*
  of collision cascade at two different angles of incidence, 24–25
  distribution of implanted species, 25*f*
  at two impact energies, 21*f*
Trehalose, 225
TRIM. *See* Transport of Ions in Matter; Transport of Ions in Matter Monte Carlo simulation

U
Ultra-shallow analysis, 92–96
Useful yield, 77, 134–135

V
Vacuum systems, 61–62
Voltage offset, 49–52

W
Work function model, 30

X
XPS. *See* X-ray photoelectron spectroscopy
X-ray photoelectron spectroscopy (XPS), 1, 2*t,* 94, 140

Z
Zinc oxide mass spectrum, 11*f*

OTHER TITLES IN OUR MATERIALS CHARACTERIZATION AND ANALYSIS COLLECTION

C. Richard Brundle, *Editor*

Auger Electron Spectroscopy: Practical Application to Materials Analysis and Characterization of Surfaces, Interfaces, and Thin Films
by John Wolstenholme

A Practical Guide to Transmission Electron Microscopy
by Zhiping Luo

Spectroscopic Ellipsometry: Practical Application to Thin Film Characterization
by Harland G. Tompkins and James N. Hilfiker

Momentum Press is one of the leading book publishers in the field of engineering, mathematics, health, and applied sciences. Momentum Press offers over 30 collections, including Aerospace, Biomedical, Civil, Environmental, Nanomaterials, Geotechnical, and many others.

Momentum Press is actively seeking collection editors as well as authors. For more information about becoming an MP author or collection editor, please visit http://www.momentumpress.net/contact

Announcing Digital Content Crafted by Librarians

Momentum Press offers digital content as authoritative treatments of advanced engineering topics by leaders in their field. Hosted on ebrary, MP provides practitioners, researchers, faculty, and students in engineering, science, and industry with innovative electronic content in sensors and controls engineering, advanced energy engineering, manufacturing, and materials science.

Momentum Press offers library-friendly terms:

- perpetual access for a one-time fee
- no subscriptions or access fees required
- unlimited concurrent usage permitted
- downloadable PDFs provided
- free MARC records included
- free trials

The **Momentum Press** digital library is very affordable, with no obligation to buy in future years.

For more information, please visit **www.momentumpress.net/library** or to set up a trial in the US, please contact **mpsales@globalepress.com.**

EBOOKS
FOR THE
ENGINEERING
LIBRARY

Create your own Customized Content Bundle — the more books you buy, the higher your discount!

THE CONTENT

- *Manufacturing Engineering*
- *Mechanical & Chemical Engineering*
- *Materials Science & Engineering*
- *Civil & Environmental Engineering*
- *Electrical Engineering*

THE TERMS

- *Perpetual access for a one time fee*
- *No subscriptions or access fees*
- *Unlimited concurrent usage*
- *Downloadable PDFs*
- *Free MARC records*

For further information, a free trial, or to order, contact:
sales@momentumpress.net

Secondary Ion Mass Spectrometry

Applications for Depth Profiling and Surface Characterization

Fred A. Stevie

Secondary ion mass spectrometry (SIMS) is a mass spectrometric technique for solid materials that can provide elemental analysis at parts per million sensitivity and lateral resolution of 50 nm. When those capabilities are combined with the ability to provide that analysis as a function of depth, SIMS has proved to be a valued technique for a wide range of applications.

This book was written to explain a technique that requires an understanding of many details in order to properly obtain and interpret the data obtained. It also will serve as a reference for those who need to provide SIMS data. The book has over 200 figures and the references allow one to trace development of SIMS and understand the many details of the technique.

Fred A. Stevie is a senior researcher at the Analytical Instrumentation Facility in North Carolina State University (NCSU). His experience with SIMS exceeds 30 years and covers a wide range of applications. He has been an analyst in major analytical facilities in Bell Laboratories and NCSU and is familiar with the capabilities of multiple techniques. Fred has authored or co-authored books on SIMS and focused ion beams and more than 200 technical publications. He also holds 20 patents related to surface analysis.

MOMENTUM PRESS
ENGINEERING